ISSN number 0971 - 9709

The Journal of Indian Geophysical Union

VOLUME 21, ISSUE 2 | MARCH 2017

AN OPEN ACCESS BIMONTHLY JOURNAL OF IGU

EDITORIAL OFFICE
Indian Geophysical Union, NGRI Campus, Uppal Road, Hyderabad- 500 007
Telephone: +91 -40-27012799; 27012734; Telefax:+91-04-27171564
E. mail: jigu1963@gmail.com, website: www.j-igu.in

The Open Access Journal with six issues in a year publishes articles covering
Solid Earth Geosciences; Marine Geosciences; and Atmospheric, Space and Planetary Sciences.

Annual Subscription

Individual ₹ 1000 per issue and Institutional ₹ 5000 for six issues

Payments should be sent by DD drawn in favour of "The Treasurer, Indian Geophysical Union", payable at Hyderabad, Money Transfer/NEFT/RTGS (Inter-Bank Transfer), Treasurer, Indian Geophysical Union, State Bank of Hyderabad, Habsiguda Branch, Habsiguda, Uppal Road, Hyderabad- 500 007
A/C: 52191021424, IFSC Code: SBHY0020087, MICR Code: 500004020, SWIFT Code: SBHYINBB028.

For correspondence, please contact, Hon. Secretary, Indian Geophysical Union, NGRI Campus, Uppal Road, Hyderabad - 500 007, India; Email: igu123@gmail.com; Ph: 040 27012799

ISSN: 0257-7968 (Thomson Reuters)
ISSN: 0971-9709 (NISCAIR)

Approved as ESCI journal by Thomson Reuters
Cited in Indian Citation Index (ICI), New Delhi
Evaluated by NISCAIR, New Delhi

CONTENTS

Editorial

I am happy to tell that the editorial on **MAGMA**, published in January, 2017 issue received positive comments from elders Dr.Rabinarayan Mishra and Dr.Y.V.Ramana; former a well known geologist from Geological Survey of India and the later a well known High Pressure and Rock Mechanics expert from NGRI. Dr.Ramana in response to my request through the editorial of January issue for an intellectual debate/interaction on definition of **MAGMA** has sent the following, as an additional input. I am sure the readers will be happy to go through the details and keep the debate active. I urge my young research friends to learn from such highly motivated elders and strengthen their knowledge base, making their research output recognised by the peers.

Dr.Y.V.Ramana has sent the following:

------I am writing my views to sustain the discussions with a positive note.

"**MAGMA** connotes geological materials, subcrustal in nature, taking the form of solid to semisolid state, or states, derived from the prevailing interior Pressure and Temperature conditions creating a mass with a semi-viscous to viscous formation states responding to form elasto - plastic flows introducing creep enabling periodic, or even aperiodic flows of extensive rocky materials; whose movement, movements or displacements cause to be causative factors for earthquakes, coupled with massive structural upward lifts, subduction zones, major fault zones, changes in oceanic rifts, geologic plate movements (major or minor), volcanic eruptions, etc., whose cumulative effect over a geological time scale to restore a cyclical balance through even continental drift.

MAGMA formation is very complex dependent on multiple variable factors, mostly Natural in origin over geologic time scales that are mostly cumulative and earthquakes are Telltales for humans to understand and draw inferences within the realms of the scientific investigator, or researcher governed by his / her analytical comprehension and limitations of knowledge. The presence or the existence of Magma is the causative factor for the very classification of crust, mantle, and core, as well as the further subdivision of upper mantle, lower mantle, outer core and inner core supported by geological and geophysical picturization of mother earth.

Dynamic earth has a regenerative process or processes of its own, with its own cyclical systems, equilibrium states at different depths, changing P and T conditions and so on, apart from the influence of the other planets in the earth's solar system, of which it is a part, and

the influence of these being more visible in the oceanic part with its tidal changes, atmospheric changes; as well as ionospheric variations impacting communications.

Trust these views find a place in the Journal, as well as the proposed discussions on Magma".

The above details communicated by Dr.Ramana are interesting.

As we need to make use of the present discussion to have better insight in to **MAGMA** composition, I place below an interesting article. The cited study helps to know about how the mantle melts, to understand **MAGMA** composition. Geochemical and isotopic data suggest that the source regions of oceanic basalts may contain pyroxenite in addition to peridotite. In order to incorporate the wide range of compositions and melting behaviours of pyroxenites into mantle melting models, Lambart et al (2016) have developed a new parameterization, Melt-PX, which predicts near-solidus temperatures and extents of melting as a function of temperature and pressure for mantle pyroxenites.

Before going into specifics of the above study let us know in detail about mantle composition.

"The bulk of the Earth's volume is composed of the mantle—the layer of silicate rocks sandwiched between the dense, hot core and the thin crust. Although the mantle is mostly solid rock, it's generally viscous: Slowly, over millions of years, the material within the layer drifts, driving tectonic plates together and apart. Thus, the mantle's influence can be seen on the planet's surface on both large and small scales—from fuelling volcanoes and seafloor expansion down to the composition and characteristics of igneous rocks. The mantle is a heterogeneous mixture of peridotite and pyroxenite, largely due to the continuous subduction of basaltic oceanic crust. This is becoming increasingly clear as our studies of basaltic **MAGMA** chemistry grow ever more detailed. However, nearly all models of mantle melting assume homogenous peridotite compositions. A few experimental studies have studied pyroxenite melting, and there have been some attempts at empirical modeling of melting of heterogeneous mantle. Igneous rocks composed primarily of pyroxenes, minerals that contain 40% more silicon than olivine—may also be a source of oceanic lavas".

New research by Lambart et al. seeks to better model how pyroxenites influence melting that occurs in the mantle. Pyroxenites make up between 2% and 10% of the upper mantle, depending on the region, but determining the amount of pyroxenites in hot mantle plumes that reach the surface requires more information. Researchers have found that at the same pressure, pyroxenites tend to melt at lower temperatures than peridotites, which means that any pyroxenites in peridotite-rich mantle regions might make up a larger portion of the liquid material than their small fraction of mantle bulk would suggest. To understand how the varying source materials in the mantle contribute to the characteristics of igneous rocks at the surface, researchers need to understand the melting characteristics of pyroxenites—a broad and variable group of rocks. That variability in composition makes predicting the phase changes of pyroxenites more complicated. And that complexity means that current models of mantle melting, like pMELTS, overestimate the temperature range over which pyroxenites melt. So, the authors created a new parameterization for mantle melting models that seeks to rectify the problem. The new parameterization accounts for the fact that temperature, pressure, and the bulk chemical composition of the rocks together determine their near-solidus temperature. The authors used a compilation of 183 experiments on pyroxenites with 25 varying chemical compositions, carried out over pressures from 0.9 to 5 gigapascals (GPa) and temperatures ranging from 1150°C to 1675°C. They charted the temperature when 5% of the materials was molten and the temperature at which clinopyroxene, a dominant mineral in pyroxenites, in each sample was gone—parameters that are easy to detect accurately and consistently. This analysis helped the authors create a new model based on experimental data from the literature, dubbed Melt-PX, which predicts the temperature at which the pyroxenites start to melt within 30°C and the amount of melting within 13%. It showed that at low pressure—less than 1 GPa— pyroxenites melt at lower temperatures than peridotites, but as pressure increases, more and more pyroxenites melt at higher temperatures than peridotites. Lambart et al is the first study to make a thermodynamic model of pyroxenite melting based on the experimental studies and represents an important step forward in accurate modeling of heterogeneous mantle melting. The model produced (Melt-PX) will be an important tool for future studies looking at **MAGMA** compositions and trying to use them to understand melting conditions in the mantle. As the new model will be a useful tool to understand **MAGMA** composition it ultimately helps researchers have a window into the Earth and the source of oceanic basalts. (Citation: Journal of Geophysical Research: Solid Earth, doi:10.1002/2015JB012762, 2016).

Let us know from the learned the necessity to know more about oceanic basalts, to keep the debate on **MAGMA** interesting. I am stressing this as many processes originating from deeper depths are linked to near surface features due to the primary contribution made by **MAGMA**.

Deciphering the Bay Of Bengal`s Tectonic origins

Since the day I led a Deep seismic Refraction team to bring out crustal velocity-depth model of West Bengal basin in 1988, I have been fascinated by the intricate subsurface crustal images of the study area. It was evident from then that the link between continental and oceanic segments is rather blurred and unique. And as such one has to view at various hidden mysteries of the oceanic and continental segments of this part of South Asia, by integrating both geologic and geophysical signatures not only to decipher the Bay of Bengal`s tectonic origin but also the entire continental span from the West Bengal and Bangladesh coastal corridor to Tibet crossing Himalayas. I felt happy to go through an interesting article published in 15th Oct, 2016 issue of EOS, while hearing soothing music from my favourite TV musical channel.

I cover below some salient points of this article in EOS and the original article published in JGR, hoping our youngsters will be benefitted.

"Although researchers have long understood that the tectonic evolution of the Bay of Bengal, located east of India, is intertwined with the opening of the Indian Ocean, the specifics of these events have yet to be unravelled. Because the standard methods of resolving the age and origin of the underlying crust—the crucial information needed to solve this puzzle—have so far yielded ambiguous results. Talwani et al(2016) have combined new, multidisciplinary data sets to obtain a better understanding of the region's tectonic history. They are able to decipher the tectonic evolution of the Bay of Bengal, a puzzle which has not been satisfactorily solved in the past. They are also able to shed new light on origin of the buried 85°E Ridge. They have done so by incorporating a number of disparate items into a unified solution. These items are the marine magnetic anomalies in the Western Basin of the Bay of Bengal, the Rajmahal and Sylhet traps, and Deep Seismic Sounding lines in India, a prominent magnetic anomaly doublet and seismic Seaward Dipping Reflectors in Bangladesh, and a new precise gravity map of the Bay of Bengal. They have identified seafloor-spreading magnetic anomalies ranging in age from 132 Ma (M12n) to 120 Ma (M0) in the Western Basin. These anomalies are "one sided"; the conjugate anomalies lie in the Western Enderby Basin, off East Antarctica. The direction of spreading was approximately NW-SE, and the half-spreading rates varied from 2.5 to 4.0 cm/yr. With the arrival of the Kerguelen plume around M0 time, seafloor spreading was reorganized and a new spreading axis opened at or close to the line joining the Rajmahal and Sylhet traps. The prominent magnetic anomaly doublet connecting the Rajmahal and Sylhet traps indicates that these traps are not individual eruptions at about 118 Ma, but rather, together, define the new line of opening. Spreading started at this line, and subsequently, India changed direction from west to north. The new oceanic crust, thus generated, underlies Bangladesh and the Eastern Basin of the Bay of Bengal and is younger than 118 Ma. The western boundary of the new ocean floor is a transform fault, which was generated by the spreading axis jump. This transform fault appears as the 85°E Ridge, and further north, on land, as a negative free-air gravity anomaly strip. A unique feature of the northern boundary of the new oceanic crust is that due to the later deposition of enormous sediments derived from the Himalayan orogeny, it lies onshore Bangladesh, in contrast to most continent-ocean boundaries in the world, which lie offshore. Despite the progress made in this study, many questions remain, according to the researchers. Additional studies, including a seismic refraction survey, will be necessary to further refine the details regarding this region's complex tectonic evolution". (Citation: Journal of Geophysical Research: Solid Earth, doi:10.1002/ 2015JB012734, 2016).

During 1988 to 1990 NGRI DSS project covered 4 seismic refraction profiles covering a significant part of West Bengal basin. Number of scientific publications (mostly by me and my younger colleagues)have come out in print. One of the articles clearly pointed out that the path of Kerguelen hot spot track followed NW-SE trend covering both oceanic and continental segments of West Bengal basin. As researchers could not cover in the similar way relevant segments of Bangladesh proper crustal velocity –depth models of the entire span of west and east Bengal basin could not be built to substantiate the proposed continental extension of Oceanic crust proposed by Talwani et al (2016). Composite deep refraction and seismic reflection data based structural models in co-ordination with other geophysical results can bring out the suggested presence of region's complex tectonic evolutionary details indicating presence of a new spreading centre along a line that now joins two volcanic provinces, called the Rajmahal and Sylhet traps. In this context a paper (in press) in Geophys. J. Int. (2017) doi: 10.1093/gji/ggw461 by Damodara et al (2017) is interesting. They have analysed first arrival refraction and later arrival wide angle reflection data (DSS data) using travel-time tomography along four profiles. The models have been successfully assessed for their reliability by checkerboard tests. The study identifies a regional feature, known as the Shelf break or the Hinge zone, where stable Indian shield ends and a sharp increase in sediment thickness occurs. The Hinge zone may represent the relict of continental and proto-oceanic crustal boundary formed during the rifting of India from Antarctica. The similar processing procedure could be used in deciphering the overall characteristics of unique crustal fabric of wider Bengal basin that contains both Rajmahal and Sylhet traps. It is time for NGRI DSS project to have a collaborative programme with Bangladesh, using the good offices of SAARC secretariat. Once data acquisition is accomplished and an integrated crustal velocity-depth model is produced, as stated by Talwani (2016) many issues pertaining to area specific and region`s complex tectonic evolution can be resolved.

In this issue

This issue contains 9 research articles, apart from the editorial and News at a glance. I do hope you would enjoy reading all the contents. Quality of many articles has been considerably improved by the stellar role played by learned reviewers including a couple of editorial board members. I thank both the authors and evaluators for the excellent contributions.

I thank one and all for the continued support extended to JIGU.

P.R.Reddy

Congratulations :

ISRO's PSLV-C37 Successfully Launched 104 Satellites in a Single Flight on 15th February, 2017. After successful expedition by Mangalyan voyager to Mars this success further confirms the outstanding capabilities of Indian Space scientists. We extend our warm greetings and congratulate one and all associated with this launch---

.... Editorial Board of JIGU & Executive committee of IGU

Elastic Wave propagation and the Coriolis force -- Recent Scientific Achievement

Earthquake generated seismic waves (elastic waves) propagate through Earth and scatter off places where material properties change suddenly, notably at the core-mantle boundary. To investigate whether rays of elastic waves are deflected by Earth`s rotation Roel Sneider and collaborators used the seismometers of USArray. They found that even after eight hours after a major earthquake, elastic waves continue to propagate along the great circle defined by the earthquake site and the array. The absence of any deflection indicates that seismic rays co-rotate with Earth. In other words the ray is not subject to the Coriolis force. Intuitively, the reason is that seismic waves are carried by a medium-the rotating Earth. In case of electromagnetic waves, which are not carried by a medium, it is significantly different: The direction of propagation of electromagnetic waves is not influenced by Earth`s rotation.

The study further pointed out that polarization of P-waves (Longitudinal) does not change in response to the Coriolis force, where as for S-waves (transverse) whose polarization is in a plane perpendicular to the propagation direction, in contrast to P-waves the polarization of S waves does rotate. Measuring the change in S-wave polarization due to Earth`s rotation presents a challenge because transverse elastic waves do not propagate for long in a pure S-wave state. By measuring the individual polarizations and difference in polarization between ScS and ScS2 waves the researchers have noticed the polarization change due to inhomogeneities in Earth`s structure is opposite in direction for eastward and westward propagating waves. But the polarization change induced by the Coriolis force is always clockwise in the Northern Hemisphere, no matter the direction of propagation. Roel Sneider et al (2016) concluded from their study that given a measurement of polarization rotation in an S wave, the Coriolis induced component can be subtracted to give the contribution from inhomogeneities alone, an approach that might lead to a better understanding of how Earth`s structure influences seismic waves (**Citation:** Roer Sneider et al, 2016, Vol 69, no 12, pp-90 & 91).

J. Ind. Geophys. Union (March 2017)
v.21, no.2, pp: 83-95

Modeling of Marine Magnetotelluric Response across 85^0E Ridge: A Numerical Simulation

K.S.N. Murthy[1,2], K. Veeraswamy*[1] and Prasanta K. Patro[1]
[1]CSIR – National Geophysical Research Institute, MT-DRS Group, Hyderabad, India
[2]Geological Survey of India, Training Institute, Hyderabad, India
*Corresponding Author: kv.swamy@gmail.com

ABSTRACT
85^0E Ridge in the Bay of Bengal region is one of the most interesting and enigmatic geotectonic features in the Indian off-shore region with its surprisingly low free-air gravity anomalies. As the marine field studies are highly expensive, it is proposed here, to simulate Marine Magneto Telluric (MMT) response across this ridge to estimate the resolvability of layer parameters like thickness and resistivity followed by period band to penetrate the signal to the desired depth using forward modeling. Similar to land MT measurements, the MT data acquired in the marine environment also gets distorted due to coast effect. In order to derive this response, a synthetic initial model has been considered which extends to 800 km on either side of the coast line and down to 600 km depth with a water column of 4 km. A finite element algorithm has been utilized to accommodate inclined continental shelf in the numerical model. In the period range of 40-4000 sec, Ridge response is well reflected in the apparent resistivity, phase, magnetic field components (Hx, Hy), and Tipper in TE and TM modes, whereas electric field components (Ex, Ey) are less pronounced. The present study reveals that the distortion in MMT responses due to coast effect is noticeable up to 200 km from the sea-land boundary for periods between 10 and 4000 sec. As the 85^0E Ridge is located at a distance of 500 km from the coast, the MMT measurements made here are free from coast effect. Data needs to be acquired for a period of at least 8 days to get more than 10 stacks of 4096 sec and therefore for better results.

Key words: 85^0E Ridge, Magnetotellurics, Finite elements, Marine Electromagnetics, Coast-effect, Northeastern Indian Ocean.

INTRODUCTION

The 85^0E Ridge is an enigmatic and aseismic volcanic feature located in the northeastern Indian-Ocean which covers from Mahanadi basin in the north to the Afanacy Nikitin Seamount (ANS) in the south. This North-South oriented ridge extends from 19^0N to 6^0S in a curvilinear shape (Figure 1). The northern part of the ridge is covered by thick pile of Bengal Fan sediments where as in the south it joins the ANS at 5^0S through isolated buried hills raised above sea level (Curray et al., 1982; Liu et al., 1982; Curray and Munasinghe, 1991; Muller et al., 1993; Gopala Rao et al., 1997; Subrahmanyam et al., 1999; Krishna, 2003; Krishna et al., 2014, Shreejith et al., 2011). Two volcanic features in the Bay of Bengal (BOB) are 90^0E Ridge and 85^0E Ridge and the crustal age of BOB is early Cretaceous. From the geological and geophysical data sets it is inferred that 90^0E Ridge is the result of post-outburst phase of Kerguelen hotspot (Duncan and Richards, 1991). But understanding the evolution of 85^0E Ridge is still a complex problem with the abnormal geophysical responses recorded over it.

Therefore additional geophysical evidences like those from Marine Magneto Telluric (MMT) investigations, which are essentially Electromagnetic (EM) induction techniques, can help resolving the problem. Globally MMT technique has been developed and used for delineating resistivity structure in the offshore region (Constable et al., 1998; Key and Constable, 2002; Baba, 2005; Heinson et al., 2005; Kasaya et al., 2005; Constable et al., 2009; Baba et al., 2010). In the Gulf of Kutch region of western India Harinarayana et al., (2008) had conducted MMT investigations and delineated the resistivity structure.

Origin and Evolutionary history of 85^0E Ridge

Curray and Munasinghe (1991) proposed that the trace of Crozet hotspot is the representation of 85^0E Ridge and ANS formed between 117 and 70 Ma but the geochemistry of the ANS and Crozet hotspot do not match together. Later Muller et al., (1993) proposed that another hot spot, which is located underneath the eastern Conrad Rise on the Antarctic plate, is the cause of formation of 85^0E Ridge. On the basis of geophysical studies, it has been inferred that the 85^0E Ridge formed due to the short lived volcanic activity during the late Cretaceous had later joined with the already existing ANS during late Paleocene (Figure 1). Recently, Bastia et al., (2010b) also favored that the ridge formation is due to the hot spot activity, but the source of the volcanism is unknown. According to Krishna (2003), the thick pile of Bengal fan sediments caused the compactness of the underlying material as well as basement rocks and the properties of all the rocks changed. When the

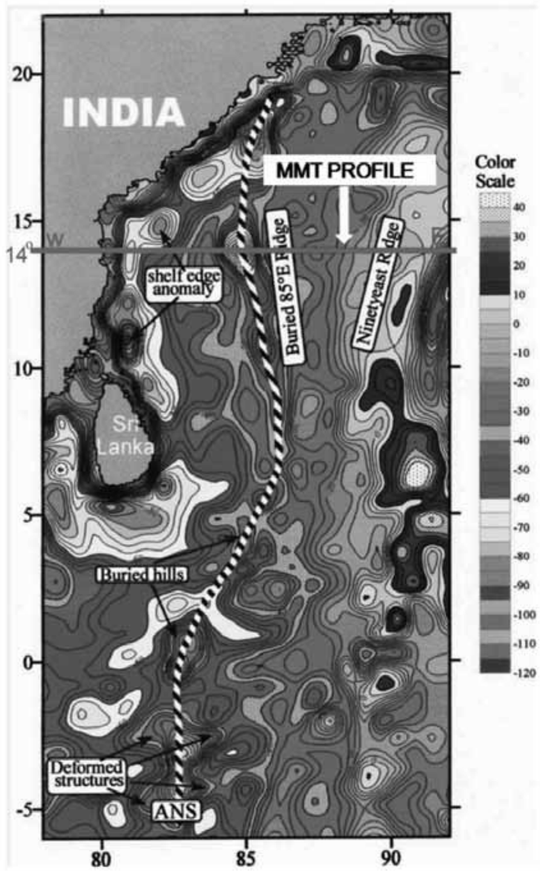

Figure 1. Marine Magnetotelluric (MMT) Profile along 14^0N latitude plotted over free-air gravity anomaly map of the northeastern Indian Ocean across the 85^0E Ridge. Curved line indicates the continuity of the 85^0E Ridge, isolated buried hills and Afanacy Nikitin Seamount (ANS) (after Krishna, 2003).

volcanic activity had taken place, the overlying sediments transformed to metasediments with more compactness than the ridge material which was at higher temperature. Here the situation is that the lower density ridge material is overlaid by higher density metasediments, showing negative free-air anomaly where as in the case of ANS absence of metasedimentary cover might be the cause for the positive free-air anomaly. He also adds that the ridge was formed in the intraplate tectonic system when the lithosphere underneath is about 35 Ma.; the formation of ANS and oceanic lithosphere taken place simultaneously and later on the ANS activated in Paleocene by the hot spot forming the 85^0E Ridge and elevated above sea level. The deformation activity like erosion and subsidence on the ANS caused the northern and southern parts to disappear and buried.

Structural features and Bathymetry in Bay of Bengal

Bay of Bengal (BOB) is the largest in size (Gopala Rao et al., 1993) and one of the largest sedimentary basins in the world which forms the northeastern part of the Indian Ocean. It lies between 22^0N - 7^0S latitudes and 80^0E - 93^0E longitudes. BOB is bordered by India and Sri Lanka in the West, Bangladesh in the North, Myanmar and Andaman Nicobar Islands in the East. The two prominent structural features in the BOB are 85^0E Ridge and 90^0E Ridge. These structural features are covered by thick pile of sediments brought by major rivers (e.g. Godavari, Mahanadi, Ganga, Brahmaputra etc.) and deposited during the pre- and post-collision of India with Asia. The continental margin is characterized by a very narrow (150-200 m) zone (Kader et al., 2013), continental shelf followed by a steep continental slope and deep abyssal plains with smooth topography (Curray et al., 1982). The thickness of the water column in the northern end of BOB is small and depth to sea bed occurs at less than 2000 meters. Bathymetry in the central BOB is relatively flat and having a water column of ~3000 meters (Figure 2). Sea floor gradient increases from north to south (Sarma et al., 2000). The bathymetry along 14^0N latitude and cutting across 85^0E Ridge is also shown in Figure 2.

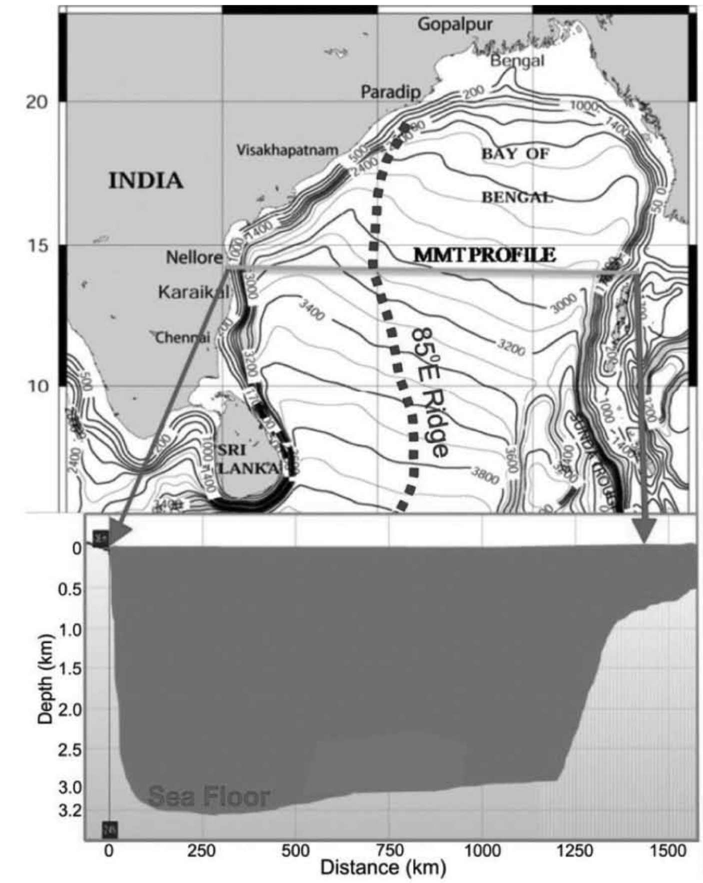

Figure 2. MMT profile across 85^0E Ridge plotted over detailed physiographic map of the Bay of Bengal using bathymetry data. Contour interval is variable up to 3000 m water depth. Bottom panel shows the variation in sea water thickness along the profile.

Earlier Geophysical Investigations

Many geophysical investigations (Bathymetric, Gravity, Magnetic, Seismic reflection etc.) were carried out to estimate the physical parameters of the 85^0E Ridge (Figure 3a-d), which are in turn useful to predict the past geodynamical history of ridge formation and tectonic evolution. From the free-air gravity anomaly map, the 85^0E Ridge appears as a strong curvilinear zone of negative gravity anomaly of about -80mgal surrounded by two small peaks of positive gravity anomalies (Figure 3b). The anomaly is discontinuous in its N-S strike, wider (120km) in the north (of 14^0 N) and narrower (40km) in the south (Choudhuri et al., 2014). Further North (15^0N to 16.5^0N) the ridge is not well pronounced. Again its signature appears from 17^0N and extends up to 19^0N. Presence of the Ridge is identified in Mahanadi basin recently by using high quality seismic reflection data (Bastia et al., 2010a). The southern part of the ridge from 11^0N to 2^0N takes maximum curvature and joins straight with ANS. The negative anomaly becomes positive from south of 5^0N to the ANS (Shreejith et al., 2011; Choudhuri et al., 2014).

The magnetic anomalies are asymmetric over the 85^0E Ridge. Alternative positive and negative magnetic streaks are distributed throughout the ridge (Figure 3a). According to Michael and Krishna (2011), the ridge was formed during the rapid changes in earth's magnetic field. During Cretaceous period, oceanic crust formed under the super long normal polarity phase. But the ridge was formed when the polarity of earth's magnetic field reversed from positive to negative. The cause for the alternative magnetic streaks could be due to the ridge topography and polarity contrast between the oceanic crust and ridge material. From the magnetic dating by Michael and Krishna (2011), the ridge formation is supported by the hotspot volcanism by using the distributed normal and reversed magnetization patterns which resembles changes in the Earth's geomagnetic field polarities related to magnetic chrons; and also that the formation of the ridge started at ~80Ma in the Mahanadi basin and finally ended in the vicinity of the ANS at ~55Ma.

On the basis of seismic reflection surveys, Michael and Krishna (2011) have identified two phases of depositional sedimentary sequences over the 85^0E Ridge, i.e., pre-

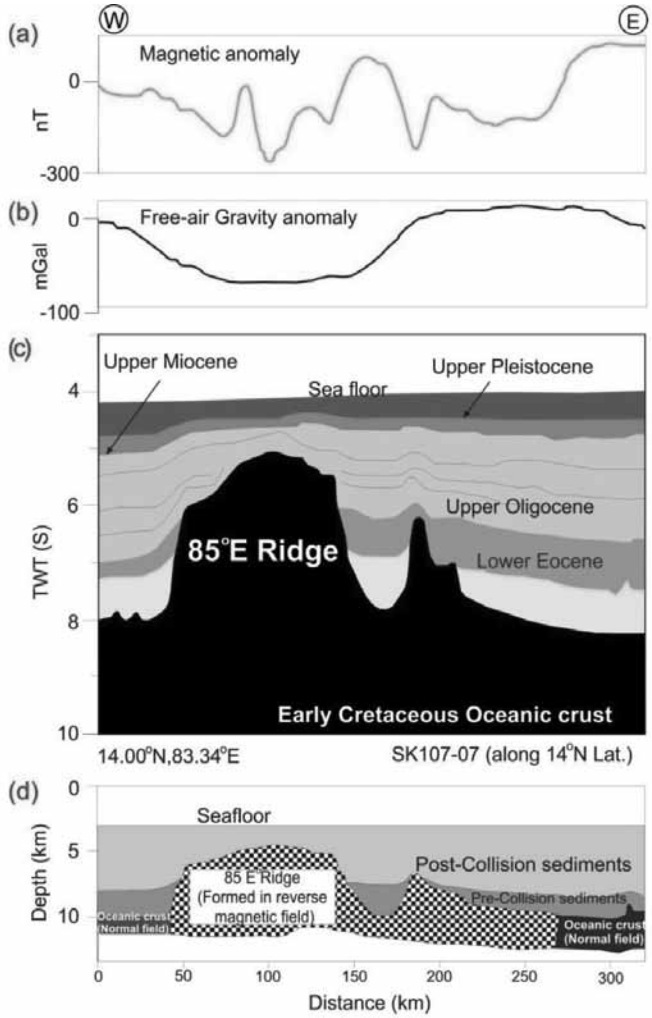

Figure 3. (a) Magnetic anomaly, (b) Free-air gravity anomaly, (c) Interpreted Seismic reflection data along 14^0N Latitude running from Eastern margin of India to Andaman Islands and (d) Crustal section derived from magnetic data (after Michael and Krishna, 2011).

collision and post-collision between India and Asia (Figure 3c,d). During the pre-collision time (end of Cretaceous) the Mahanadi and Godavari rivers deposited the sediments over the ridge. And here the lower Eocene boundary makes the margin between these two. There after collision had taken place and the sediments deposited are from the Ganga and Brahmaputra rivers. The thickness of the sedimentary column decreases from north to south. They recorded the two-way travel time (TWT) of sediments at different latitudes along 15.5^0N, 14.64^0N, 14^0N, 13^0N as 2.4s, 2.8s, 0.8s, 1.7s respectively. The pre-collision metasediments have attained higher velocities and densities due to the greater depth and age than the post-collision sediments. According to Shreejith et al., (2011), the negative free-air gravity anomaly observed over the 85^0E Ridge could be explained by the combination of (i) flexure at the Moho boundary, (ii) high density metasedimentary rocks on either side of the ridge and (iii) thick pile of low density Bengal fan sediments over the ridge.

Origin and evolution of the 85^0E Ridge has been evaluated by different authors on the basis of geophysical and tectonic signatures. Ramana et al., (1997) have proposed two concepts for the evolution of the ridge. They are: i) due to the stretching and compressional forces acted on the lithosphere during the major plate reorganization at the time of K-T superchron, which might have led to shearing of lithosphere, and/or ii) due to horizontal compressional forces acting on the passive continental margin leading to the sagging followed by deformation produced by the buckling instability of the oceanic plate. Krishna (2003) believes that the ridge was formed in the intra-plate setting due to the hotspot activity. Based on the ridge magnetic pattern and the geomagnetic polarity time scale, Michael and Krishna (2011) opined that the

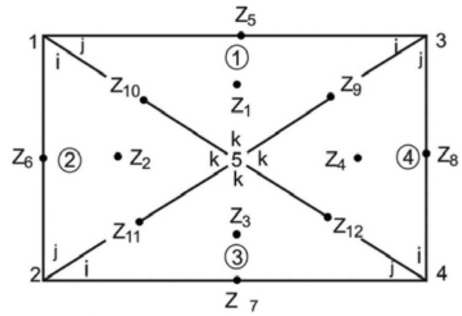

Figure 4. Triangular and rectangular elements, their ordering conventions and evaluation points (after Wannamaker et al., 1987) used for finite element modeling. Z1-Z4 correspond to depths to the centroid of each triangle, Z5 - Z12 represents depth to the boundary midpoint, Nos. 1 – 4 are triangular elements and i, j, k triangular element nodal labels.

ridge was formed in the Mahanadi basin at ~80 Ma by the short lived hotspot activity and continued southwards and ended in the vicinity of the ANS at ~55 Ma. Recently Choudhuri et al., (2014) proposed that the Indian plate moved over the hotspot and the material from mantle rose up to the sea surface and caused the bulge in lithosphere. The eruptions initially took place on the continent and moved to proto oceanic crust and finally to oceanic crust. This causes the development of depocentres which favors the sediment deposition. As the plate motion continues towards north, the volcanic foci moved further south and younger volcanic foci formed in its trail. The negative gravity anomaly observed over the 85^0E ridge, has been attributed to continental origin as in case of Laxmi Ridge in the Arabian Sea (Shreejith et al., 2011). But they also mentioned that there are many limitations in explaining the other aspects like NW-SE oriented oceanic fracture zones delineated in the western basin, which obliquely cut the 85^0E ridge.

The diversity of concepts put forth from earlier studies can be resolved by integrating with MMT data which gives the resistivity variation in the vicinity of the ridge. Prior to taking up highly expensive data acquisition in the marine environment, MMT forward modeling has been initiated over the ridge in the present study to determine the resolvability of different ridge parameters. The modeling is carried out using the finite element solution (Wannamaker et al., 1987) which has some advantages over the usual softwares currently in use.

Two dimensional modeling

Wannamaker et al., (1987) program is a stable finite element algorithm for 2-D Magnetotelluric modeling which solves directly for secondary variations in electrical and magnetic fields. In general, while computing for total fields, the finite element programs produce erroneous numerical results at low frequencies. However, this inaccuracy is more severe for transverse magnetic results (TM) as compared to Transverse electric (TE). The present program overcomes such a difficulty with numerical accuracy at lower frequencies as it computes the secondary field variations. The equations are solved using the approximation that there is no change in the primary field within each triangular area (depths Z1 - Z4), as shown in Figure 4. Once again, the primary field has been considered as constant along the boundary of each triangular element and is calculated at mid-points of the boundary (depths Z5 – Z12) as shown in Figure 4.

Mesh Design

In the present study, a finite element mesh has been utilized to calculate the secondary field variations (Coggon, 1971) at low frequencies as it gives better values as compared to total field (Wannamaker et al., 1987). The mesh design is comprised of rectangular elements, with constant column width and row heights in a given rectangular cell (Figure 4). Again the rectangular element is divided into four triangular elements within each of which the impedivity and admittivity are constant. Such a construction through triangular elements, allows us to consider the sloping boundaries, like continental shelf, in the simulating model. The unknown secondary fields parallel to strike are calculated by piecewise linear functions defined over each triangular sub region. The field is specified using three linear shape functions whose amplitudes are unity at one node and zero at other two nodes. The primary field is constant within each triangular element and it is evaluated at the centroid of each triangular area. The evaluations of triangular cells are in anti-clock wise direction in which Z1 is the first and Z4 is the fourth triangular cell.

In general, Dirichlet's boundary conditions are applied at all mesh boundaries for solving the magnetotelluric problems. By convention, on the left hand side earth layering has been considered as the host layering for the remaining anomalous conductivity medium. Zero boundary conditions have been applied for the left side as its edges are located at large distances from the anomalous zone. In

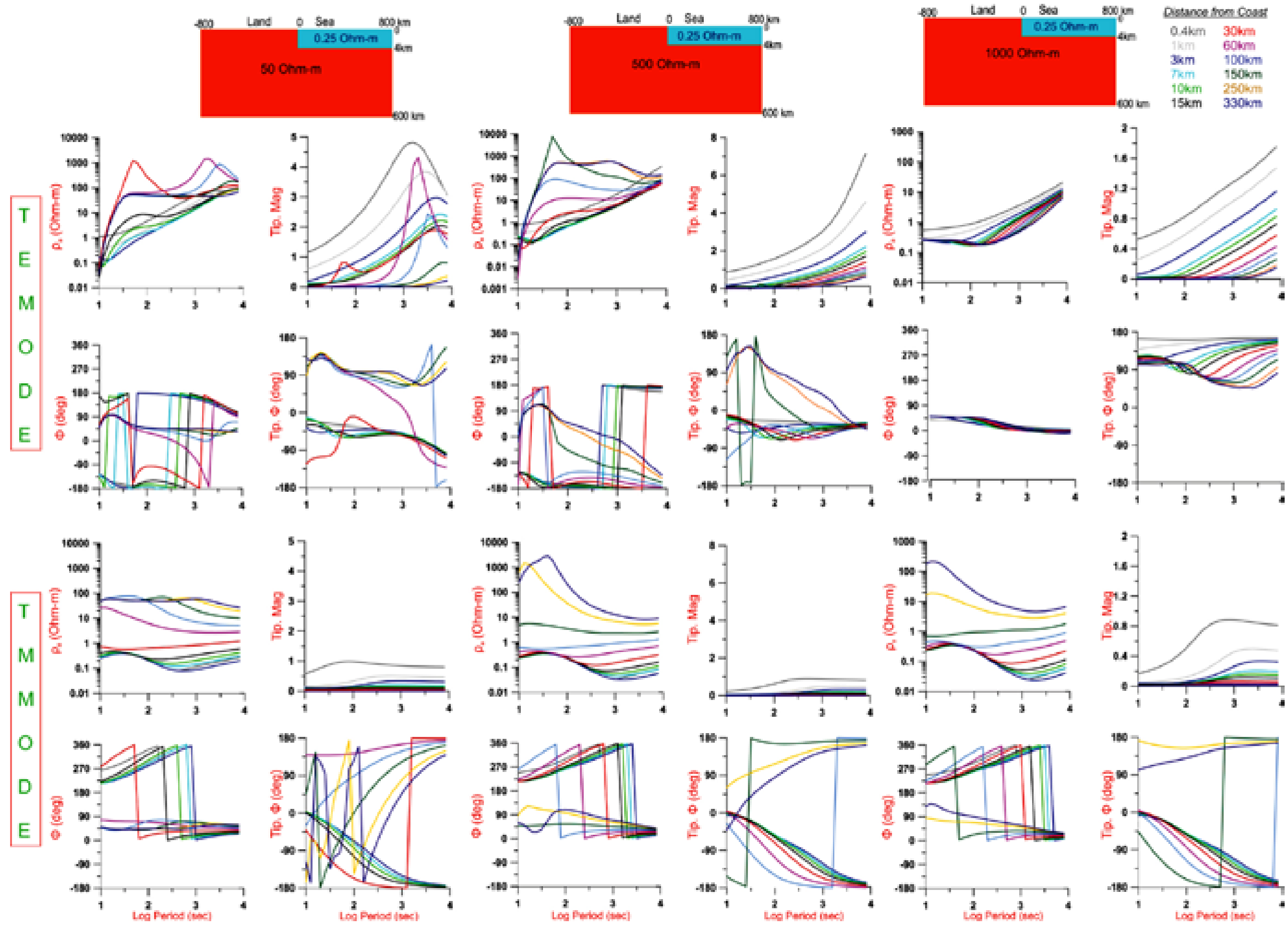

Figure 5. Synthetic modeling of the MMT response which includes only two bodies, i.e., sea water and single host with different resistivities to calculate the extent to which the MMT data is affected by coast. Coast effect is observed in the period range of 10-4000 sec and the extent of the data distortion limited up to 200 km. As the distance and period increases coast effect decreases in TE mode, where as in TM mode coast effect is increasing at longer periods and decreasing with increase in distance.

case, the right layering differs from the left layering, then conductivity inhomogeneity layering can be considered to extend indefinitely towards right hand side to infinite distance. Therefore, non-zero boundary conditions apply at right side at infinite distance. This program has been used to accommodate the inclined boundaries like continental slope and bathymetry in the BOB to simulate MMT response (like Ex, Ey, Hx, Hy, Rho-a, Phase etc.). The results, when plotted along the profile for various MMT parameters, show the ridge resolvability under thick pile of sediments.

SUMMARY AND DISCUSSION OF RESULTS

Variation in MMT response due to Coast effect

The MT data acquired on the land side will be affected by the marine environment in TE and TM mode responses (Veeraswamy, 1993; Singh et al., 1995; Rodriguez et al., 2001; Malleswari and Veeraswamy, 2014) due to large conductivity contrast between the ocean (0.25 Ohm-m) and continent (1000 Ohm-m). For 2-D model this coast effect is considerable for marine Magnetotelluric data (Key and Constable, 2011) and geo magnetic response derived from the induced currents flowing parallel to the coast. The maximum distortion in amplitude and phase response in general occurs at a definite range of period at a specific distance from the coast. Based on the model considered, it is possible to identify the characteristic period and distance with the host resistivity and the ocean depth. The coast effect does not mask the subsurface conductivity anomalies but it is sensitive to the sea floor. When the sloping coast is considered, the distortion in data may shift according to the volume of water displaced. The characteristic period is defined as the product of host resistivity and square of ocean depth where as characteristic distance is the product of host resistivity and ocean depth (Worzewski et al., 2012). Electrical conductivity structures in the offshore region

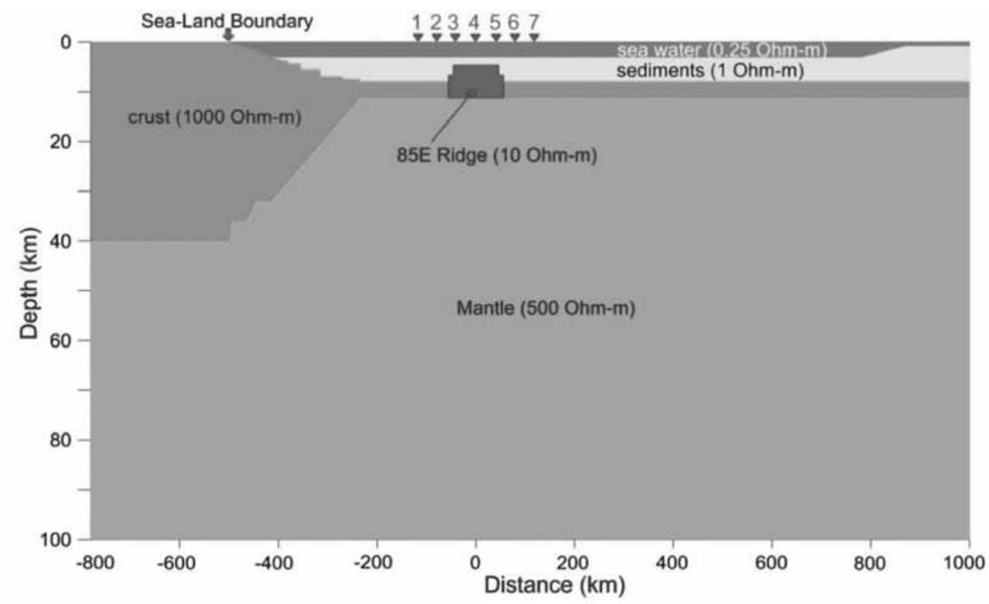

Figure 6. Two dimensional model utilized to compute MMT response across the 85^0E Ridge embedded in thick pile of sediments under ocean environment with corresponding resistivities.

were earlier delineated by using magneto variational (Arora et al., 2003; Baba, 2005) and magnetotelluric (Constable et al., 1998; Key and Constable, 2002, 2011; Baba and Chave, 2005; Kapinos and Brasse, 2009; Baba et al., 2010) investigations.

In the present study, the resolution analysis has been carried out for the coast effect with the half space and vertical water column with uniform thickness. The considered initial model (Figure 5 & 6) extends to 800 km on either side of the coastline and down to 600 km depth with sea water thickness as 4 km. Near the coastline the grid width is as small as 25 m in the offshore region and it increases to 1.3 times for the subsequent grids. Three different land resistivities (50 Ohm-m, 500 Ohm-m and 1000 Ohm-m) have been considered to estimate the effect of coast on MMT measurements. In all models the resistivity and thickness of sea water are taken as 0.25 Ohm-m and 4 km respectively. Figure 5 shows the variation in different MMT responses with period. Various curves correspond to response at different distances from the coast for both TE and TM modes. As shown in Figure 5, the MMT response is affected more by the coast for the models with host resistivities 50 Ohm-m and 500 Ohm-m as compared to 1000 Ohm-m. Key and Constable (2011) earlier did similar modeling while interpreting the data collected in the offshore of northeastern Japan. They observed single narrow positive peak in TE mode apparent resistivity at 100 sec period when the site is located at more than 100 km from the coast. In the present numerical study also a single narrow positive peak is seen for the same distance and period mentioned. However, this peak is migrated to 1000 sec when the site is moved to 200 km. The coast effect produces maximum variation in apparent resistivities for TE mode when the site is located between 30 km and 60 km, while for TM mode such variation is not evident. A fluctuation in apparent resistivity can be noticed when the land resistivity is 50 Ohm-m and an increasing apparent resistivity with period can be seen when the land resistivity is 1000 Ohm-m. The apparent resistivity is distorted when the station is located at less than 100 km from the coast, afterwards the effect is reduced and Tipper attains maximum between 300 and 3000 sec while Phase gets distorted when the station is located at <100 km. Tipper phase is positive when the station is at >100 km and it is negative when station is at <60 km. Phases show large negative response at maximum coast effect i.e. at <100 km. Tipper component is decreasing towards the ocean but there is a high magnitude at longer periods from 100 sec to 10000 sec and the distances from 30 km to 100 km from coast. From this analysis, it can be concluded that the MMT measurements shall be distorted when the site is located at less than 200 km from the coast and thereafter the coast effect is negligible.

Variation in MMT response across 85^0E Ridge

The two dimensional model used to compute the MMT response, should consider the environment of the ridge which includes sediments, water column, crust (land and marine) and mantle with the respective resistivities and thicknesses. Variations in crustal thickness are also considered all along the profile (i.e. on land and offshore). The numerical model considered here, starts from land and passes through continental shelf, continental slope,

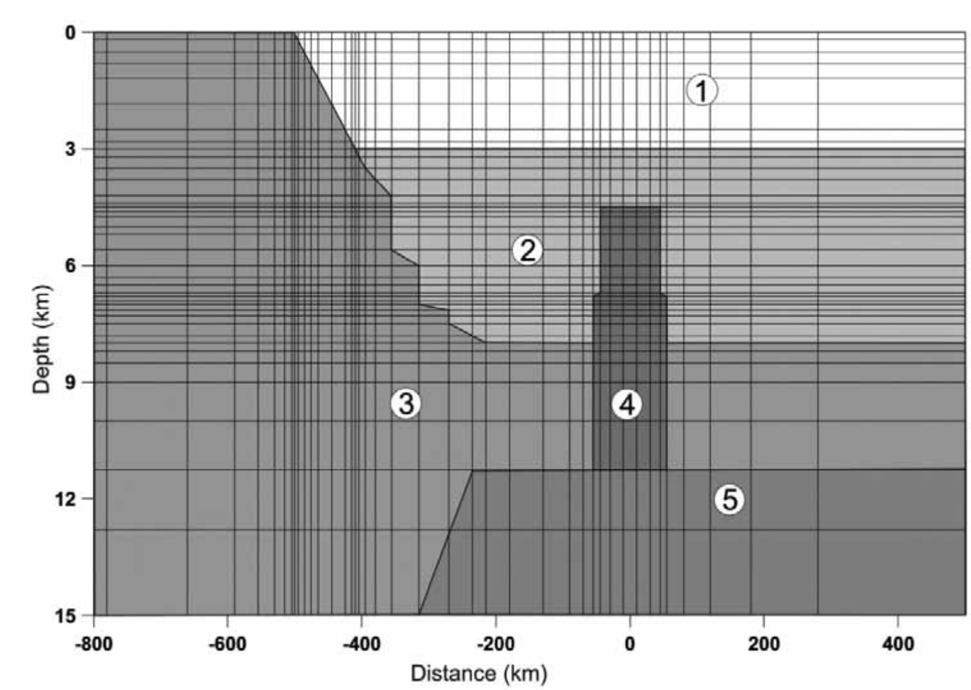

Figure 7. A section of the mesh used to generate marine MT data. The mesh geometry utilized here allows triangular sub-elements which tolerates elements with large aspect ratios. Nos. 1, 2, 3, 4, 5 represents Sea, Marine Sediments, Crust, Ridge and Mantle respectively.

Table 1. Resistivity and thickness parameters used for different formations in 2-D modeling during simulation.

Formation	Resistivity (Ohm-m)	Thickness (km)	Remarks/Reference
Sea water	0.25	0 – 3.0	As per bathymetry
Sediments	1	5.0	Constable (1990)
Ridge (variable)	10, 100, 1000	6.5	To accommodate both conductive and resistive ridge material
Crust	1000	11.5 - 40	Joseph et al., (2000) Matsuno et al., (2010)
Mantle	500	- - -	Baba et al., (2010)

continental rise and finally ends after 85^{0}E Ridge (Figure 6). The resistivities and thicknesses considered for different zones of the model are given in Table-1. As shown in Figure 6 the water column thickness varies towards ocean side. The numerical model was developed using the information across the 85^{0}E Ridge i.e., width and thickness of the ridge, pre- and post-collision sediments, crustal thickness etc. (Michael and Krishna, 2011) and passing through 14^{0}N latitude.

Numerical forward modeling has been carried out for 2D model (Figure 6) of the coastline and seafloor along the profile in order to study the nature of the distortion in the MT responses. Sea floor topography along a 1000 km long profile was discretized into different cells with variable widths of 5 to 20 km in the anomalous region (Figure 7). The entire model mesh was considered for more than 5000 km wide to make sure distortions from the sea floor topography in the central portion did not corrupt the 1D boundary conditions assumed along the sides of the model. The model has been divided into six regions viz. air, ocean, marine sediments, crust, ridge and mantle (or underlying half space) and the corresponding grid used for numerical modeling is shown in Figure 7.

Figure 8 shows the apparent resistivity and phase responses along the MMT profile for both TE and TM modes showing the coast effect and ridge effect at different periods. The coast effect is clearly visible when the sites are located in the continental shelf region. The TE mode parameters are more sensitive to larger distances as compared to TM mode. The distortion in TE and TM modes is maximum when the sites are located at <200 km from the vertical coast. This effect is defined here as

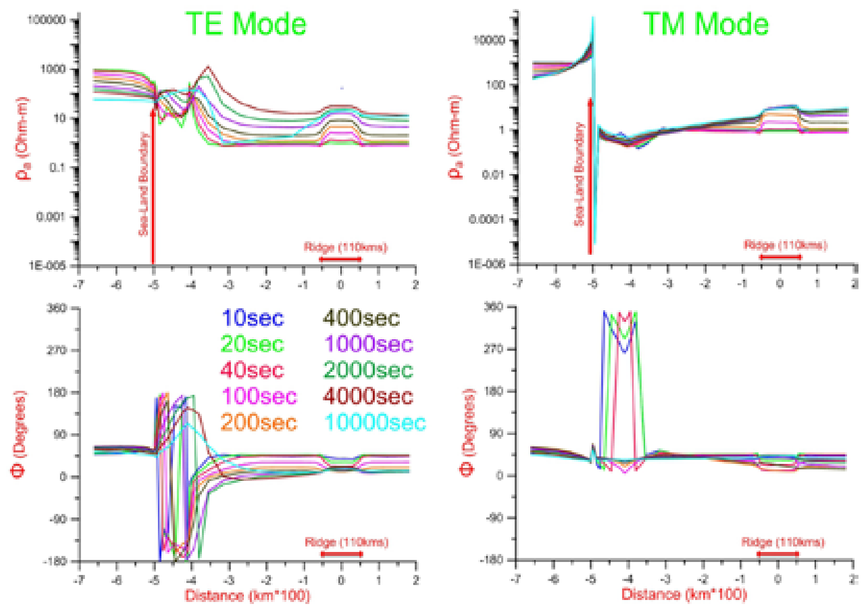

Figure 8. Apparent resistivity and phase variations along the MMT profile for both TE and TM mode showing the coast effect and the ridge effect at different period bands. TE mode data is strongly affected by the coast. The coast effect is limited to 200 km from the coastline. It is evident from this figure that the coast effect is negligible in the region of 85^{0}E Ridge.

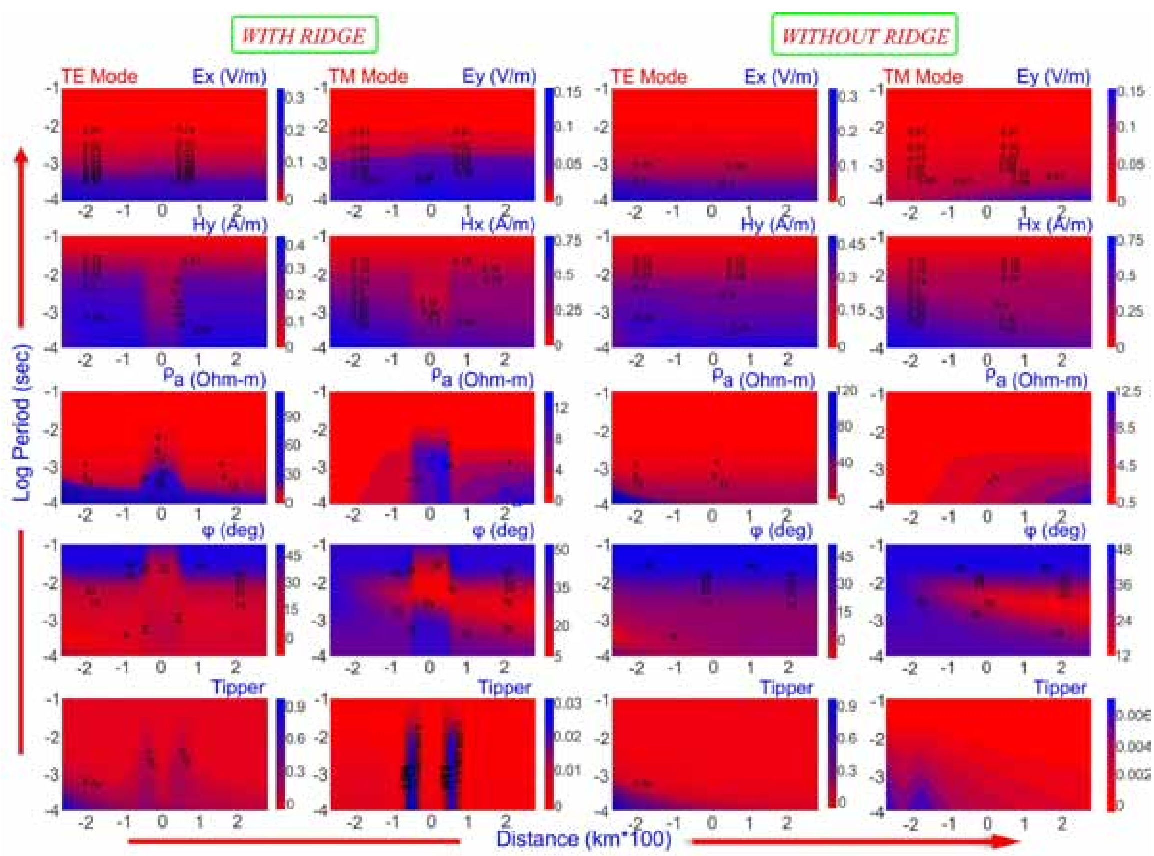

Figure 9. MMT parameters of TE and TM mode showing the variation in response due to the ridge. For the sake of comparison, response without ridge is also shown. Parameters like Horizontal magnetic field components (Hx, Hy), apparent resistivity (ρ_a), phase (ϕ) and Tipper showing the clear response when the ridge is present where as Horizontal electrical field components (Ex, Ey) are less affected in both TE and TM modes. Vertical resolution of the ridge is well pronounced in TM mode parameters as compared to TE mode.

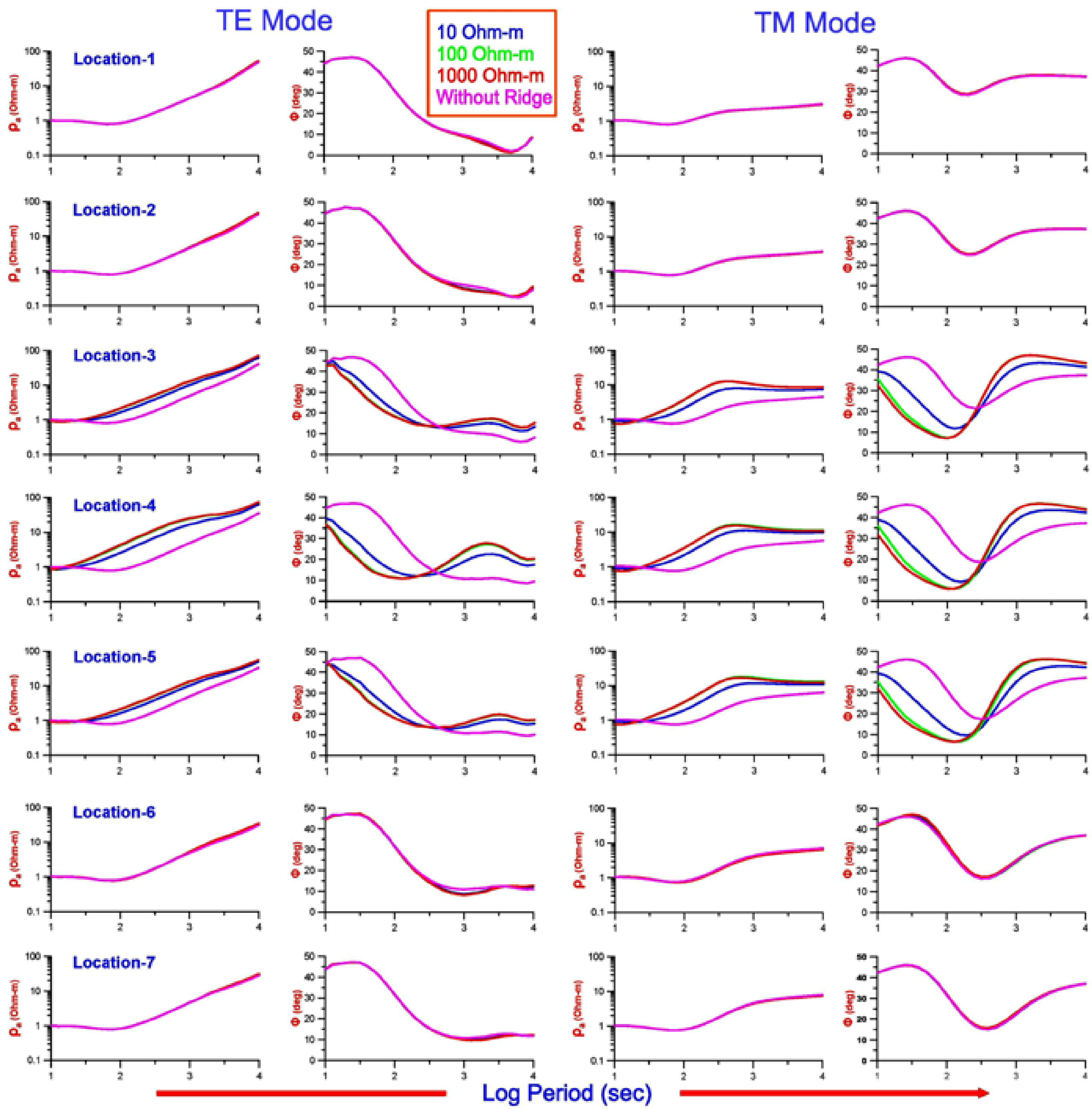

Figure 10. MMT response (apparent resistivity and phase) at different locations across the ridge with different ridge resistivities. The ridge effect is clearly seen in phase response of the TM mode as compared to TE mode. As the resistivity of the ridge increases the variation in apparent resistivity and phase response attains maximum towards centre of the ridge.

the maximum coast effect and extending up to 200 km. As the ridge is lying at 500 km from the coast, there is no coast effect on the ridge. In the same figure the ridge is well resolved in the period band of 40-4000 sec.

The data recording duration is another important factor that needs to be analyzed. Generally LF3 band has to be chosen to acquire data, wherein the sampling interval is 0.5 sec. So, after 4096 sec there are 8192 samples. During the processing the LF3 data has to be filtered with 32x filter to transform the data in to LF4 band (Friedrichs, 2007). Then one will have 256 samples with 16 sec sampling rate which is not enough for Fast Fourier Transform (FFT) computations. As a prerequisite, for a standard FFT with 4096 points, it is necessary to have 16 times of that data. Therefore, 18.2 hours (16 * 4096) recording time is essential to get one stack of 4096 sec. Hence, it is necessary to acquire data for a period of 8 days to get 10 stacks which is the minimum requirement in relatively less noisy areas. On the basis of the present numerical study, it can be surmised that the MMT surveys carried out for Hydrocarbon exploration within the EEZ (0-370 km away from the coast), it is necessary to consider the effect of coast up to 200 km from the sea-land boundary.

In order to view the two dimensional response of the ridge, the MMT parameters are plotted as pseudo sections and are shown in Figure 9. For the sake of comparison models with and without ridge are plotted. The model with ridge shows the ridge response in an excellent way; where as the model without ridge is clear from the response of the ridge. In each model, transverse electric and transverse magnetic modes are shown to estimate the parameters to what extent they are responding to the ridge presence. Parameters like Horizontal magnetic field components (Hx, Hy), apparent resistivity (ρa), phase (ϕ) and Tipper showing the clear variation in the response when the ridge is present, where as Horizontal electrical field components (Ex, Ey) are less distorted in both TE and TM modes. Vertical resolution of the ridge is well pronounced in TM mode parameters as compared to TE mode. Vertical flanks of the ridge are well resolved in the TM mode tipper response.

The MMT response at different stations across the ridge is shown in Figure 10. Results are plotted for seven stations with a station spacing of 35 km, out of which three of them are lying directly above the ridge and remaining four placed on either side of the ridge. Variation in apparent resistivity against period is plotted with four curves in which three curves are representing the ridge resistivity of 10 Ohm-m, 100 Ohm-m and 1000 Ohm-m and another curve is without ridge. The three resistivity values considered here are representative of ridge material when it is made up of mantle (or) oceanic crustal (or) continental crustal material. On the basis of numerical simulation, it can be surmised that the ridge response is prominent in the TM mode phase as compared to TE mode phase. As the resistivity of the ridge increases the variation in apparent resistivity and phase response rises towards center of the ridge.

CONCLUSIONS

Marine Magnetotelluric measurements are relatively more expensive and it is advisable to estimate through modeling, the resolvability of different parameters of tectonic features like ridges before conducting the field measurements. Keeping this in view, the MMT response at different locations across the 85^0E Ridge has been generated by numerical simulation. Interestingly, the computed results reveal that (i) the coast effect on MMT measurements can be seen in the entire continental shelf and continental slope regions, (ii) the coast effect is negligible on the MMT measurements made over the 85^0E Ridge as it is located at ~500 km east of coast line in the Bay of Bengal, (iii) the 85^0E Ridge is more visible in TM mode response as compared to TE mode in the period range of 40-4000 sec, (iv) horizontal magnetic field components (Hx, Hy) are more sensitive as compared to electric field components (Ex, Ey), and (v) MMT data needs to be acquired for a period of at least 8 days to get more than 10 stacks of 4096 sec.

ACKNOWLEDGEMENTS

The authors are thankful to Dr.V.M. Tiwari, Director, CSIR-National Geophysical Research Institute, Hyderabad for kind permission to publish this study. We thank Prof.P. E. Wannamaker for sparing the modeling algorithm. Though this study/activity is initiated under GEOSCAPE project, major part of it has been done under INDEX project supported by CSIR, New Delhi. We are thankful to Dr. Nandini Nagarajan and Dr. M.R.K. Prabhakar Rao for useful suggestions and apt reviewing to enhance the quality of the manuscript. We thank Prof.B.V.S.Murty for editing the manuscript. We thank Chief Editor for his support and encouragement.

Compliance with Ethical Standards

The authors declare that they have no conflict of interest and adhere to copyright norms.

REFERENCES

Arora, B.R., Subba Rao, P.B.V., and Nagar, V., 2003. Electrical conductivity signatures of Plume Lithosphere Interactions in the Indian Ocean, Memoir Geological Society of India, v.53, pp: 393-418.

Baba, K., 2005. Electrical Structure in Marine Tectonic Settings, Surveys in Geophysics, v.26, pp: 701-731.

Baba, K., and Chave, A.D., 2005. Correction of seafloor Magnetotelluric data for topographic effects during inversion, Journal of Geophysical Research, B12105, doi:10.1029/2004JB003463., v.110.

Baba, K., Utada, H., Goto, T.N., Kasaya, T., Shimizu, H., and Tada, N., 2010. Electrical conductivity imaging of the Philippine Sea upper mantle using seafloor Magnetotelluric data, Physics of the Earth and the Planetary Sciences, v.183, pp: 44-62.

Bastia, R., Radhakrishna, M., Das, S., Kale, A.S., and Catuneanu, O., 2010a. Delineation of the 85^0E ridge and its structure in the Mahanadi Offshore Basin, Eastern Continental Margin of India (ECMI), from seismic reflection imaging, Marine and Petroleum Geology, v.27, pp: 1841-1848.

Bastia, R., Radhakrishna, M., Srinivas, T., Nayak, S., Nathaniel, D.M., and Biswal, T.K., 2010b. Structural and tectonic interpretation of geophysical data along the Eastern Continental Margin of India with special reference to the deep water petroliferous basins, Journal of Asian Earth Sciences, v.39, pp: 608-619.

Choudhuri, M., Nemeok, M., Stuart, C., Welker, C., Sinha, S.T., and Bird, D., 2014. 85°E Ridge, India – Constraints on its Development and Architecture, Journal Geological Society of India, v.84, pp: 513-530.

Coggon, J.H., 1971. Electromagnetic and electrical modeling by the finite element method, Geophysics, v.36, pp: 132-155.

Constable, S.C., 1990. Marine electromagnetic induction studies. Surveys in Geophysics, v.11, pp: 303-327.

Constable, S.C., Orange, A.S., Hoversten, G.M., and Morrison, H.F., 1998. Marine magnetotellurics for petroleum exploration Part I: A sea-floor equipment system, Geophysics, v.63, pp: 816–825.

Constable, S., Key, K., and Lewis, L., 2009. Mapping offshore sedimentary structure using electromagnetic methods and terrain effects in Marine Magnetotelluric data, Geophysical Journal International, v.176, pp: 431–442.

Curray, J.R., Emmel, F.J., Moore, D.G., and Russel, W.R., 1982. Structure, tectonics, and geological history of the northeastern Indian Ocean; In: The Ocean Basins and Margins, The Indian Ocean (eds) Nairn A E and Stehli F G (New York: Plenum), v.6, pp: 399–450.

Curray, J.R., and Munasinghe, T., 1991. Origin of the Rajmahal Traps and the 85°E Ridge: Preliminary reconstructions of the trace of the Crozet hotspot, Geology, v.19, pp: 1237-1240.

Duncan, R.A., and Richards, M.A., 1991. Hot spots, mantle plumes, flood basalts, and true polar wander, Rev. Geophysics, v.29, pp: 31–50.

Friedrichs, B., 2007. MAPROS Software Manual. Metronix, Germany, pp: 126.

Gopala Rao, G.C., Bhattacharya, M.V., Ramana, V., Subrahmanyam, T., Ramprasad, K.S., Krishna, A.K., Chaubey, G.P.S., Murty, K., Srinivas, D.M., Reddy, S.I., Ashalata, B., Subrahmanyam, C., Mital, G.S., Drolia, R.K., Rai, S.N., Ghosh, S.K., Singh, R.N., and Majumdar, R., 1993. Analysis of Multi-Channel and Magnetic Data Along Seismic Reflection 13^0 N Latitude Across the Bay of Bengal, Marine Geophysical Researches, v.16, pp: 225-236.

Gopala Rao, D., Krishna, K.S., and Sar, D., 1997. Crustal evolution and sedimentation history of the Bay of Bengal since the Cretaceous, J. Geophys. Res., v.102, pp: 17747-17768.

Harinarayana, T., 2008. Marine Magnetotelluric and Marine Seismic study in Gulf of Kutch region, Gujarat, India, Project Report Submitted to DGH, New Delhi., pp: 97.

Heinson, G., White, A., and Lilley, F.E.M., 2005. Rifting of a passive margin and development of a lower-crustal detachment zone: Evidence from Marine Magnetotellurics, Geophysical Research Letters, DOI: 10.1029/2005GL022934., v.32.

Kader, A., Chowdhury, Z.R., Uddin, M.M., Hoque, E., and Basak, S.C., 2013. Bathymetric study of the Bay of Bengal based on open source satellite and sounding data, International Journal of Geomatics and Geosciences, v.4, pp: 116-124.

Kapinos, G., and Brasse, H., 2009. Some notes on bathymetric effects in marine Magnetotellurics, motivated by an amphibious experiment at the South Chilean margin, Freie Universit¨at Berlin, Fachrichtung Geophysik, Malteserstr-12249., pp: 74-100.

Kasaya, T., Goto, T.N., Mikada, H., Baba, K., Suyehiro, K., and Utada, H., 2005. Resistivity image of the Philippine Sea Plate around the 1944 Tonankai earthquake zone deduced by Marine and Land MT surveys, Earth Planets Space, v.57, pp: 209–213.

Key, K., and Constable, S., 2002. Broadband marine MT exploration of the East Pacific Rise at $9^0$50'N. Geophysical Research letters, doi:10.1029/2002GL016035., v.29.

Key, K., and Constable, S., 2011. Coast effect distortion of marine Magnetotelluric data: insights from a pilot study offshore northeastern Japan, Physics of the Earth and the Planetary Interiors, v.184, pp: 194-207.

Krishna, K.S., 2003. Structure and evolution of the Afanasy Nikitin seamount, buried hills and 85^0E ridge in the northeastern Indian ocean, Earth and Planetary Science Lett., v.209, pp: 379-394.

Krishna, K.S., Bull, J.M., Ishizuka, O., Scrutton, R.A., Jaisankar, S., and Banakar, V.K., 2014. Growth of the Afanasy Nikitin Seamount and its relationship with the 85^0E Ridge, northeastern Indian Ocean, J. Earth Sys. Sci., v.123, pp: 33-47.

Liu, C.S., Sandwell, D.T., and Curray, J.R., 1982. The Negative Gravity Field over the 85^0E Ridge, Journal of Geophysical Research, v.87, pp: 7673-7686.

Malleswari, D., and Veeraswamy, K., 2014. Numerical simulation of coast effect on magnetotelluric measurements, Acta Geod Geophy., v.49, pp: 17-35.

Matsuno, T., Seama, N., Evans, R.L., Chave, A.D., Baba, K., White, A., Goto, T., Heinson, G., and Boren, G., 2010. Upper mantle electrical resistivity structure beneath the central Mariana subduction system. Geochemistry Geophysics Geosystems, doi:10.1029/2010GC003101., v.11.

Michael, L., and Krishna, K.S., 2011. Dating of the 85^0E Ridge (northeastern Indian Ocean) using marine magnetic anomalies, Current Science, v.100, pp: 1314-1322.

Muller, R.D., Royer, J.Y., and Lawver, L.A., 1993. Revised plate motions relative to the hotspots from combined Atlantic and Indian Ocean hotspot tracks, Geology, v.21, pp: 275-278.

Joseph, E.J., Toh, H., Fujimoto, H., Iyengar, R.V., Singh, B.P., Utada, H., and Segawa, J., 2000. Seafloor electromagnetic induction studies in the Bay of Bengal, Marine Geophysical Researches, v.21, pp: 1-21.

Ramana, M.V., Subrahmanyam, M., Chaubey, A.K., Ramprasad, T., Sarma, V.L.N.S., Krishna, K.S., Desa, M. and Murthy, G.P.S., 1997. Structure and Origin of the 85^{0}E Ridge, Jour. of Geophysical Research, v.102, pp: 17995-18012.

Rodriguez, O.D., Fucugauchi, J.U., Arzate, J.A., and Enriquez, O.C., 2001. Coast effect in Magnetotelluric soundings over the Yucatan peninsula, Mexico, Geofisica International, v.40, pp: 31-41.

Sarma, K.V.L.N.S., Ramana, M.V., Subrahmanyam, V., Krishna, K.S., Ramprasad, T., and Desa, M., 2000. Morphological features in the Bay of Bengal, Journal of Indian Geophysical Union, v.4, pp: 185-190.

Singh, U.K., Yash Kant, and Singh, R.P., 1995. Effect of coast on Magnetotelluric measurements in India, ANNALI DI GIOFISICA, v.38, pp: 331-335.

Sreejith, K.M., Radhakrishna, M., Krishna, K.S., and Majumdar, T.J., 2011. Development of the negative gravity anomaly of the 85^{0}E Ridge, northeastern Indian Ocean - A process oriented modeling approach, Journal of Earth System Science, v.120, pp: 605–615.

Subrahmanyam, C., Thakur, N.K., Gangadhara Rao, T., Khanna, R., Ramana, M.V., and Subrahmanyam, V., 1999. Tectonics of the Bay of Bengal: New insights from satellite gravity and ship-borne geophysical data, Earth Planet.Sci. Lett., v.171, pp: 237-251.

Veeraswamy, K., 1993. Quantitative demarcation of coast-effect over Saurashtra peninsula, Proceedings of IGU seminar on Perspectives and Prospects in Geosciences towards the New Industrial policy, pp: 130-140.

Wannamaker, P.E., John, A.S., and Rijo, L., 1987. A stable finite element solution for two-dimensional magnetotelluric modeling, Geophys.J.R.astr.Soc., v.88, pp: 277-296.

Worzewski, T.W.D., Jegen, M., and Swidinsky, A., 2012. Approximations for the 2-D coast effect on marine magnetotelluric data, Geophy. J. Int., v.189, pp: 357-368.

A Map of Earth`s Viscous Crust-- Recent Scientific Achievement

On long scales of length and time, Earth`s crust and upper mantle flow like stiff liquid. To understand how the rocks deform under geologic stresses, one needs to know their viscosity—a property that depends on the rock temperature, strain rate and composition. Among those features variations in composition, specifically trace amounts of water and magma, are the most difficult to determine but exert a strong influence on the rock`s behaviour (Marc Hirschmann and David Kohistedt, Physics Today, March, 2012, page 40). The hotter, wetter, or more molten a rock the weaker it is. Fortuitously, the same factors that weaken a rock and lower its viscosity also make it more electrically conductive. Since the last 6 decades, researchers have been able to infer resistivity profiles as a function of depth in crustal and mantle rocks from variations in magnetic and electric fields measured Earth`s surface using magnetotelluric (MT) imaging. Recently an US and an Australian scientist jointly have derived an empirical conversion factor to determine viscosity variations from two-dimensional variations in electrical resistivity obtained from an MT survey across the western US. The researchers calibrated the magnitudes of the viscosity variations with geodynamic flow models to produce a viscosity map. The map predicts the region`s rough surface topography, crustal deformation and mantle upwelling more accurately than do standard geological models. The upwelling identifies spots of potential earthquakes or volcanism. (**Citation**: L.Liu, D.Hasterok, Science 353, 1515, 2016).

J. Ind. Geophys. Union (March 2017)
v.21, no.2, pp: 96-104

Inversion of well log data using improved shale model for determination of petrophysical parameters

Ajay Malkoti*[1], Nimisha Vedanti[1] and A.K. Bhattacharya[2]

[1]Academy of Scientific and Innovative Research, CSIR-NGRI, India-500007

[2] Indian Institute of Technology, Kharagpur, West Bengal, India-721302

*Corresponding Author: ajmalkoti@gmail.com

ABSTRACT

Estimation of petrophysical parameters from well logs is an important procedure in reservoir characterization. Here we present a method, based upon improved estimates of average mineralogical composition of shale, to estimate the petrophysical parameters from the well log data of a sandstone reservoir. The shale response is dependent of its distributional characteristics which is difficult to model. Shale response has a large influence on the inversion algorithm, which affects the parameter estimation. Thus to mitigate its effect in forward modelling we used the improved estimates of an average shale-mineralogical-composition model (SMCM). A genetic algorithm (GA) based inversion was carried out for correct estimation of petrophysical parameters. This improved algorithm was tested for the applicability on the synthetic data and then applied on - well log data of Ankleshwar field, cambay Basin, India. The result for synthetics exibited good match with the assumed model and worked well even in presence of large noise. In Ankleshwar reservoir, parameters estimated using this method were compared with the industry provided values and with earlier studies. It was found that our results are in good agreement with them. The average error between the ankleshwar well data and its synthetics, generated for inverted parameters, was found to be about 6.27%. Major advantages of this approach are mitigation of cumulative error, enhanced resolution and capability to generate missing logs. This algorithm has also demonstrated its capability in delineating the finer details of the formation.

Key words: Inversion, Genetic Algorithm(GA), shale-mineralogical-composition model (SMCM), Well-log data, Ankleshwar field.

INTRODUCTION

In exploration geophysics, well-log data is widely used to estimate the petrophysical parameters of the formation in the vicinity of the borehole. Some useful parameters are porosity, permeability, fluid saturation and mineral composition of the formation. Inversion methods are used to obtain estimates of these vital petrophysical parameters necessary to characterize the formation. Efficacy of an inversion scheme depends upon the choice of model used for obtaining log. Along with that, the inversion schemes (linear or some local optimization method) suffer from several drawbacks (Menke, 2012; Sen and Stoffa, 2013). Thus, accurate estimation of petrophysical parameters from the well logs requires a realistic model which can describe the log behaviour/response accurately and a robust inversion scheme.

The log response is generally computed using the weighted sum of the log responses for each mineral/ fluid present in rock, called linear model. Here weights/ parameters are assigned on the basis of fractional percentage of respective minerals/fluids. In practice, we are interested in determining depth distribution of these parameters (e.g. porosity, water and hydrocarbon saturation, shale and sand volume, etc.). It is an inverse problem which can be treated using linear inversion techniques (Menke, 2012). Many authors such as Mayer & Sibbit (1980), Alberty and Hashmy (1984), and Mezzatesta, et al., (1988) utilised the various logs such as Gamma ray log (GR), Self-potential log (SP), Neutron log (NPHI), Density log (DEN), Sonic log (DT) jointly to estimate petrophysical parameters. It is important to note that some parameters (viz. shale) may represent the volume of a mineral assemblage which may vary. For linear problem we assume that constitution of this mineral assemblage is known. Usually, the ratio of number of logs (or data) to parameters in such linear problems varies between 1 and 2 which is quite low for parameter estimation. To increase data to parameter ratio we can include more data by using other logs which are governed by non-linear relationships.

Non-linear models have a non-proportional relation between the input and output of the model. The forward model for well logs depends upon the fractional volume content of the mineral/fluid present in matrix/pore as well as on the structural or distributional (e.g. dispersed, laminar, etc.) character of the rock. For example, various models proposed in literature for resistivity logs are non-linear in nature. The resistivity log can be explained using a non-linear empirical relation given by Archie (1942). It is important to note that this model does not work for every geological scenario. For example in case of shaly-sands, resistivity log may show anomalous high values of conductivity due to high cation exchange capacity (CEC) of clay minerals (Serra, 1984). This effect is observed when the aluminium ions present over the surface of clay gets replaced by other ions such as Fe++ or Mg++. It makes aluminosilicate sheets of clay negatively charged, causing accumulation of loosely held positive charge ions near its surface. These accumulated positive ions can be easily mobilized, resulting in high conductivity. CEC depends upon the surface area or distributional characteristics of shale which makes its estimation hard for shaly formation, as shale occurs in various forms (laminar, dispersed and structural) with different surface areas. Clay minerals (Kaolinite, Illite, Montmorillonite, Vermiculite, etc.) present in shale have different CEC due to different physical and molecular structures. Various authors made attempts to address this issue and proposed different models for shaly formation (Worthington, 1985). Simandoux (1963) approximated this effect by considering total resistance of pore fluid and shale as two resistors in parallel. Different models have been proposed for laminated clay (Poupon et al., 1954) and dispersed clay (Schlumberger, 1975) to take care of clay distribution. However some resistivity models e.g. Waxman and Smith model (WSM) (1968) and Dual water model (DWM) (Clavier et al., 1977) are distribution independent. WSM assumes that the clay particles increase the conductivity of the formation while DWM assumes that only cations increase the conductivity of clay bound water. However these two models require some additional parameters e.g. WSM requires estimates of specific cation conductance and CEC whereas DWM requires resistivity and saturation values for bound and free water in the formation. Hence use of these models is not advisable as they involve extra parameters to calculate the log response. In this study we have used the Indonesian formulae (Poupon and Leveaux, 1971) to calculate the resistivity log response due to two reasons; first, it's practically proven and second, the parameters used to define the response do not add any new parameter to our set of parameters.

In the forward modelling the SMCM plays an important role. Most of the available literature on estimating SMCM is based upon argillaceous part of clay (Perrin, 1971; Ridgway 1982; Shaw, 1981; Sellwood & Sladen 1981). Hiller (2006) provided a new average SMCM for which he analysed 105 samples and estimated both, argillaceous as well as non-argillaceous component of shale. This kind of data was not available earlier. Thus using this model, the log response for the shale can be determined more precisely using appropriate inversion technique.

From the literature it is evident that several inversion techniques exist. However, a close scanning of these details from the literature, it is noticed from the linear and non-linear inversion techniques GA based Stochastic inversion is better. Our focus is on reasonable understanding of Ankleswar reservoir composition by proper use of available borehole data, as deligently as possible with faster convergence, limiting computational costs. As such we do not go into details of relative merits and limitations of various inversion methods. Bearing this in mind, we will be using the forward modelling set of equation as described in (Dobroka & Sazabo, 2011, Szucs & Civan, 1996) with improved estimates of SMCM. Non-linear nature of modelling equations limits the use of linear inversion methods and/or local optimization schemes (Gill et al., 1981; Dimri, 1992; Vedanti et al., 2005). Thus, inversion for the petrophysical parameters will be carried out using the global optimization approach. In the current study we employ the Genetic Algorithm (GA) (Holland, 1975) to estimate the petrophysical parameters. The applicability of the method is demonstrated on synthetic log data and then it is applied on well log data of Ankleshwar oilfield, situated in Cambay basin, India. The estimated petrophysical parameters form Ankleshwar logs are compared with that of provided by the Oil and Natural Gas Corporation Ltd. (ONGC) and Vadapalli et al., (2014) and the results are in good agreement.

Theory and Algorithm

In a borehole, the geologic formation consists of two main components - 1) lithological matrix, and 2) fluid(s) entrapped in this matrix. The fluid filled pores may contain water or hydrocarbon and the lithology may consists of different rocks e.g. shale, sandstone, etc. The rocks again can be treated as an assemblage of different minerals. The log response equation assumes that the logging tools respond mainly to the compositional characteristics of rock, not to their structure (Serra, 1984; Schlumberger, 1989). It means that the components present at a given depth only affect the behaviour of log at that depth. Assuming this, we can calculate the synthetic log at any depth by summing weighted individual response of tool, corresponding to each component, as:

$$L^{LOG} = \phi_e S_{xo} L_w^{LOG} + \phi_e (1 - S_{xo}) L_{hc}^{LOG} + V_{sh} L_{sh}^{LOG} + (1 - V_{sh} - \phi_e) \sum_{i=1}^{n} V_i L_i^{LOG} \quad (1)$$

Here L^{LOG} represent the log response (L) for a given log tool for a mineral/fluid at 100% saturation of the material indicated in subscript. The subscripts *'w'*, *'h'*, *'sh'*, *'i'* represents the log reading in water/mud filtrate, hydrocarbon, shale and i[th] mineral/fluid in matrix respectively. Parameters act as weight here represented by f_e, effective porosity; S_W and S_{XO}, saturation in un-invaded zone and flushed zone respectively and V_i the volume of i[th] mineral/fluid. Eq (1) can be used to determine the response of many logs e.g. GR, SP, Neutron, Density, etc. GR log response can be written as:

$$L^{GR} = \phi [L_w^{GR} S_{xo} + L_{hc}^{GR} (1 - S_{xo})] + V_{sh} L_{sh}^{GR} + \sum_{i=1}^{n} V_i L_i^{GR} \quad (2)$$

Table 1. The table above shows the average composition of average shale.

Average Shale content	Hiller (2006)
Quartz	23.9
Feldspar	3.7 (K-spar) 2.4 (Plag.)
Carbonate	7.5 (Calcite) 1.3(Dolomite) 0.5 (Siderite)
Fe-Oxide	0.8
Clay minerals	47.7 (Di-clay) 7.5 (Tri-clay)
Other minerals	0.5 (Pyrite)
Organic matter	--

Log response equation for resistivity of flushed zone (R_{XO}) and uninvaded zone (R_W) can be written using Indonasian Equation as:

$$\frac{1}{\sqrt{R_{xo}}} = \left[\frac{V_{sh}^{1-\frac{V_{sh}}{2}}}{R_t} + \sqrt{\frac{\phi^m}{aR_{xo}}}\right]\sqrt{S_{xo}^n} \tag{3}$$

$$\frac{1}{\sqrt{R_w}} = \left[\frac{V_{sh}^{1-\frac{V_{sh}}{2}}}{R_t} + \sqrt{\frac{\phi^m}{aR_w}}\right]\sqrt{S_w^n} \tag{4}$$

Here R_t, R_W, R_{XO}, represent the true resistivity of formation, resistivity of formation water, and resistivity of flushed zone water respectively. Cementation constant, saturation exponent, and tortuosity factor are represented by 'm', 'n' and 'a' respectively.

It can be seen that logs governed by eq (1) are very much dependent on L_w, L_{hc}, L_{sh}, and L_i. The response with respect to given SMCM is very important since its contents greatly affect the linear response equations (e.g. GR and SP) while its fractional volume affects the resistivity log. In this study we have used the average SMCM model given by Hiller (2006) (Table 1). The fractional volume of all the components was estimated utilizing the XRF data, which is more accurate than earlier methods/data.

Using the improved shale model we obtain L_{sh}^{log} and thus provided improved forward log response equations (eq. 1, 3, 4). Using these equations we can obtain petrophysical parameters using GA inversion.

The non-linear nature of the log response equations insinuates us to use the global optimization technique. So in this study we have used the evolution based optimization method called Genetic Algorithm (GA) given by John Holland (1975). In this technique each solution is treated as an individual or a chromosome. We used "Binary ladder" computational notation as it simplifies the application of GA operators (viz. crossover, mutation, selection, etc.) (Goldberg, 1989). It starts by initializing a pool of individuals, called population. From the population, two individuals are selected randomly and crossover operator is applied to them. This operator makes them exchange part of their chromosome after the crossover point. Mutation operator introduces variation in these two chromosomes by changing or flipping the random bit of their chromosome. Thus obtained individuals (chromosome) are evaluated on the basis of a fitness function, which determines its chances of survival/selection for the next population set. Finally a selection process is used to determine which individual will go to next generation. Its analogue can be treated as roulette wheel where each individual of population have area proportional to its fitness and the individual having more area will have more chance of selection. However this does not guarantee that an individual with high fitness must get selected so an individual with low fitness may also remain in next population. The above process is performed over a given number of generations or till the termination criteria is met. In short we apply all above genetic operator in given sequence to create a next generation from the present generation.

The results obtained after optimization can be accessed for its quality by degree of fitness of data. For this particular problem of petrophysical parameter estimation we define the fitness function as difference between observed real well log and synthetics in least square sense.

$$f = \sqrt{\frac{1}{N}\sum_i^N \left[\frac{d_i^{obs} - d_i^{syn}}{d_i^{obs}}\right]^2} \tag{5}$$

While minimizing the above fitness function different constraints can be imposed on parameters. First constraint imposed on any component is because of the maximum fractional volume (100%) it can occupy in a lithology (i.e. $0<V_{sh}$, V_{ma}, V_i, $\phi<1$). For our reservoir, we have constrained the porosity in range of 5-35% (i.e. $0.05<\phi<0.35$) and water saturation for flushed zone and uninvaded zone as $0.6<S_{xo}<1$ and $0.2<S_w<1$- respectively. An additional

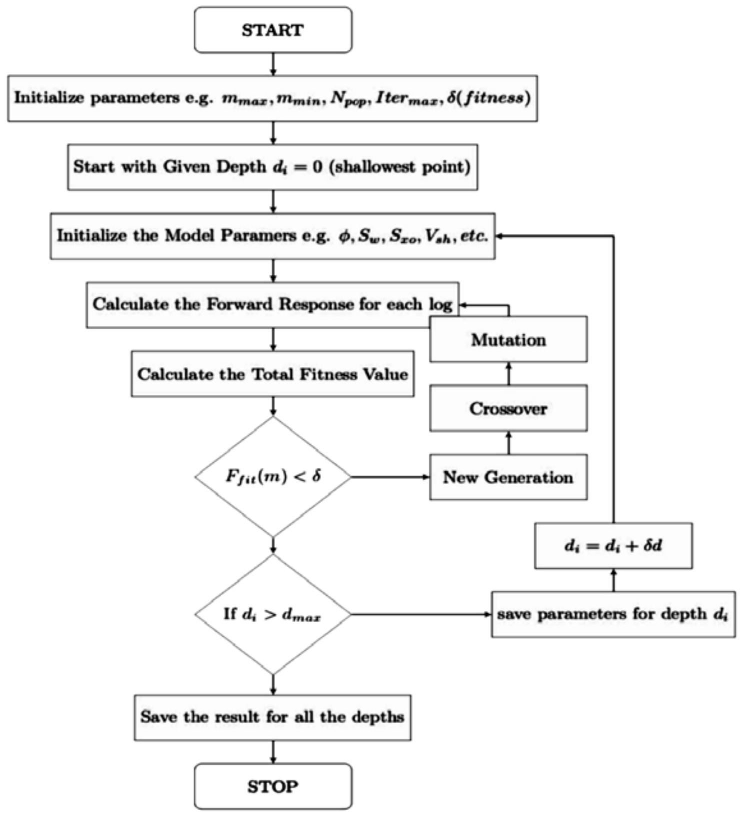

Figure 1. Algorithm for optimization of well log parameters at each depth point.

constraint equation, ϕ–V_{sh}+V_{mc}+V_i=1, can be imposed on parameters as the total volume occupied by all minerals along with void space (or porosity) in a rock is the volume of unit cube.

Numerical implementation of GA optimization is shown in Figure 1. In first step the parameters required by GA optimization algorithm, such as m_{min} and m_{max}, (vectors containing the minimum and maximum value for each parameters respectively), $Iter_{max}$ (maximum no of generation), δ (minimum error to terminate the loop), etc are initialized. GA optimization of fitness function is done at each depth point (d_i) starting from shallowest to deepest depth point (d_{max}) by stepping through δd. To retrieve the petrophysical parameters viz. ϕ, S_w, S_{xo}, V_{sh}, etc., Optimization at a depth is achieved by application of genetic operators on a set of population repeatedly until the criteria of maximum generation or δ has met. As soon as either of these conditions meet, the results (optimized parameters) are saved and it proceeds for the next depth point.

In this algorithm we have assumed that the response recorded by a logging tool is affected by the minerals/fluids present in horizontal section of the formation at that depth and thus the parameters obtained after inversion belong to that depth point only. As this inversion algorithm is associated with a particular depth point we can call it a point inversion algorithm. However in reality, the log response is also affected by the nearby layers thus to account for this effect, a weighted average response of adjacent layers may be assigned to that depth point. It should be noted that in order to use this method to invert real field data, it is desired to have some priori geological knowledge to limit number of components. Generalizing a model by considering a large number of components reduce the data to parameter ratio and makes the problem less over-determined or even-determined.

APPLICATIONS

Synthetic data application:

The inversion algorithm described above has been tested on synthetic log data. Synthetic logs were generated using an assumed petrophysical model shown in Figure 2. In this model, first and fourth layer are assigned general values for overburden and underburden, while second and third layers in this model correspond to the cap and reservoir rocks respectively. The second layer 6m-10m has very low porosity and high amount of shale (V_{sh}= 50%). The third layer (10-13 m) is mainly composed of sand with negligible fraction of shale possessing a high porosity ϕ = 30%. This layer has some residual oil as the difference in saturation of flushed zone and of un-invaded zone is non zero i.e. $S_{xo} - S_w = 0$. Using this model, ideal response of logs (Figure 3) was generated using forward modelling eq (1), (3), and (4). Synthetic log was generated by addition of Gaussian noise to ideal responses. Experiments were carried out with various levels of noise, however here we have shown only large noise (10%) case is shown in Figure 3. Petrophysical parameters obtained after inversion are shown in Figure 3 and we found that this algorithm worked well on synthetic data logs.

Real data application:

We applied the algorithm on well logs of Ankleshwar field of Cambay basin, India (Figure 4) to estimate the petrophysical parameter. Ankleshwar oil field has four major formations viz. Telwa, Ardol, Kanwa, and Hazad. Telwa and Kanwa are primarily shale while the Ardol and Hazad are alternation of sandstone and shale. Hazad formation possesses the reservoir characteristics and out of its different sand layers (S1, S2, S3 and S4) only two (S3 and S4) are major producing layer. These two layers are being studied for CO_2 enhance oil recovery (EOR). We used one of the Ankleshwar well (ANK-W1) data which has been well-studied for reservoir characterization and thus it was considered as a standard for comparing our results. A thin coal layer is also present in payzone being studied but we have not considered coal in our parameter set. The reason is- first, it would be having a negligible effect on the log response; second, for inversion it would increase the number of parameters and thus might lead to erroneous results. With this a priori information about lithology, we have carried out the inversion only for the S4 sand layer of Hazad formation. The results for petrophysical parameters obtained after GA based inversion are presented in Figure 5 and compared with the results provided by the industry (ONGC) as well as with the earlier studies carried out by Vadapalli et al., (2014).

RESULTS AND DISCUSSION

For inversion of the noisy-synthetic-well-logs (Figure 3) using the GA based inversion. We have used 6 logs and 7 constraining equations to retrieve 5 parameters. Number of parameter to be estimated is reduced to 4 due to constraining equation on total volume and thus give us the data to parameter ratio is 3.25. Synthetic study result shows that even for very high value of noise in synthetics, this scheme could recover the petrophysical parameters (Figure 2) satisfactorily except for S_{xo}, which was not retrieved accurately and its value is restricted nearby 0.8. The reason for such behaviour for S_{xo} could be lesser number of constraints for its estimation. S_{xo} represent water filled pores which have zero effect on GR and SP logs and thus resulting in lesser number of constraining equations for S_{xo}. However the valued for S_w were much more consistent unlike S_{xo}. Reason behind this is S_w influences the deep resistivity log, while having a negligible effect on other logs. Hence for S_w the inversion process is reduced to a one to one mapping from data to parameter space, i.e. from resistivity log directly.

Inversion results for Ankleshwar field well data show that the real logs have a good match with the synthetics logs, generated using the inverted parameter (Figure 5) with an average error of 6.27%. The small mismatch between the results can be attributed to the limitations of our model which comes primarily from two sources; first, due the relationships which govern the forward model and second, the number of constraining equations to maintain the threshold ratio. The forward modelling should be accurate so that it can generate the log response precisely. We have discussed several models in introduction but still there is a requirement of one single model to describe the effects caused due to contents as well as due to structure. Presence of several parameters brings non uniqueness of the solution into the picture, which can be mitigated only by constraining the parameter's bound. That is why we assert that our inversion requires the ratio of modelling equations (including constraints) and model parameters to be as large as possible. To explain this, let us consider two parameters constrained by three or more equations. In a two dimensional plot these constraining lines would cover some closed area, known as feasible region. If we add more and more such constraints, the feasible region becomes smaller and when this area becomes small enough we may get best possible solutions. If we have less data or constraints for a given depth point then we will have lesser options for selection of mineralogical components. Here we can use available geological information to ignore some components and deal with lesser number of parameters. Thus in this study we limited our model to the reservoir formation whose lithology is mostly known.

We found that the GA estimated parameter V_{sh} shows a strong correlation with given GR and SP logs. The S4 layer of Hazad formation can be further divided into different sand layers viz. S4.1 (1112.5-1116.0m), S4.2 (1119.0-1122.0m), S4.3 (1124.0-1130.5m), and S4.4 (1134.0-1138.0m). These sand layers presence can be clearly seen as the zones marked by high porosity, low GR and low shale. A comparision of parameters estimated using GA algorithm with that provided by the industry (ONGC) and Vadapalli et al., (2014) is presented in Figure 5. Industry has provided ϕ and S_w values, whereas the Vadapalli et al., (2014) provided ϕ , Vsh, and Vsd values. It can be observed that the ϕ estimates for all three are in good agreement. However, our method predicts significantly higher value

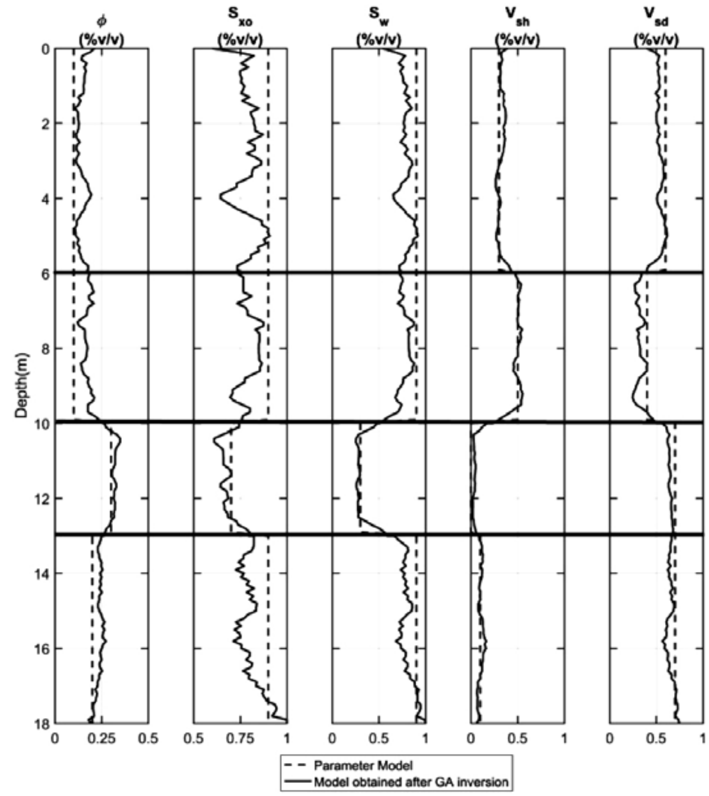

Figure 2. Parameter model (Porosity, ϕ; Water saturation, S_w or S_{xo}; Shale Volume, V_{sh}; and Sand Volume, V_{sd}) used to create the synthetic logs and the inverted parameters obtained, using the noisy synthetic logs.

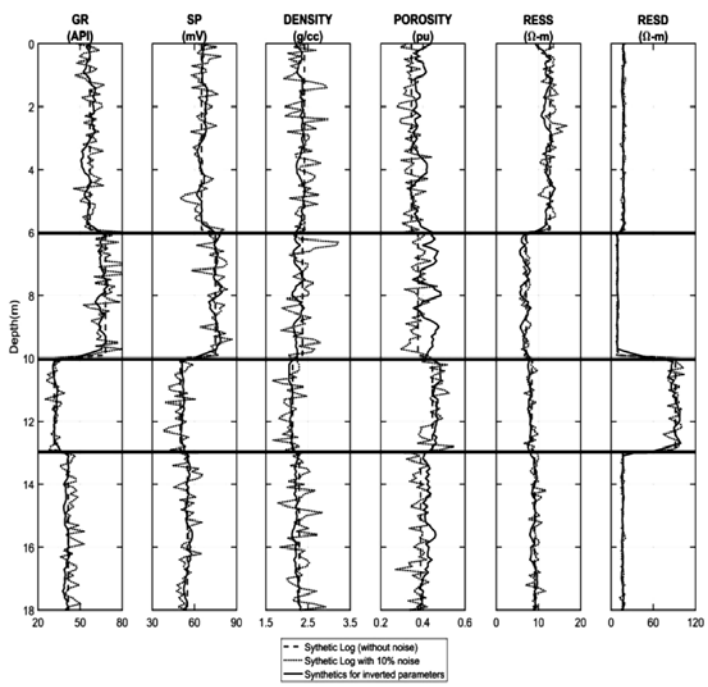

Figure 3. The response for the assumed parameter model (shown in Figure 2) without noise (ideal case) and with 10% noise (realistic case) are shown above. The logs generated for parameters obtained after inversion of noisy data are also shown. Various logs shown above are- Gamma Ray- GR; Self Potential-SP; Density-DENS; Neutron Porosity- NPOR; Shallow Resistivity- RESS; and Deep Resistivity- RESD.

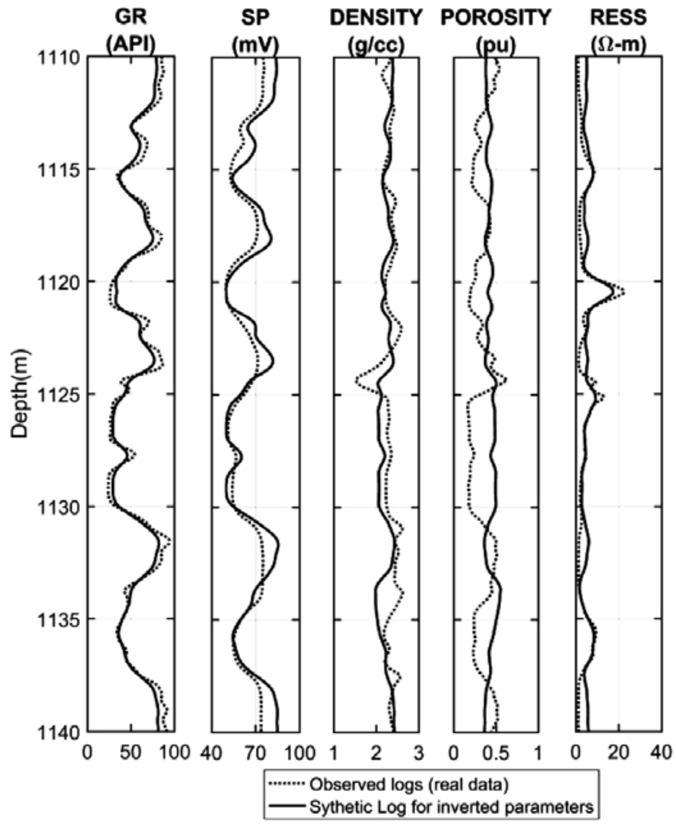

Figure 4. Comparison of real/observed borehole log with the synthetic log (generated using inverted parameters) for Ankleshwar borehole data.

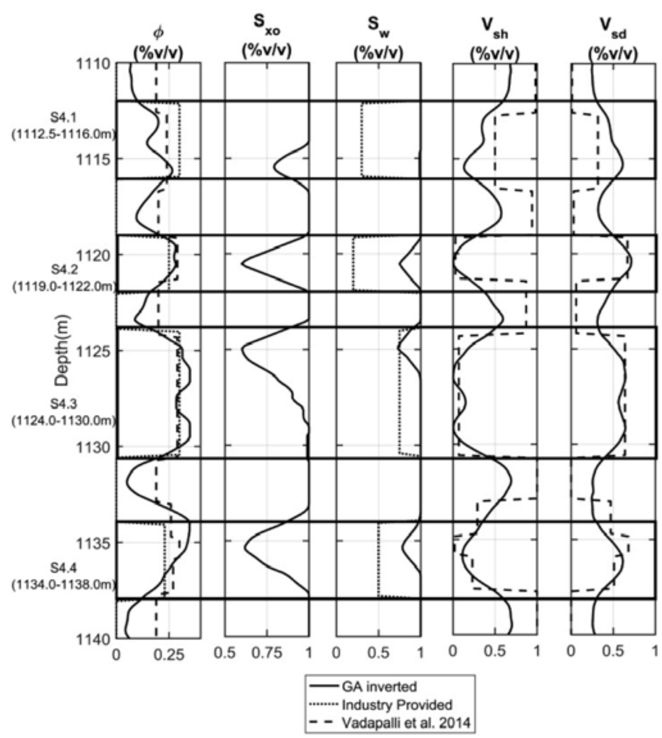

Figure 5. Comparison of petrophysical parameters for Ankleshwar borehole data. GA inversion results, industry provided results and results from Vadapalli et al., (2014) are shown.

of S_w than the industry provided values. This difference between GA inverted results and the values provided by the industry could be a result of assumptions, or some error made in conventional procedure used by the industry. The error originated at some step may grow while going through subsequent steps in processing and finally produce cumulatively large error. In our method we mitigated this cumulative error problem as we are utilizing all the logs simultaneously for parameter estimation. Our results are also in good agreement to all three parameters (ϕ, V_{sh} and V_{sd}) estimated by Vadapalli et al., (2014). In addition to this our method brings out the finer features of well log by detecting the sub layers of shale and sand present within the formation which is another advantage of our approach. The estimated petrophysical properties using this method can be used directly for interpretation as well for generation of missing log(s). Often, in industry provided data, some logs are missing which might be required by a researcher for further processing/interpretation. In this scenario we can generate these logs using log response equations for which we can use our inverted petrophysical parameters model as an input. However its practical application is yet to be tested and verified.

CONCLUSIONS

We have carried out inversion of well log data for estimation of the petrophysical parameters using a non-linear model with precise estimates of shale using the GA optimization technique. This technique was successfully tested on synthetic data and then applied on Ankleshwar field well data. The field data inversion was carried out for the S4 sand layer of Hazad formation which is being considered for CO_2 –EOR and we found that our results are in good agreement with the information provided by the industry. This technique has limitation if there are a large number of parameters with few constraints. In this scenario parameters must be limited by some a priori knowledge of lithology of the formation. In this scenario parameter must be limited by some means. However the advantages of this method are- applicability to any formation, robust inversion method as it works even in presence of high noise, mitigating the error propagation problem to some extent by simultaneously inverting data for different parameters, finer resolution as it brings out the finer details of lithology, and capability of generating missing logs.

ACKNOWLEDGEMENTS

AM would like to express sincere thanks to University Grant Commission for JRF scholarship. Authors are thankful to ONGC for providing the data. We thank Director NGRI for giving permission to publish this paper. We also thank Dr. Dhananjay Kumar and Chief Editor of JIGU for their valuable suggestions.

Compliance with Ethical Standards

The authors declare that they have no conflict of interest and adhere to copyright norms.

REFERENCES

Alberty, M., and Hashmy, K., 1984. Application of ULTRA to log Analysis, SPWLA 25th Annual Logging Symposium, pp: 1-17.

Archie, G. E., 1942. The electrical resistivity log as an aid in determining some reservoir characteristics, Petroleum Transactions of AIME, v.146, pp: 54–62.

Clavier, C., Coates, G., and Dumanoir, J., 1977. The theoretical and experimental bases for the "dual water" model for the interpretation of shaly sands, Society of Petroleum Engineers Journal, v.24, no.2, pp: 153-168.

Dimri, V. P., 1992. Deconvolution and inverse theory - application to geophysical problems, Elsevier Science Publishers, Amsterdam.

Dobroka, M., and Sazabo, N. P., 2011. Interval inversion of well-logging data for objective determination of textural parameters. Acta Geophysica, v.59, no.5, pp: 907-934.

Gill, P. E., Murray, W., and Wright, M. H., 1981. Practical Optimization, Academic Press.

Goldberg, D. E., 1989. Genetic Algorithms in Search, Optimization, and Machine Learning. Addison-Wesley Longman Publishing Co., Inc., Boston, MA, USA.

Hiller, S., 2006. Appendix A. Mineralogical and chemical data, in GM Reeves, I Sims, and JC Cripps eds., Clay materials used in construction: London. Geological Society, Engineering Geology Special Publications, v.21, pp: 449-459.

Holland, J. H., 1975. Adaptation in Natural and Artificial Systems: An Introductory Analysis with Applications to Biology, Control, and Artificial Intelligence. The University of Michigan Press, Ann Arbor.

Mayer, C., and Sibbit, A., 1980. GLOBAL, a new approach to computer-processed log interpretation. Presented at the 55th Ann. Fall Tech. Conf. at Dallas, Tex, Soc. Petr. Eng. AIME.

Menke, W., 2012. Geophysical Data Analysis: Discrete Inverse Theory, Third Edition, Academic Press (Elsevier).

Mezzatesta, A., Rodriguez, E., and Frost, E., 1988. Optima: a statistical approach to well log analysis. Geobyte, v.3, pp: 56-69.

Perrin, R. M. S., 1971. The Clay Mineralogy of British Sediments. Mineralogical Society, London, pp: 247.

Poupon, A., Loy, M. E., and Tixier, M. P., 1954. A Contribution to Electric Interpretation in Shaly Sands, Journal of Petroleum Technology, pp: 29–34.

Poupon, A., and Leveaux, J., 1971. Evaluation of Water Saturations in Shaly Formations. Society of Petroleum and Well Log

Analyst Transcation, 12th Annual Logging Symposium, pp: 1-2.

Ridgway, J. M., 1982. Common Clay and Shale:Great Britain Instiute of Geological Science, Mineral Resources Consultative Committee. Mineral Dossier 22.

Schlumberger, 1975. A Guide to Wellsite Interpretation for the Gulf Coast. Schlumberger Offshore Services.

Schlumberger, 1989. Log Interpretation Principle/Applications, Schlumberger Educational service.

Sellwood, B. W., and Sladen, C. P., 1981. Mesozoic and Tertiary argillaceous units, distribution and composition. Quarterly Journal of Engineering Geology, v.14, pp: 263-276.

Sen, M., K., and Stoffa, P. L., 2013. Global Optimization Methods in Geophysical Inversion. Cambridge University Press.

Serra, O., 1984. Fundamentals of well-log interpretation volume 1-The acquisition of logging data. Development in Petroleum Science No 15A, Elsevier, Amsterdam..

Shaw, H. F., 1981. Mineralogy and petrology of the argillaceous sedimentary rocks of the UK, Quarterly Journal of Engineering Geology, v.14, pp: 277-290.

Simandoux, P., 1963. Dielectric measurements in porous media and application to shaly formation: Revue de L'Institut Français du Pétrole, v.18, pp: 193–215.

Szucs, P., and Civan, F., 1996, Multi-layer well log interpretation using the simulated annealing method, Journal of Petroleum Science and Engineering, v.14, no.3, pp: 209-220

Vadapalli, U., Srivastava, R. P., Vedanti, N., and Dimri V. P., 2014. Estimation of Permeability of a sandstone reservoir by fractal and Monte Carlo simulation approach: a case study, Nonlinear Processes in Geophysics, v.21, pp: 9-18.

Vedanti, N., Srivastava, R. P., Sagode, J., and Dimri, V. P., 2005. An efficient non-linear Occam's inversion algorithm with analytically computed first and second derivatives for DC resistivity sounding, Computers & Geosciences, v.31, pp: 319-328.

Waxman, M. H., and Smits, L. J. M., 1968. Electrical conductivities in oil-bearing shaly sand, Society of Petroleum Engineers Journal, v.8, pp: 107–122.

Worthington, P.F., 1985. The evolution of shaly-sand concepts in reservoir evaluation, The Log Analyst, pp: 23–40.

J. Ind. Geophys. Union (March 2017)
v.21, no.2, pp: 105-115

Geotechnical investigations in the southern part of Ahmedabad district, Gujarat, India

Sarda Thokchom*[1], B.K. Rastogi[1], N.N. Dogra[2] and Vasu Pancholi[1]

[1]Institute of Seismological Research, Gandhinagar, Gujarat, India
[2]Department of Applied Geology, Kurukshetra University, Kurukshetra, India
*Corresponding Author: sarda.1331@gmail.com

ABSTRACT

Geotechnical investigations of soil consisting of surface and subsurface studies are performed in the southern part of Ahmedabad district in Gujarat state of western India. Surface investigations include detailed geological and geomorphological mapping, whereas subsurface investigations involved selected drilling, soil sampling and laboratory analysis of the samples. About 700 samples were collected at every 1.5m depth interval from 64 boreholes, each of about 50 m depth for soil classification. The study area is covered by alternate layers of fine and coarse grained sediments. We used Standard Penetration Test (SPT)-N values, Soil Bearing Capacity (SBC) and Soil Bearing Pressure (SBP) for soil classification. The SPT-N values are noted during drilling while the SBC and SBP are estimated from the soil properties. The measured soil properties both physical and mechanical include: density, specific gravity, permeability, stiffness, strength, grain size analysis, liquid limit, plasticity index and shear strength parameters (Cohesion co-efficient and Friction Angle). A relationship has been obtained between SBC and N-values derived from the above studies.

Key words: Geotechnical investigation, Engineering geology, Geotechnical properties, Surface exploration, subsurface exploration.

INTRODUCTION

The study area, about 50km in N-S direction and 20km in E-W direction, lies in the southern part of Ahmedabad district, bordering Bhavnagar district of Gujarat. It is situated on the western flank of the Gulf of Cambay while the northern end of the area is about 50 km south of Ahmedabad.

Geotechnical investigation involves analysis of the soil composition to determine its structure and strength index by surface as well as by subsurface exploration. Surface exploration includes geological mapping, remote sensing and geophysical surveys. We prepared geomorphological map and soil maps from the geological mapping and remote sensing studies. The geophysical surveys provided information on the faults and structure of deep layers of sediments and rocks. The subsurface exploration involves soil sampling by test pits and trenching, followed by laboratory testing of the samples to obtain the subsurface soil properties.

In geotechnical engineering, classification of soil is mainly done in accordance with their physical and mechanical properties such as density, specific gravity, permeability, stiffness, strength etc. The investigation involves soil classification according to IS code, estimation of safe bearing capacity (SBC) and safe bearing pressure (SBP) based on shear parameters of soils in selected boreholes. Seismic site classification based on blow count obtained from standard penetration test (SPT – N values) was carried out according to National Earthquake Hazard Reduction Program (NEHRP). This study provides preliminary guidelines for construction and for land use planning.

GEOLOGY OF THE STUDY AREA:

The study area is situated at the western side of South Cambay basin. The area is covered by about 100m thick Quaternary alluvium and 250 m of Tertiary sediments deposited on the subsiding side of the Cambay basin. The Quaternary formations exposed in the study area include the tidal deposits brought by marine agencies and flood plain deposits brought by fluvial agencies. The Cambay basin is formed at the end of the Cretaceous due to rifting of the western continental margin of India (Biswas, 1982). It is a 500 km long and 50-60 km wide basin trending NNW-SSE. The sediments are marine up to Miocene, while the lower Pleistocene deposits are fluvio-marine indicating shallow marine and continental condition. The topography of the Cambay basin varies between 80 to 100 m. The first major transgression during Quaternary took place only in middle Pleistocene. The evidences of tectonism, differential uplifts within the graben (Ghosh, 1982; Sareen, 1993), eustatic changes in the base level, uplifts of the Aravalli mountain ranges and faulting (Ahmed, 1986) during middle to late Quaternary, can be seen in the form of entrenched rivers and cliffy banks. The study area is almost flat, gently sloping towards east with elevations ranging between 2-12 m, and thus the major drainage in this region flows from west to east.

Three main creeks trending NW-SE are present in the study area; first creek is in the northern most part of the study area originating from Gorasu village, second is in the central part and third is along the southern most boundary of the study area. The tidal flats are 8-10 km wide and numerous creeks cut tidal flats. All the water bodies of this region are full during the monsoon/post monsoon season but dry for the rest of the year. Rivers are also ephemeral since the region falls under semi arid climatic zone.

Rivers drain the Saurashtra peninsula and erode the Deccan Trap and deposit the finer sediments along the present day mud flats. Mud flats are present all along the south-eastern part of the study area and gradually merge with the Gulf of Cambay. Mud flats are formed all along the coastline trending NE-SW. Towards west of the present day Mud Flats are the Old Mud Flat deposits, which cover almost the whole study area. Presence of the older mud flats also indicates that the region was submerged under the sea water in the past. These older mud flats are at present at higher elevation than the high tide level and do not get water logged by the sea water. Salt Flats are present all along the western margin of the present day mud flats fringing the water logged area as well as all along the tidal creeks. The saline sea water from the Gulf enters the mud flats and the creeks and gives rise to low lying salt encrusted flat valleys, which are almost flat to gently sloping towards the sea. In the study area, all the salt flats are present along the three major creeks.

ESTIMATION OF SOIL PROPERTIES:

Soil property details are given below. Detailed exposition of these properties could be obtained from standard published articles/ internet.

Standard Penetration Test (SPT):

SPT is an in-situ dynamic penetration test designed to provide information on the geotechnical properties of soil. It is commonly used to check the consistency of stiff or stony cohesive soils and weak rocks, by driving a standard 50 mm outside diameter thick walled sampler into soil using repeated blows of a hammer falling through 76 cm. The measured SPT blow count (N_{SPT}) is normalized for the overburden stress at the depth of the test and corrected to a standardized value of $(N_1)_{60}$ using the recommended correction factors given by Robertson and Fear (1998):

$$(N_1)_{60} = N_c * (C_N * C_E * C_B * C_R * C_S)$$

Where, C_N = Overburden Pressure, C_E = Hammer Energy, C_D = Bore Hole Diameter, C_S =Presence or Absence of Liner, C_R = Rod Length.

Plastic limit (W_p):

It is defined as the minimum water content of the soil at which the soil will just begin to crumble into pieces (plastic behaviour). Clay has finer particles and has higher Plastic limit as compared to silt.

Liquid Limits (W_l):

Liquid Limit (LL) is the minimum water content at which soil changes from plastic to a liquid behavior. The Liquid limit is the measure of water content at which the soil paste groove gets vanished in 25 blows.

Plasticity Index (I_p):

It is the range of water content within which a soil behaves as plastic substance. When a sandy soil is used the plastic limit must be determined first. In case where, plastic limit is equal to liquid limit the plasticity index is treated as Zero. Plasticity Index (I_p) of a soil is estimated using the following equation

$$W_p = W_l - W_p$$

where, W_l = Liquid limit of the soil
W_p = Plastic limit of the soil

Grain Size Analysis:

The percentage of various sizes of particles in a given dry soil sample is determined by means of particle size analysis. Particle size analysis can be performed by the Sieve Analysis (for coarse soil fraction) and Sedimentation Analysis (for fine soil fraction < 75μ).

Sieve Analysis preferably is used if the soil size is 0.075 mm or more in diameter/size. When the size of the soil is less than 0.075 mm, usually sedimentation analysis is used. Sieving is carried out by arranging various sieves of different mesh sizes. Wt% of each mesh/sieve size is evaluated using the following equation:

$$\text{Wt \% of a size fraction} = (\omega/W) \text{ X } 100,$$

where, ω = weight retained in a sieve
W = total weight of the sample

Sedimentation Analysis is based on the principle of Stokes law and evaluated using hydrometer:

$$\nu = cr^2$$

where, ν = settling velocity
r = radius of the particles
c = a constant

The hydrometer reading is taken at different intervals of time from which the size of the largest particles suspended at those times is determined.

Soil Classification:

The classification of soil is carried out according to Indian Standards (IS-1498-1970). According to this classification,

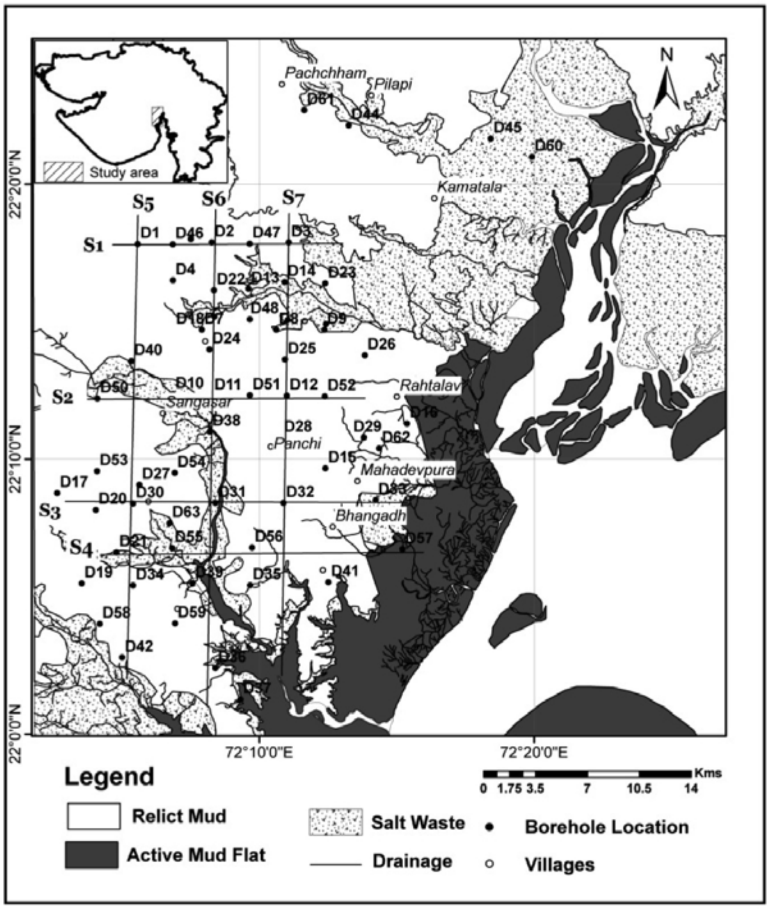

Figure 1. Geomorphology of the study area along with the borehole locations and selected cross sections.

soil is divided into coarse soil (gravel and sand) and fine soil (silt and clay). Classification of soil using plasticity chart provides comparison of soil at equal liquid limits. Toughness and dry strength increase with increasing plasticity index.

In the plasticity chart A-line is drawn which separates clay from silt. The soils that lie above the A-line are clay while those below the A line are silt. A-line has a linear equation between the liquid limit (W_l) and the plasticity index (I_p):

$$I_p - 0.73(W_l - 20)$$

Plasticity index of 4 to 7 indicates transition zone of clay and silt.

Cohesion co-efficient (C: kg/cm^2) and Friction Angle (Ø: Degree):

Cohesion co-efficient (C: kg/cm^2) and Friction Angle (Ø: Degree) are shear strength parameters. The shear strength is important in determining the bearing capacity for foundations, stability of slopes or cuts and calculating the pressure exerted by a soil on a retaining wall. For the present study, direct Shear test is performed as per IS 2720(13)-1986 to determine the bearing capacity of foundation.

GEOTECHNICAL PROPERTIES OF THE STUDY AREA:

As stated above, the present study area is covered with thick fluvio-marine sediments. In order to know the geotechnical characteristics of the subsurface lithology, 64 boreholes varying in depth from 30 to 100 m (as shown in Figure1) were, for collecting both disturbed and undisturbed samples for laboratory analysis.

The Standard Penetration Tests (SPT) were conducted as per IS- code (IS 2131, 1981) at every 3m depth interval in all boreholes to determine the SPT-N values.The SPT-N values at depth of 3m and 6m were generally low, less than 10 and 20 respectively. With increase in depth the measured SPT-N values increase due to the densification of sediments and overburden stress. The SPT-N values above 50 blow counts were encountered at an average depth of 15m. In some boreholes, sudden increase in SPT-N values was observed which may be due to the presence of gravel layers at that particular depth.

Water table of the study area was obtained from borehole data collected during drilling. The water table is shallow and varies from 1m to 3.9m. Soil samples were collected as per IS: 2132 (1986) for determination of the physical properties of sediments. Determination of index properties of sediments was carried out according to IS: 2131 (1985). After laboratory analysis, the boreholes were classified into two categories i.e. domination of fine grained and coarse grained soils, based on presence of more than 60% clayey, silty and sandy soils in each borehole. Physical properties of the sediments and SPT-N values were plotted separately for the fine and coarse grained categories of boreholes against the depth (Figures 2 & 3). It is observed that in both categories, the fine content (%) is high, nearly 100% down to the depth of 8 km. Fine content decreases to less than 40% below 8 to 20m in coarse grained dominating boreholes (Figure 2a). Below 20m depth, approx. 50% of samples for both categories are sandy and 50% are silty and clayey soil. The liquid limit (LL) for the fine grained soil boreholes was generally higher, ranging from 35-60 (Figure 2b). The coarse grained soil boreholes, on the other hand, show LL values 20 to 30 (Figure 3b). Plasticity index of the fine grained soil is also higher than the coarse grained soil.

Soil classification is carried out as per IS-1498-1970. The fine-grained soil can be classified as silty soil with intermediate plasticity to clayey soil with high to low plasticity. Only a few of them are silty soil with high plasticity (Figure 4). The coarse grained soil, on the other hand, can be classified as poorly sorted sand (SP) to silty sand (SM).

VERTICAL CORRELATION OF GEOTECHNICAL PARAMETERS

The boreholes are vertically correlated using geotechnical parameters and SPT- N values along seven different cross sections (Figure 1), four along EW direction (S_1 to S_4) and three along N-S direction (S_5 to S_7). Locations of cross sections are shown in Figure 1 and soil profiles are shown in Figures 5 and 6. The vertical profiles show that the entire study area is covered by fine grained sediment with intermediate to low plasticity having an average depth of 15m which reaches to 30m at a few locations. The fine grained layer is followed by the coarse grained sediment with an average thickness of 20m. Low SPT-N value (N_{SPT}) less than 15 were encountered at depth 6m except in boreholes D51 and D16 in Section-S_2**,** and in borehole D17 in Section-S_4**.** N_{SPT} greater than 15 but less than 50 were found at the depth 6m to 30m. N_{SPT} greater than 50 were found at depths 30m and below.

ESTIMATION OF FOUNDATION PARAMETERS

Safe Bearing Capacity (SBC) and Safe Bearing Pressure (SBP) are the two main parameters for designing foundation structure. These parameters are estimated considering shear and consolidation characteristics of the sub surface sediments. SBC and SBP have been estimated for 20 borehole locations. Results are presented for six boreholes (Table 1). For SBC estimation, the soil parameters like cohesion, angle of friction, specific gravity and corrected N values are used for foundation depth of 3m with width and length of 3m. The ground water level factor is considered along with the permissible 25 mm settlement of the footing.

The results show that the SBC value varies between 8.56t/m^2 and 45.04t/m^2. The low SBC in borehole D22 is due to silty sand with low plasticity and low $(N1)_{60}$ at 3m depth. On the other hand, the high SBC in borehole D61 is due to clayey nature of the soil at this particular depth. The plot of SBP with corrected N value (Figure 7) shows that the SBP increases with increase of N values.

SITE CLASSIFICATION

Site classification is an important part of the present study as the study area is expected to undergo extensive construction activities in near future. It is necessary to have subsurface litholog to estimate the effects of earthquake. Site classification can be carried out based on three different parameters i.e. undrained shear strength (S_u), SPT-N (N_{SPT}) and shear wave velocity (Vs) (NEHRP, 2000). The parameters used to define site classification are based on the upper 30m of the site profile (NEHRP, 2003). We used N_{SPT} for the site classification. The equivalent shear stiffness values of soil based N_{SPT} values over 30m depth can be estimated by using the following equation:

$$N_{30} = \frac{\sum_{i=1}^{n} d_i}{\sum_{i=1}^{n} \left(\frac{di}{N_i}\right)}$$

where, N_{30} is the measured N_{SPT} value without correction and should not be taken greater than 100 blows/ft, of distinctly different soils and rocks are segregated by a number that ranges from 1 to n in the upper 30m. Average N_{30} values were calculated using equation1. The calculated N_{30} ranges from 8 to 57 and classification according to the US National Earthquake Hazard Reduction Program (NEHRP) is given in Table 2. It is observed that the entire study area comes under the site 'class D' which belongs to stiff soil except in four boreholes out of total 64 (three of which come under the site class-E (soft soil) and one in site class-C (much dense soil).

Detailed site classification at every 3m depth were carried out using average N_{SPT} values down to 3m (**N_3**), 6m (**N_6**), 9m (**N_9**), 12m (**N_{12}**), 15m (**N_{15}**) and 18m (**N_{18}**) depth and classified them as per NEHRP site classification.

Figure 8 shows site classification of the study area at different depths of 3m, 6m, 9m, 12m, 15m and 18m. At 3m depth soft soil is revealed over a major part of the

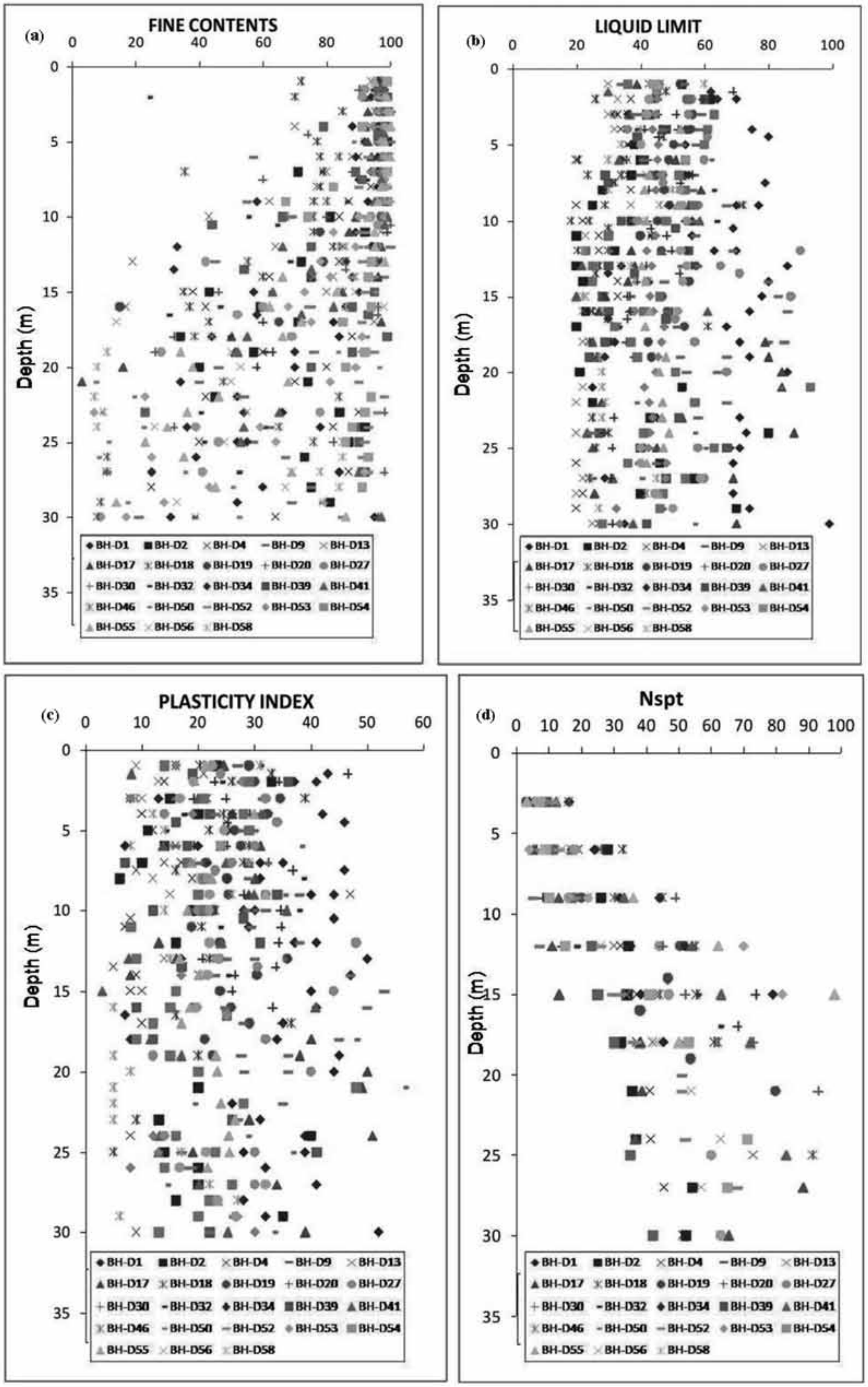

Figure 2. Plot of geotechnical properties (Fine content, Liquid Limit, Plasticity Index and SPT-N value) for fine grained dominated boreholes.

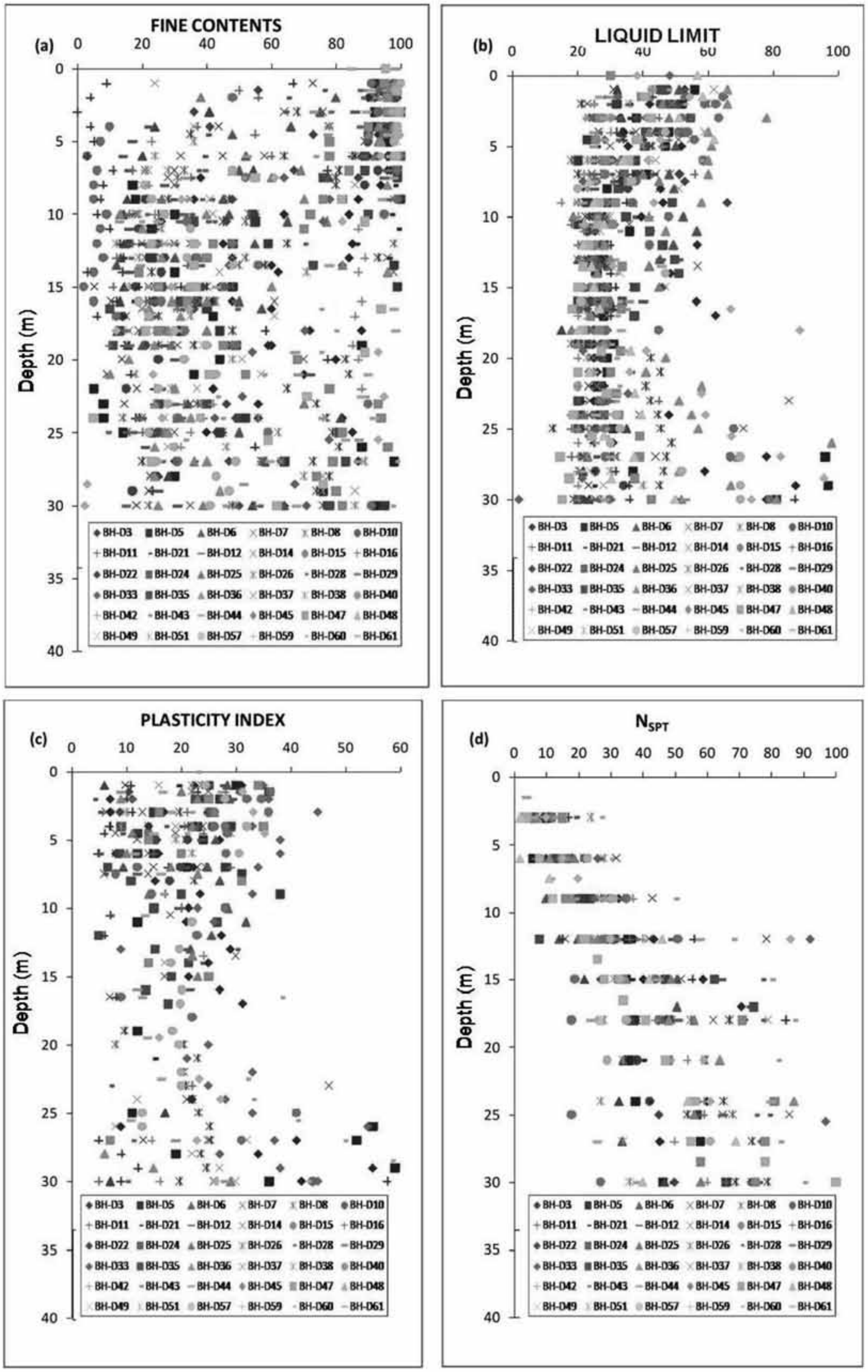

Figure 3. Plot of geotechnical properties (Fine content, Liquid Limit, Plasticity Index and SPT-N value) for coarse dominated boreholes.

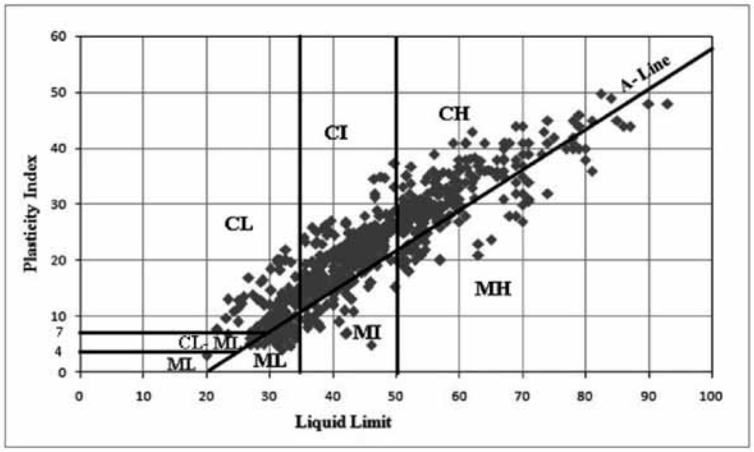

Figure 4. Classification of Fine Grained Soil for the study area based on plasticity chart as per IS**: 1498 – 1870**. Plasticity Index and Liquid Limit for each of 645 samples are shown by diamonds. The letter C indicates clay and M indicates silt. Subsequent letters L, I and H indicate low, intermediate and high plasticity, respectively.

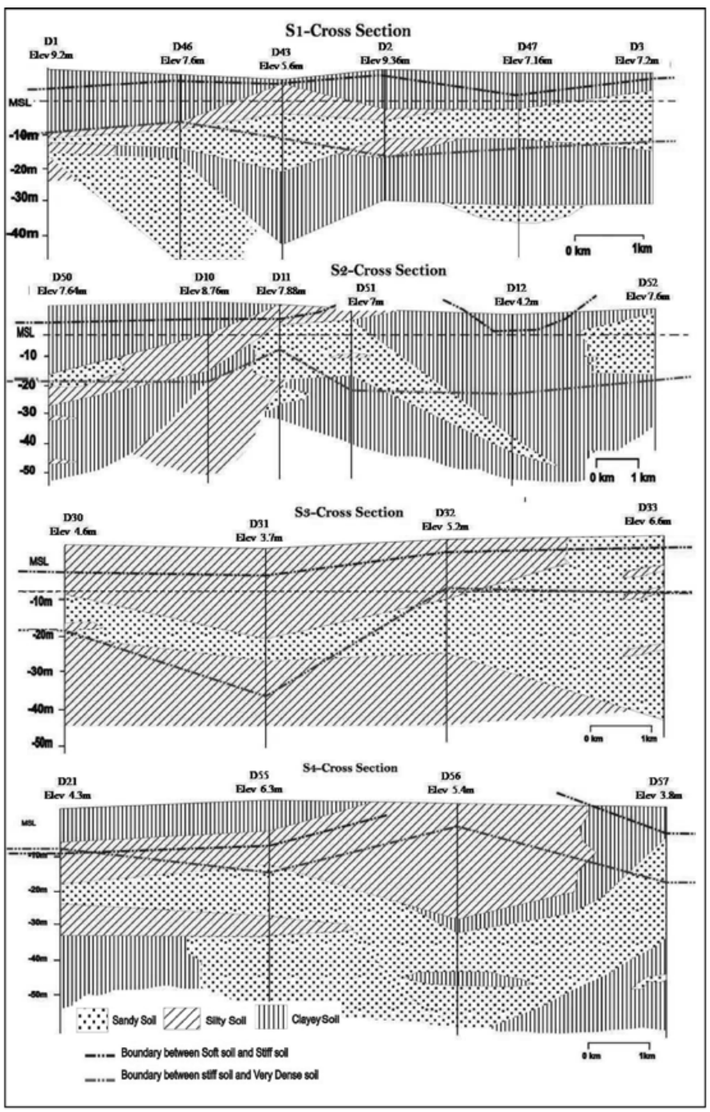

Figure 5. Soil profiles along west to east (see Figure 1).

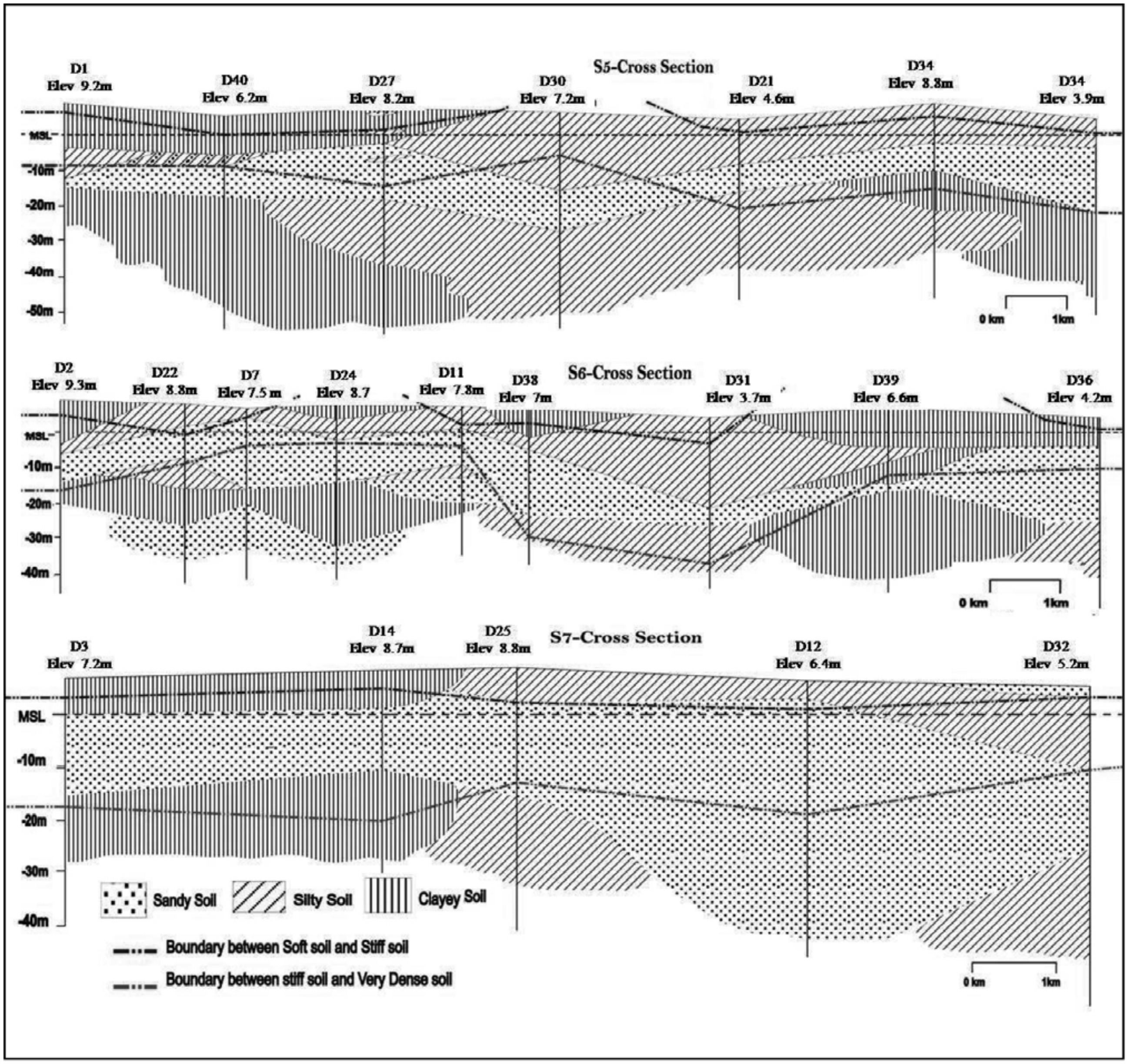

Figure 6. Soil profiles along north to south (see Figure 1).

Table1. Estimated SBP and SBC at 3m footing depth for selected boreholes in the study area.

Bore Hole No.	Water Table (in m)	Depth of Footing, D (in m)	Width of Footing, B (in m)	Water Table Factor	Corrected "N" value	Settlement / Unit Pressure (in mm)	Safe Bearing Pressure (in t/m^2)	Safe Bearing Capacity (in t/m^2)
D9	2.4	3	3	0.5	4	190	2.63	16.95
D22	2	3	3	0.5	6	160	3.12	8.56
D25	1.5	3	3	0.5	14	22	22.71	14.96
D26	2.1	3	3	0.5	15	20.5	24.38	29.63
D32	2.5	3	3	0.5	10	36	13.88	30.9
D61	2.44	3	3	0.5	8	58	8.62	45.04

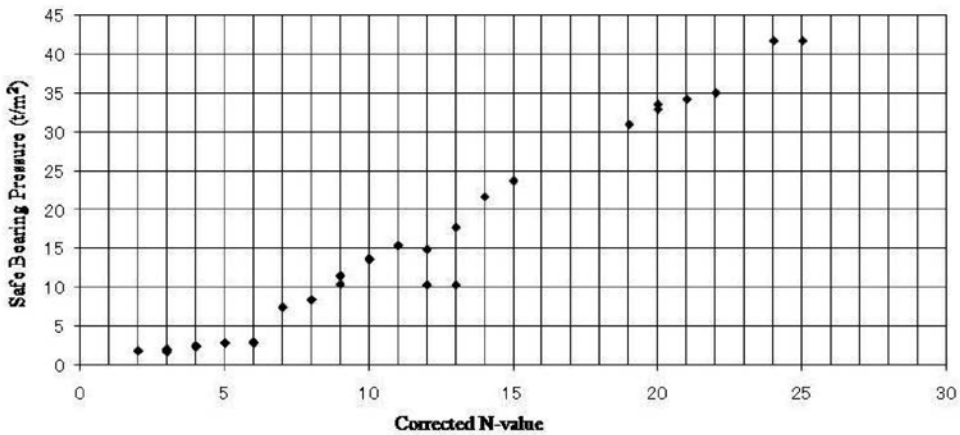

Figure 7. Graph showing a linear relationship between SBP and corrected N- values.

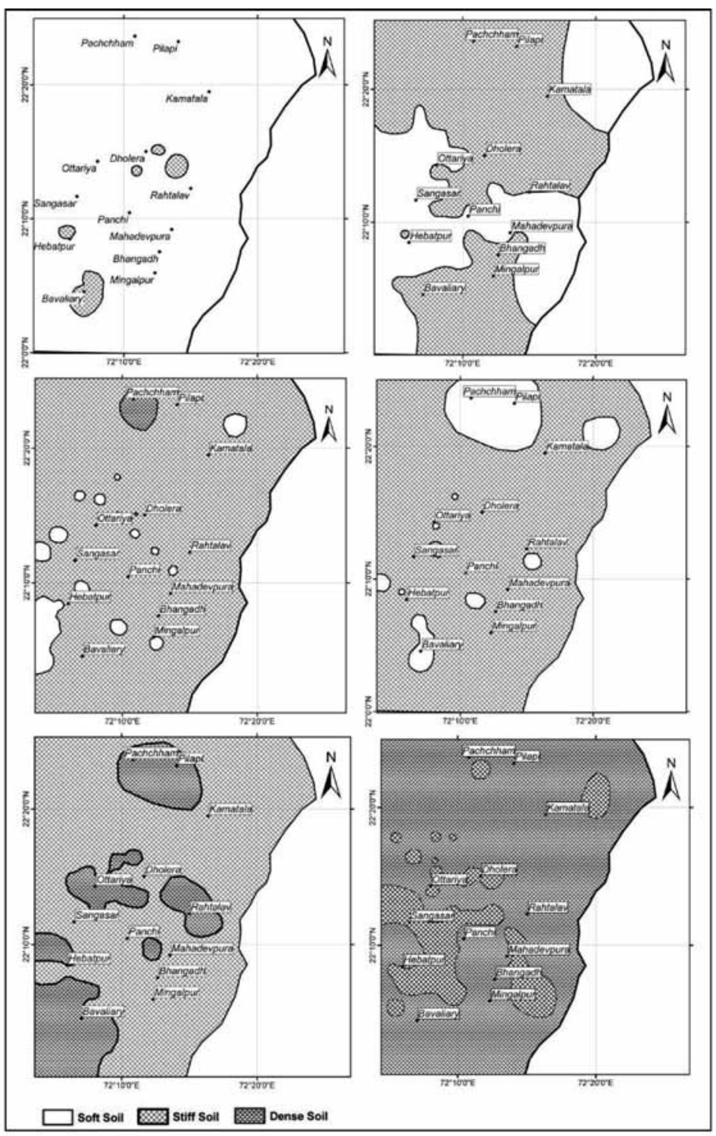

Figure 8. Distribution of different soil types based on SPT-N value according to NEHRP.

Table 2. Seismic site classification as per NEHRP.

Site Class	N_{SPT} value (N_{30})	Shear wave velocity (V_s)	Undrained shear strength (S_u)
Site-E (Soft soil)	<15	(< 180 m/s)	(< 50 kPa)
Site-D (Stiff soil)	15-50	(180 to 360 m/s)	(50 to 100 kPa)
Site-C (Very dense soil/ soft rock)	>50	(360 to 760 m/s)	(> 100 kPa)

area with small patches of stiff soil in the southern part at borehole D39 and D59 and at the central part at boreholes D2, D9 & D26. At the depth of 6m, the area shows soft soil and stiff soil in almost equal proportions. Northern and southern parts are characterized by stiff soil while the middle and north eastern portions are characterized by soft soil. At the depth of 9m, the entire area is covered by stiff soil with small patches of soft soil in southern part. Dense soil is found in the northern part in and around borehole D61. At the depth of 12m, the entire area is covered by the stiff soil with two patches of soft soil in northern part and a few small patches in the southern part. At the depth of 15m, there is no soft soil. Relatively denser soil occupies the northern part, central part and south western part while the stiff soil occupies the remaining portion. At the depth of 18m, the entire area is covered by the dense soil with small patches of stiff soil in the southern part.

DISCUSSION AND CONCLUSIONS

Geotechnical investigations, carried out using samples from 64 boreholes down to the depth of around 50m indicate that the study area is covered by fine grained sediments down to depth of 8m. The sediments are classified as silt with intermediate to low plasticity and clay with high to low plasticity. Site classification based on the measured SPT-N value and the US National Earthquake Hazard Reduction Program (NEHRP) indicates that the study area in general comes under class -D i.e. the soil in the area is stiff in nature for depth exceeding 3m. Such a type of soil possesses sufficient strength suitable for infrastructure development. For high rise buildings, detailed investigation should be carried out before construction to estimate low frequency amplification due to the possibility of large Kutch earthquakes. Safe Bearing Capacity of soils having N>15 (stiff soil) is acceptable but not for 3m top soft soil having N<15.

The present study provides preliminary guidelines to geotechnical engineers and researchers for land use planning and other constructional activities.

ACKNOWLEDGEMENTS

The study was funded by Gujarat Infrastructure Development Board and GICCL. Authors are grateful to Dr. M. Ravi Kumar, Director General, ISR for permission to publish the work and Dr. Sumer Chopra, Director for his support. Thanks are due to Dr. J.R.Kayal for constructive review and suggestions. Authors thank Dr. M.R.K. Prabhakara Rao and Chief Editor for apt editing of the manuscript.

Compliance with Ethical Standards

The authors declare that they have no conflict of interest and adhere to copyright norms.

REFERENCES

Ahmed, F., 1986. Geological evidence bearing on the origin of the Rajasthan desert (India), Proceedings of Indian National Science Academy v.52, pp: 1285–1306.

Biswas, S.K., 1982. Rift basins in western margins of India and their hydrocarbon prospects with special reference to Kutch basin, Am. Assoc. Petrol. Geol., v.10, pp: 1497-1513.

Ghosh, R.N., 1982. Regl. Conf. Min, Ener. Reso. SE Asia Manila, Philippines 1982, pp: 111-126.

IS: 1498 -1970. Indian Standard Classification and identification of soils for general engineering purposes, First revision, Bureau of Indian Standards, New Delhi.

IS: 2131-1981. Method for standard penetration test for soils. Bureau of Indian Standards, New Delhi.

IS: 2131- 4, 1981. Method of test for soils. Part-4: Grain size analysis. Second revision. Bureau of Indian Standards, New Delhi.

IS: 2132-1986. Code of Practice for Thin- Walled tube sampling of soils. Second revision. Bureau of Indian Standards, New Delhi.

IS: 2131-5, 1985. Method of test for soils. Part-5: Determination of Liquid and Plastic limit. Second revision. Bureau of Indian Standards, New Delhi.

IS: 2720-1986. Method of test for soils. Part-13: Direct Shear test. Second revision. Bureau of Indian Standards, New Delhi

National Earthquake Hazards Reduction Program (NEHRP), 2000. Recommended Provisions for Seismic Regulations for New buildings and Other Structures, FEMA 368, Building Seismic Safety Council, Federal Emergency Management Agency, Washington DC.

National Earthquake Hazards Reduction Program (NEHRP), 2003. Recommended Provisions for Seismic Regulations for New buildings and Other Structures, FEMA -450, Building Seismic Safety Council, Federal Emergency Management Agency, Washington DC.

Robertson, P.K., and Wride (Fear) C.E., 1998. "Cyclic liquefaction and its evaluation based on the SPT and CPT", In Proc. of the 1996NCEER Workshop on Evaluation of Liquefaction Resistance of Soils. Edited by T.L. Youd and I.M. Idriss, NCEER-97-0022

Sareen, B.K., Tandon, S.K., and Bhola, A.M., 1993. Slope deviatory alignment, stream network and lineament orientation of Sabarmati river system, Neotectonic activity in the mid-late Quaternary. Current Science., v.64, pp: 827–836.

J. Ind. Geophys. Union (March 2017)
v.21, no.2, pp: 116-123

Assessment of Liquefaction potential of soil in Ahmedabad Region, Western India

V.K. Dwivedi*[1], R.K. Dubey[2], S. Thockhom[1], V. Pancholi[1], S. Chopra[1] and B.K. Rastogi[1]

[1]Institute of Seismological Research, Raisan, Gandhinagar
[2]Indian School of Mines, Dhanbad
*Corresponding Author: geovinay@gmail.com

ABSTRACT

Estimation of liquefaction resistance, also called Cyclic Resistance Ratio (CRR) of soil, is an important aspect of geotechnical earthquake engineering; it is one of the most important secondary effects of earthquake which causes severe damages to engineering structures. The liquefaction potential is estimated in terms of factor of safety (FS). The present study involves evaluation of liquefaction potential of soil in the Ahmedabad city area, which dominantly consists of sandy to silty sediments and is witnessing significant constructional activities in recent times. Standard Penetration Test (SPT) data from 23 boreholes are collected for analysis. The SPT N-values were corrected for the estimation of CRR. Results of the study indicate that the soil in Ahmedabad city area is much compact, water table is much low and SPT- N values are high, which imply that liquefaction potential is much low. However, it is advisable to perform site specific detailed geotechnical investigation in case of high rise structure and or heavy engineering structures.

Key words: Geotechnical, SPT N-value, Cyclic Resistance Ratio (CRR), Cyclic Stress Ratio (CSR), liquefaction susceptibility, Factor of Safety (FS).

INTRODUCTION

Liquefaction is a phenomenon wherein a mass of soil loses a large percentage of its shear resistance when subjected to cyclic loading induced by earthquakes and flows like a liquid (Sladen et al., 1985). The phenomenon of liquefaction of soil has been brought to the attention of researchers after the great Niigata (1964) and Alaska (1964) earthquakes. It is a phenomenon in which the strength and stiffness of a soil is reduced by earthquake shaking. Liquefaction and related phenomenon have been responsible for tremendous amounts of damage due to earthquakes around the world (Yanagisawa, 1983; Borcherdt, 1991; Morales et al., 1995). Many structures, foundations and slopes did experience failures due to liquefaction during the earthquakes of Dhubri, Assam (1930), Bihar-Nepal (1934), Niigata (1964), San Fernando (1971), Tangshan (1979), Loma Prieta (1989), Kobe (1995), Koyna (1995), Turkey (1998), Chi-Chi, Taiwan (1999), Bhuj (2001), and the Great East Japan earthquake (2011).

India and its surrounding regions have witnessed large earthquakes in the recent past like Muzaffarabad (2005), Sumatra (2004), Bhuj (2001) and Nepal (2015). Such earthquakes have caused great destruction and damages to both low rise and high rise buildings and other engineering structures. The Kachchh rift basin in Gujarat region witnessed the 2001 large earthquake (Mw7.6) which caused widespread liquefaction, ground failures, huge damages and loss of lives (e.g. Rao and Mohanty, 2001, Rastogi, 2001, Dubey and Dar, 2015).

Thus, the progressive expansion of safe human settlements requires practical understanding of the impact of possible natural hazards like earthquakes, landslides and subsidence on built environment and necessitates systematic development with minimum risks. The investigation related to the estimation of liquefaction susceptibility of an area is considered to be one of the basic mandatory requirements of systematic planning of urbanization. The Ahmedabad city in Gujarat sate located in the western part of India is an industrial capital with many big petrochemical complexes and scientific organizations and institutes. The city is experiencing great thrust in constructional activities and expanding its settlement area due to increased population and industrialization. In view of the above, it becomes necessary to investigate liquefaction hazard, which is one of the major secondary effects of an earthquake. In the present study, site classification and evaluation of liquefaction potential in terms of factor of safety for different sites in the developed as well as in the developing parts of the Ahmedabad city area are carried out on the basis of SPT N-values (Idriss and Boulanger, 2004). These results are much useful to assess the risk associated with earthquake, which is crucial for ensuring safety of the engineering constructions.

Geology of Ahmedabad city

Ahmedabad is one of the largest cities in India with a population of around 6.2 million (Census 2011). It is located between latitudes N22° 50´ to N23° 10´ and

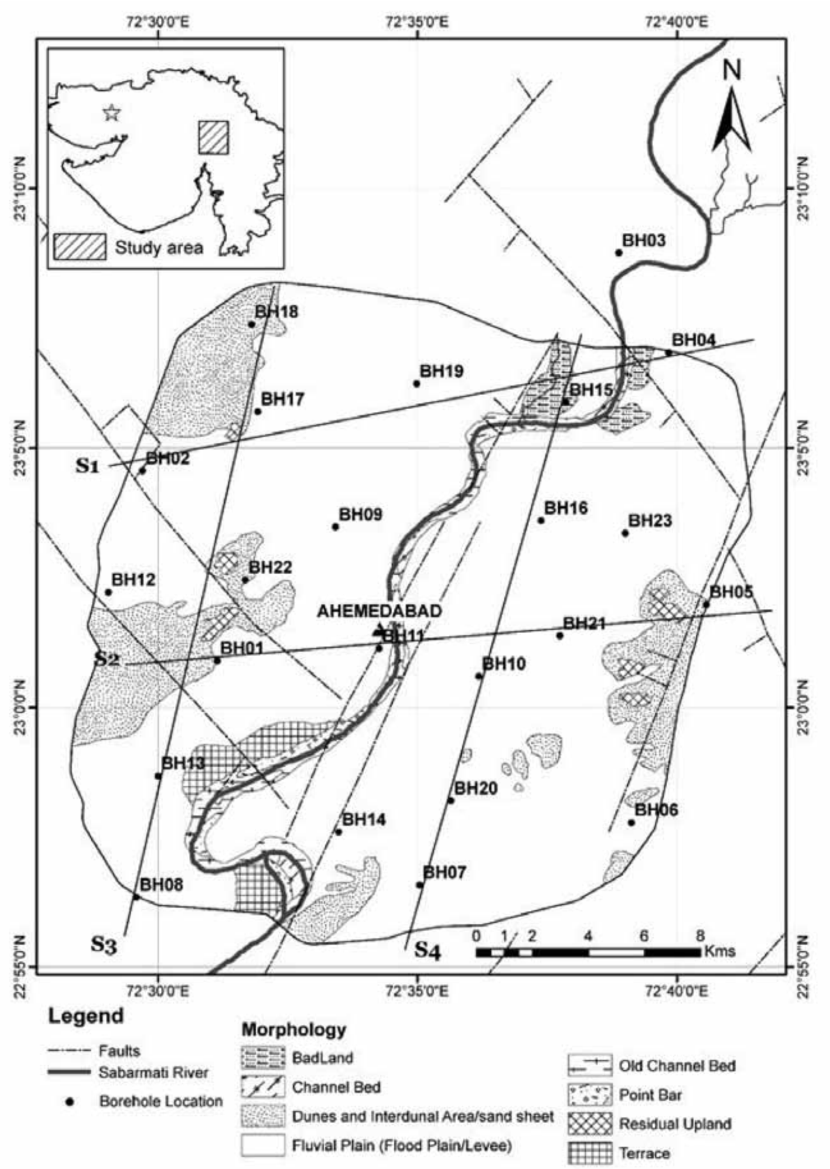

Figure 1. The map shows borehole locations, geomorphic features and selected profiles (S1-S4) in the study area. Inset: Map of Gujarat state, rectangle shows the study area, and the star indicates epicentre of the 2001 Bhuj earthquake Mw 7.7.

longitudes E 72° 26´ to E72° 43´ with an average elevation of 53m from the mean sea level (MSL). It is situated on the thick continental Quaternary sequences of Sabarmati basin, deposited by the erosion of hills of Aravalli mountains (Tandon et al., 1997). The Quaternary succession of the Sabarmati basin consists of conglomerate, sandy and silty soils and can be divided into four stratigraphic subdivisions viz. Waghpur Formation, Sabarmati Formation, Mahesana Formation and Akhaj Formation. The Waghpur Formation is characterized by well sorted fine buff sand, while the Sabarmati Formation is the youngest formation and consists of unconsolidated alluvium derived from Aravalli mountains (Sareen, 1992; Tandon et al., 1997). Geomorphologically, the study area can be divided into residential upland, low land, dune and inter-dunal regions with a few water reservoirs or ponds. The low land regions are further classified into flood plain, bad land, terrace, point bar, channel bar and recent channel. The Sabarmati river flows through the middle of the Ahmedabad city (Figure 1), which dries up in summer leaving only a small stream of water. Topographically, the study area is almost flat in nature except few small hills of Thaltej-Jodhpur Tekra. The average annual rainfall in the study area is 635 mm. According to Bureau of Indian Standards (BIS), the present study area falls under seismic zone III (IS-1893-Part I, 2002). The city has suffered severe damages at some places during the 2001 Bhuj earthquake, although the epicenter was ~250 km away from the main city.

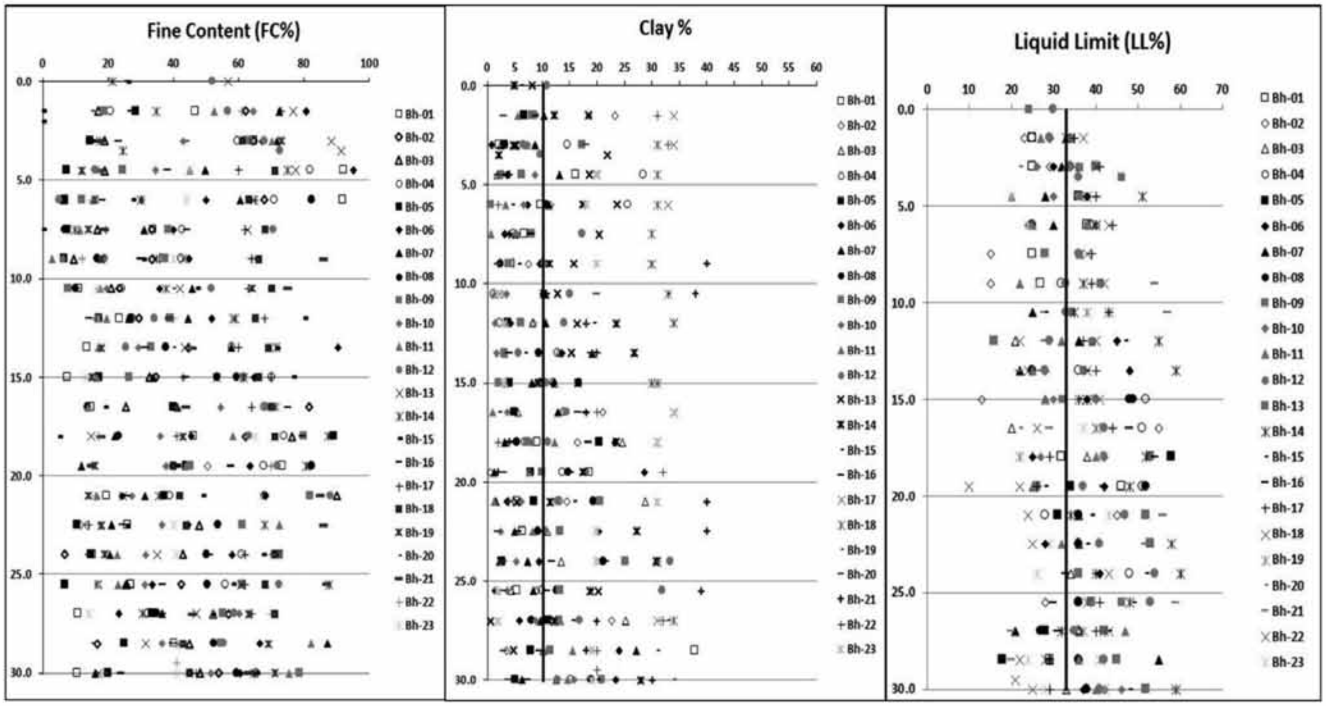

Figure 2. Fine content, clay % and liquid limit.

Geotechnical Investigations

In order to study the subsurface lithological characteristics of the region, a total of 23 boreholes (11 of 80m depth, six of 40m depth and five of 35m depth) were drilled at different locations (Figure 1). During drilling the soil samples, both disturbed and undisturbed, were collected for geotechnical investigation. The standard penetration tests were conducted, as per IS-code, at the depth interval of every 3m in the boreholes. The normalised SPT-N blow counts and lithology were recorded during sampling in the field. The depth of the water table measured during drilling was found to vary between 3m and 50m. Some variations in water table were, however, observed during different seasons, like that in monsoon and in summer. The SPT-N values measured are generally low in the shallow depths. The blow counts greater than 50 are generally encountered at depths of 6m to 9m which indicates that some shallow layers of the study area are prone to liquefaction. The measured SPT-N value N_{SPT}) however, depends on many factors such as hammer types, samplers used, drilling methods, types of rod used during drilling, borehole size, test procedure, etc. (Schmertmann and Palacios, 1979; Kavacs et al., 1981; Farrar et al., 1998; Sivrikaya and Togrol, 2006). Hence, the measured SPT blow count is first normalized for the overburden stress at the depth of the test and corrected to a standardized value of (N1)60. Using the recommended correction factors given by Robertson and Fear (1996), the corrected SPT blow count is calculated using the following equation (1):

$$(N_1)_{60} = N_{SPT} \cdot (C_N \cdot C_E \cdot C_B \cdot C_R \cdot C_S) \ \ldots \qquad (1)$$

where, C_N = overburden correction factor, C_E = hammer energy correction factor, C_B = borehole diameter correction factor, C_r = rod length correction factor, C_s = correction factor for presence or absence of liner in borehole. The corrected N-Value "(N1)60" is further corrected for fine content on the basis of revised boundary curves derived by Idriss and Boulanger (2004) for cohesion-less soils. The fine content corrected SPT-N values, $(N_1)_{60cs}$ were finally used for evaluation of soil liquefaction in the present investigation. The other geotechnical parameters required for the evaluation of soil liquefaction, such as grain sizes, specific gravity, consistency limits, moisture content etc., were determined as per IS code in the geotech laboratory. Fine content (silt and clay) percentage, and liquid limit against depth for all the boreholes were plotted, which suggest that the area has variable soil types with low overall percentage of clay, with an average value of 30% (Figure 2)

Vertical Correlation of Sub-surface lithology

Four cross sections, two east-west (S1, S2) and two north-south (S3, S4), were made for vertical correlation of the subsurface lithology of the study area (Figure 1). The section

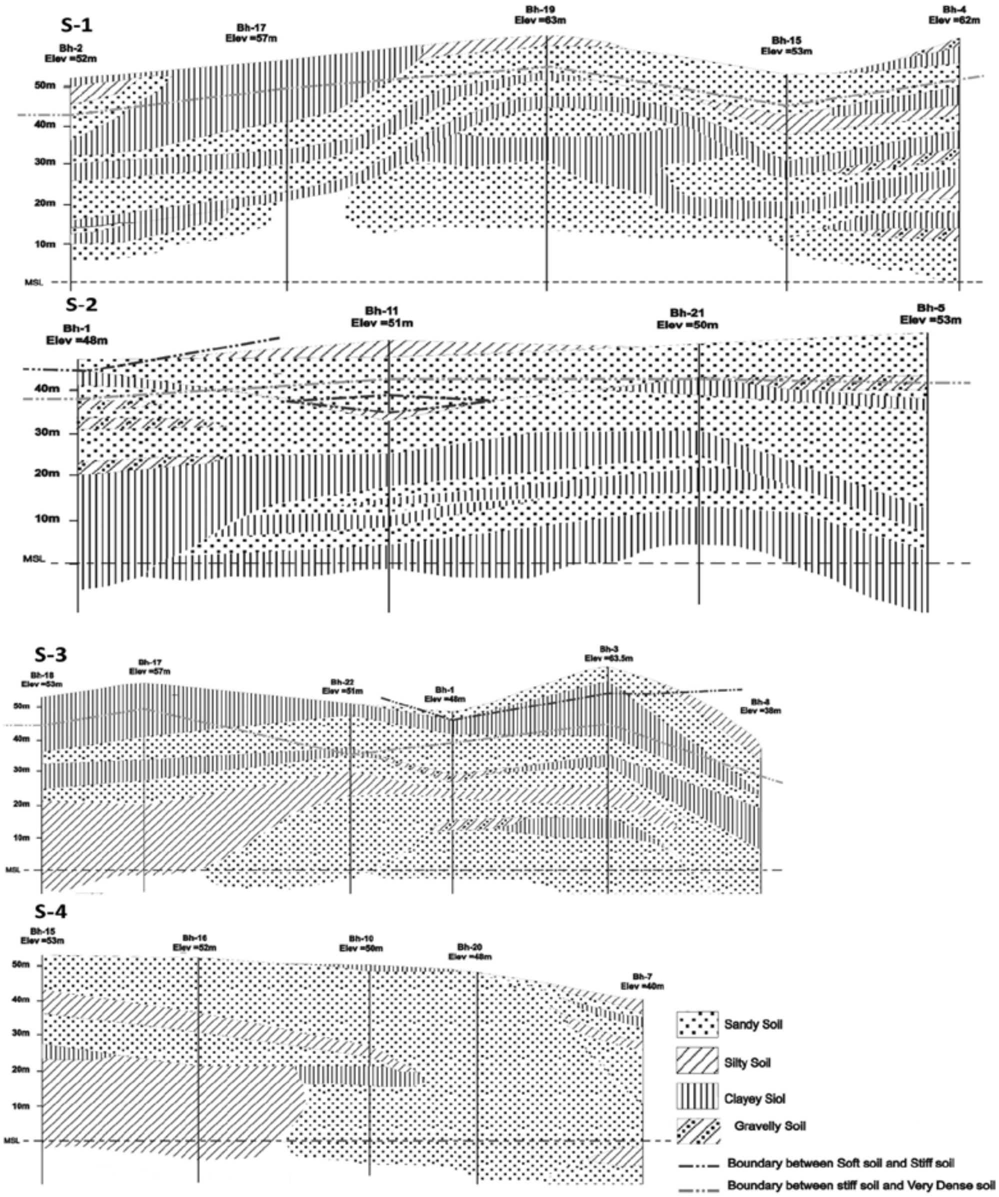

Figure 3. Vertical sections (S1-S4 shown in figure 1) of the sub-surface lithology.

S1 suggests that the subsurface lithology is characterized by fine grained clayey material at the topmost layer, which gets thicker towards the western side down to 15m. Silty soil is found in the middle part of the section with a thickness of 3m. This is followed by a layer of sandy soil with two thin layers of clayey soil. The SPT N-values were found to be greater than 50 blows at an average depth of 9m and at near surface in the eastern most part of the section.

In S2 section, the topmost lithology is characterized by sandy soil, which continued down to the depth of 25m with some lenticular layey and gravelly deposits in the western and eastern corners of the section (Figure 3). The sandy layer overlies a clayey layer, which has two lenticular shape sandy deposits with thickness of 1.5m and 3m present at depths of 30m and 35m, respectively in the middle part of the section. The SPT N-values were found to be greater than 50 blows at an average depth of 10m, while at 15m depth near Sabarmati river, the SPT- blows suddenly decreases to 14, may be due to the presence of thin clayey layer in the section.

In S3 section, the clayey sediment occupies the top layer with a thickness of 20m in the northern part and gets thinner in the middle part of the section (Figure 3). This clayey layer is followed by thick sandy deposits, which continue down to 50m with ~ 6m thick clayey layer and gravelly sediment in the middle part. The SPT N-values were found to be more than 50 blows at an average depth of 9m in northern and southern parts, whereas it was found to be more than 50 blows at a depth of 15m in the middle part of the section.

The S4 section consists of sandy deposits down to 50m with small patches of clay (Figure 3). In the northern part, the sediments are silty. The SPT N-values were found to be greater than 50 blows at an average depth of 6m in northern and at 10m in the southern part.

Liquefaction Evaluation

It is well known that coarse grained sediments i.e. sandy soils are potentially vulnerable to liquefaction. However, liquefaction in fine grained soil especially in silts and silty-clay are major issues in liquefaction assessment. In 1999 the Kocaeli (Turkey) earthquake and the Chi-Chi (Taiwan) earthquake, widespread liquefaction induced damages occurred in cohesive soil sites, which include partial settlements or complete bearing failures of shallow founded structures (Seed et al., 2003).

Liquefaction susceptibility of the fine grained sediments is usually assessed following the procedure of Andrews and Martin, (2000). If the sediments are susceptible to liquefaction then factor of safety against liquefaction is estimated at a particular depth. Seed and Idriss (1971) proposed a simplified procedure, termed as Cyclic Stress Method. In this method, earthquake induced loading, characterized in terms of the Cyclic Stress Ratio (CSR), is compared with the liquefaction resistance represented in terms of the Cyclic Resistance Ratio (CRR). The CSR is calculated using Equation (2):

$$\left(CSR = 0.65\left(\frac{\alpha_{max}}{g}\right)\left(\frac{\sigma_{vo}}{\sigma_{vo}'}\right)r_d\right) \quad \ldots\ldots (2)$$

where, 0.65 (α_{max} /g) = 65% of the peak cyclic shear stress; α_{max} =peak horizontal acceleration at the ground surface generated by the earthquake; g = acceleration due to gravity; σ_{vo} =total overburden stress; $\sigma_{vo'}$ = effective overburden stress; and r_d = stress reduction coefficient. Liao and Whitman (1986) proposed an empirical formulae to estimate average values of r_d.

r_d =1.0 – 0.00765z (for z ≤ 9.15 m), r_d= 1.174 – 0.0267z (for 9.15 < z ≤ 23 m), where, z= depth below ground surface in meters.

The Ahmedabad city area is in zone III as per seismic zoning map of India (BIS 2000), where expected PGA is 0.16g. Trivedi (2011), however, estimated different PGA values for various sites of Ahmedabad city the maximum PGA being 0.19g. Taking note of these values, in the present study we have considered PGA 0.2g and 0.3g for the evaluation of liquefaction.

The CRR is a function of the soil properties and the magnitude of an earthquake. Higher magnitude earthquakes induce more cycles of shaking than lower magnitude earthquakes. Thus larger magnitude earthquakes will induce liquefaction at a lower CSR than a lower magnitude earthquake (Youd and Idriss, 2001). CRR can be estimated using standard penetration test (SPT) as proposed by Idriss and Boulanger (2004).

The value of CRR for a magnitude 7.5 earthquake and an effective vertical stress σ_{vo} =1 atmosphere can be calculated based on (N_1) 60cs using the following equation proposed by Idriss and Boulanger (2004):

$$\text{CRR}= \exp\left\{\frac{(N_1)60cs}{14.1} + \left(\frac{(N_1)60cs}{126}\right)2 - \left(\frac{(N_1)60cs}{23.6}\right)3 + \left(\frac{(N_1)60cs}{25.4}\right)4 - 2.8\right\} \ldots\ldots (3)$$

$$(N_1)_{60cs} = (N_1)_{60} + \Delta N1_{60}$$

$$\Delta(N_1)_{60} = \exp\left[1.63 + \frac{9.7}{FC+0.001} - \left(\frac{15.7}{FC+0.001}\right)(N_1)_{60} = N_c(C_N * C_E * C_B * C_R * C_S)\right.$$

where the various correction factors C_N , C_E ,C_B, C_S ,C_R are as explained at equation 1 earlier and FC is fine content. The results of the liquefaction assessment are presented in terms of factor of safety (FS) against liquefaction:

$$\text{FS}= (\text{CRR7.5/ CSR})\ \text{MSF} \quad \ldots\ldots\ldots\ldots. (4)$$

CRR curves represent the liquefaction susceptibility for a magnitude of 7.5. Therefore, the factor of safety is multiplied with a magnitude scaling factor (MSF). Various values of MSF have been proposed based on empirical data (Youd et al., 2001). In the present study, MSF value 1.32 for M 6.0 suggested by Seed and Idriss (1982) is used for the analysis.

The evaluation of liquefaction of Ahmedabad city zone was performed in 23 boreholes with 138 blows data for PGA 0.2g and 0.3g down to depth of 20m. The layers having corrected SPT N-values greater than 50 were considered as non- liquefiable. In the present study, three different classes of liquefiable status were provided based on the factor of safety. Factor of safety (FS) less than 1 at particular depth was classified as liquefiable (Seed and Idriss, 1971), FS between 1 and 1.2 as marginally liquefiable and FS greater than 1.2 as non- liquefiable (Ulusay and Kuru 2004; Seed and Idriss, 1982).

The results obtained from liquefaction evaluation are assessed as (i) CSR vs. $(N_1)_{60cs}$ and (ii) factor of safety with depth (Figures 4 and 5). The CSR with $(N_1)_{60cs}$ defines the liquefiable condition as per Youd et al., (2001) guidelines. Samples which are liquefiable fall on the right side of the curve (FC=35%) and are composed of sandy and silty soil with intermediate to low plasticity. Marginally liquefiable samples fall between the curves of FC= 35% and FC≤ 5%. The samples falling on the left side of the curve (FC≤ 5%) are classified as non-liquefiable. In the present study out of 138 SPT- samples, for PGA value 0.2g, only two samples are found marginally liquefiable, and remaining non- liquefiable. About 97% of the investigated samples from different depths show non-liquefiable potential and only 3% are marginally liquefiable. For PGA value 0.3g,

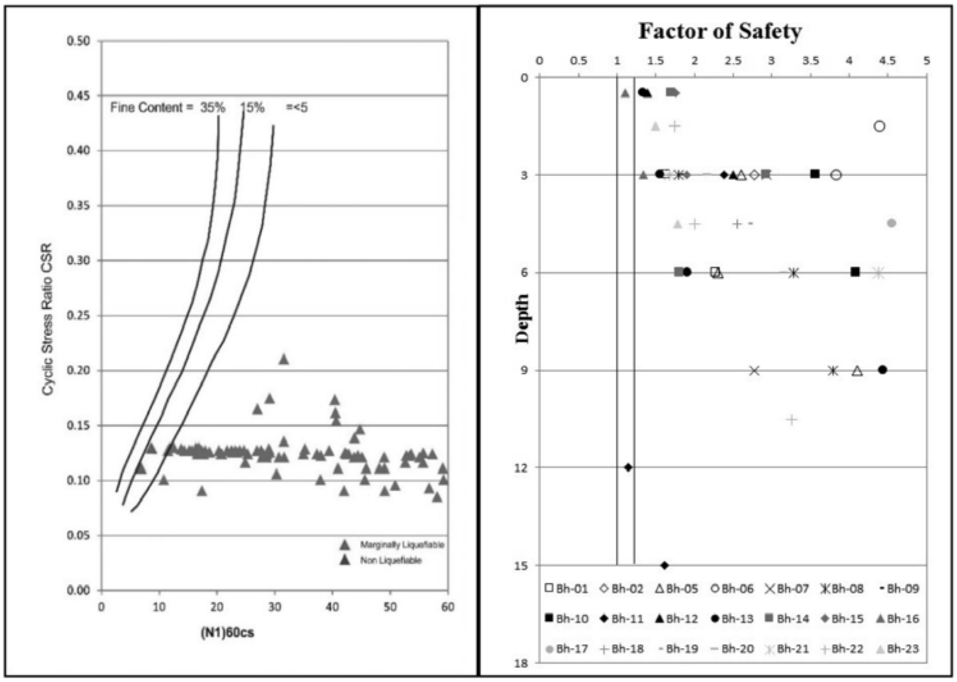

Figure 4. Plot showing CSR/$(N_1)_{60cs}$ and factor of safety against liquefaction for 0.2 g.

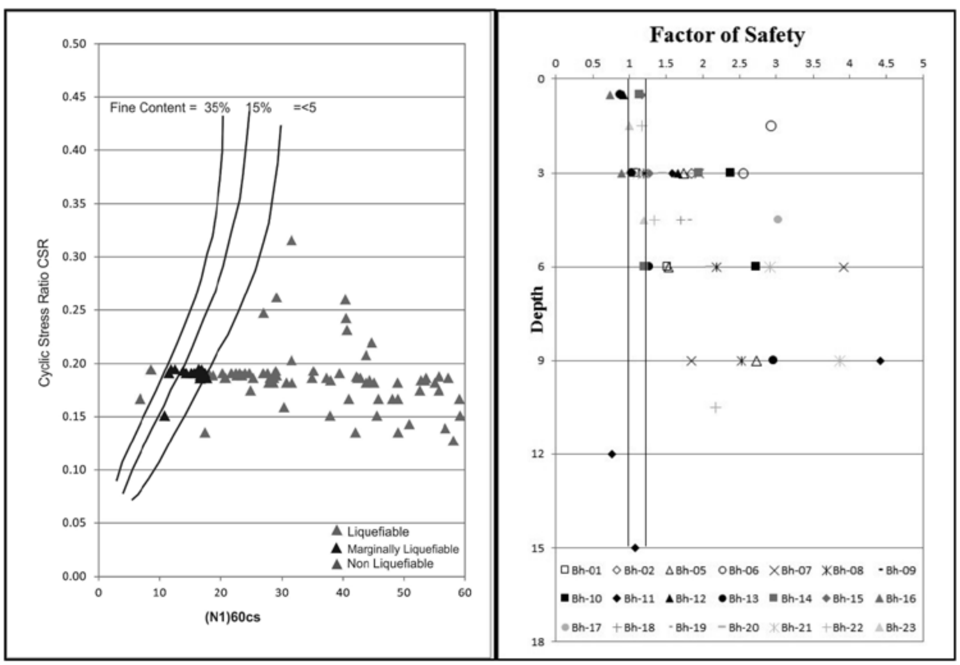

Figure 5. Plot showing CSR/$(N_1)_{60cs}$ and factor of safety against liquefaction for 0.3 g.

two samples are found liquefiable, nine are marginally liquefiable and remaining are non-liquefiable. About 90% of the investigated samples from different depths show non-liquefiable potential with only 8% as marginally liquefiable and only 2% liquefiable. The plot of factor of safety against liquefaction with depth shows that the area has high SPT N-values. Since, the N- values are high, the estimated FS for most of the samples were also relatively high. Liquefiable layers are found at depths of 12m and 15m with FS values of 0.185 and 0.174, respectively. However, marginally liquefiable layers are found down to the depth of 6m and one at 18m. Liquefaction below the depth of 10m is not expected since the sediments below this depth have higher relative densities.

Table1. Estimated factor of safety for PGA 0.2g and 0.3g at different boreholes.

Liquefaction Borehole No.	Depth of Liquefiable layers (m)	Factor of safety		Description	
		0.2g	0.3g	0.2g	0.3g
01	3.0	1.42	1.09	Non Liquefiable	Marginally Liquefiable
08	3.0	1.58	1.09	Non Liquefiable	Marginally Liquefiable
11	12.0	0.69	0.76	Liquefiable	Liquefiable
	15.0	0.93	1.04	Liquefiable	Marginally Liquefiable
13	3.0	1.41	1.04	Non Liquefiable	Marginally Liquefiable
14	6.0	1.12	1.20	Marginally Liquefiable	Marginally Liquefiable
16	3.0	1.19	0.89	Marginally Liquefiable	Liquefiable
21	3.0	1.48	1.11	Non Liquefiable	Marginally Liquefiable
22	1.5	1.75	1.16	Non Liquefiable	Marginally Liquefiable
23	1.5	1.5	1.01	Non Liquefiable	Marginally Liquefiable
	4.5	1.3	1.19	Non Liquefiable	Marginally Liquefiable

DISCUSSION AND CONCLUSIONS

The lithological variations delineated from 23 boreholes suggest that the Ahmedabad city area consists of different layers of gravel, sand and silty-clay. The sediment layers encountered in the boreholes have shown distinct variations in their thickness and shapes from location to location. The top six layers of five boreholes are found susceptible to liquefaction of which one borehole shows liquefiable potential and six of them show marginally liquefiable potential for PGA 0.3g. For PGA of 0.2g, no layer shows factor of safety less than 1.0 i.e. liquefiable, two layers show factor of safety between 1.0-1.2, i.e. marginally liquefiable (Table 1). Liquefaction in these layers may occur due to the presence of sandy-soil in the Clayey Sand (SC) layers. Besides, the water table is found at low levels except in boreholes BH08, BH07 and BH20 where it is at 3.5m, 5.2m and 6m, respectively. It is observed that the liquefiable layers are mostly confined to the central part of the city. Liquefaction is not observed below 10m due to the compaction and fine contents except in BH-11 at the depth of 12 m for PGA 0.2g and at depth 12m and 15m for PGA 0.3g at BH-11.

A total of eight layers at five different boreholes were found to be susceptible to liquefaction; out of which six comprises of top layers (down to 10 m depth). It can be concluded that the study area is marginally liquefiable at six layers in two boreholes in the western part, two boreholes in the eastern part and one borehole in the central part.

The different parameters analyzed in the present study indicate high compaction and presence of low water-table which give high SPT N-value and less liquefiable layers. Hence, it can be concluded that the study area is safe for construction activities. However, detailed site specific geotechnical investigations are required in case of high-rise constructions and heavy engineering structures.

ACKNOWLEDGEMENTS

The authors are grateful to Dr. M. Ravi Kumar, Director General, Institute of Seismological Research (ISR), Gandhinagar, Gujarat, India for his kind support and encouragement for doing this research work. The second author is thankful to the Director, Indian School of Mines, Dhanbad-826004 for his kind support and encouragement. The study was supported by the Ministry of Earth Sciences under the project MoES/P.O.(Seismo)/1(41)/2009. Thanks are due to Prof.J.R.Kayal for constructive review and suggestions. They also thank Prof.B.V.S.Murty for editing the manuscript. We thank the Chief Editor for his support and encouragement.

Compliance with Ethical Standards

The authors declare that they have no conflict of interest and adhere to copyright norms.

REFERENCES

Andrews, D.C.A., and Martin, G.R., 2000. "Criteria for Liquefaction of Silty Soils", Proc. 12th WCEE, Auckland, New Zealand.

Borcherdt, R.D., Wentworth, C.M., Glassmoyer, G., Fumal, T., Mork, P., and Gibbs, J., 1991. On the Observation, Characterization, and Predictive GIS Mapping of Ground Response in the San Francisco Bay Region, California, Proc of 4th International Conference on Seismic Zonation, v.3, pp: 545-552.

Dubey, R.K., and Dar, J.A., 2015. Geotechnical susceptibility constraints on seismicity of Karewa Group and its implication in Quaternary earthquakes around Kashmir Valley, India. Geotech Eng and Geol Eng (in Press)., pp: 1-13.

Farrar, J. A., Nickell, J., Alien, M. G., Goble, G., and Berger, J., 1998. Energy loss in long rod penetration testing. Terminus

Dam liquefaction investigation, proceeding of the ASCE specialty conf. on Geotechnical Earthquake Engineering and soil dynamics in Seattle, v.75, pp: 554-567.

Idriss, I. M., and Boulanger, R. W., 2004. "Semi empirical procedure for evaluation liquefaction potential during earthquake" Proceeding joint conference, The 11th International conf. of soil dynamics and earthquake engineering (SDEE), the 3rd international conf. on Earthquake Geotechnical Engineering (ICEGE), Berkeley California. pp: 32-56.

IS 1893: Part 1 2002. Criteria for earthquake resistant design of structures – Part 1: General provisions and buildings. Bureau of Indian Standards, New Delhi Japan Road Association (2002) Specifications for Highway Bridges, Part V Earthquake Resistant Design

Kovacs, W. D., Salomone, C. A., and Yokel, F. Y., 1981. Energy measurement in the Standard Penetration Test U. S. Department of Commerce and National Bureau of Standards, Washington. D.C.

Liao, S. S. C., and Whitman, R. V., 1986. A catalog of liquefaction and non- liquefaction occurrences during earthquakes. Research Report, Department of Civil Engineering, Massachusetts Institute of Technology, Cambridge, Mass.

Morales, E.M., Tokimatsu, K., Kojima, H., Kuwayama, S., Abe, A., and Midorikawa, S., 1995. 'Liquefaction-induced damage to buildings in 1990 Luzon earthquake; discussion and closure', Journal of Geotechnical Engineering, v.121, no.5, pp: 453–454.

Rao, K.S., and Mohanthy, W.K., 2001. The Bhuj Earthquake and Lessons for the Damages, IGS Newsletter, v.33, pp: 3-10.

Robertson P.K., and Fear. C. E., 1996. "Soil liquefaction and its evaluation based on SPT and CPT: Paper presented at NCEER Workshop on Evaluation of Liquefaction Resistance, Jan. 4-5, 1996, Salt Lake City, Utah.

Rastogi, B. K., Gupta, H., Mandal, P., et al., 2001. "The deadliest stable continental region earthquake occurred near Bhuj on 26 January 2001", Journal of Seismology (2001)5:609. October 2001, v.5, pp: 609–615

Schmertmann, J. H., and Palacios, A. V., 1979. Energy dynamics of SPT J. Geotech Eng. Div. v.105, no.8, pp: 909-926.

Seed, H. B., and Idriss, I. M., 1982. Ground Motions and Soil Liquefaction During Earthquakes. Monograph, Earthquake Engineering Research Institute, Berkeley, California, v.134, no.5.

Seed, H.B., and Idriss, I.M., 1971. Simplified procedure for evaluation of soil liquefaction potential. Journal of the soil mechanics and foundation division, v.97, no.9, pp: 1249-1273.

Seed, R. B., Cetin, K. O., Moss, R. E. S., Kammerer, A. M., Wu, J., Pestana, J. M., Riemer, M. F., Sancio, R.B., Bray, J.D., Kayen, R. E., and Faris, A., 2003. "Recent Advances in Soil Liquefaction Engineering: A Unified and Consistent Framework", 26th Annual ASCE Los Angeles Geotechnical Spring Seminar, Keynote Presentation, H.M.S. Queen Mary, Long Beach, California, April 30, 2003.

Sivrikaya, O., and Togrol, E., 2006. Determination of undrained strength of fine grained soil by means of SPT and application in Turkey. Eng. Geol., v.86, no.1, pp: 2-69.

Sladen, J. A., Holeander, R. D., and Krahn, J., 1985. The liquefaction of sands- a collapse surface approach; Canadian Geotechnical Journal., v.22, pp: 564-578.

Tandon, S. K., Sareen, B. K., Rao, M. S., and Singhvi, A. K., 1997. Aggradation history and luminescence chronology of Late Quaternary semi-arid sequences of the Sabarmati basin, Gujarat, western India; Palaeogeography Palaeoclimatology Palaeoecology., v.128, pp: 339-357

Trivedi, S.S., 2011. Soil amplification studies of Ahmedabad region, International Conference on Current Trends in Technology, 'Nuicone – 2011'.

Ulusay, R., and Kuru, T., 2004. 1998 Adana-Ceyhan (Turkey) Earthquake and a Preliminary Microzonation Based on Liquefaction Potential for Ceyhan Town, Natural Hazards 32: 59. doi:10.1023/B:NHAZ.0000026790.71304.32

Yanagisawa, 1983. Damage to structures due to liquefaction in the Japan Sea earthquake of 1983, Disaster, December 1983: DOI: 10.1111/j.1467-7717.1983.tb00833.x.,v.7, no.4, pp: 259–265.

Youd, T. L., Idriss, I.M., Andrus, R. D., Arango, T., Castro, G., Christian, J. T., Dobry, R., Liam finn, W. D., Harder, L. F., Hynes, M. E., Ishihara, K., Koster, J. P., Laio, S. S. C., Marcuson, W. F., Martin G. R., Mitchell J. K., Moriwaki Y., Power M. S., Robertson P. K., Seed R. B., and Stoke, K. H., 2001. " Liquefaction resistance of soil; Summery report from the 1996 NCEER and 1998 NCEER/NSF workshop on evaluation of liquefaction resistance of soil Journal of Geotechnical and Geoenvironmental Engineering, ASCE, v.127, no.10, pp: 817-833.

Youd, T.L., Member, ASCE, Idriss, I.M., Fellow, ASCE, 2001. Liquefaction Resistance of Soils: Summary Report from the 1996 NCEER and 1998 NCEER/ NSF Workshops on Evaluation of Liquefaction Resistance of Soils, J Geotech. and Geoenvironmental Eng., v.27, no.4, pp: 297-313.

J. Ind. Geophys. Union (March 2017)
v.21, no.2, pp: 124-131

A note on the origin of Clinopyroxene megacrysts from the Udiripikonda lamprophyre, Eastern Dharwar Craton, southern India

Ashutosh Pandey, Rohit Pandey, Dinesh Pandit, Praveer Pankaj and N.V. Chalapathi Rao*

Electron Probe Micro Analyzer (EPMA) Laboratory, Department of Geology
Banaras Hindu University, Varanasi-221005 India
*Corresponding Author: nvcr100@gmail.com

ABSTRACT

Abundant sub-rounded to sub-angular and centimeter-sized clinopyroxene megacrysts constitute a conspicuous feature of the Udiripikonda lamprophyre, located in the Eastern Dharwar craton, Southern India. These clinopyroxene megacrysts, at times, are also associated with minor amounts of biotite. The megacrysts lack reaction-rim or any other disequilibrium textures generally displayed by crustal and mantle xenocrysts/xenoliths entrained in such volatile-rich magmas. Cr_2O_3-impoverished (< 0.1 wt%) nature of the clinopyroxene megacrysts preclude them from being chrome-diopside, derived from the disaggregation of upper mantle rocks, and commonly found entrained in kimberlites,. The clinopyroxene megacrysts ($Wo_{47.43-49.20}En_{32.44-33.64}$ $Fs_{13.73-15.03}$; $Ac_{3.32-4.69}$) and associated biotite (Mg#: 0.84- 0.90) are compositionally similar to the clinopyroxene ($Wo_{43.68-47.76}$; $En_{37.47-44.58}$; $Fs_{8.36-12.31}$; $Ac_{2.70-3.38}$) and biotite (Mg#: 0.84- 0.88) occurring as liquidus phases within the host lamprophyre. Clinopyroxene barometry reveals an overlapping pressure estimates for megacrysts (9.8 to 12.4 kbar) and phenocrysts (8.4 to 10.1 kbar). Likewise, the Ti-in-biotite geothermometry also suggests an overlapping temperature range of 957ºC to 1097ºC and 904ºC to 1069ºC for megacrystal suite and phenocrysts respectively at pressure of ~10 kbar. The clinopyroxene ± biotite megacrysts of this study are, thus, inferred to be cognate products which crystallized under high- to medium-pressure conditions during the evolution of lamprophyre magma.

Key words: Clinopyroxene, Megacryst, Lamprophyre, Udiripikonda, Dharwar Craton, Southern India.

INTRODUCTION

Megacrysts (> 1 cm) of discrete minerals such as clinopyroxene, mica, amphibole, ilmenite etc have been documented from deep-mantle derived rock types such as kimberlites, and alkali-basalts (Dawson and Smith, 1977; Wass, 1979; Boyd et al., 1984; Colville and Novak, 1991); but an understanding of their origin remains unclear. A variety of models- ranging from cognate (Boyd and Nixon, 1978; Schulze, 1987) through xenocrystal (Jones et al., 1987; Davies et al., 2001) to metasomatic (Pivin et al., 2009; Kopylova et al., 2009) and even magma-mixing (Brooks and Printzlau, 1978) have been proposed to account the genesis of these megacrysts. Occurrence of megacrysts in general, and those of clinopyroxene in particular, is rare in lamprophyres but nevertheless has been recorded in the literature (see Brooks and Rucklidge, 1973; Praegel, 1981; Larsen, 1981; Neal and Davidson, 1989; Brodie and Cooper, 1989; Jaques and Perkin, 1994). The purpose of this note is to document the occurrence of rare clinopyroxene megacrysts from a lamprophyre dyke from the Udiripikonda, eastern Dharwar craton, southern India, and to deduce their plausible origin from textural relations, chemical composition and pressure-temperature estimations.

GEOLOGICAL SETTING

The lamprophyre of this study was reported by the Geological Survey of India (Ravi et al., 1998) and occurs as ~1 km long and 1.2 m wide N70ºW trending dyke near the village of Udiripikonda (14º49'33.6"N; 77º19'40.6"E). The Udiripikonda lamprophyre intrudes the granite-gneisses (Peninsular Gneissic Complex) of the Eastern Dharwar Craton, southern India (Figure 1A) is located in the Wajrakarur kimberlite field, where tens of kimberlites confined to distinct clusters ranging in age from Mesoproterozoic (ca. 1090 Ma) to Late Cretaceous (ca. 90 Ma) age were reported (Kumar et al., 2007; Chalapathi Rao et al., 2013, 2016). The lamprophyre is melanocratic and is characterized by crustal xenoliths (felsic material of quartz and feldspar derived from the country granitoids). A number of greenish colored megacrysts (Figure 1B) of clinopyroxene varying in size up to 2 cm are conspicuous and widespread in this dyke.

PETROGRAPHY

Petrographic studies show that the host lamprophyre has typical panidiomorphic-porphyritic texture dominated by phenocrysts and microphenocrysts of clinopyroxene,

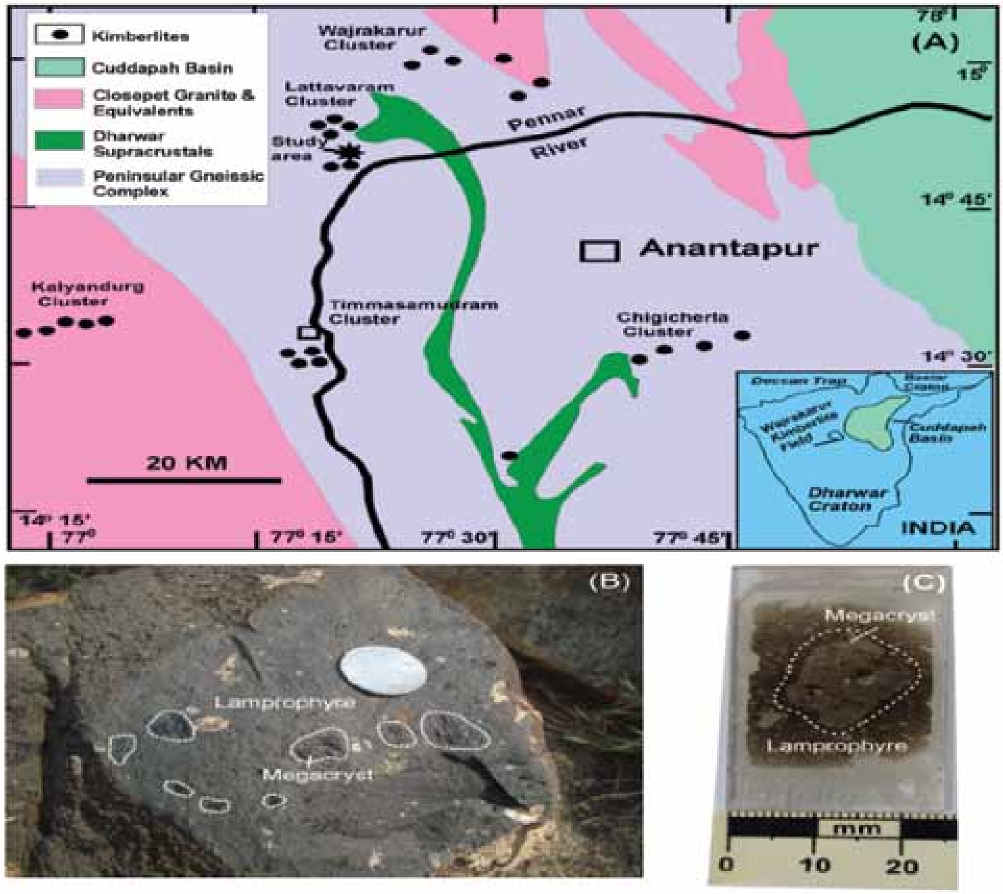

Figure 1. (A) Geological map of the Wajrakarur kimberlite field in the eastern Dharwar Craton, southern India, showing various kimberlite clusters (after Nayak and Kudari, 1999) and location of lamprophyre (Udiripikonda) of this study. (B) Outcrop of the Udiripikonda lamprophyre displaying megacrysts (encircled by white dotted patterns). The diameter of the 2 rupee coin shown is 2.4 cm. (C) An overview photograph of the megacryst in a thin section.

biotite and olivine in a groundmass of feldspar and its bulk-geochemistry classifies it to belong to alkaline lamprophyre variety (cf. Rock, 1991). Detailed petrology and geochemistry of the lamprophyre are beyond the scope of this paper and will be addressed elsewhere. The clinopyroxene megacrysts vary in their shape from sub-rounded to sub-angular, with the former in great majority, and display sharp contacts with the host lamprophyre (Figure 1B and C). Some of the megacrysts are altered but a majority of them are fresh (Figure 2A). None of the studied megacrysts display kelyphitic rims or any other disequilibrium textures displayed commonly by the entrained crustal and mantle xenocrysts/xenoliths in the host magmas. A few of the megacrysts also contain biotite in association with clinopyroxene (Figure 2B) and both of them exclude any effects of deformation.

RESULTS

Mineral chemistry was determined by a CAMECA-SXFive electron microprobe (EPMA) at the Department of Geology, Banaras Hindu University, Varanasi, using wavelength-dispersive spectrometry and a LaB_6 filament. An accelerating voltage of 15 kV, a beam current of 10 nA and a beam diameter of 1 μm along with TAP, PET and LLIF crystals were employed for major elements. A number of natural and synthetic standards were used for calibration. After repeated analyses it was found that the error on major element concentrations is <1% whereas the error on trace elements varied between 3-5%.

EPMA studies revealed the megacrystic clinopyroxene ($Wo_{47.43-49.20}$ $En_{32.44-33.64}$ $Fs_{13.73-15.03}$; $Ac_{3.32-4.69}$) as well as that present as phenocrysts in the host lamprophyre ($Wo_{43.68-47.76}$; $En_{37.47-44.58}$; $Fs_{8.36-12.31}$; $Ac_{2.70-3.38}$) which are essentially diopsidic in nature (see Table 1; Figure 3A). They are all calcic [Ca/(Ca+Mg) >0.49] and magnesian [Mg#: 0.80-0.90] and display a strong overlap in their composition. All of their Cr_2O_3 contents are essentially <0.1 wt% and exclude the compositional field of chrome-diopside megacrysts, which are considered to be either disaggregated fragments of garnet- and spinel-bearing mantle peridotites or even those megacrysts of cognate origin found in

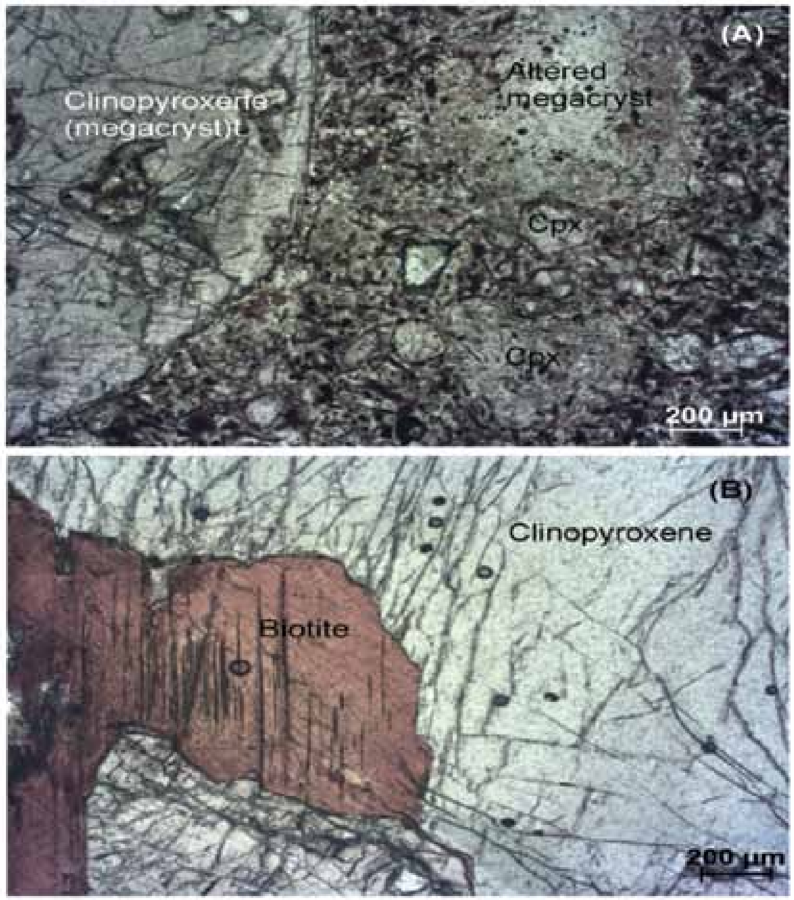

Figure 2. (A) Photomicrographs of the Udiripikonda lamprophyre showing megacrystic and phenocrystic phases of clinopyroxene (cpx) in the host lamprophyre. Note also the presence of an altered megacryst. Plane polarized light; (PP/U1/4). (B) Photomicrograph showing the association of biotite with megacrystic clinopyroxene Plane polarized light; (PP/U1/4).

kimberlites (Figure 3B). The biotite associated with the megacrystic diopside also displays a strong compositional overlap with the phenocrystal biotite in lamprophyre in terms of MgO, FeO, SiO_2, Al_2O_3 and Mg# (0.84 – 0.88) (see Table 2; Figure 4A and B). However, the megacrystic mica is relatively are more enriched in TiO_2, BaO and F contents than those occurring as phenocrysts (Table 2).

Clinopyroxene Geobarometry

Experimental investigation on high Ca-pyroxenes demonstrate that Ti and Al content in clinopyroxene depends on the temperature of crystallization in the range of 1230ºC to 900ºC (Gerke et al., 2005). Ti and Al content in clinopyroxene from the megacrystic suite corresponds to a temperature range of 1000ºC to 900ºC and is indistinguishable with that (1100ºC to 900ºC) of the phenocrystic clinopyroxene in host lamprophyres (see Table 1) with both of them displaying an overlap with the stability field of high Ca-pyroxene (Figure 5A). Occurrence of clinopyroxenes in igneous rocks is also sensitive to the pressure of crystallization (Nimis 1995) and can be applicable to determine the crystallization conditions of alkaline ultramafic magma such as lamprophyres following the clinopyroxene geobarometric formulation of Putirka (2008). Geobarometric calculations based on Putirka [2008, Equation (1) below] using the composition of clinopyroxenes from megacrystic suite and phenocrysts of this study indicate an overlapping range of crystallization pressure between 9.8 to 12.4 kbar and 8.4 to 10.1 kbar, respectively (Table 1).

$$P\ (\text{kbar}) = 3205 + 0.384*(T + 273.15) - 518*\ln(T + 273.15) - 5.62*Mg + 83.2*Na + 68.2*DiHd + 2.52*Al^{VI} - 51.1*DiHd^2 + 34.8*EnFs^2 \quad (1)$$

where T is in ºC; cations in clinopyroxene formula calculated on 6 oxygen basis;

$$Al^{IV} = 2 - Si;\ Al^{VI} = Al - Al^{IV};$$

Jd = Al^{VI} or Na, whichever is less; if excess Al^{IV} remains after forming Jd;

CaTs = Al^{IV} – Jd, if Al^{IV}>CaTs; CaTi = (Al^{IV} – CaTs)/2; CrCaTs = Cr/2;

Table 1. Mineral chemistry (oxide wt%) of the clinopyroxene from the megacryst suite and host lamprophyre of this study. Pressure estimation based on Putirka (2008) in equation (1) at 1000ºC temperature.

	Megacryst suite					Lamprophyre (Phenocrysts)				
	PP/U1/4									
SiO_2	45.40	46.86	46.76	45.12	46.10	45.80	50.21	46.36	46.65	47.22
TiO_2	1.69	2.17	2.32	2.28	1.94	3.12	0.89	2.59	2.39	2.22
Al_2O_3	8.22	8.39	7.79	8.03	8.23	8.57	6.39	8.55	7.86	7.93
Cr_2O_3	0.03	0.08	0.11	0.01	0.01	0.10	0.37	0.03	0.00	0.03
FeO	8.92	8.42	8.38	8.99	8.24	6.77	4.97	7.08	6.62	6.77
MnO	0.26	0.00	0.13	0.06	0.00	0.15	0.05	0.22	0.25	0.04
MgO	10.94	11.06	11.45	10.90	11.23	12.36	14.97	12.37	12.72	12.99
CaO	22.80	21.70	22.04	22.73	22.78	21.78	20.42	21.44	22.06	21.45
Na_2O	0.99	1.19	0.87	1.06	0.85	0.70	0.87	0.90	0.80	0.69
K_2O	0.01	0.04	0.08	0.00	0.01	0.00	0.06	0.00	0.00	0.00
Total	99.26	99.91	99.94	99.18	99.41	99.33	99.21	99.56	99.34	99.33
Cations for 6 oxygen atoms										
Si	1.732	1.759	1.758	1.724	1.744	1.720	1.851	1.737	1.751	1.765
Ti	0.048	0.061	0.066	0.065	0.055	0.088	0.025	0.073	0.067	0.062
Al	0.370	0.371	0.345	0.361	0.367	0.379	0.278	0.377	0.347	0.349
Cr	0.001	0.002	0.003	0.000	0.000	0.003	0.011	0.001	0.000	0.001
Fe_t	0.265	0.264	0.263	0.237	0.261	0.212	0.153	0.222	0.208	0.212
Mn	0.008	0.000	0.004	0.002	0.000	0.005	0.002	0.007	0.008	0.001
Mg	0.622	0.619	0.642	0.621	0.634	0.692	0.823	0.691	0.711	0.724
Ca	0.932	0.873	0.888	0.930	0.923	0.876	0.806	0.860	0.887	0.859
Na	0.074	0.086	0.063	0.078	0.062	0.051	0.062	0.066	0.058	0.050
K	0.000	0.002	0.004	0.000	0.001	0.000	0.003	0.000	0.000	0.000
Total	4	4	4	4	4	4	4	4	4	4
Wo	48.64	47.43	47.78	48.61	49.20	47.76	43.68	46.66	47.43	46.56
En	32.49	33.64	34.54	32.44	33.76	37.72	44.58	37.47	38.04	39.26
Fs	15.03	14.23	14.28	14.85	13.73	11.76	8.36	12.31	11.42	11.48
Ac	3.84	4.69	3.40	4.10	3.32	2.76	3.38	3.55	3.11	2.70
Mg#	0.90	0.80	0.81	0.89	0.85	0.84	0.88	0.85	0.88	0.84
Ca/(Ca+Mg)	0.60	0.59	0.58	0.60	0.59	0.56	0.49	0.55	0.55	0.54
P (kbar)	10.7	12.4	9.8	10.5	9.8	8.4	9.6	10.1	9.0	8.7

DiHd = Ca – CaTi – CaTs – CrCaTs; and EnFs = (Fe + Mg – DiHd)/2;

Ti-in-Biotite Geothermometry

Biotite composition from the megacrystic suite and phenocrystic phase of Udiripikonda lamprophyre are essentially confined to the primary biotite field (see also Figure 5B; Nachit et al., 1985). It has been highlighted before, that TiO_2 content in biotites from megacrystic suite is relatively higher in comparison to phenocrystic biotites from host lamprophyres. Experimental investigations have demonstrated that Ti solubility in mica increases with temperature and decreases with pressure (Robert 1976). As a result, Ti substitution in biotite can be very useful in geothermometric estimation (Henry et al., 2005). Recently, Wu and Chen (2015) proposed Ti-in-biotite geothermometry based on empirical calibration over a wide range of pressure conditions [Equation (2) below].

$$T\ (^{\circ}C) = \mathrm{Exp}[6.313 + 0.224*\ln(X_{Ti}) - 0.228*\ln(X_{Fe}) - 0.499*\ln(X_{Mg}) + 1.5*P] \quad (2)$$

Where P is in kbar; cations in biotite formula calculated on 22 oxygen basis;

$X_Z = Z/(Fe + Mg + Al^{VI} + Ti)$,

Z = Fe, Mg, Ti;

Calculation of Ti-in-biotite geothermometry suggests an overlapping temperature range of 957ºC to 1097ºC and 904ºC to 1069ºC for megacrystic suite and phenocrysts

Table 2. Mineral chemistry (oxide wt%) of the micas from megacryst suite and host lamprophyre of this study. Temperature estimation based on the formulation of Wu and Chen (2015) in equation (2) at 10 kbar pressure.

	Megacryst suite					Lamprophyre (Phenocrysts)				
	PP/U1/4									
SiO_2	34.59	34.07	35.32	33.60	34.89	34.12	32.41	31.55	29.85	31.56
TiO_2	11.89	7.64	7.08	10.19	7.00	4.77	5.89	8.76	7.81	8.07
Al_2O_3	13.28	14.62	13.60	13.92	14.33	13.67	13.77	12.65	12.84	13.73
Cr_2O_3	0.05	0.11	0.09	0.07	0.10	0.00	0.00	0.00	0.00	0.00
FeO	13.96	16.88	18.73	18.37	19.17	21.00	21.02	22.17	21.72	20.86
MnO	0.10	0.00	0.00	0.08	0.06	0.12	0.21	0.46	0.45	0.33
MgO	12.24	10.67	10.14	9.46	9.43	8.06	8.41	7.81	7.90	8.33
CaO	0.20	0.07	0.17	0.10	0.05	0.41	0.63	0.73	3.09	0.38
BaO	0.55	0.73	0.51	0.11	0.18	0.19	0.21	0.14	0.19	0.14
Na_2O	0.49	0.27	0.36	0.29	0.32	0.68	0.20	0.39	0.21	0.31
K_2O	8.24	8.96	8.54	8.22	8.59	7.76	7.68	6.88	6.96	7.46
F	0.42	0.44	0.24	0.09	0.20	0.00	0.00	0.00	0.00	0.06
Total	96.00	94.46	94.80	94.50	94.32	90.80	90.42	91.55	91.00	91.22
Cations for 22 oxygen atoms										
Si	5.186	5.280	5.457	5.190	5.412	5.544	5.315	5.149	4.957	5.136
Al	2.347	2.671	2.476	2.535	2.588	2.456	2.661	2.433	2.513	2.633
Cr	0.006	0.013	0.011	0.008	0.013	0.000	0.000	0.000	0.000	0.000
Al	0.000	0.000	0.000	0.000	0.033	0.162	0.000	0.000	0.000	0.000
Ti	1.340	0.890	0.823	1.184	0.817	0.584	0.727	1.075	0.975	0.988
Fe(ii)	1.750	2.187	2.419	2.373	2.487	2.853	2.882	3.025	3.016	2.838
Mn	0.012	0.000	0.000	0.011	0.008	0.016	0.030	0.063	0.063	0.046
Ba	0.032	0.045	0.031	0.006	0.011	0.012	0.013	0.009	0.012	0.009
Mg	2.735	2.465	2.336	2.178	2.181	1.952	2.055	1.899	1.955	2.020
Ca	0.031	0.011	0.028	0.017	0.008	0.072	0.111	0.127	0.549	0.065
Na	0.141	0.082	0.109	0.086	0.095	0.214	0.063	0.124	0.067	0.097
K	1.576	1.772	1.683	1.619	1.699	1.609	1.607	1.433	1.474	1.549
F	0.197	0.213	0.118	0.046	0.100	0.000	0.000	0.000	0.000	0.033
Total	15.354	15.628	15.491	15.253	15.451	15.475	15.463	15.338	15.582	15.415
Mg#	0.61	0.53	0.49	0.48	0.47	0.41	0.42	0.39	0.39	0.42
T (°C)	1097	988	957	1090	978	904	954	1069	1035	1042

respectively (see Table 2), at a pressure of ~10 kbar, which is obtained from clinopyroxene geobarometry.

Rock (1991) highlighted two important criteria to distinguish between a xenocrystic/xenolithic and cognate origin of the megacrysts found in the lamprophyres: (i) compositional disparity with the equivalent minerals in the groundmass, and (ii) presence of reaction rims or resorption features in case of xenocrysts. A compositional similarity between the megacrystic and liquidus phases and lack of disequilibrium textures rule out a xenocrystic/xenolithic origin of the megacrysts, in this study, and instead imply their genetic relation with the lamprophyre. This is further supported by the fact that the mica reported from mantle-derived xenoliths is typically a phlogopite rather a biotite and absence of any deformation in the megacrysts (see O'Reilly and Griffin, 2013). Note that deformation is a common, but not essential, feature of many of the studied mantle-derived xenoliths and xenocrysts. A cumulate-origin for the megacrysts is also not favoured owing to the strong compositional overlap displayed by the diopsides of the two paragenesis. Pressure-temperature estimates on the clinopyroxene and biotite from megacrysts and phenocrysts (above) reveal their overlapping characteristics. A relative paucity of Ba and F in the groundmass mica (see Table

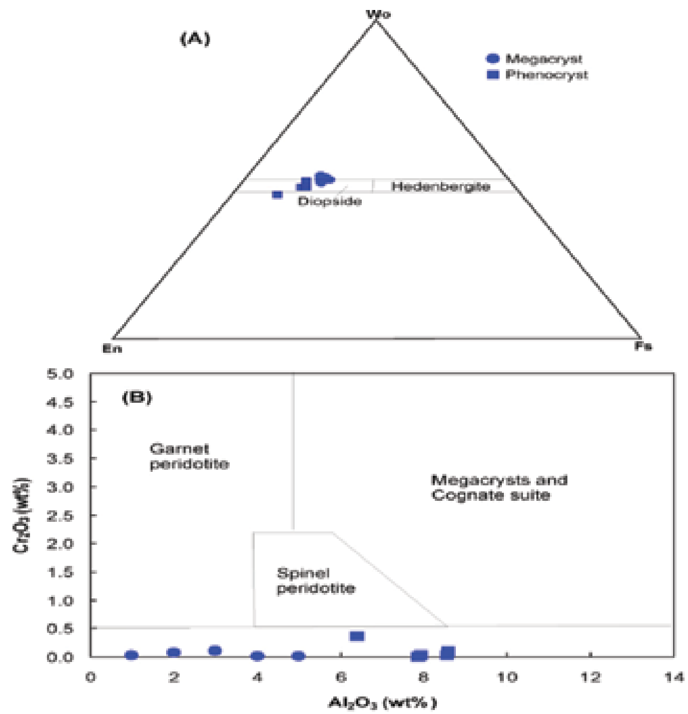

Figure 3. (A) Diopsidic nature of the megacrystic and phenocrystic clinopyroxene in the standard pyroxene ternary plot. Note their compositional similarity. (B) Al_2O_3 (wt%) versus Cr_2O_3 (wt%) of the clinopyroxene megacrysts and phenocrysts of this study in the compositional fields of clinopyroxene xenocrysts, megacrysts and cognate suite found in kimberlites (after Ramsay, 1992). Note the conspicuously lower chromium contents of the megacrysts as well as phenocrysts of this study. Symbols remain the same as in Figure 3A.

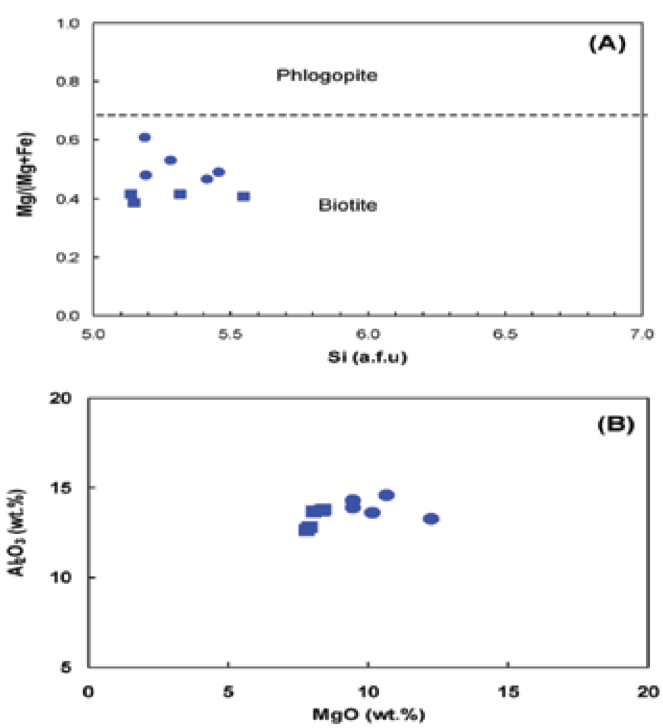

Figure 4. (A) Si (atoms per formula unit) versus Mg/(Mg+Fe) mica classification diagram (after Reider et al., 1998) for the megacrystic and phenocrystic micas from this study. (B) MgO (wt%) versus Al_2O_3 (wt%) binary plot of the biotites of this study showing their overall compositional similarity. Symbols remain the same as in Figure 3A.

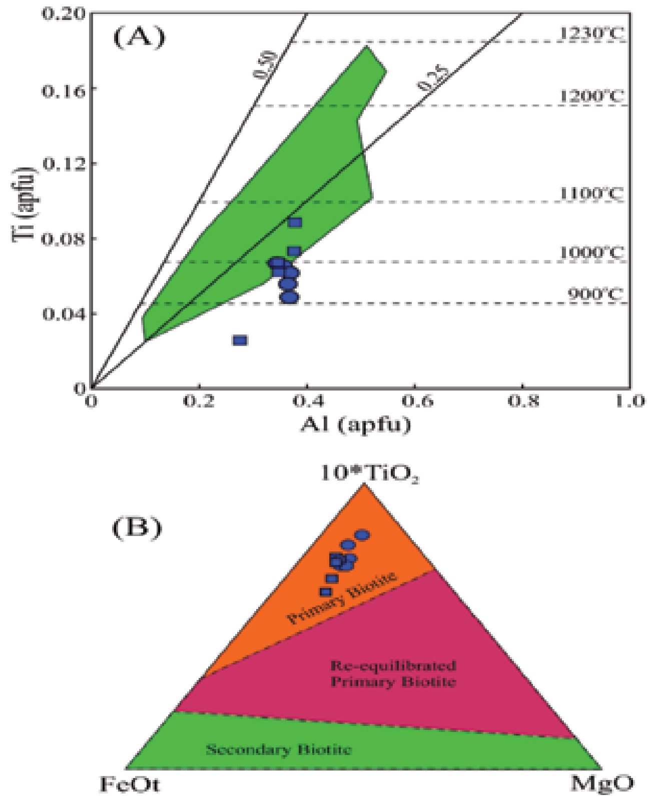

Figure 5. (A) Ti versus Al contents (atoms per formula unit) diagram with the stability field of high Ca-pyroxene (after Gerke et al., 2005) for megacrystic and phenocrystic clinopyroxene from this study. (B) Primary nature of biotite from the TiO_2-FeO_t-MgO triangular diagram (after Nachit et al., 1985) for the megacrystic and phenocrystic micas from this study. Symbols remain the same as in Figure 3A.

2), perhaps, reflects the depletion of these elements in the lamprophyre melt due to their incorporation whilst crystallization of the earlier formed megacrysts. Possible early crystallization of the clinopyroxene megacrysts is also indicated by the sub-rounded nature (Figure 1 and 2) reflecting the abrasion during the ascent of the lamprophyre magma. Further studies, deploying multi-instrumental analytical techniques such as LA-ICP-MS, on these megacrystic nodules from Udiripikonda lamprophyre are required to firmly ascertain and constrain their genesis.

ACKNOWLEDGEMENTS

NVCR thanks Dr P.R. Reddy, Chief Editor, for kind invitation to contribute this manuscript for publication in JIGU. Financial assistance from DST-SERB in the form of a major research project (Project No: IR/S4/ESF-18/2011 dated 12.11.2013) made this study possible. JRFs to AP and RP by CSIR are gratefully acknowledged. DP thanks DST-SERB for a Research Scientist position. Authors are thankful to Prof. B.V.S. Murty for constructive review and apt editing of the manuscript.

Compliance with ethical Standards

The authors declare that they have no conflict of interest and adhere to copyright norms.

REFERENCES

Boyd, F.R., Dawson, J.B., and Smith, J.V., 1984. Granny Smith diopside megacrysts from the kimberlites of the Kimberley area and Jagersfontein, South Africa. Geochim. Cosmochim. Acta v.48, pp: 381-384.

Boyd, F.R., and Nixon, P.H., 1978. Ultramafic nodules from the Kimberley pipes, South Africa. Geochim. Cosmochim. Acta v.42, pp: 1367-1382.

Brodie, C.G., and Cooper, A.F., 1989. Nodule associations from ouachitite and camptonite lamprophyres. Western Otago and south Westland, New Zealand. Geol. Soc. Austral. Spec. Publ., v.14, pp: 545-559.

Brooks, C.K., and Rucklidge, J.C., 1973. A Tertiary lamprophyre dike with high pressure xenoliths and megacrysts from Wiedemanns Fjord, East Greenland. Contrib. Mineral. Petrol., v.42, pp: 197-212.

Brooks, C.K., and Printzlau, I., 1978. Magma mixing in mafic alkaline volcanic rocks: The evidence from relict phenocrystal phases and other inclusions. J. Volcanol. Geoth. Res., v.4, pp: 315-331.

Chalapathi Rao, N.V., Wu, F.Y., Mitchell, R.H., Li, L.Q., and Lehmann, B., 2013. Mesoproterozoic U–Pb ages, trace element and Sr–Nd isotopic composition of perovskite from kimberlites of the Eastern Dharwar craton, southern India: distinct mantle sources and a widespread 1.1 Ga tectonomagmatic event. Chem. Geol., v.353, pp: 48–64.

Chalapathi Rao, N.V., Dongre, Wu, F.Y., and Lehmann, B., 2016. A Late Cretaceous (ca. 90 Ma) kimberlite event in southern India: Implication for sub-continental lithospheric mantle evolution and diamond exploration. Gondwana Res., v.35, pp: 378-398.

Colville, A.A., and Novak, G.A., 1991. Kaersutite megacrysts and associated crystal inclusions from the Cima volcanic field, San Bernardino County, California. Lithos, v.27, pp: 107-114.

Davies, G.R., Spriggs, A.J., and Nixon, P.H., 2001. A non-cognate origin for the Gibeon kimberlitemegacryst suite, Namibia: implications for the origin of Namibian kimberlites. J. Petrol., v.42, pp: 159-172.

Dawson, J.B., and Smith, J.V., 1977. The MARID (mica-amphibole-rutile-ilmenite-diopside) suite of xenoliths in kimberlite. Geochim. Cosmochim. Acta, v.41, pp: 309-323.

Gerke, T.L., Kiline, A.I., and Sack, R.O., 2005. Ti-content of high-Ca pyroxenes as a petrogenetic indicator: an experimental study of Mafic Alkaline Rocks from the Mt. Erebus volcanic region, Antarctica. Contrib. Mineral. Petrol., v.148, pp: 735-745.

Henry, D.J., Guidotti, C.V., and Thomson, J.A., 2005. The Ti-saturation surface for low-to-medium pressure metapelitic biotites: implications for geothermometry and Ti-substitution mechanisms. Am. Mineral., v.90, pp: 316-328.

Jaques, A.L., and Perkin, D.J., 1984. A mica, pyroxene, ilmenite megacryst-bearing lamprophyre from Mt. Woolooma, northeastern New South Wales.J Australian Geol and Geophys, v.9, pp: 33-40.

Jones, R.A., 1987. Strontium and neodymium isotopic and rare earth element evidence for the genesis of the megacrysts in kimberlites of southern Africa. In: P.H. Nixon (Ed) Mantle Xenoliths, John Wiley and Sons, UK, pp: 711-724.

Kopylova, M.G., Nowell, G.M., Pearson, D.G., and Markovic, G., 2009. Crystallization of megacrysts from proto kimberlitic fluids: Geochemical evidence from high-Cr megacrysts in the Jericho kimberlite. Lithos, v.112s, pp: 284-294.

Kumar, A., Heaman, L.A., and Manikyamba, C., 2007. Mesoproterozoic kimberlites in South India: a possible link to 1.1 Ga global magmatism. Precambrian Research. v.154, pp: 192-204.

Larsen, J.G., 1981. Medium-pressure crystallization of a monchiquitic magma-evidence from megacrysts of Drever's block, Ubekendt Ejland, West Greenland. Lithos v.14, pp: 241-261.

Nachit, H., Razafimahefa, N., Stussi, J.M., and Carron, J.P., 1985. Composition chimique des biotites et typologie magmatique des granitoids. Comtes Rendus Hebdomadaires de lÁcademie des Sciences, v.301 no.11, pp: 813-818.

Nayak, S.S., and Kudari, S.A.D., 1999. Discovery of diamond-bearing kimberlites in Kalyandurg area, Anantapur district, Andhra Pradesh.Curr.Sci., v.76, pp: 1077–1079.

Neal, C.R., and Davidson, J.P., 1989. An unmetasomatised source for the Malaitan alnoite (Soloman Island): Petrogenesis involving zone refining, megacryst fractionation, and assimilation of oceanic lithosphere. Geochim. Cosmochim Acta v.53, pp: 1975-1990.

Nimis, P., 1995. A clinopyroxene geobarometer for basaltic systems based on crystal-structure modeling. Contrib. Mineral. Petrol., v.121, pp: 115-125.

O'Reilly, S.Y., and Griffin, W.L., 2013. Mantle metasomatism. In: Harlov, D.E. and Austrheim, H. (Eds) Metasomatism and the Chemical Transformation of Rock, Lecture Notes in Earth System Sciences, DOI 10.1007/978-3-642-28394-9_12., pp: 471-533.

Pivin, M., Femenias, O., and Demaiffe, D., 2009. Metasomatic mantle origin for Mbuji-Mayi and Kundelungu garnet and clinopyroxene megacrysts (Democratic Republic of Congo). Lithos, v.112s, pp: 951-960.

Praegel, N.O., 1981. Origin of ultramafic inclusions and megacrysts in a monchiquite dyke at Streap, Inverseness-shire, Scotland. Lithos, v.14, pp: 305-322.

Putirka, K.D., 2008. Thermometers and barometers for volcanic systems. Rev. Mineral. Geochem., v.69, pp: 61-120.

Ramsay, R.R.,1992. Geochemistry of diamond indicator minerals. Unpublished PhD thesis, University of Western Australia, pp: 246.

Ravi, S., Bhaskara Rao, K.S., and Rao, K.R.P., 1998. Search for kimberlites in the granite-greenstone-terrain in the central segment of Wajrakarur kimberlite field, Anantapur district, Andhra Pradesh. Records. Geol. Surv. India., v.132, no.5, pp: 40-41.

Reider, M., Cavazzini, D., Yakonov Y.S.D., Frank-Kamenetskii, V.A., Gottardi, G., Guggenheim, S., Koval, P.V., Muller, G., Neiva, A.M.R., Radoslovich,E.W., Robert J.L,, Sassi, F.P., Takeda, H., Weiss, Z., and Wones, D.R., 1998.Nomenclature of micas. Can. Mineral., v.36, pp: 905-912.

Robert, J.L., 1976. Titanium solubility in synthetic phlogopite solid solutions. Chem. Geol., v.17, pp: 213-227.

Rock, N.M.S., 1991. Lamprophyres. Blackie, New York, pp: 285.

Schulze, D.J., 1987. Megacrysts from alkali volcanic rocks. In: Nixon, P.H. (Ed) Mantle xenoliths. John Wiley and Sons, UK, pp: 433-451.

Wass, S.Y., 1979. Multiple origins of clinopyroxenes in alkali basaltic rocks. Lithos, v.12, pp: 115-132.

Wu, C.M., and Chen, H.X., 2015. Revised Ti-in-biotite geothermometer for ilmenite or rutile-bearing crustal metapelites. Sci. Bull., v.60, pp: 116-121.

J. Ind. Geophys. Union (March 2017)
v.21, no.2, pp: 124-139

Bedrock Structural Controls on the Occurrence of Sinkholes : A Case Study from Chintakommadinne Area, Part of Cuddapah Basin, South India

M. Prasad[1], M. Ramakrishna Reddy[1] and V. Sunitha*[2]

[1]Dept of Earth Sciences, Yogi Vemana University, Kadapa, Andhra Pradesh
[2]Dept of Geology, Yogi Vemana University, Kadapa, Andhra Pradesh
*Corresponding Author: vangala_sunitha@yahoo.com

ABSTRACT

Heavy precipitation in the Chintakommadinne area in the Y.S.R Kadapa District, Andhra Pradesh during November 2015 has induced ground subsidence resulting in rapid increase in the frequency of 15 sinkhole occurrences. Most susceptible to future sinkhole development, determined by different factors: (1) bedrock type has the most significant impact on predicting sinkhole risk, (2) proximity to faults, lineaments (3) sudden recharge and raise in the groundwater table, and (4) depth of overlying soil to bedrock has an existent yet insignificant effect on sinkhole development. Alignment of sinkholes mainly occurs along strike of bedding. Enhanced rock solution and conduit formation correlates with carbonate units of greater limestone purity and finer grain size, suggesting some lithologic control on karst formation. Density of sinkhole occurrence tends to increase in areas where water-table fluctuations are large. Given the correspondence between geologic structures such as faults, geologic maps showing such structural data are useful tools for predicting future sinkhole occurrence.

Key words: Sinkholes, Structural control, Karst Topography, Buggavanka River, Cuddapah Basin

INTRODUCTION

Sinkholes can be of artificial, natural or combined origin as studied and observed in urban and rural areas in various regions (Beck, 1991; Aisong and Jianhua, 1994; Salvati and Sasowsky, 2002; Williams, 2003; Beck, 2004; Waltham et al., 2005). Sinkhole collapses in urban areas however, may be a man-made result of a forgotten and covered as well as outdated sewer system, of which its real magnitude appears to be a potential risk of unknown proportions. Such sinkholes may be absolutely devastating in the area where they appear and the appearance itself may be with signs or without any warning. Prominent examples of sinkholes appeared in recent years in the United States like the Macungie Sinkhole in 1986 (Dougherty and Perlow, 1988), Daisetta Sinkhole in 2008 (Paine et al., 2009), and in Guatemala City, Guatemala 2007 and 2010 (Hermosilla, 2012) and even in desert areas like in Kuwait (Shaqour, 1994). Man induced sinkholes are associated with the increasing industrialization and urbanization of cities and the intense human economic activity in the investment of the corresponding hydrological systems (Reese et al., 1997; Gutiérrez et al., 2007; Brinkmann et al., 2008; Gutiérrez et al., 2009). Based on significantly high economic damages caused by sinkholes in urban areas, the monitoring and detection with geophysical tools and geographic as well as historic data of sinkholes has recently been a major focus in city planning and hazard prevention (Orndorff and Lagueux, 2000; Lei et al., 2004; Gutiérrez-Santolalla et al., 2005; Gutierrez et al., 2008; Brinkmann et al., 2008; Bruno et al., 2008; Kaufmann and Romanov, 2009; Krawczyk et al., 2012; Margiotta et al., 2012). It is of fundamental interest to society, and authorities, to identify their potential distribution and to prevent the occurrence of further sinkholes, and assess the potential economic damage and loss of lives.

STUDY AREA

The study area lies in Chintakomma Dinne Revenue Mandal of YSR (Kadapa) District of Andhra Pradesh, India as shown in the Figure 1, bounding with latitudes from 14° 20' 41" N to 14° 29' 51"N and longitudes 78° 39' 1.11"E to 78° 56' 37.57"E. In geological point of view this area falls in south western part of Proterozoic Cuddapah Basin. Physiographically this area form part of the Palakonda hills with average rainfall of 700mm. The area of study experiences tropical weather climate with 28-30^0 C during November to January and 40-45^0 C during April-May. Based on the Agro-climatic conditions the District falls both in Southern and scarce rainfall zone.

METHODOLOGY

A systematic approach was made to carry out the present study. Detailed field survey was carried out in the areas where the sink holes were distributed and all the location information were collected by using Global Positioning

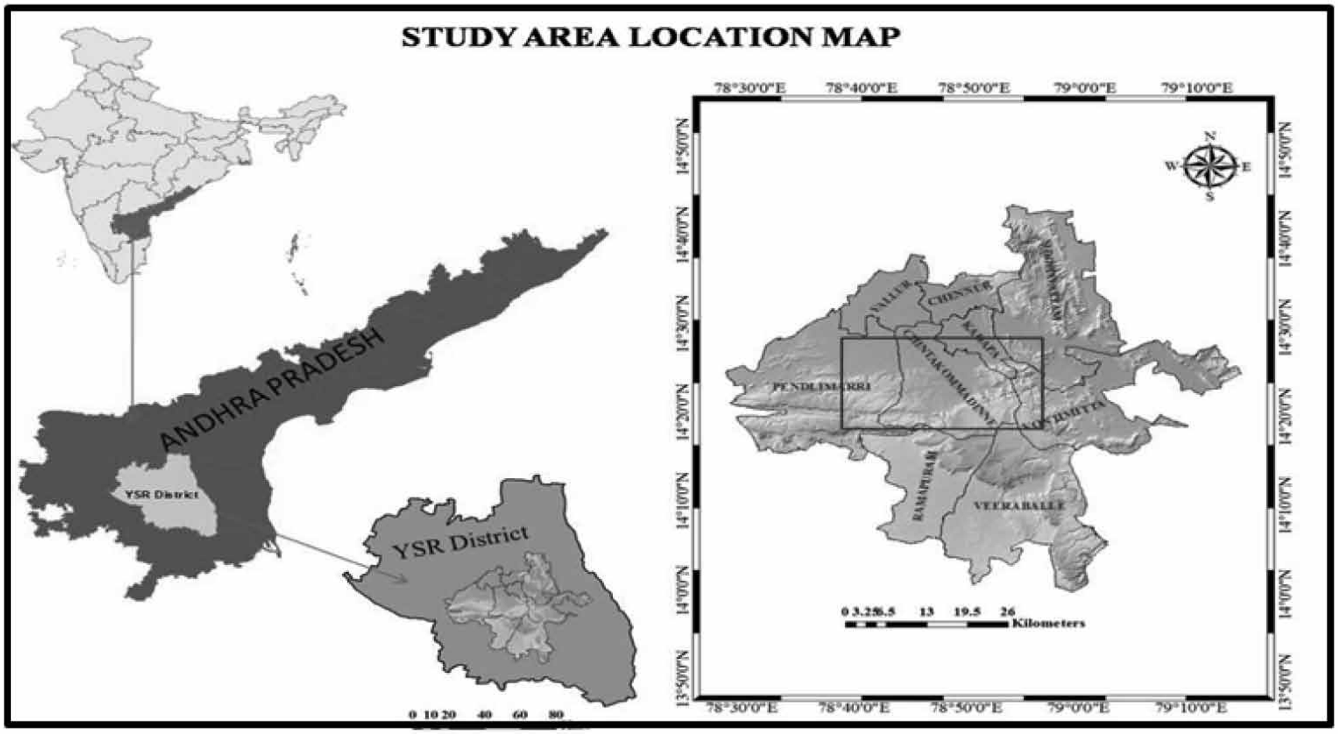

Figure 1. Location map of the study Area.

System (GPS) and SOI Toposheet No: 57J/11 and 57J/15. The GPS points were imported to Google earth software. Identification of closed depressions was aided through the use of Google Earth data, and these locations were compared with the GPS Data. These compared sink holes locations were exported to ArcGIS10 software. Digital Elevation Model was constructed by using SRTM DEM. These sink holes data were added as layer file within a Geographic Information System (GIS), Identified depressions were field-checked. The thematic layers of information viz. DEM, Geology map and sink hole location data permitted the qualitative observations between sinkholes and geologic structure.

RESULTS AND DISCUSSIONS:

Lithological control

Karst topography is the landscape that is formed due to dissolution of soluble rocks like limestone. During the present study the relationship between karst features and geologic structures is well documented. On a large scale, the geologic attributes determine the exposure of a limestones terrain to the karst processes (White et al., 1970). At a medium scale geologic structures determine the flow paths in karst quifers (Parizek, 1976; Nelson, 1988). At a small scale, geologic structures have a significant impact upon the ultimate morphology of conduit systems (Ford and Ewers, 1978; White, 1988; Palmer, 1991). Karst development is characterized by well-developed and integrated underground drainage systems, long segments of losing and disappearing streams, long segments of gaining streams, hundreds of caves, thousands of sinkholes, and dozens of major springs, some of which are world class. The generation of these karstic depressions is related to the dissolution of carbonate and evaporitic rocks. Sinkholes in evaporite karst areas occur worldwide (Klimchouk et al., 1996).

From a geological point of view, the rocky substrata of the study area is mainly constituted by Shales, Lime stones and unconsolidated sediments in the northen part and by Limestone and Quarzites in the southern part (Figure 2). These rock types, belong to different stratigraphic units (Papaghni, Nallamalai and Kurnool groups), are juxtaposed by means of a E-W oriented, Northerly dipping fault boundary. This boundary occurs due to major faulting between the Koilakuntla Limestone and the Quartzite Formations of Kurnool Group and Birankonda (Nagari) formation of Nallamalai group of Cuddapah Supergroup. The major drainage in the study area is Buggavanka River, (Bugga = Spring ; Vanka = Stream) and it is tributary to the Pennar River.

Structural control:

Sinkholes are a common feature used to identify subsurface lineaments or "photo-linears" (Littlefield et al., 1984;

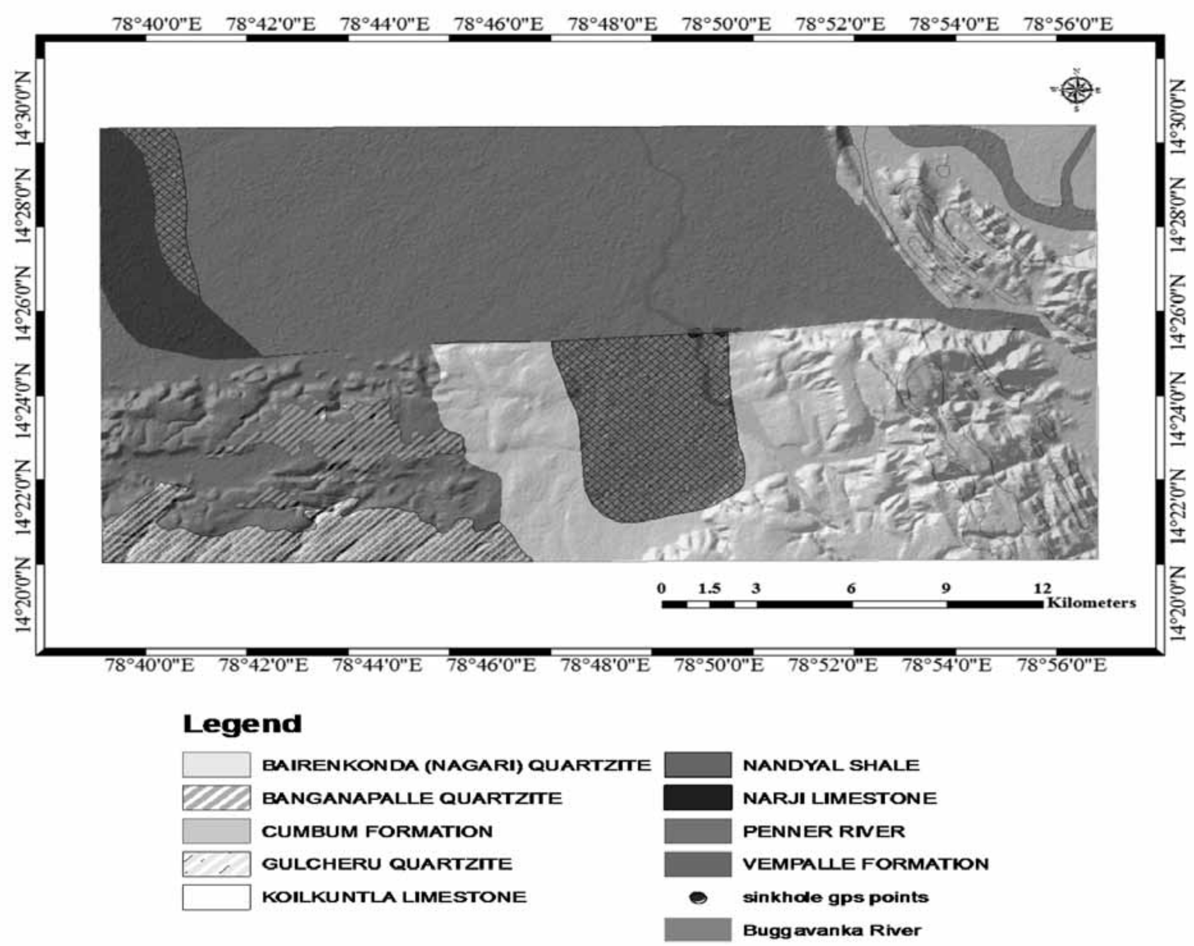

Figure 2. Generalized Geological map showing the various litho units and GPS locations of the sink holes(black circles)in the study area.

Howard, 1968; Kastning, 1983; Orndorff and Lagueux, 2000). Thus, sinkhole alignments are considered an indication of preferential flowpaths for groundwater (Elvrum, 1994; Taylor, 1992). Secondary permeability features, such as fractures, faults, and bedding planes, are frequent in telogenetic limestones, such as those in Kentucky, due to brittle deformation during uplift and exhumation (Vacher and Mylroie, 2002). Fault offsets often produce geologic boundaries for karst development. Irrespective of their origin, these fracture traces play an important role in the direction of groundwater flow (Taylor, 1992). Interestingly, while some sinkholes align with known faults, other faults have no overlying sinkholes, and many sinkhole alignments suggest currently unknown faults or fracture traces (Florea, 2005). Sinkhole GIS data, combined with field reconnaissance, is a proven tool for tracing significant medium-scale structural features in Kentucky (Florea, 2002). Additionally, the ability of the sinkhole GIS data to assist in identifying yet unknown structural features is a valuable resource unanticipated at the beginning of digitization (Florea, 2005).

The complex history of the Cuddapah Basin dates back to the Palaeoproterozoic. It records tectonic events that shaped the SE margin of proto-India from when it became part of Columbia (Saha 2002; Rogers and Santosh 2004; Santosh 2010). N-S trending major fault (around 30 km) in the study area(south western part of the Cuddapah Basin) is the major structure control for the formation of sink holes as shown the figure 3 all the sink holes that are produced along the fault zone, which acts as the boundary between the Nandyal Shale, Koilakuntla Limestone and the Bairankonda Quartzite Formations.

Hydromorphology:

The regional scale analysis indicates that the karst collapse sinkholes are not the mere response to the concurrence of the climatic and lithological conditions which commonly favour the development of karst processes, the occurrence of such landforms appearing strongly influenced by distinctive structural and hydrogeological conditions. These evidences point to the important role played by

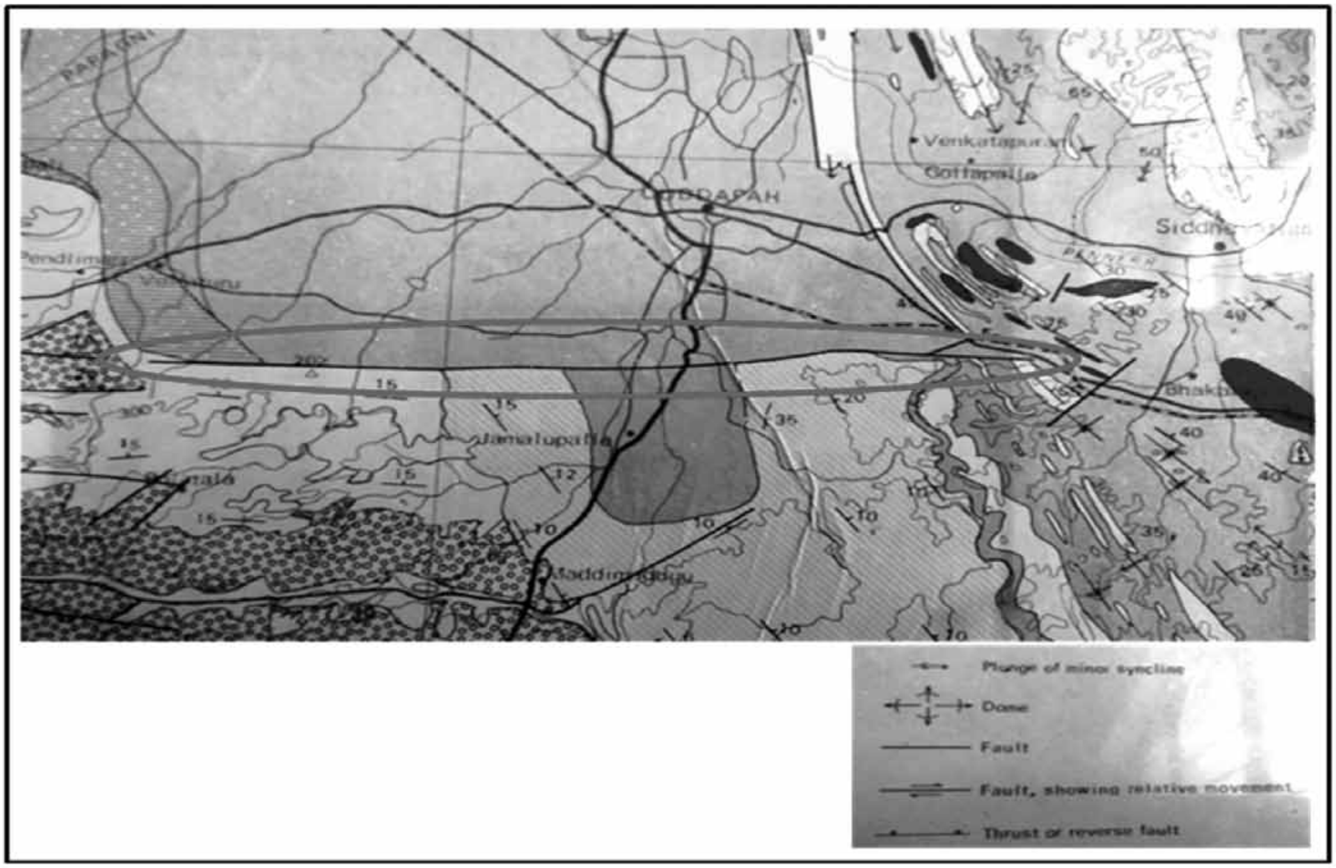

Figure 3. A portion of Geological & Mineral Map of Cuddapah Basin (GSI, 1981) on 1: 2,50,000 Scale. Showing the major fault in the study area (E-W trending dark line in red circle)

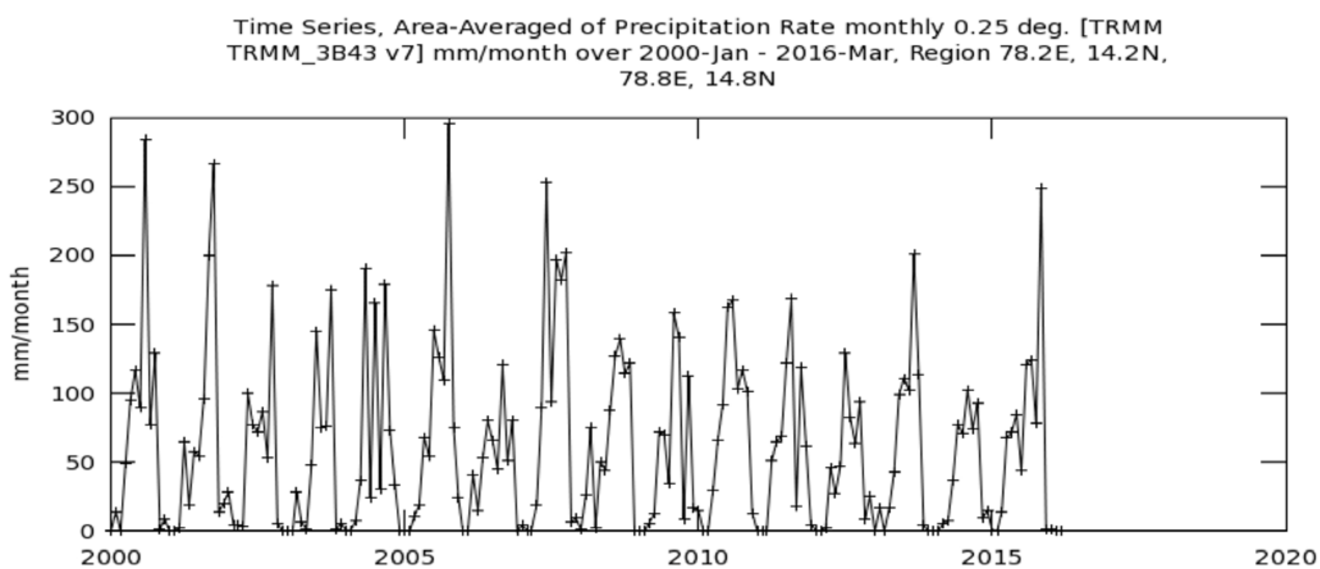

Figure 4. Goddard Earth Sciences Data and Information Services Center 2016. NASA TRMM satellite based time series area averaged map of the study area shwoing the monthly average rainfall from January, 2000 to March, 2016.

Figure 5. A&B: sinkholes in Buggavanka River near Bugga Ramalingeswara temple; C: sinkholes human by induced activity (about 20 feet height overhead water storage tank submerged) F: subsidence due to vegetative stress; E: turbid water from the adjacent bore well; G&H : Collapse ; I: News paper article on sinkholes (Andhrajyothi Telugu Daily 2015).

extensional fault zones in the migration of deeply derived fluids, thus suggesting that active faults, in particular, represent preferential pathways for fluid rising and mixing with shallow groundwater. In addition, a focus on the relationships between karst collapse sinkholes and extensional fault zone properties has shown how the fault length and depth, and the dimension of the damage zone, influence the sinkhole formation and evolution (Antonio et al., 2013).

Shales, quartzites, limestones / dolomites of the Proterozoic Cuddapah basin are the dominant lithounits in the area of present study. Ground water occurs under water table conditions in weathered portion of the formation and the thickness of the weathered portion is around 10 m bgl. Ground water is developed in weathered portion through large diameter dug wells (6m). As the pressure on ground water increases, the water levels were lowered and the yields from dug wells decreased and occasionally dried up in the drought years (CGWB, 2013). Decline in water levels cause loss of support to the bedrock roofs over cavities and to surface material overlying openings in the top of bedrock. Alternate swelling-shrinking and support-withdrawal caused by seasonal fluctuations in water level tend to disrupt the cohesiveness of unconsolidated surfacial material and promote collapse (Williams, 2003; Sinclair, 1982).

Analysis of the causes of the sinkholes

After heavy rain fall during the month of November 2015 (248mm) (Goddard, 2016) as shown in the figure 4 out of 700mm annual average rainfall, around 15 sinkholes were developed in and around Nayanori palle, Balijapalle villages in Chintakomma dinne mandal (The Hindu national daily, 2015). Among these majority of sinkholes were formed with in the Buggavanka River and adjoining areas. Google earth Imagery shows that the locations of sink holes (before and after their formation) along a major fault zone falling in the study area (see Figure 3). These sink holes were filled with groundwater (Figure 5 A & B). By analyzing and integrating geology structures, Remote Sensing data, the rainfall data and CGWB reports, it is concluded that the area was dried up due to prolonged drought caused by scanty rainfall leading to over exploitation of groundwater. Subsequently heavy rain fall in the upstream side of the Buggavanka dam resulted in flooding, there by causing sudden recharge and raise in groundwater table leading to shrinkage of ground along the weak zones controlled by the major fault.

CONCLUSIONS

This study identifies the main triggering factors for the development of land subsidence and sinkhole formation. During the present study it is concluded that around 15 sinkholes were developed in and around Nayanori palle, Balijapalle villages in Chintakommadinne mandal after heavy rain of 248 mm fall during the month of November 2015. The study indicate that Geology, Geomorphology, structural information combined with hydrologic data is crucial for predicting future sinkhole susceptibility. From the analysis conducted in this study, it was found that sinkhole risk was most sensitive in the area underlain by carbonate bedrock in the region where the rock types are mainly limestone and dolomites.

ACKNOWLEDGEMENTS

First author is highly thankful to the Department of Science and Technology (DST-INSPIRE) Govt. of India, for providing INSPIRE Fellowship under AORC Scheme. Thanks are due to Prof.N. Balayerikala Reddy and Dr.V.Raghu for useful suggestions to enhance the quality of the manuscript. They also thank Dr.V.V.Sesha Sai for editing the manuscript. We thank the Chief Editor for his support and encouragement.

Compliance with Ethical Standards

The authors declare that they have no conflict of interest and adhere to copyright norms.

REFERENCES

Aisong, D., and Jianhua, J., 1994. Land subsidence, sinkhole collapse and earth fissure occurrence and control in China. Hydrological Sciences journal, v.39, no.3, pp: 245-256.

Andhrajyothi Telugu daily, Kadapa District edition. 22nd Nov 2015.

Antonio Santo., Alessandra Ascione., Stefano Mazzoli., and Nicoletta, Santangelo., 2013. Structural control on karst collapse sinkhole formation Geophysical Research Abstracts, EGU2013-8197, EGU General Assembly., v.15.

Beck, B.F., 1991. On calculating the risk of sinkhole collapse. In Appalachian Karst. Proceedings of the Appalachian Karst Symposium.

Beck, B.F., 2004. Soil piping and sinkhole failures. In Enyclopedia of caves. White WB (ed). Elsevier: New York; pp: 523–528.

Brinkmann, R., Parise, M., and Dye, D., 2008. Sinkhole distribution in a rapidly developing urban environment: Hillsborough County, Tampa Bay area, Florida. Engineering Geology, v.99, no.3, pp: 169-184.

Bruno, E., Calcaterra, D., and Parise, M., 2008. Development and morphometry of sinkholes in coastal plains of Apulia, southern Italy. Preliminary sinkhole susceptibility assessment. Engineering Geology, v.99, no.3, pp: 198-209.

CGWB, 2013. Central Ground Water Board Ministry of Water Resources, Government of India, groundwater brochure, YSR District (Kadapa), Andhra Pradesh Southern Region Hyderabad.

Dougherty, P. H., and Perlow Jr, M., 1988. The Macungie Sinkhole, Lehigh valley Pennsylvania: Cause and repair. Environmental Geology and Water Sciences, v.12, no.2, pp: 89-98.

Elvrum, C.D., 1994. Relationship of fracture traces and sinkholes to stratigraphy and groundwater in the Inner Bluegrass karst region, Kentucky (MS Thesis), University of Kentucky, Lexington, Kentucky, pp: 138.

Florea, L.J., 2002. Detection of Iapetan rifting (Rome Trough tectonism) by kuaternary karstification: Pulaski County, Kentucky, in Hydrogeology and Biology of Post Paleozoic Karst Aquifers, Karst Frontiers: Proceedings of the Karst Waters Institute Symposium, pp: 192–208.

Florea, L., 2005. Using state-wide GIS data to identify the coincidence between sinkholes and geologic structure. Journal of Cave and Karst Studies, v.67, no.2, pp: 120–124

Ford, D.C., and Ewers, R.O., 1978. The development of limestone cave systems in the dimension of length and depth: Canadian Journal of Earth Science, v.15, pp: 1783–1798.

Goddard Earth Sciences Data and Information Services Center, 2016. TRMM (TMPA) Precipitation L3 1 day 0.25 degree x 0.25 degree V7, version 7, Goddard Earth Sciences Data and Information Services Center (GES DISC), Accessed [Enter

User Data Access Date at] http://disc.gsfc.nasa.gov/datacollection/TRMM_3B42_Daily_7.html (missing in the text)

GSI, 1981. Published Geological and Mineral map of Cudaph Basin (1; 250000), Maps and Cartography Division Geological Survey of India. Bandlaguda, Hyderabad.

Gutiérrez-Santolalla, F., Gutiérrez-Elorza, M., Marín, C., Desir, G., and Maldonado, C., 2005. Spatial distribution, morphometry and activity of La Puebla de Alfindén sinkhole field in the Ebro river valley (NE Spain): applied aspects for hazard zonation. Environmental Geology, v.48, no.3, pp: 360-369.

Gutiérrez, F., Galve J.P., Guerrero, J., Lucha, P., Cendrero, A., Remondo, J., Bonachea, J., Gutiérrez, M., and Sánchez J.A., 2007. The origin, typology, spatial distribution and detrimental effects of the sinkholes developed in the alluvial evaporite karst of the Ebro River valley downstream of Zaragoza city (NE Spain). Earth Surface Processes and Landforms, v.32, no.6, pp: 912-928.

Gutierrez, F., Cooper, A. H., and Johnson, K. S., 2008. Identification, prediction, and mitigation of sinkhole hazards in evaporite karst areas. Environmental Geology, v.53, no.5, pp: 1007-1022.

Gutiérrez, F., Galve, J. P., Lucha, P., Bonachea, J., Jordá, L., and Jordá, R., 2009. Investigation of a large collapse sinkhole affecting a multi-storey building by means of geophysics and the trenching technique (Zaragoza city, NE Spain). Environmental Geology, v.58, no.5, pp: 1107-1122.

Howard, A.D., 1968. Stratigraphic and structural controls on landform development in the Central Kentucky Karst: NSS Bulletin, v.30, no.4, pp: 95–114.

Hermosilla, R. G., 2012. The Guatemala City sinkhole collapses. Carbonates and evaporites, v.27, no.2, pp: 103-107.

Kastning, E.H., 1983. Karstic landforms as a means to interpreting geologic structure and tectonism in carbonate terranes, in Abstracts with Programs - Geological Society of America, v.15, no.6, pp: 608.

Kaufmann, G., and Romanov, D., 2009. Geophysical investigation of a sinkhole in the northern Harz foreland (North Germany). Environmental geology, v.58, no.2, pp: 401- 492.

Klimchouk, A., Lowe, D., Cooper, A., Sauro, U., 1996. Gypsum karst of the World. International Journal of Speleology, v.25, no.3-4, pp: 307.

Krawczyk, C.M., Polom, U., Trabs, S., and Dahm, T., 2012. Sinkholes in the city of Hamburg—New urban shear-wave reflection seismic system enables high- resolution imaging of subrosion structures. Journal of Applied Geophysics v.78, pp: 133–143.

Lei, M. T., Li, Y., Jiang, X. Z., Gan, F. P., and Meug, Y., 2004: Preliminary study on the technology and method of sinkhole collapse monitoring and prediction: As an example of sinkhole collapse monitoring station in Zhemu Village, Guilin City. The Chinese Journal of Geological Hazard and Control, v.15, no.7, pp: 142-147.

Littlefield, J.R., Culbreth, M.A., Upchurch, S.B., and Stewart, M.T., 1984. Relationship of Modern Sinkhole Development to Large-Scale Photolinear Features, in Beck, B.F., ed., 1st Multidisciplinary Conference on Sinkholes, pp: 189–195.

Margiotta, S., Negri, S., Parise, M., and Valloni, R., 2012. Mapping the susceptibility to sinkholes in coastal areas, based on stratigraphy, geomorphology and geophysics. Natural hazards, v.62, no.2, pp: 657-676.

Nelson, J.W., 1988. Influence of joints and fractures upon the hydrogeology of a karst terrane, in Symposium Proceedings of the International Conference on Fluid flow in Fractured Rocks, pp: 432–446.

Orndorff, R.C., and Lagueux, K.M., 2000. Using geographic information systems (GIS) to determine geologic controls on the distribution of sinkholes in the Ozarks of south-central Missouri, in Abstracts with Programs - Geological Society of America, v.32, no.3, pp: 38.

Paine, J. G., Collins, E. W., Wilson, C. R., Buckley, S., and John, A., 2009. Preliminary investigations of subsidence, collapse, and potential for continued growth of the Daisetta Sinkhole, Liberty County, Texas., pp: 17.

Palmer, A.N., 1991. The origin and morphology of limestone caves: Geological Society of America Bulletin, v.103, pp: 1–21.

Parizek, R.R., 1976. On the nature and significance of fracture traces and lineaments in carbonate and other terranes, in Karst Hydrology and Water Resources;, Karst hydrology: V. Yevjevich (ed.), v.1, pp: 47–108.

Reese, A. J., Cantrell, A., and Scarborough, J., 1997. Sinkhole and drainage planning in Johnson City, Tennessee. The Engineering Geology and Hydrogeology of Karst Terranes, pp: 265-271.

Rogers, J. J. W., and Santosh, M., 2004. Continents and Supercontinents. Oxford University Press, Oxford.

Saha, D., 2002. Multi-stage deformation in the Nallamalai fold belt, Cuddapah basin, South India – Implications for Mesoproterozoic tectonism along southeastern margin of India. Gondwana Research, v.5, pp: 701– 719.

Santosh, M., 2010. A synopsis of recent conceptual models on supercontinent tectonics in relation to mantle dynamics, life evolution and surface environment. Journal of Geodynamics, v.50, pp: 116–133.

Salvati, R., and Sasowsky, I. D., 2002. Development of collapse sinkholes in areas of groundwater discharge. Journal of Hydrology, v.264, pp: 1–11.

Shaqour, F., 1994. Hydrogeologic role in sinkhole development in the desert of Kuwait. Environmental Geology, v.23, no.3, pp: 201-208.

Sinclair, W.C., 1982. Sinkhole development resulting from ground-water withdrawal in the Tampa area, Florida. United States Geological Survey Water Resources Division. USGS, WRI, 81-50.

Taylor, C.J., 1992. Ground water occurrence and movement associated with sinkhole alignments in the Inner Bluegrass karst region of Central Kentucky [MS Thesis]: University of Kentucky, Lexington, Kentucky, pp: 113.

The Hindu national daily, December 5, 2015.http://www.thehindu.com/news/national/andhra-pradesh/rain-causing-sinkholes-in-calcreterich-kadapa/article7950559.ece

Vacher, H.L., and Mylroie, J.L., 2002. Eogenetic karst from the perspective of an equivalent porous medium: Carbonates and Evaporites, v.17, no.2, pp: 182–196.

Waltham, T., Bell, F., and Culshaw, M., 2005. Sinkholes and Subsidence. Springer: Chichester. Springer: Praxis

White, W.B., Watson, R.A., Pohl, E.R., and Brucker, R., 1970. The central Kentucky karst: Geographical Review, v.60, no.1, pp: 88–115.

White, W.B., 1988. Geomorphology and Hydrology of Karst Terrains: Oxford University Press, New York, pp: 464.

Williams, P., 2003. Dolines. In Encyclopedia of Caves and Karst Science, Gunn J (ed). Fitzroy Dearborn: New York, pp: 304 –310.

J. Ind. Geophys. Union (March 2017)
v.21, no.2, pp: 140-147

Determination of Urban Dust Signatures through Chemical and Mineralogical Characterization of Atmospheric Dustfall in East Delhi (India)

Anshu Sharma, Saumya Singh and U.C. Kulshrestha*
School of Environmental Sciences, Jawaharlal Nehru University, New Delhi 110067
*Corresponding Author: umeshkulshrestha@gmail.com

ABSTRACT
The fine road dust particles contribute a dominant fraction of ambient concentration of air particulates in urban areas. The road dust carries toxic pollutants such as heavy metals and polyaromatic hydrocarbons (PAHs) etc. exerting a significant influence on air quality. This study is aimed to analyze the chemical, mineralogical and morphological characteristics of the dustfall deposition during the period from November 2013 to February 2014 in east Delhi. The research findings of this study confirm that the vehicular traffic is a significant cause for high deposition flux of the dustfall resulting in a possible health hazard for roadside population. Average dustfall flux was observed to be 310 mg/m^2/day and the average pH of aqueous extract of dustfall samples was noticed as 7.7. SEM results showed the dust particles were irregular in shape representing spherical, rectangular, platy and angular shapes. Their diameter ranged from 1.5-151.5μm. Ca, Si, and Al were the major contributors in dust indicating that the dustfall is weathered material of local rock which consists of calcium aluminum silicates. Other heavy metals such as Zn, Cu contributed primarily from vehicular traffic while Fe, Al, and Mn mainly from suspended road dust. C particles seen in the dustfall samples might be due to interaction of atmospheric dust with industrial and vehicular emissions.

Key words: Road dust, vehicular traffic, SEM-EDX, heavy metals, dustfall.

INTRODUCTION

Dust is one of the leading aerosol types which plays a very significant role in the modulation of atmosphere and climate (Tegen and Fung, 1995; Kulshrestha, et al., 2003b, Singh et al., 2004). Dust aerosols impact the radiation budget of Earth's atmosphere directly by scattering and absorbing solar and terrestrial thermal radiations, and indirectly by changing cloud optical properties and lifetimes (Lacis, 1995; Liao and Seinfeld, 1998). Due to its large active surface area, mineral dust can also affect gas-phase concentrations of ozone, as well as nitrate, sulfate, and the formation of photochemical smog (Underwood et al., 2001; Dentener et al., 1996; Dickerson et al., 1997).

Fine solid particles on road surfaces are also a significant source of air pollution in urban areas (Thorpe and Harrison, 2008; Amato et al., 2009, 2011). Road dust consists of soil minerals, organic matter (derived from vegetation) and potentially toxic pollutants emitted from various anthropogenic sources (Gunawardana et al., 2012; Rogge et al., 1993). Dust particles function as a carrier of other pollutants which is largely dependent on the chemical composition, shape, size, and their sources (McBride, 1994). Traffic-related pollutants include tire and brake abrasion products, combustion exhaust and pavement wear (Rogge et al., 1993; Kreider et al., 2010; Amato et al., 2011). There is an increasing concern about this nano- and micro-sized particles because of their possible adverse effects on the human health and environment (Inoue et al., 2006). Therefore, the present study was carried out to determine the influence and contribution of suspended road dust to the free-falling dust particles through their chemical and morphological characterization at site in east Delhi which represents very typical urban characteristics in north India. This study will be helpful in understanding the sources of dust pollution in order to develop the appropriate strategies for the mitigation of dust pollution, further helping in reducing ambient particulate matter levels in the city.

MATERIAL AND METHODS

Study area

The samples of atmospheric dust were collected at Babarpur (28^{o}41'N and 77^{o}16'E) region, located near Shahdara Industrial Area of east Delhi. The site represents an Industrial-cum-residential zone. As per census of 2011, the population density of this area is estimated to be 36,155 per km^2. The area of study around Shahdara has several industries such as plastic, packaging and metal processing. The area has very high traffic density especially the trucks which are the major sources of the nitrogen dioxide (NO_2) and *sulfur dioxide* (SO_2) in the locality. The site has nearly two busy roads nearby (300 m north and south) running

Table 1. Comparison of dustfall fluxes at worldwide.

Sampling site	Country	Deposition flux ($mg/m^2/day$)	References
Delhi	India	310.3	Present study
Delhi	India	96.6	Kumar et al., (2014)
Jharia coal mining (Commercial)	India	461.8	Rout et al., (2014)
Jharia coal mining (Residential)	India	318.8	Rout et al., (2014)
Miami, Florida	USA	0.7	Prospero et al., (1987)
French Alp	France	5.7	Angelis and Gaudichet, (1991)
Coast Mountain, BC	Canada	29.8	Owens and Slaymaker, (1997)
Namoi Valley	Australia	85.9	Cattle et al., (2002)
Northern Nigeria	Africa	435.2	McTainsh and Walker, (1982)
Guagzhou	China	124.2	Zhao et al., (2010)

east westerly. The sampling was carried out at a residential building located 2km away from Shahdara and about 300 m away from Babarpur bus terminal, which is considered as very busy terminal.

Sample collection and analysis

Dustfall Sample collection:

Dustfall samples were collected in a plastic tray (500 cm^2, polypropylene) which placed on the terrace of the building (about 10 meters from the ground surface) on the basis of 7 days ambient exposure. The sampling was carried out from November, 2013 to February, 2014 (Kumar et al., 2014). The tray was carefully weighted before and after the collection for obtaining the amount of deposited dust. The tray was thoroughly cleaned with high quality deionized water and dried before the collection of next sample. Total four samples were collected during this period, representative of each month. The collected amount of dust samples were wrapped in aluminum foil and stored in refrigerator at 4°C till further analysis.

The total dustfall weight was calculated by the difference of m_1 and m_2, and the dustfall fluxes were calculated by using the following formula (Gupta et al., 2015a):

$$DF = (m_2\text{-}m_1) / A \times d$$

Where DF is the total dustfall flux ($mg/m^2/day$), m_1 is the initial weight of tray, m_2 is the final weight of the tray in mg, A is the surface area of plastic tray (m^2) and d is the number of days for which tray was exposed in the open air.

Chemical Analysis:

0.2g of the sample was transferred to a centrifuge tubes following adding 10ml ultrapure water. The sample was then sonicated for half an hour at 1 Hz in an ultrasonicator in order to extract water soluble components. Finally, the sample was filtered with Whatman 41 filter. Major anions (F^-, Cl^-, NO_3^- and SO_4^{2-}) and cations (Na^+, K^+, NH_4^+, Ca^{2+} and Mg^{2+}) were determined in the aqueous extract of dustfall by Ion Chromatography (Metrohm 883 Basic IC Plus). Details of ionic analysis are given elsewhere (Singh et al., 2014).

Morphological and elemental Analysis:

Surface morphology and elemental analysis of the dust samples were carried out using SEM-EDX (Carl Zeiss AG-EVO 40 Series model). SEM images were taken for identifying the shape and size of dust particles in the sample at different magnifications. More details about the SEM analysis are given in Gupta et al., (2015c).

Quality Assurance and Quality Control (QA/QC)

The quality of sampling and analysis was ascertained by analyzing blank of tray. All the cationic and anionic species had area below the detection limit in the blank. Calibration of methods and quantification of components were carried out using MERCK reference standards (CertiPUR).

RESULTS AND DISCUSSION

Dustfall fluxes at Trans-Yamuna region

Dustfall fluxes varied from 185 to 447 $mg/m^2/day$ with an average flux value 310 $mg/m^2/day$. Kumar and coworkers (2014) have reported an average dustfall flux 95.82 $mg/m^2/day$ at different sites of Delhi. Therefore, these fluxes are considered higher at this site. Such higher fluxes can be attributed to the suspended soil dust, road dust and increasing construction activities (Kumar et al., 2014). In addition, changing land use pattern in urban regions is also a significant source of global atmospheric dust (Tegen and Fung, 1995). Table 1 gives the comparison of dustfall

Table 2. Dustfall flux and pH of aqueous extract.

Sample No.	Sampling duration	Dust Flux ($mg/m^2/day$)	pH
1	01/11/2013-07/11/2013	185	7.9
2	29/11/2013-05/12/2013	446.7	7.6
3	03/01/2014-10/01/2014	182.2	7.7
4	09/02/2014-16/02/2014	427.5	7.6
	Average	310.3	7.7

fluxes at different sites worldwide. It is indicated that the dustfall deposition fluxes are very high at the tropical sites as compared to temperate sites.

pH of dustfall extract

The pH of aqueous extract of dustfall was found to be in the range of 7.55 - 7.96, (Table 2) clearly showing the alkaline nature of atmospheric dust. Such high pH of alkaline atmospheric dustfall extract suggests the dominance of crustal components particularly, the presence of carbonates and bicarbonates of Ca (Kulshrestha et al., 2003a). $CaCO_3$ rich soil of this region contributes to a major fraction of atmospheric dust in Indian region (Kulshrestha et al., 1999; Jain et al., 2000).Very similar range of pH was found at different sites of Delhi (Kulshrestha et al., 2003b).

Chemical characterization of dustfall

Figure 1 shows the variation of dustfall flux and dustfall fluxes of major ions in the samples. Dustfall deposition fluxes mainly depend upon the particle density and the size (Hicks et al., 1986). Higher the mass mean diameter of particles, greater will be their dustfall deposition flux. SO_4^{2-} and NO_3^- particles, which are mainly originated from anthropogenic activities, showed almost rates to those of the soil-derived elements. This suggests the possibility of association with such particles. Variation of Ca^{2+} and Na^+ fluxes is in accordance with dustfall fluxes suggesting that these are originated from soil. According to earlier studies origin of Ca^{2+} has been reported from soil (Kulshrestha et al., 2003b; Kumar et al., 2014). Generally, Ca^{2+}, Mg^{2+}, K^+ are considered as initial components which are found abundant in the atmosphere (Rahn, 1976; Kulshrestha et al., 1998). However, biomass burning and other combustion sources have also been responsible for K^+ emissions (Andrae et al., 1990; Simoneit, 2002). The Na^+ and Cl^- ions are contributed by sea salts as major fraction. However, Na^+ is also contributed by local soils in this region (Lakhani et al., 2007) while Cl^- is also contributed by some industrial units such as combustion of municipal waste, waste incineration, vehicles exhaust etc. (Singh et al., 2014; Moffet et al., 2008).

The fluxes of the major ions decreased in the following order $Ca^{2+} > K^+ > Na^+ > Mg^{2+} > NH_4^+ > SO_4^{2-} > NO_3^- > Cl^- > F^-$ (Figure 2). Among cations, the fluxes of Ca^{2+} were observed to be highest with mean value 3.56 ± 1.16 $mg/m^2/day$ followed by K^+, Na^+, Mg^{2+} and NH_4^+. Relative percentage of Ca^{2+} among major ions is about 59%, which shows the dominance of crustal components, i.e. $CaCO_3$ in dustfall, rich in soil of India region (Kulshrestha et al., 1996; 1998). Fluxes of K^+ and Na^+ were found to be 0.58 ± 0.05 and 0.45 ± 0.13 $mg/m^2/day$, contributing 9% and 7%, respectively. This may be due to their common origin as a crustal component. In coarse mode, K^+ origin is mostly considered from soil dust (Li et al., 2008; Shen et al., 2009) while in fine mode it is contributed by biomass burning (Andrae et al., 1990). Among cations, Mg^{2+} and NH_4^+ have recorded lower fluxes with average mean value 0.23 ± 0.04 (4%) and 0.1 ± 0.07 (2%) $mg/m^2/day$ respectively.

Among the anions, SO_4^{2-} had the maximum fluxes with mean value 0.50 ± 0.32 $mg/m^2/day$ followed by NO_3^-, Cl^-, and F^-. The largest source of sulfate could be the oxidation of sulfur dioxide (SO_2) emitted from the burning of fossil fuels, biomass, coal in thermal power plants and vehicular exhaust (Jain et al., 2000; Gupta et al., 2015b). High levels of NO_3^- (0.42 ± 0.33 $mg/m^2/day$) may be contributed by vehicular emission, as the site was surrounded by two major roads. Cl^- (0.22 ± 0.16 $mg/m^2/day$) may be due to complicated sources such as sea salts, vehicles exhaust, waste disposal or wood burning, etc., (Perrino et al., 2011; Andrea et al., 1990). SO_4^{2-}, NO_3^- and Cl^- contribute about 8%, 7% and 4% respectively of total ions. The alkaline nature of dust in Indian region promotes SO_4^{2-} and NO_3^- scavenging through dry deposition forming secondary aerosols such as $CaSO_4$ and $Ca(NO_3)_2$ (Kulshrestha, 2013; Kulshrestha et al., 2003b).

Morphological observations of Dust

Morphological analysis of the dustfall was carried out using SEM-EDX technique. SEM images revealed that the particles were fine to coarse in size diameter ranging from 1.5 μm -151.5μm. The dustfall was dominated by spherical, irregular, long, tubular, grapes like structure, aggregated and rhombic shape of particles. Images of dust particles with

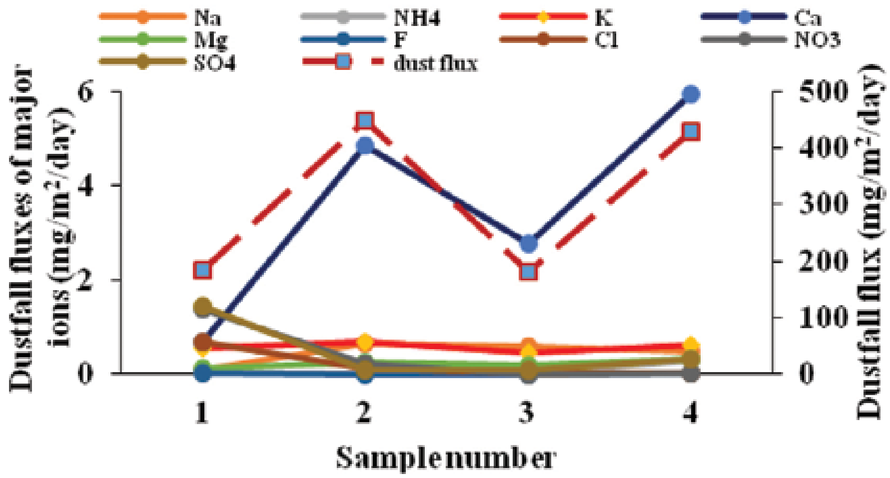

Figure 1. Variation of dust fall flux and major ion fluxes from Nov.2013 to Feb. 2014.

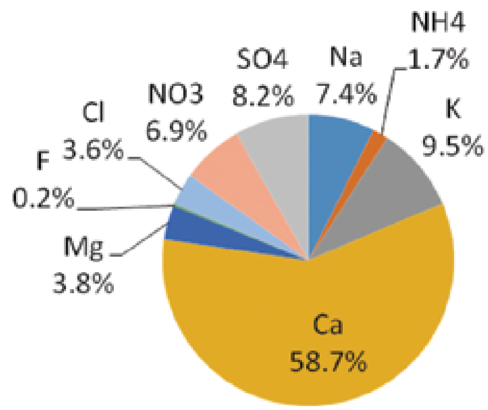

Figure 2. Relative percentage contribution of major ions in dustfall.

different magnifications are shown in Figure 3 (A to I). Almost similar morphological features have been reported in dustfall in this region (Mishra et al., 2015; Kumar et al., 2014; Pachauri et al., 2013). The various shapes of dust particles might be due to their emission from different sources, geological characteristics, and meteorological parameters. Elemental and morphology of dust particles are controlled by wind direction and geology of that area (Zarasvandi et al., 2011).

The rounded shaped particle with smooth surface (Figure 3B) are considered as soot particles and fly ash. The presence of soot particles may be due to emissions from vehicular traffic, thermal power plants, and other industrial units located in and around Delhi. Soot particles at residential and commercial site is indicating of domestic coal burning and biomass burning (Rout et al., 2014). Some rounded shaped particles was found with specific shape pattern having with rough surface (Figure 3C). These particles showed the presence of pollens. Figure 3D shows grossular structure of the particles. In the earth's crust the major type of chemical compound is composed of about 72% of aluminosilicate group in terms of weight (Cong et al., 2010; Van Malderen et al., 1996). Aluminosilicate particles are mainly composed of Si and Al oxides with varying amount of K, Mg, Ca, and Fe. Similar results were observed by other coworkers in this region (Kumar et al., 2014; Pachauri et al., 2013). Some grape like structure of the particles (Figure 3E) are similar to the structure of a big aged carbon fractal comprising of carbon monomers (Mishra et al., 2015). Due to vehicular emission or combustion activities including tire abrasion and fly ash from asphalt, fresh carbon fractals (open long chain fractals) are released in the atmosphere which reside in the atmosphere for long time and form close fractals (closed chain compact fractal) due to surface tension and particle dynamics. In our study, we found some triangular structures (termed as triangular flaky structure) (Figure 3F) and flattened crust like particles (Figure 3I). The flattened structures are of oblate shape and thicker than the flakes. Mishra and coworkers (2015) suggested that the layered structure particles inferred to be

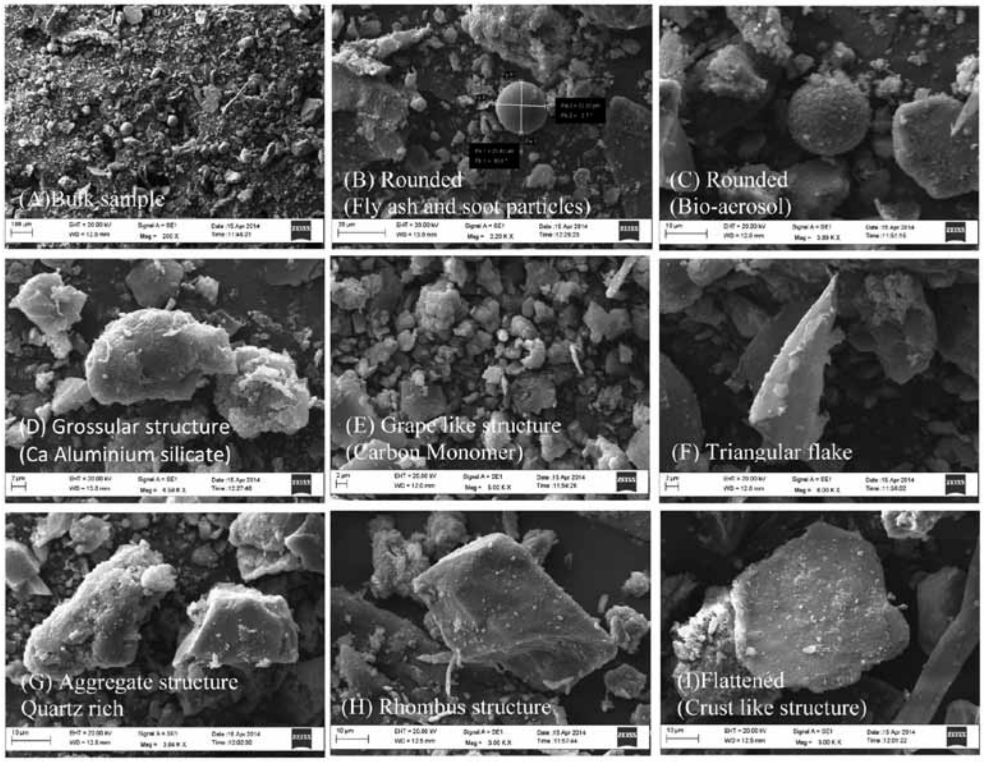

Figure 3. (A to I) SEM Images of dust particles with different magnifications.

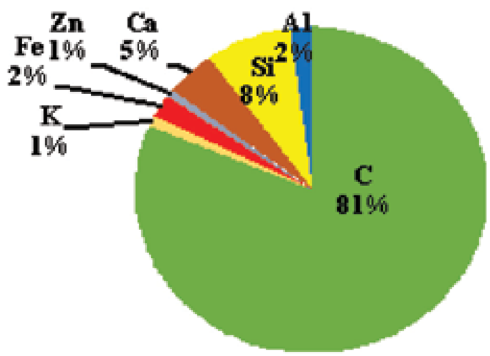

Figure 4. Average elemental composition of dust sample (excluding oxygen %).

rich in calcite and quartz. Figure 3G shows some irregular aggregate structure. Zhao and coworkers (2010) found that the irregular granular aggregates are the marker of construction dust and normal granular were markers of road dust. Angular crust like particles was found to be rich in quartz while some angular particles were found to be rich in C, N, O and Si (Mishra et al., 2015).

Elemental composition of Dustfall particles

Figure 4 illustrates the elemental composition of dust samples as determined by SEM-EDX. It shows the relative contribution of various elements which are present in the dust in major quantity. Oxygen was excluded due its very high contribution about 75% of the mass. As the figure clearly shows carbon, silicon and calcium has the highest percentage among all the elements contributing 81%, 8% and 5%, respectively. Similar results have also been observed by Kumar et al., (2014) in south Delhi area. It has been found that dust particles over urban areas have been multifold enriched with carbon as compared with local soil (Mishra and Kulshrestha, 2016; Kulshrestha et al., 2012). Dust particles due to their suspension in air have greater possibility to interact with various air pollutants allowing the adsorption of gases and other particulates including carbonaceous aerosols (Kumar et al., 2014).

In addition, copper and sulfur were also present in trace amount. The dust consisted of oxides of carbon, calcium, silicon, iron, aluminum, potassium, zinc, copper and sulfur. Such contribution indicated that the dustfall is a mixture of natural as well as anthropogenic emissions. Presence of metals such as zinc and copper indicated an influx of industries while contribution of zinc and sulfur indicates the influx of diesel combustion particularly from heavy duty vehicles. Presence of oxides of aluminum, silicon, calcium, iron, and potassium suggested that the dust is primarily of crustal origin.

CONCLUSIONS

The present study mainly carried out around Shahdara Industrial Area reveal that the road dust suspension and industrial emissions have significant effect on the chemical characteristics of atmospheric dust in East Delhi. The pH of dustfall suggest that the atmospheric dust is alkaline in nature. High rate of dustfall indicate the effect of increasing urbanization and decreasing forest cover. Deforestation and construction activities due to rapid urbanisation are significant factors resulting in increase in the atmospheric dust. The alkaline nature of dust in Indian region promotes SO_4^{2-} and NO_3^- scavenging through dry deposition forming secondary aerosols such as $CaSO_4$ and $Ca(NO_3)_2$. High correlation between of Cl- with NO_3^- and SO_4^{2-} suggested their emissions from biomass burning and waste incinerations. Morphologies of dust indicated that the major constituents of the urban dust are derived from industrial and vehicular activities including tire abrasion, fly ash from asphalt and combustion byproducts. The elemental analysis further indicated that C, Si and Ca as the major elements of dustfall, while traces of Cu and Zn were also recorded.

ACKNOWLEDGEMENTS

We sincerely thank CSIR-UGC, DST PURSE, New Delhi for the financial support to carry out this research work. Analytical assistance provided by Advance Instrumentation Research Facility (AIRF), JNU, New Delhi is also gratefully acknowledged. The authors are thankful to Dr. Gyan Prakash Gupta for reviewing the manuscript and providing useful suggestions to enhance the quality of the manuscript. They also thank Dr.V.V.Sesha Sai for editing the manuscript. We thank the Chief Editor for his continued support, guidance and encouragement.

Compliance with Ethical Standards

The authors declare that they have no conflict of interest and adhere to copyright norms.

REFERENCES

Amato, F., Pandolfi, M., Escrig, A., Querol, X., Alastuey, A., Pey, J., Perez, N., and Hopke, P.K., 2009. Quantifying road dust resuspension in urban environment by multilinear engine: a comparison with PMF2, J Atmos. Environ., v.43, pp: 2770–2780.

Amato, F., Pandolfi, M., Moreno, T., Furger, M., Pey, J., Alastuey, A., Bukowiecki, N., Prevot, A.S.H., Baltensperger, U., and Querol, X., 2011. Sources and variability of inhalable road dust particles in three European cities, J Atmos. Environ., v.45, pp: 6777–6787.

Andrae, M. O., Talbot, R. W., Berresheim, H., and Beecher, K. M., 1990. Precipitation chemistry in Central Amazonia, J. Geophys. Res., v.95, no.16, pp: 987–16,999.

Angelis, M. De., and Gaudichet, A., 1991. Saharan dust deposition over Mont Blanc (French Alps) during the last 30 years, J Tellus B., v.43, no.1, pp: 61–75.

Cattle, S. R., McTainsh, G. H., and Wagner, S., 2002. Eolian dust contributions to soil of the Namoi Valley, northern NSW, Australia," J Catena., v.47, no.3, pp: 245–264.

Cong, Z., Kang, S., Dong, S., Liu, X., and Qin, D., 2010. Elemental and Individual Particle Analysis of Atmospheric Aerosols from High Himalayas, J Environ. Monit. Assess., v.160, pp: 323–335.

Dentener, F. J., Carmichael, G. R., Zhang, Y., Lelieveld, J., and Crutzen, P. J., 1996. Role of mineral aerosol as a reactive surface in the global troposphere, J Geophysical Research: Atmospheres., v.101, no.D17, pp: 22869-22889.

Dickerson, R. R., Kondragunta, S., Stenchikov, G., Civerolo, K. L., Doddridge, B. G., and Holben, B. N., 1997. The impact of aerosols on solar ultraviolet radiation and photochemical smog, Science., v.278, no.5339, pp: 827-830.

Gunawardana, C. H., Goonetilleke, A., Egodawatta, P., Dawes, L., and Kokot, S., 2012. Source characterisation of road dust based on chemical and mineralogical composition, J Chemosphere., v.87, pp: 163–170.

Gupta, G. P., Singh, S., Kumar, B., and Kulshrestha, U. C., 2015a. Industrial dust sulphate and its effects on biochemical and morphological characteristics of Morus (Morus alba) plant in NCR Delhi, J Environmental monitoring and assessment., v.187, no.3, pp: 1-13.

Gupta, G. P., Kumar, B., Singh, S., and Kulshrestha, U. C., 2015b. Deposition and Impact of Urban Atmospheric Dust on Two Medicinal Plants during Different Seasons in NCR Delhi.

Gupta, G. P., 2015c. Study of dry deposition of particulates on foliar surface and its effect on biochemical constituents of selected plant species of national capital region, India,Thesis.

Hicks, D.B., 1986. measuring dry deposition: a reassessment of the state of art, J Water, Air, and Soil Pollution., v.30, pp: 5–90.

Inoue, M., Murase, A., Yamamoto, M., and Kubo, S., 2006. Analysis of volatile nanoparticles emitted from diesel engine using TOF-SIMS and metal-assisted SIMS (MetA-SIMS), J Applied Surface Science., v.252, pp: 7014–7017.

Jain, M., Kulshrestha, U. C., Sarkar, A. K., and Parashar, D. C., 2000. Influnce of crustal aerosols on wet deposition at urban and rural sites in India, v.34, pp: 5129-5137.

Kreider, M.L., Panko, J.M., McAtee, B.L., Sweet, L.I., and Finley, B.L., 2010. Physical and chemical characterization of tire-related particles: comparison of particles generated using different methodologies, J Sci. Total Environ., v.408, pp: 652–659.

Kulshrestha, U., 2013. Acid rain : In Encyclopedia of environment management.S.E. Jorgensen, (ed.) Taylor & Francis: New York, v.1, pp: 8-22.

Kulshrestha, U. C., Kumar, B., Gupta, G. P., Singh, S., and Kulshrestha, M. J., 2012. Defining criteria for good habitats: importance of bioaerosols, black, carbon and trace gases, J Indian Journal of Air Pollution Control., v.7, pp: 24–30.

Kulshrestha, U.C., Kulshrestha, M.J., Sekar, R., Sastry, G.S.R., and Vairamani, M., 2003a. Chemical characteristics of rainwater at an urban site of south-central India, J Atmos. Environ., doi:10.1016/S1352-2310(03)00266-8., v.37, pp: 3019-3026.

Kulshrestha, M. J., Kulshrestha, U. C., Parashar, D. C., and Vairamani, M., 2003b. Estimation of SO4 contribution by dry deposition of SO2 onto the dust particles in India, J Atmos. Environ., v.37, no.22, pp: 3057-3063.

Kulshrestha, U.C., Jain, M., Mandal, T.K., Gupta, P., Sarkar, A.K., and Parashar, D.C., 1999. Measurements of acid rain over Indian Ocean and surface measurements of atmospheric aerosols at New Delhi during INDOEX pre- campaigns, J Curr. Sci., v.76, no.7.

Kulshrestha, U. C., Saxena, A., Kumar, N., Kumari, K. M., and Srivastava, S. S., 1998. Chemical composition and association of size-differentiated aerosols at a suburban site in a semi-arid tract of India, J Atmospheric Chemistry, v.29, no.2, pp: 109-118.

Kulshrestha, U. C., Sarkar, A. K., Srivastava, S. S., and Parashar, D. C., 1996. Investigation into atmospheric deposition through precipitation studies at New Delhi (India), J Atmospheric Environment., v.30, no.24, pp: 4149-4154.

Kumar, B., Verma, K., and Kulshrestha, U.C., 2014. Deposition and Mineralogical Characteristics of Atmospheric Dust in relation to Land Use and Land Cover Change in Delhi (India), J Geography Journal., v.11.

Lacis, A. A., 1995. Climate forcing, climate sensitivity, and climate response: A radiative modeling perspective on atmospheric aerosols, J Aerosol forcing of climate., pp: 11-42.

Lakhani, A., Parmar, R. S., Satsangi, G. S., and Prakash, S., 2007. Chemistry of fogs at Agra, India: Influence of soil particulates and atmospheric gases, J Environmental monitoring and assessment., v.133, no.1-3, pp: 435-445.

Li, J., Zhuang, G., Huang, K., Lin, Y., Xu, C., and Yu, S., 2008. Characteristics and sources of air-borne particulate in Urumqi, China, the upstream area of Asia dust, J *Atm Environment.*, v.42, no.4, pp: 776-787.

Liao, H., and Seinfeld, J. H., 1998. Radiative forcing by mineral dust aerosols: sensitivity to key variables, J of Geophysical Research., v.103(D24), pp: 31637-31645.

McBride, M.B., 1994. Environmental Chemistry of Soil. Oxford University Press, New York.

McTainsh, G. H., and Walker, P. H., 1982. Nature and distribution of Harmattan dust, J Zeitschrift fur Geomorphologie, v.26, no.4, pp: 417–435.

Mishra, M., and Kulshrestha, U., 2016. Estimation of Carbonaceous Emission Impact on Urban Soil-Dust in Delhi, J Climate Change, DOI 10.3233/JCC-160023., v.2, no.2, pp: 119–127.

Mishra, S.K., Agnihotri, R., Yadav, P.K., Singh, S., Prasad, M.V.S.N., Praveen, P.S., Tawale, J.S., Rashmi, Mishra, N.D., Arya, B.C., and Sharma, C., 2015. Morphology of Atmospheric Particles over Semi-Arid Region (Jaipur, Rajasthan) of India: Implications for Optical Properties.

Mishra, S. K., Agnihotri, R., Yadav, P. K., Singh, S., Arya, B. C., and Sharma, C., 2015. Morphology of atmospheric particles over Semi-Arid region (Jaipur, Rajasthan) of India: Implications for optical properties, J Aerosol Air Qual. Res, v.15, pp: 974-984.

Moffet, R. C., Desyaterik, Y., Hopkins, R. J., Tivanski, A. V., Gilles, M. K., Wang, Y., ... and Mugica, V., 2008. Characterization of aerosols containing Zn, Pb, and Cl from an industrial region of Mexico City, J Environmental science & technology, v.42, no.19, pp: 7091-7097.

Owens, P.N., and Slaymaker, O., 1997. Contemporary and post-glacial rates of aeolian deposition in the Coast Mountains of British Columbia,Canada, J GeografiskaAnnalerA: Physical Geography., v.79, no.4, pp: 267–276.

Pachauri, T., Singla, Y., Satsangi, A., Lakhani, A., and Kumari, K.M., 2013. SEM-EDX Characterization of Individual Coarse Particles in Agra, India, J Aerosol and Air Quality Research., v.13, pp: 523–536.

Perrino, C., Tiwari, S., Catrambone, M., Dalla Torre, S., Rantica, E., and Canepari, S., 2011. Chemical characterization of atmospheric PM in Delhi, India, during different periods of the year including Diwali festival, J Atmospheric Pollution Research., v.2, no.4, pp: 418-427.

Prospero, J. M., Nees, R. T., and Uematsu, M., 1987. Deposition rate of particulate and dissolved aluminum derived from Saharan dust in precipitation at Miami, Florida, J Geophysical Research-Atmospheres., v.92(D12), pp: 14723–14731.

Rahn, K. A., 1976. The chemical composition of the atmospheric aerosol. Graduate School of Oceanography, University of Rhode Island.

Rogge, W.F., Hildemann, L.M., Mazurek, M.A., and Cass, G.R., 1993. Sources of fine organic aerosol. 3. Road dust, tire debris, and organometallic brake lining dust: roads as sources and sinks, J Environ. Sci. Technol., v.27, pp: 1892–1904.

Rout, T.K., Masto, R. E., Padhy, P. K., George, J., Ram, L.C., and Maity, S., 2014. Dust fall and elemental flux in a coal mining area PII: S0375-6742(14)00135-6.

Shen, Z., Cao, J., Arimoto, R., Han, Z., Zhang, R., Han, Y., and Tanaka, S., 2009. Ionic composition of TSP and PM 2.5 during dust storms and air pollution episodes at Xi'an, China, J Atmospheric Environment, v.43, no.18, pp: 2911-2918.

Simoneit, B. R., 2002. Biomass burning—a review of organic tracers for smoke from incomplete combustion, J Applied Geochemistry., v.17, no.3, pp: 129-162.

Singh, S., Gupta, G. P., Kumar, B., and Kulshrestha, U. C., 2014. Comparative study of indoor air pollution using traditional and improved cooking stoves in rural households of Northern India, J Energy for Sustainable Development, v.19, pp: 1-6.

Singh, R. P., Dey, S., Tripathi, S. N., Tare, V., and Holben B., 2004. Variability of aerosol parameters over Kanpur, northern India, J Geophys. Res., D23206, doi: 10.1029/2004/jD004966., v.109.

Tegen, I., and Fung, I., 1995. Contribution to the atmospheric mineral aerosol load from land surface modification, J Geophysical Research., v.100(D9), pp: 18707.

Thorpe, A., and Harrison, R.M., 2008. Sources and properties of non-exhaust particulate matter from road traffic: a review, J Sci. Total Environ., v.400, pp: 270–282.

Underwood, G. M., Song, C. H., Phadnis, M., Carmichael, G. R., and Grassian, V. H., 2001. Heterogeneous reactions of NO_2 and HNO_3 on oxides and mineral dust: A combined laboratory and modeling study, J. Geophys. Res., v.106, no.D16, pp: 18055–18066.

Van Malderen, H., Van Grieken, R., Bufetov, N.V., and Koutzenogii, K.P., 1996. Chemical Characterization of Individual Aerosol Particles in Central Siberia, J Environ. Sci. Technol., v.30, pp: 312–321.

Zarasvandi, A., Carranza, E. J. M., Moore, F., and Rastmanesh, F., 2011. Spatio-temporal occurrences and mineralogical-geochemical characteristics of airborne dusts in Khuzestan Province (southwestern Iran), *J Exploration.*, v.111, no.3, pp: 138–151.

Zhao, X. P., Ackerman, A., and Guo, W., 2010. Dust and smoke detection formulti-channel imagers, J Remote Sensing., v.2, no.10, pp: 2347–2368.

How do you find an Exoplanet?—Recent publication

In his book "How do you find an Exoplanet" the author explains the four key methods that have been used to discover exoplanets-planets that orbit around stars other than the Sun. Those are the radial velocity method, observations of transits, analysis of gravitational microlensing and direct imaging. His aim is to make his presentation accessible to anyone with an understanding of freshman physics. As per Samantha J.Thompson of University of Cambridge, UK (who has reviewed the book), readers with an understanding of Kepler`s laws or even just Newtonian gravity find the topics covered to be comprehensive and the progression of topics easy to follow. She further states that the story built by the author helps readers identify with the author. She points out that even those who grew up in a city with hardly any awareness of the night time stars above could be bitten by the astronomy bug. (**Source**: Physics Today, Nov 2016, vol 69, no 11, pp.59 & 60 & Johnson Asher Johnson, Princeton University Press, 2016. $ 35, 178 pges; ISBN 978-0-15681-1).

J. Ind. Geophys. Union (March 2017)
v.21, no.2, pp: 148-152

Winter precipitation climatology over Western Himalaya: Altitude and Range wise study

M S Shekhar*[1], N Narasimha Rao[1], Surendar Paul[2], S C Bhan[3], G P Singh[4] and Amreek Singh[1]

[1]Snow and Avalanche Study Establishment, Research and Development Centre, Sector 37 Chandigarh - 160036, India
[2] India Meteorological Department Chandigarh - 160036, India
[3]India Meteorological Department, Mausam Bhawan, Lodhi Road, New Delhi- 110 003 India
[4]Department of Geophysics, Institute of Science, Banaras Hindu University, Varanasi-221005 India
*Corresponding Author: sudhanshu@sase.drdo.in

ABSTRACT

An Attempt has been made in this study to find the Climatology of winter precipitation over western Himalaya region (WH). Characteristics of Precipitation Variation Trends (PVT) with different altitude regions and Himalayan ranges have been analysed by using monthly cumulative precipitation data from 81 surface observatories of western Himalaya from 1971-2013. With respect to elevation, western Himalaya is divided into three altitude regions and four Himalayan ranges. The altitude regions considered for study are below 1500m, 1500-3500m and above 3500m respectively. Results show that more than 80 % of the stations under study indicates strong negative precipitation tendency rate over western Himalaya. Simple linear regressions have been used for trend analysis. The statistical significance of winter precipitation trends has also been studied by using Mann-Kendall method. The results confirm the decreasing trends in winter precipitation there by indicating the impact of climate change and precipitation variability in western Himalayan region.

Key words: Precipitation Variation Trend, Western Himalaya, Climatology, Mann-Kendall test, Range and altitude.

INTRODUCTION

The Himalayan Mountains play an important role in shaping the weather and climate system of Indian subcontinent. The main weather systems which bring precipitation in western Himalayan region are Western Disturbances (WDs) during wintertime and monsoon phenomenon during summer time. The summer monsoon dominates the climate from June to September and WDs dominate the climate form November to April. During winter i.e. December, January, February (DJF), WDs yield enormous amount of precipitation over northern India (Lang and Barros, 2004 and Dimri and Mohanty, 2009), which is important for overall ecology and socioeconomic requirements of the region. Himalayan climatology with special reference to extreme rainfall events in the context of global climate change has been studied by Joshi and Rajeevan (2006). Bhutiyani et al., (2007) and Shekhar et al., (2010) attempted studies to understand the impact of climate variability and precipitation and temperature trends in Himalayan region. Many studies have brought out the topographic effects on precipitation (Barros and Lettenmaier, 1994 and Liao et al., 2007), whereas a limited few have analysed the relationship between precipitation variation trends (PVT) and topography (Ma and Fu, 2007). Altitude is generally accepted as the most common topographic variable used to explain spatial variations in precipitation such as precipitation enhancement through orographic uplift. It may be noted that in Switzerland, depending on the region, altitude explains 0–90% of the variance of mean annual precipitation (Sevruk, 1997). The effect of altitude, however, is not always positive. Lu et al., (2008) discussed the negative correlation between summer precipitation and altitude in China and found that the correlation is becoming stronger with increased global warming.

PRESENT STUDY:

A primary objective of the present study is to preliminarily understand the relationship between Precipitation Variation Trend (PVT) and altitude of Himalayan Ranges over Western Himalaya; and thereby opening a direction to further understand the trends in precipitation patterns with larger number of topographic variables, such as orientation, slope, and exposure etc. especially in Western Himalayan region.

DATA AND METHODOLOGY

Data

In the present study 81 observation stations of Snow and Avalanche Study Establishment (DRDO) and India Meteorological Department (IMD), which are well distributed over WH are chosen for analysing data of winter season. The stations under study have been categorised into three altitude regions and four ranges as given in Table 1.

Table 1. Categories of Altitude and Himalayan ranges.

Altitude Regions	Western Himalayan ranges
1. altitude < 1500 m (28)	1. Pir Panjal (PP) (50)
2. altitude between 1500 m to 3500 m (44)	2. Shamshawari (SH) (8)
3. altitude > 3500 m (9)	3. Great Himalaya (GH) (16)
	4. Karakoram (KK) (7)

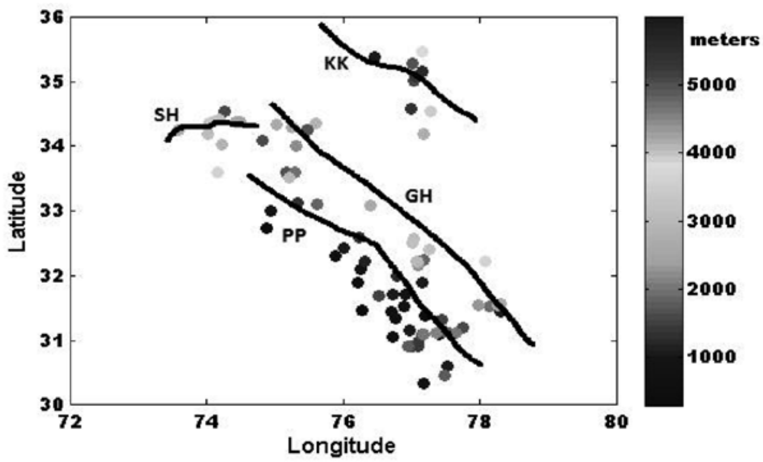

Figure 1. Indian Western Himalaya and data observation stations showing the altitude in meters above mean sea level; KK-Karakoram Range, SH-Shamshawari Range, GH- Great Himalaya Range, PP- Pir Panjal Range; Latitude and Longitude in Degrees).

Figure 1 shows the locations of 81 surface observatories in the Indian Western Himalaya. To maximize data quality, the annual stations, ordinary climatological stations, and observation stations with any missing data (a month without measured precipitation data) were removed. Ultimately, data collected from 1971 to 2013 from these 81 stations were considered for analysis. The present study is restricted to the winter season, where precipitation is measured only from November to April.

Methodology

Simple linear regression has been used to calculate the precipitation tendency rate as $X_t = a_0 + a_1t$; Here, t is time from 1971 to 2013, and X_t is the estimated monthly mean precipitation by simple linear regression. The regression coefficient is $a_1=dX_t/dt$, and the precipitation tendency rate is $b=a_1x10$, with units of mm/10 a. A positive value indicates an increasing trend, and a negative value indicates decreasing trend. The regression coefficient indicates quantitatively the relationship between t and X_t. The Mann–Kendall (MK) test being a widely used nonparametric technique for detecting monotonic trends in hydrological and meteorological time series (e.g., Gemmer et al., 2011), the same MK test for trend analysis to test the statistical significance (passing the 95% significance level) is used in the present study.

RESULTS AND ANALYSIS:

In Figure 2 are shown scatter plots between the winter PVT and altitudes and ranges in the Western Himalaya region. In addition to these the spatial distribution of winter PVT and winter precipitation patterns (shown in Figures 3 and 4) were also analysed.

The relationship between winter PVT, altitude regions and Himalayan Ranges

Figure 2 indicates overall negative winter precipitation variation trends for all altitudes and ranges in western Himalayan region. The decreasing tendency rate has been observed within (±10mm/10a) in lower altitudes and within ±50 mm /10a in middle and upper altitude regions. The findings clearly indicate that decreasing trends are more in middle and higher altitudes compared to lower altitudes. The overall negative tendency rate has been observed in all the Western Himalayan ranges except for Shamshawari Range, wherein positive tendency rate has been observed. A Complete negative tendency rate has been observed in Karakoram Range. The Spatial distribution of the winter precipitation tendency rate is shown here in Figure 3 Spatially positive tendency rate is dominant in the western part, whereas the tendency rate is negative in Eastern, Middle and Southern parts of Western Himalaya respectively.

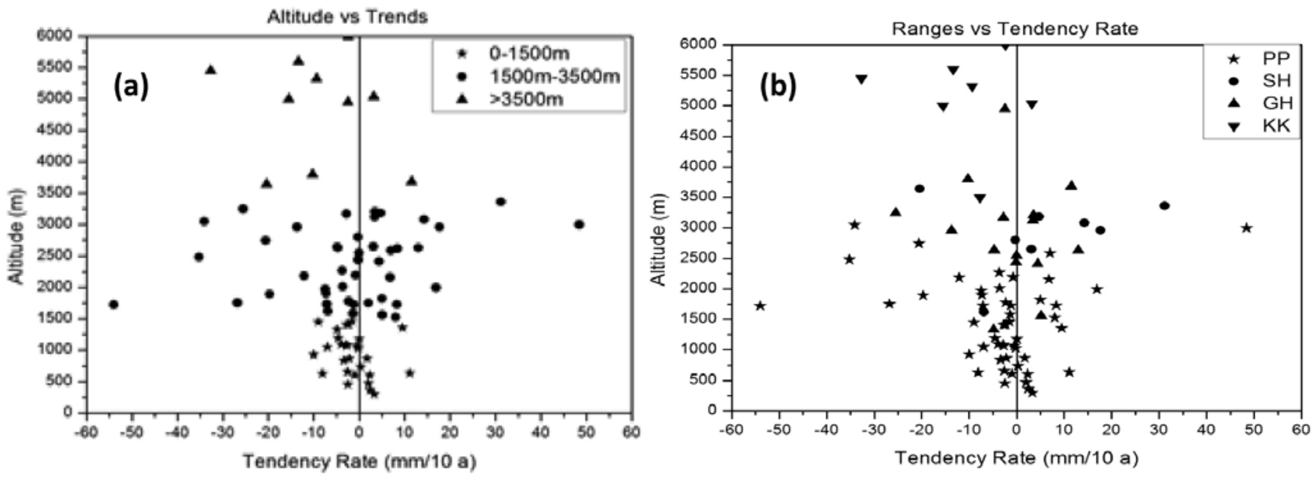

Figure 2. Scatter plots of the winter precipitation tendency rate versus (a) altitude regions and (b) Himalayan Ranges.

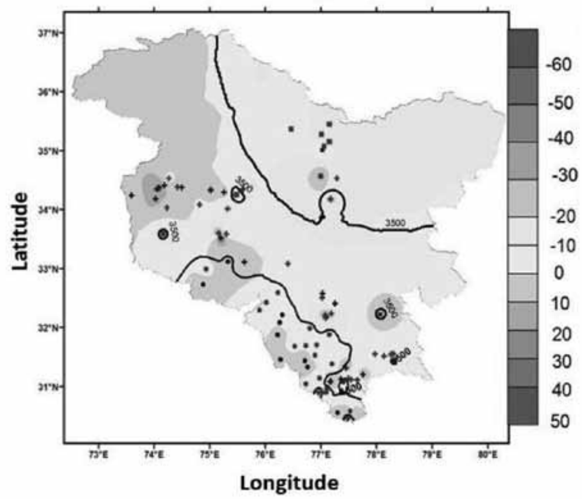

Figure 3. Spatial distribution of the winter precipitation tendency rate b (mm/10a). Black solid lines are 1500m and 3500m contour lines ;(•, +, □) represent the points 0- 1500m, 1500-3500m and above 3500m, respectively. Blue (•, +, □) represents positive, and red (•, +, □) negative.

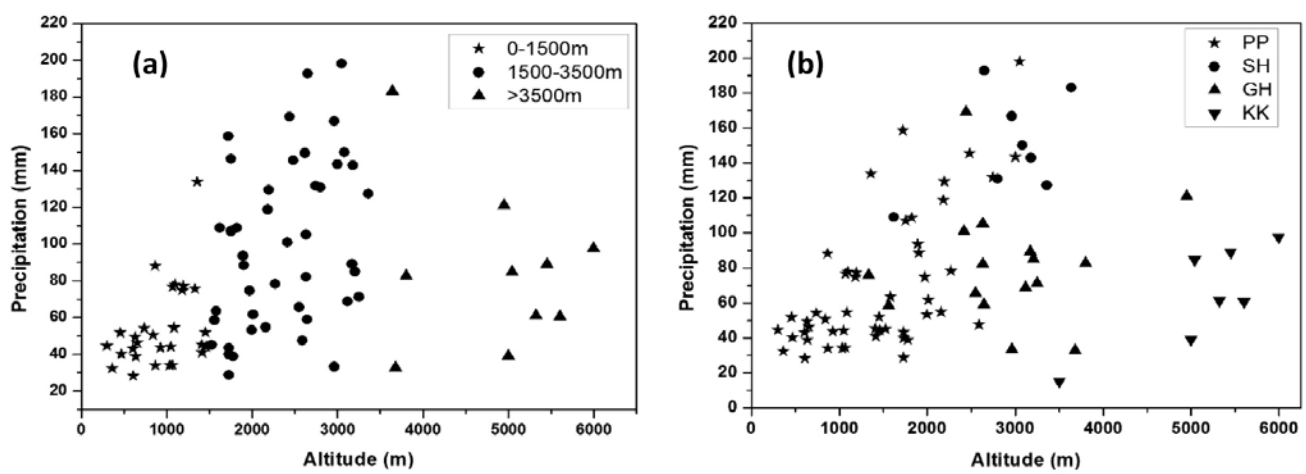

Figure 4. Scatter plots of the regional winter precipitation versus (a) altitude regions and (b) Himalayan Ranges.

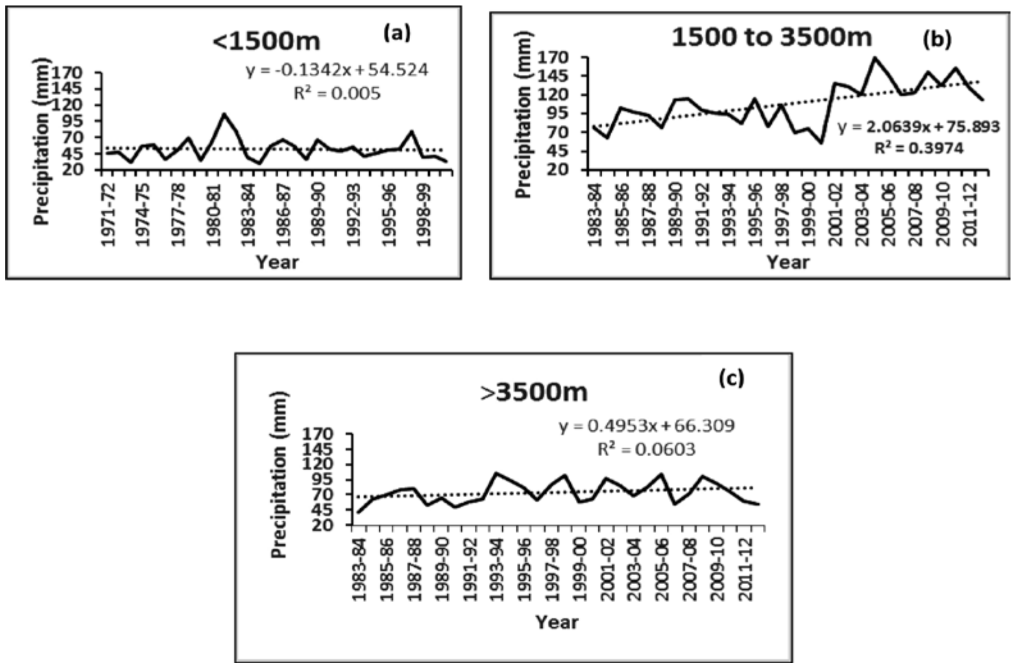

Figure 5. Trends in precipitation over different altitude zones of Himalaya.

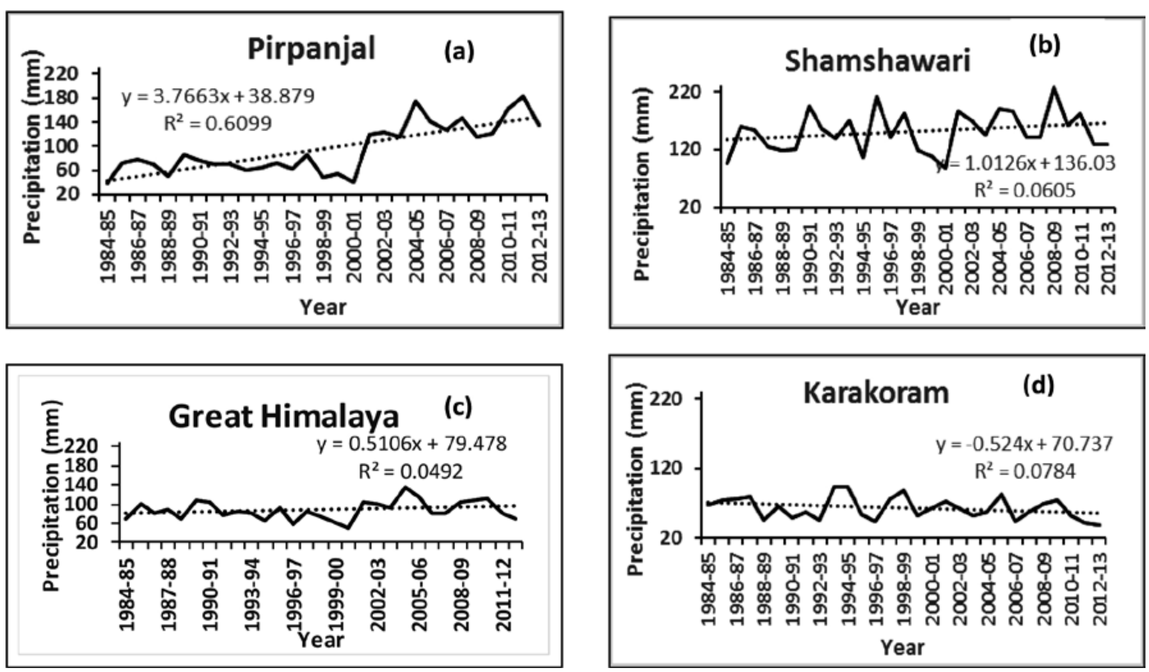

Figure 6. Trends in precipitation over different ranges of Himalaya.

Winter precipitation patterns for different altitude regions and Ranges in Western Himalaya.

Mean winter precipitation patterns indicate more precipitation in middle altitudes as compared to other altitudes (Figure 4a). The maximum Mean winter precipitation has been observed in middle altitudes region (1500-3500 m) with value up to 200 mm. Mean precipitation for lower and upper altitudes is about 80 and 125mm respectively. Similarly, maximum winter precipitation pattern is observed in Shamshawari range followed by Great Himalaya, Pir Panjal and Karakoram ranges respectively (Figure 4b). In Shamshawari, the precipitation value ranges from 125 to 200 mm. In Pir Panjal the values are 80 mm for majority of stations except for a few stations where the values are up to 200mm. The

Precipitation values in Great Himalaya and Karakoram ranges are 125 and 100 mm respectively. The trends in winter precipitation (altitude wise) are depicted in Figure 5. Altitude wise decreasing precipitation trends has been observed in lower altitudes and increasing in middle and upper altitudes. Significant positive trend is observed in middle altitude region and no significant trends are present in lower and upper altitudes.

The range wise trends in winter precipitation are shown here in Figure 6. An overall increasing trend in precipitation has been seen in all ranges except the Karakoram. There are no significant trends in Great Himalaya, Shamshawari and Karakoram, whereas significant trend is found in Pir Panjal only. The study on climatology of fresh snowfall over Western Himalaya by Shekhar et al., (2010) indicates decreasing trends in snowfall in all the ranges of Western Himalaya. The decreasing trends in snowfall and increasing trends in total precipitation clearly indicate the increasing liquid precipitation i.e. rainfall in these ranges of Himalaya in the warming environment due to recent climate change and global warming. The trend in precipitation in Karakoram remains the same i.e. decreasing. This may be due to the fact that this range is situated in higher altitude which gets precipitation throughout the year in the form of snowfall only.

CONCLUSIONS

Range and altitude wise climatology of winter precipitation over western Himalaya region has been studied. Negative tendency rate of precipitation is observed in all the ranges of Western Himalaya except for Shamshawari where the rate is positive. Spatially positive tendency rate is dominated in western part and negative in Eastern, Middle and Southern parts of Western Himalaya respectively. Precipitation shows decreasing trends in lower altitudes and increasing trends in middle and upper altitude regions. However, the trends are not significant in lower and upper altitudes but show significant positive trends in middle altitude region. The increasing trend in total precipitation and decrease in snowfall confirms the increasing rainfall in almost all the ranges of Western Himalaya except the Karakoram range and thereby confirming the setting in of the climate change and global warming over the Himalayan region.

ACKNOWLEDGEMENTS

Authors are thankful to Director SASE (DRDO) for providing the necessary support and guidance to complete this work. Contribution made by Miss Usha Devi, SRF, Hazard Assessment and Forecasting Division (HAFD) for compiling station data is duly acknowledged. Thanks are due to Dr. Jagabandhu Panda for constructive review and suggestions. They also thank Prof. B. V. S. Murty for editing the manuscript. We thank the Chief Editor for the support and guidance.

Compliance with Ethical Standards

The authors declare that they have no conflict of interest and adhere to copyright norms.

REFERENCES

Barros, A.P., and Lettenmaier, D.P., 1994. Dynamic modeling of orographically induced precipitation, Geophys Rev., v.32, no.3, pp: 265–284.

Bhutiyani, M.R., Kale, V.S., and Pawar, N.J., 2007. Long-term trends in maximum, minimum and mean annual air temperatures across the north-western Himalaya during the 20th Century. Climatic Change, v.85, pp: 159–177.

Dimri, A.P., and Mohanty, U.C., 2009. Simulation of mesoscale features associated with intensed western disturbances over western Himalayas. Meteorol Appl., v.16, pp: 289–308.

Gemmer, M., Fischer, T., Jiang, T., Su, B., and Liu, L.L., 2011. Trends in precipitation extremes in the Zhujiang River basin, South China. J. Clim. http://dx.doi.org/10.1175/2010JCLI3717.1., v.24, pp: 750–761.

Joshi, U.R., and Rajeevan, M., 2006. Trends in precipitation extremes over India, NCC Research Report No, 3/2006, National Climate Centre, Pune.

Lang, T.J., and Barros, A.P., 2004. Winter storms in central Himalayas. J Meteorol Soc Jpn., v.82, no.3, pp: 829–844.

Liao, F.Y., Hong, C., and Zheng, G.G., 2007. Review of orographic influences on surface precipitation, Meteor. Sci. Tech., v.35, no.3, pp: 309–316.

Lu, A.G., Kang, S.C., and Pang, D.Q., 2008. Altitude effect of precipitation and the influence of global warming on it in China, Ecol. Environ., v.17, no.5, pp: 1875–1878.

Ma, Z.G., and Fu, C.B., 2007. Global aridification in the second half of the 20th century and its relationship to large-scale climate background, Sci. China Ser D-Earth Sci., v.50, no.5, pp: 776–788.

Sevruk, B., 1997. Regional dependency of precipitation-altitude relationship in the Swiss Alps, Climatic Change., v.36, pp: 355–369.

Shekhar, M., Chand, H., Kumar, S., Srinivasan, K., and Ganju, A., 2010. Climate change studies over western Himalayan region., Ann. Glaciol., v.51, no.54, pp: 105-112.

J. Ind. Geophys. Union (March 2017)
v.21, no.2, pp: 153-166

Selection of optimum wavelet in CWT analysis of geophysical downhole data

Amrita Singh*[1], Saumen Maiti[1] and R.K.Tiwari[2]

[1]Department of Applied Geophysics, Indian Institute of Technology (Indian School of Mines), Dhanbad-826004, India
[2]CSIR-National Geophysical Research Institute, Hyderbad-500007, India
*Corresponding Author: saumen_maiti2002@yahoo.co.in

ABSTRACT

Continuous wavelet transform (CWT)-based scalogram analysis is appropriate for the modelling of discontinuous well log signal. The choice of appropriate mother wavelet in scalogram analysis is crucial to model the geophysical well log data precisely. Here, we examine some of the key points related to the choice of optimum wavelet for the analysis of well log signal. We used the scalogram analysis to detect the formation interface and explored the impact of each mother wavelet. Following three key indicators, e.g. (i) histogram analysis of CWT coefficient at even number scale (ii) statistical significance test of each sub- signal at even number scale and (iii) Principal component analysis (PCA) of those sub-signals are used. These key steps help to identify the precise localization of formation tops detection problem of well log data of KTB borehole, Germany. Here, five mostly used wavelet functions (Haar, Gaussian wavelet of order 1 (Gaus1), Gaussian wavelet of order 3 (Gaus3), Morlet and Daubechies wavelet of order 2 (Db2)) are employed on two sets of data: (i) spectral gamma ray (SGR) log in pilot hole and (ii) density (RHOB) log in main hole data. The comparative results suggest that Gaus1 is better among all mother wavelets rendering maximum number of occurrences of CWT coefficients in the total well log signal modelling. Statistical significance test shows that CWT coefficients and their respective scales are statistically important. The results based on PCA analysis further suggest that Gaus1 wavelet is in good agreement with the gross structure of the signal.

Key words: Continuous wavelet transform, PCA analysis, Histogram analysis, Significance test, Formation interface, KTB.

INTRODUCTION

Wavelet transform has become a very popular tool for data analysis in almost all domains of applied sciences (Sang et al., 2016; Shoaib et al., 2014). The wavelet transform-based analysis is appropriate for the investigation of the non-stationary signals, which are common in real geophysical time/space series data. Wavelet (Morlet et al., 1982), has been broadly used in time series analysis (e.g., identifying periods and duration of signal band, time series modelling/ forecasting, de-noising of time series, and identification of true components, characterization of subsurface geology/ geological rock types, litho-logical boundary identification/ modelling discontinuity etc) (Kumar and Foufoula-Georgiou, 1997; Kisi, 2009; Percival and Walden, 2000; Adamowski and Chan, 2011; Doveton, 1986; Farge, 1992; Daubechies, 1992; Chandrashekhar and Rao, 2012; Labat, 2008; Perez-Munoz et al., 2013; Liu et al., 2014; Maraun et al., 2007; Pan et al., 2008; Prokoph and Agterberg, 2000; Goupillaud et al., 1985).

However, selection of optimum mother wavelet and their time-based scale distribution of the wavelet coefficients are two important issues in any applications (Percival and Walden, 2000). Particularly, the choice of suitable mother wavelet in scalogram analysis is crucial for the precise analysis of geophysical well log data analysis (Chandrashekhar and Rao, 2012). Several studies have discussed the procedure for appropriate selection of optimum mother wavelet function. For example, Morlet wavelet is found suitable for the identification of key sedimentary cycles (Prokoph and Agterberg, 2000). The Haar is found realistic for the identification of formation interface in well logging (Pan et al., 2008). To identify fluids in wells and pay zones, Chandrashekhar and Rao (2012) experimented with various mother wavelets and performed mainly histogram analysis of CWT coefficient and found that Gaussian wavelet is the most appropriate. Therefore, there is no widely accepted consensus on the choice of the best method and selection of optimum mother wavelet and temporal scale.

Recently, several researchers have carried out experiment to search for suitable optimum wavelets for modelling (Nourani et al., 2011; Maheswaran and Khosa, 2012; Singh, 2011; Shoaib et al., 2014). Torrence and Compo (1998) recommended for choosing a non-orthogonal wavelet. They considered both 'width' and 'shape' of the signal/wavelet and performed similarity measures between wavelet and original series for finalizing better mother wavelet. Schaefli et al., (2007) reported that wavelet should be chosen such that it shows good time-frequency localization by compromising between time and scale resolution. Nourani et al., (2014) advocated a setting criterion by utilizing similarity measures between wavelet and raw series. In their work, it is explained how wavelet match with malleable depth-scale window that contracts to view small scale structures and broadens to view large-scale structures, akin to a zoom lens (Walker, 1999; Percival and Walden, 2000; Singh et al., 2016; Kumar and Foufoula-Georgiou, 1997; Javid and Tokhmechi, 2012). Particularly, Sang et al., (2016) presented a succinct way of various technical issues in wavelet analysis. They focus mainly on DWT-based analysis and its usefulness is credited by the fact that categorical distributions of DWTs are approximately uncorrelated. However, their recommendation for mother wavelet selection and scale has not resolved the ongoing debate completely. In fact, their approach may not be appropriate for CWT-based analysis where each sub-signal is intimately coupled. Recently, Chandrashekhar and Rao (2012) have done scalogram analysis and efficient histogram analysis of different CWT coefficients to select the optimum mother wavelet. The above scheme is found to be strong for particular downhole data and has been used to model the space localization of formation tops by choosing the appropriate mother wavelet. However, they did not deal with the quantitative statistical assessment and significance of the results at various scales exclusively in choosing the best mother wavelet and a more convincing careful quantitative assessment is required. Therefore, we carried out an experiment to select optimum mother wavelet and see how the associated CWT coefficients are statistically significant to explain the original signal in different scales. Moreover, our combined approach is different in a sense that we have (i) considered and compared performance of both popular orthogonal (Haar, Daubechies wavelets) and non-orthogonal (Morlet, Gaussian wavelets) wavelet in scalogram analysis for good localization in space domain, (ii) taken care of even number scales of CWT coefficients for histogram analysis, (iii) included statistical significance test analysis of the wavelet coefficients to show how the coefficients are significant in matching signal characteristics (iv) used PCA analysis to examine relative influence of each sub-signal at various even number scale using various mother wavelet on over all signal matching characteristics.

Before going to the data analysis, we briefly present the KTB data and wavelet transform theory for the completeness of the article.

MATERIALS AND METHODS

KTB borehole data

The KTB is located in the north-eastern Bavaria, southern Germany. The KTB crust consists of paragneisses, metabasites and alternations of gneiss-amphibolites, with minor occurrence of marbles, calcsilicates, orthogeneisses, lamprophyres and diorites (Pechnig et al., 1997). The maximum depths of pilot and main hole are 4 km and 9.1 km respectively. The data is digitized at 0.1524 m interval. We have used gamma ray log of pilot hole and density log of KTB main hole to model boundary via optimum wavelet selection.

Wavelet analysis via CWT

Goupillaud et al., (1985) defined a wavelet function such as

$$\psi_{u,s}(z) = \frac{1}{\sqrt{(s)}}\psi\left(\frac{z-u}{s}\right), u > 0, s \in R \tag{1}$$

where the ψ is mother wavelet, s is scale factor which depends on wavelength, u is shift parameter and z is a variable. In this framework, the transformation is performed for different sections of the convolved signal by changing s and u. Accordingly, CWT of signal $f(z)$ takes the form of

$$CWT_f(u,s) = \frac{1}{\sqrt{|s|}}\int_{-\infty}^{\infty} f(z)\psi^*\left(\frac{z-u}{s}\right)dz \tag{2}$$

where * denotes the complex conjugate. CWT was performed on different downhole data sets, like density, neutron porosity, the gamma-ray intensity, and seismic p-wave velocity and resistivity log. But in the present study, the results of gamma ray log of pilot hole and density log of main hole data in KTB are presented. Experiments were performed to select optimum mother wavelet from a pool consisting of mother wavelet namely Haar, Gaus1, Gaus3, Morlet and Db2 for the application of modelling well log data (Figure 1).

We have employed the CWT-based histogram analysis and examined their statistical significance to emulate the signal characteristics at different scales. Finally, PCA analysis of CWT coefficient was used to examine relative influence of each mother wavelet to model the well log signal boundary detection.

Optimum mother wavelet selection in CWT-based wavelet analysis and boundary detection

A complete computational procedure is presented as a flow diagram in Figure 2. Accordingly after reading the well log data CWT has been applied. Since edge effect is common problem in high value of the CWT coefficients at the edge of the scalograms (contour map of CWT coefficient), which might obscure the signal of interest, we have followed symmetric half-point method of Strang and Nguyen (1995) and Chandrasekhar and Rao (2012). The CWT coefficient was obtained by using CWT analysis with various mother wavelets.

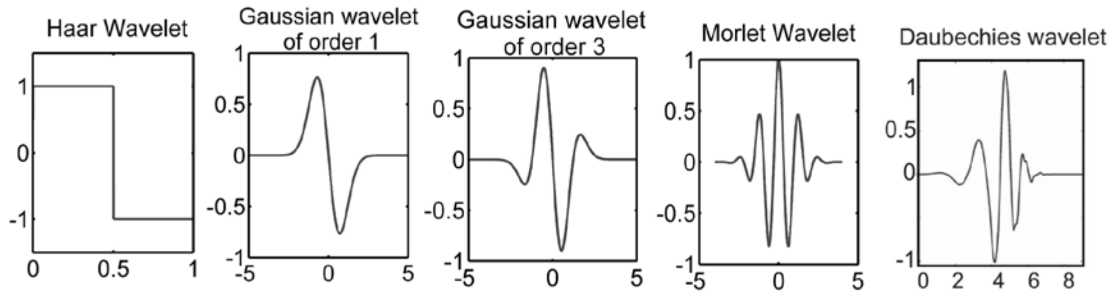

Figure 1. Shape and nature of the mother wavelet used in the present study (a) Haar, Gaus 1, Gaus 3, Morlet and Db2.

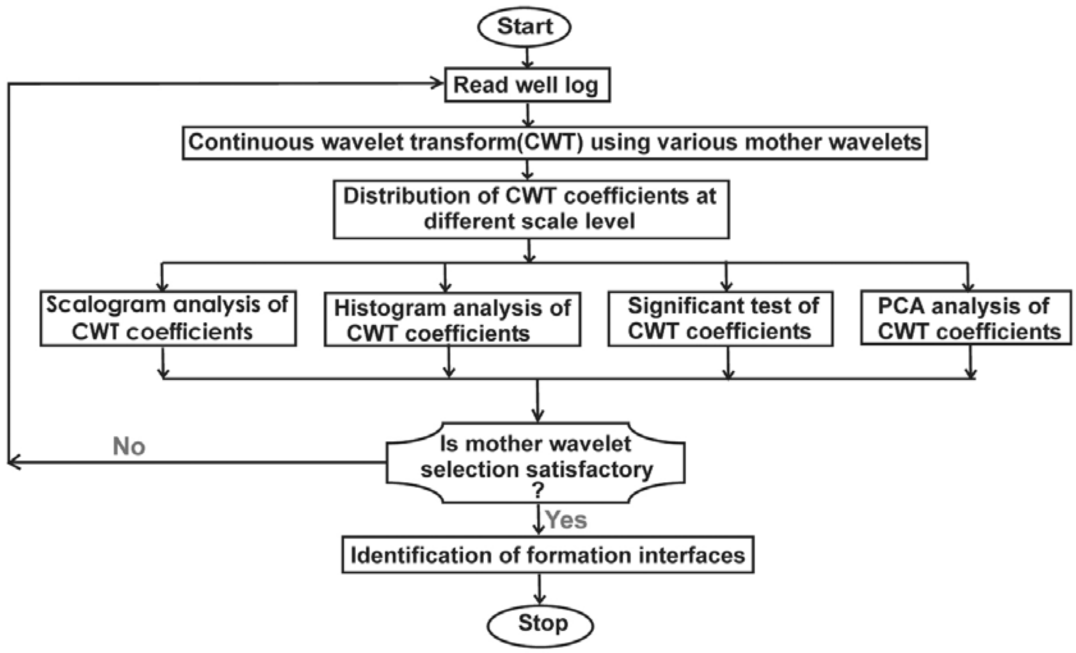

Figure 2. Basic flow diagram of CWT-based boundary detection and mother wavelet selection.

Then histogram analysis, statistical t-test by function t-test2, and PCA-based analysis were conducted on the obtained CWT coefficient distribution at even number scale. The best mother wavelet was chosen with highest histogram peak, t-test results (h=0 and p-value less than 1.0) and central characteristics of PCA results in PC1 and PC2 because, in most of the cases using PC1 and PC2, the output data variance is explained to the extent of 90%. At the end of the boundaries, interfaces are detected by using the best mother wavelet and are given in the table 2 and 3.

RESULTS AND DISCUSSIONS

Histogram analysis

Histograms of absolute normalised value of CWT coefficients were prepared for entire well log signal using various mother wavelets. The histogram analysis plot of gamma ray log of KTB pilot hole is presented in figure 3b.

Figure 3b demonstrates that maximum number of occurrence of CWT coefficients is close to 1300 for Haar wavelet, which is slightly lower than the results obtained by the Gaus1. Figure 3b implies that maximum number of occurrence of CWT coefficient for Gaus 3, Db2 and Morlet are around 1400, 1100 and 1000 respectively. Figure 4a shows the scalogram of density log of KTB main hole.

Figure 4b reveals that maximum number of occurrence of CWT coefficients is almost equal to 2000 whereas for Gaus1 it is close to 2100. The maximum number of occurrence of CWT coefficient for Gaus 3, Db2 and Morlet are around 1900, 1750 and 1150 respectively (Figure 4b).

Therefore, histogram-based CWT coefficient suggests that Gaus1 mother wavelet is better among the other wavelets being currently used for matching the gross signal characteristics. Conversely, it can be said that Gaus1 shows a better similarity between wavelet and original signal. It may be noted that CWT-based scalogram analysis gives the CWT coefficient (Amplitude) distribution against depth

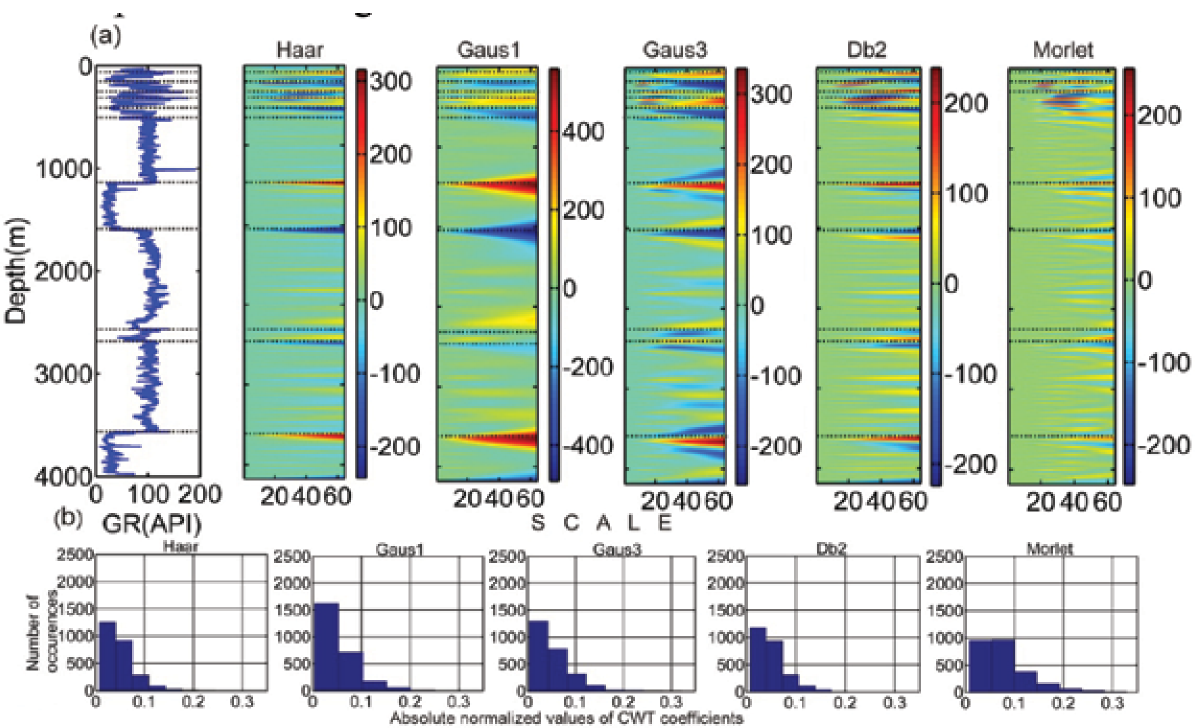

Figure 3. (a) Scalogram plots of gamma ray log data obtained from depth range 28 m to 4000 m at KTB pilot hole corresponding to Haar, Gaus1, Gaus3, Db2, and Morlet wavelets (b) Histogram analysis of CWT coefficients corresponding to Haar, Gaus1, Gaus3, Db2 and Morlet mother wavelet applied on gamma ray log.

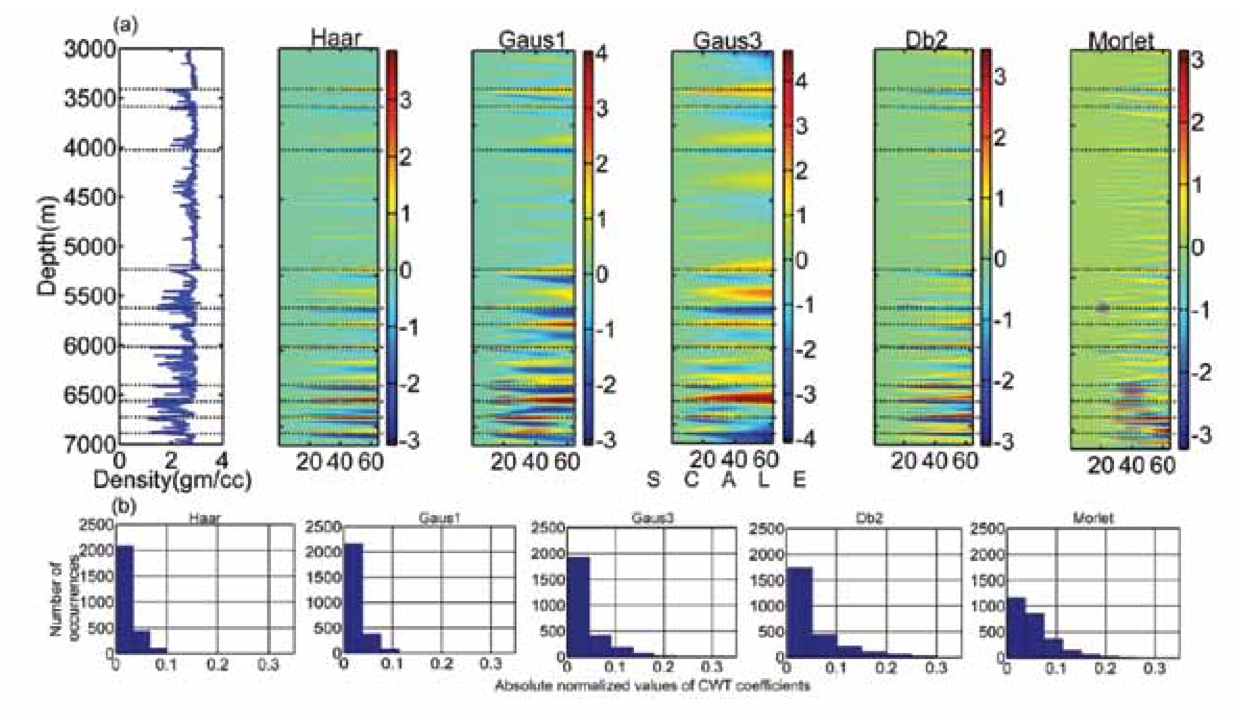

Figure 4. (a) Scalogram plots of density log data obtained from depth range 3000 m to 7000m at KTB main hole corresponding to Haar, Gaus1, Gaus3, Db2, and Morlet wavelets (b) Histogram analysis of CWT coefficients corresponding to Haar, Gaus1, Gaus3, Db2 and Morlet mother wavelet applied on density log.

Table 1. Significance test of the gamma ray log of pilot hole (P) and density log of main hole (M) data using various wavelets of Haar, Gaus1, Gaus 3, Db2 and Morlet. Here $Ph_{Haar,Gaus1}$ means h value using Haar and Gaus1 wavelets in pilot hole data and $Mh_{Haar,Gaus1}$ means h value using Haar and Gaus1 wavelets in main hole data. Others are denoted similarly.

Parameter of Hypothesis t- test	Level 1	Level 2	Level 3	Level 4	Level 5	Level 6
$Ph_{Haar,Gaus1}$ $PpH_{aar,Gaus1}$	0 0.97	0 0.60	0 0.81	0 0.37	0 0.47	0 0.41
$Ph_{Haar,Gaus3}$ $Pp_{Haar,Gaus3}$	0 0.36	0 0.34	0 0.70	0 0.53	0 0.81	0 0.95
$Ph_{Haar,Db2}$ $Pp_{Haar,Db2}$	0 0.87	0 0.78	0 0.26	0 0.17	0 0.46	0 0.44
$Ph_{Haar,Morlet}$ $Pp_{Haar,Morlet}$	0 0.89	0 0.94	0 0.71	0 0.36	0 0.96	0 0.50
$Mh_{Haar,Gaus1}$ $Mp_{Haar,Gaus1}$	0 0.41	0 0.30	0 0.13	0 0.25	0 0.51	0 0.55
$Mh_{Haar,Gaus3}$ $Mp_{Haar,Gaus3}$	0 0.55	0 0.01	0 0.32	0 0.61	0 0.92	0 0.99
$Mh_{Haar,Db2}$ $Mp_{Haar,Db2}$	0 0.23	0 0.33	0 0.06	0 0.13	0 0.31	0 0.63
$Mh_{Haar,Morlet}$ $Mp_{Haar,Morlet}$	0 0.80	0 0.14	0 0.02	0 0.29	0 0.86	0 0.18

of the well log. From the scalogram figure (3a & 4a), one can identify the litho-facies boundary zones by utilizing the property of space localization which is particularly important to identify the boundary of the litho-facies/ and/ or pay zones in well log analysis. This analysis is particularly significant because the maximum occurrence of CWT coefficient is related to the resolution of the scalogram, which in turn, helps identifying formation boundary. Therefore, it may be noted that optimum mother wavelet selection is critical for similarity measurement between wavelet and original log data in the space-localization of CWT based well log analysis.

Statistical significance test for CWT coefficient at various scales

We performed t-test by the function ttest2 between CWT coefficient distributions using different mother wavelets at various even numbers of scales with 5% significance level. Table 1 demonstrates the statistical significance test results between CWT coefficient of Haar and Gaus1 mother wavelet of scale 2, 4, 8, 16, 32 and 64 of the gamma ray log of KTB pilot hole data. The h-value gives 0.0 for all scales (even number considered here) and p-value ranges from 0.37 to 0.97. Here, h is equal to zero, which implies that null hypothesis cannot be rejected at this point with 5% significance level. A statistical significant value ($p<1.0$) implies that CWT coefficient of Haar and Gaus 1 is pertinent to model the data at all scales. The result of hypothesis test between CWT coefficient of Haar and Gaus 3 mother wavelet of scale 2, 4, 8, 16, 32 and 64 of the gamma ray log of KTB pilot hole data is shown in table1. The h-value gives 0 for all scales (even number considered) and p-value ranges from 0.34 to 0.95. Moreover, statistical significant value ($p<1.0$) implies that CWT distribution coefficients between Haar and Gaus 3 are relevant and closely associated with each other. Similarly, the result of statistical significance test between CWT coefficient of Haar and Db2 mother wavelet of scale 2, 4, 8, 16, 32 and 64 of the gamma ray log of KTB pilot hole data is documented (Table 1). The h-value gives 0 for all scales (even number considered), while the p-value varies from 0.17 to 0.87 suggesting that CWT coefficients between Haar and Db2 are closely tied to their relevancy in current analysis. The statistical significance test result between CWT coefficient of Haar and Morlet mother wavelet of scale 2, 4, 8, 16, 32 and 64 of the gamma ray log of KTB pilot hole data is demonstrated (table 1). The h-value gives 0 for all scales (even number considered) and the p-value ranges from 0.36 to 0.94. The p-values are also found statistically significant ($p<1.0$).

Likewise, Table 1 also demonstrates the hypothesis test result between CWT coefficient of Haar and Gaus1 mother wavelet of scale 2, 4, 8, 16, 32 and 64 of the density log of KTB main hole data. The h-value gives 0 for all scales (even number considered) and the p-value ranges from 0.13 to 0.55. Here also, null hypothesis cannot be rejected with 5% significance level because the h value is found to be zero. All the p-values are found to be less than 1.0 implying that CWT coefficients of Haar and Gaus 1 corresponding to all even number scales are statistically significant to model the original gamma log variation of KTB pilot hole.

The hypothesis test result between CWT coefficient of Haar and Gaus 3 mother wavelet of scale 2, 4, 8, 16,

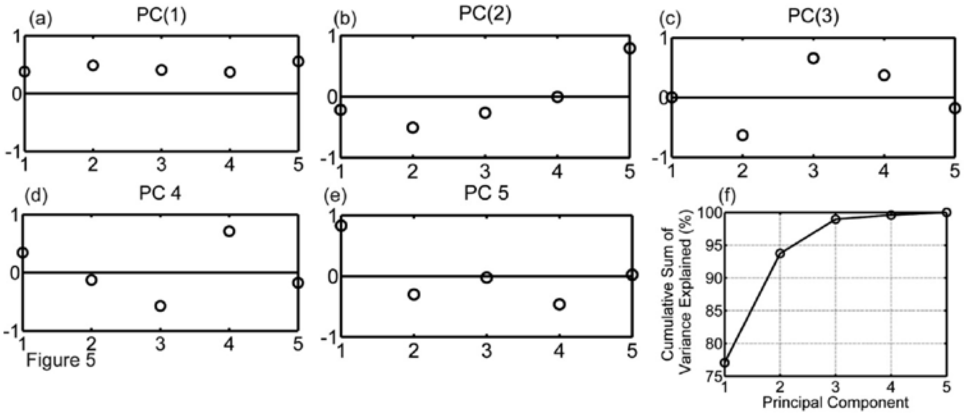

Figure 5. (a-e) PCA plot displays the impact of each variable (CWT coefficient series at scale 2 of various mother wavelets of gamma ray log of pilot hole) for modelling of well log signal. In the x-axis, position of Haar, Gaus 1, Gaus 3, Db2 and Morlet wavelet is represented by 1, 2, 3, 4, and 5 respectively. Y-axis denotes the impact of each wavelet and the value is normalized between -1 and +1. (f) The PCA analysis of well log data from cumulative sum of variance is explained by the different PCs.

32 and 64 of the gamma ray log of KTB pilot hole data is presented in Table 1. The h-value gives 0 for all scales (even number considered) and the p-value ranges from 0.01 to 0.99. The statistical significance ($p<1.0$) is closely linked to the authenticity and reliability of relevance. The result of hypothesis test between CWT coefficient of Haar and Db2 mother wavelet of scale 2, 4, 8, 16, 32 and 64 of the density log of KTB main hole data are documented in Table 1. The h-value shows 0 for all scales (even number considered) and the p-value varies from 0.13 to 0.63. The relevance between the CWT coefficient distribution of Haar and Db2 mother wavelet is distinct and noteworthy ($p<1.0$). The hypothesis test result between CWT coefficient of Haar and Morlet mother wavelet of scale 2, 4, 8, 16, 32 and 64 of the density log of KTB main hole data is provided (Table 1). The h-value gives 0 for all scales (even number considered) and the p-value ranges from 0.02 to 0.80. All the p-values are found to be less than 1.0 meaning that CWT coefficients of Haar and Morlet corresponding to all even number scales are statistically significant to model the original density log variation of KTB main hole.

PCA analysis

The Principal component analysis (PCA) is an effective tool to remove linear dependencies among variables (Jolliffe 1972). Ultimately it helps to reduce the data dimension for visualization (Ojha and Maiti 2016). Total data variance is distributed among PCs such as PC(1), PC(2), PC(3) etc. In order to represent the data characteristics satisfactorily, it is suggested to keep PCs whose eigen values are larger than 0.7 (Jolliffe, 1972).

We carried out PCA analysis of CWT coefficients at different scales obtained from CWT of gamma ray log of KTB pilot hole and density log of KTB main hole. Here, the total variables are five (i) Haar wavelet (ii) Gaus 1 wavelet (iii) Gaus 3 wavelet (iv) Db2 wavelet (v) Morlet wavelet. The results of PC on the five mother wavelets for the depth 28-4000 m interval are shown in figures 5-10 for pilot hole and figures 11-16 for main hole.

Pilot hole data

Figures 5a-e demonstrate the role of each PC corresponding to each mother wavelet for modeling well log at scale 2 and suggests that the Gaus 1 shares relatively principal role in modeling gamma ray in panel PC(1), although, mother wavelets show a significant positive involvement in PC(1) and PC(2), Gaus 1 and Morlet play key role in opposite direction. In PC(3), Gaus 1 and Gaus 3 have main role in opposite direction. In PC(4), Gaus 3 and Db2 have foremost role in opposite direction.

In PC(5), Haar has a key role opposite to Gaus 1 and Db2. Figure 5f suggests that 94% variance of the downhole data described by first two PCs. Thus, involvement of CWT coefficient data can in principle be described by first two PCs which are particularly significant in analyzing CWT coefficient of voluminous industrial data. Thus, the multivariable data set can be described using only two coordinate axes. The PCA based leading role amongst Haar, Gaus 1, Gaus 3, Db 2 and Morlet at scale 2 for the depth 28-4000 m interval of gamma ray log is demonstrated in figures 5a-e.

Figures 6(a-e) reveal the role of each PC corresponding to each mother wavelet for modeling well log at scale 4. Figures 6a-e suggest that the Gaus 3 shares relatively central role in modeling gamma ray in panel PC(1), although, mother wavelets have significant positive involvement in PC(1). In PC(2), Gaus 1 and Morlet have leading role in opposite direction. In PC(3), Gaus 1 and Gaus 3 have governing role in opposite direction. In PC (4),

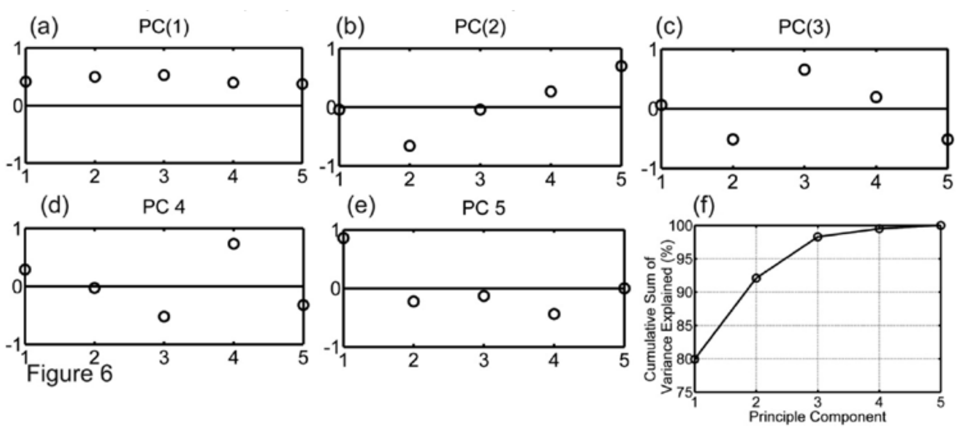

Figure 6. (a-e) PCA plot displays the impact of each variable (CWT coefficient series at scale 4 of various mother wavelets of gamma ray log of pilot hole) for modelling of well log signal. In the x-axis, position of Haar, Gaus 1, Gaus 3, Db2 and Morlet wavelet is represented by 1, 2, 3, 4, and 5 respectively. Y-axis denotes the impact of each wavelet and the value is normalized between -1 and +1. (f) The PCA analysis of well log data from cumulative sum of variance is explained by the different PCs.

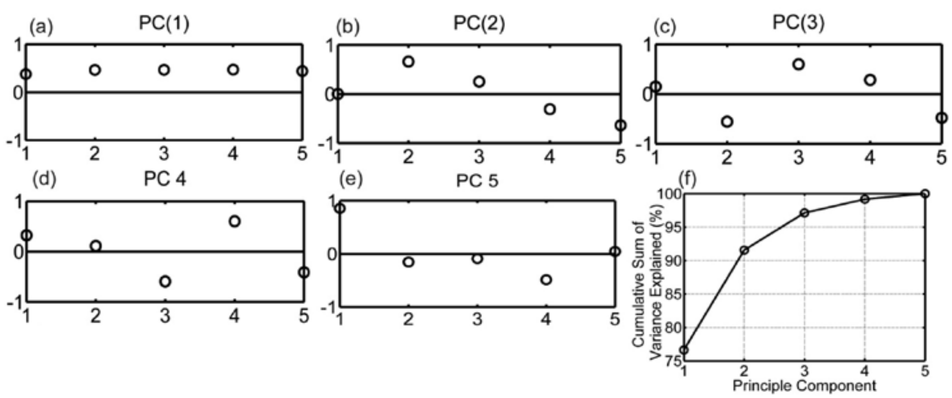

Figure 7. (a-e) PCA plot displays the impact of each variable (CWT coefficient series at scale 8 of various mother wavelets of gamma ray log of pilot hole) for modelling of well log signal. In the x-axis, position of Haar, Gaus 1, Gaus 3, Db2 and Morlet wavelet is represented by 1, 2, 3, 4, and 5 respectively. Y-axis denotes the impact of each wavelet and the value is normalized between -1 and +1. (f) The PCA analysis of well log data from cumulative sum of variance is explained by the different PCs.

Gaus 3 and Db2 have chief role but in opposite direction. In PC(5), Haar has major role opposite to Gaus 1 and Db 2. Figure 6f submits that 92% variance of the downhole data are elucidated by first two PCs.

Therefore, involvement of CWT coefficient data can in principle be described by first two PCs which are particularly significant in analyzing voluminous CWT coefficient of industrial data. Thus the multivariable data set can be described using only two coordinate axes. The PCA-based leading role among Haar, Gaus 1, Gaus 3, Db2 and Morlet at scale 4 for the depth 28-4000 m interval of gamma ray log is demonstrated in figures 6a-e.

Figure 6f suggests that 91% variance of the downhole data could be explained by first two PCs. So involvement of CWT coefficient data could in principle be described by first two PCs without losing much information, which is particularly significant in analyzing voluminous CWT coefficient of industrial data. Thus, the multivariable data set can be described using only two coordinate axes. The PCA-based significant role among Haar, Gaus 1, Gaus 3, Db2 and Morlet at scale 8 for the depth 28-4000 m interval of gamma ray log is demonstrated in figures 7a-e.

Figures 7(a-e) display the role of each PC corresponding to each mother wavelet for modeling well log at scale 8. Figure 7a-e suggest that the Db2 shares slightly prominent role in modeling gamma ray in panel PC(1), although, mother wavelets have significant positive involvement in PC(1). In PC(2), Gaus 1 and Morlet have prominent role in opposite direction. In PC (3), Gaus 1 and Gaus 3 have important role in opposite direction. In PC(4), Gaus 3 and Db 2 have significant role in opposite direction. In PC(5), Haar and Db 2 have major role in opposite direction.

Figures 8(a-e) exhibit the role of each PC corresponding to each mother wavelet for modeling well log at scale 16. Figures 8a-e suggest that the Gaus 1 shares slightly significant role in modeling gamma ray in panel PC(1), although, mother wavelets have significant positive involvement in PC(1).

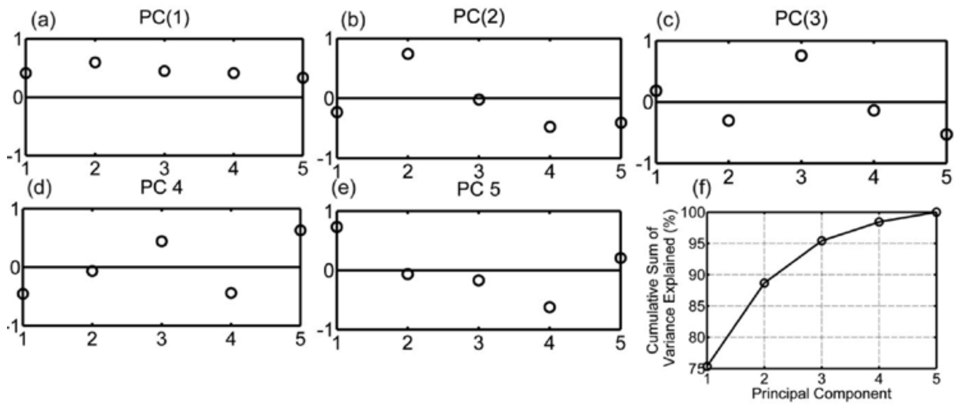

Figure 8. (a-e) PCA plot displays the impact of each variable (CWT coefficient series at scale 16 of various mother wavelets of gamma ray log of pilot hole) for modelling of well log signal. In the x-axis, position of Haar, Gaus 1, Gaus 3, Db2 and Morlet wavelet is represented by 1, 2, 3, 4, and 5 respectively. Y-axis denotes the impact of each wavelet and the value is normalized between -1 and +1. (f) The PCA analysis of well log data from cumulative sum of variance is explained by the different PCs.

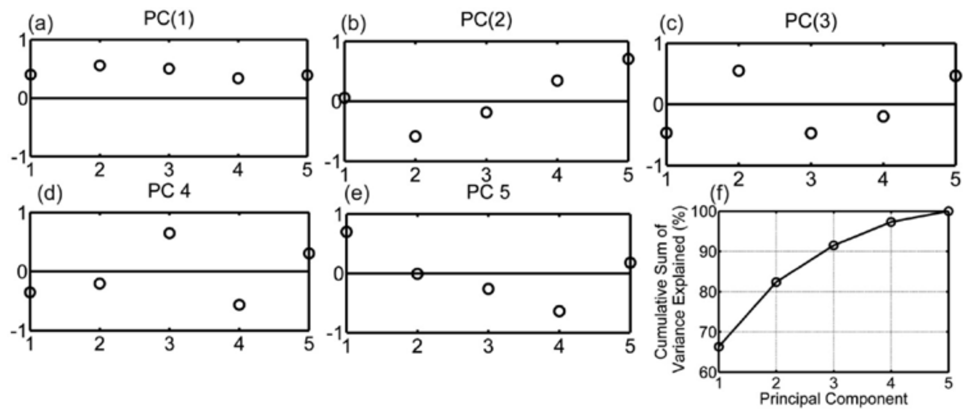

Figure 9. (a-e) PCA plot displays the impact of each variable (CWT coefficient series at scale 32 of various mother wavelets of gamma ray log of pilot hole) for modelling of well log signal. In the x-axis, position of Haar, Gaus 1, Gaus 3, Db2 and Morlet wavelet is represented by 1, 2, 3, 4, and 5 respectively. Y-axis denotes the impact of each wavelet and the value is normalized between -1 and +1. (f) The PCA analysis of well log data from cumulative sum of variance is explained by the different PCs.

As seen in PC (2) panel, Gaus1 and Morlet have significant roles but they are in opposition to each other. PC(3) demonstrates the dominance of Gaussian wavelets (order 1 and 2) but their role is in opposite direction. On the other hand, PC(4) shows that the impact and direction of influence of Db2 and Morlet are distinct. Figure 8f recommends that 89% variance of the downhole data are explained by first two PCs. Thus, the multivariat data set can be described using only two coordinate axes. The PCA based significant role among Haar, Gaus 1, Gaus 3, Db2 and Morlet at scale 16 for the depth 28-4000 m interval of gamma ray log is demonstrated in figures 8a-e.

Figures 9(a-e) show the role of each PC corresponding to each mother wavelet for modeling well log at scale 32. Figures 9a-e suggest that the Gaus 1 plays a better role in modeling gamma ray in panel PC (1), although the mother wavelets have significant positive role in PC (1). In PC(2), Gaus1 and Morlet have central role in opposite direction. In PC(3), Gaus1 and Gaus3 have significant role in opposite direction. In PC (4), Gaus3 and Db2 have significant role in opposite direction. In PC(5) Haar and Morlet play key roles in opposite direction. According to figure 9f, 82% variance of the downhole data are explained by the first two PCs. Thus, the multivariable data set can be described using only two coordinate axes. The PCA-based key role among Haar, Gaus 1, Gaus 3, Db2 and Morlet at scale 32 for the depth 28-4000 m interval of gamma ray log is demonstrated in figures 9a-e.

Figures 10(a-e) demonstrate the role of PC corresponding to each mother wavelet for modeling well log at scale 64 suggesting that the Gaus 1 shares slightly persuasive role in modeling gamma ray in panel PC(1), although, mother wavelets have significant positive involvement in PC(1). Gaus 1 and Morlet have persuasive role in PC(2) in opposite direction. Similarly in PC(3), Gauss 1 and Gaus 3 have credible roles in opposite direction. Further, one can

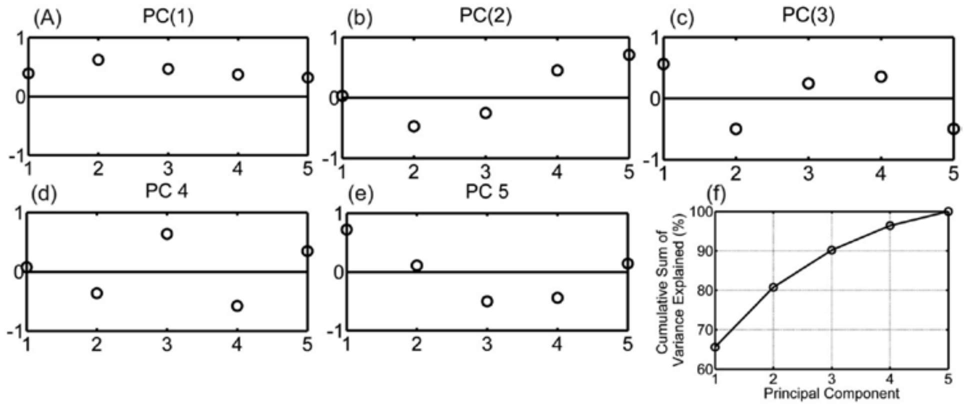

Figure 10. (a-e) PCA plot displays the impact of each variable (CWT coefficient series at scale 64 of various mother wavelets of gamma ray log of pilot hole) for modelling of well log signal. In the x-axis, position of Haar, Gaus 1, Gaus 3, Db2 and Morlet wavelet is represented by 1, 2, 3, 4, and 5 respectively. Y-axis denotes the impact of each wavelet and the value is normalized between -1 and +1. (f) The PCA analysis of well log data from cumulative sum of variance is explained by the different PCs.

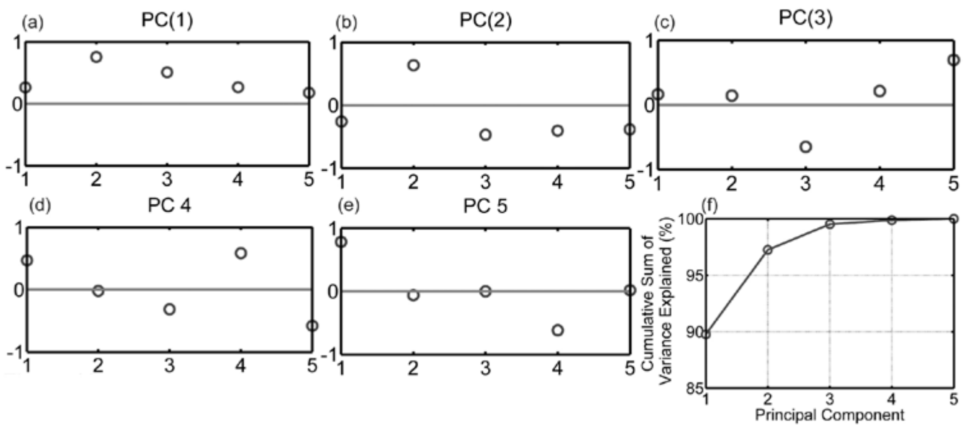

Figure 11. (a-e) PCA plot demonstrates the impact of each variable (CWT coefficient series at scale 2 of various mother wavelets of density log of main hole) for modelling of well log signal. In the x-axis, position of Haar, Gaus 1, Gaus 3, Db2 and Morlet wavelet are represented by 1, 2, 3, 4, and 5 respectively. Y-axis denotes the impact of each wavelet and the value is normalized between -1 and +1. (f) The PCA analysis of well log data from cumulative sum of variance is explained by the different PCs.

see that in PC(4), Gauss 3 and Db 2 have credible roles in opposite direction. In PC (5), Haar and Morlet have credible roles in opposite direction. Figure 10f proposes that 80% variance of the downhole data are explained by first two PCs.

Main hole data

Figures 11a-e reveals the role of each PC corresponding to each mother wavelet for modeling well log at scale 2.
Figure 11 suggests that the Gaus1 shares relatively cogent role in modeling gamma ray in panel PC(1), although, mother wavelets have significant positive involvement in PC(1). In PC(2), Gaus 1 and Gaus 3 have cogent role in opposite direction. In PC(3), Gaus 3 and Morlet have cogent roles in opposite direction. In PC(4), Morlet and Db(2) have main role in opposite direction. In PC(5) Haar has a sound role opposed to Db 2

Figure 11f reveals that 97% variance of the downhole data are explained by first two PCs. The PCA-based dominant role among Haar, Gaus 1, Gaus 3, Db2 and Morlet at scale 2 for the depth 3000-7000 m interval of density log is demonstrated in figures 11a-e. Figures 12a-e demonstrate the role of each PC corresponding to each mother wavelet for modeling well log at scale 4.

Figures 12(a-e) suggest that the Gaus 1 shares relatively sound role in modeling density log in panel PC(1), although, mother wavelets have significant positive involvement in PC(1). PC(2) panel shows the influence of Gaus 1 and Morlet are distinct but they are opposite in direction. PC(3) exhibits convincing role of Gaus 3 and Morlet wavelet although they are found in opposite direction. In PC (4), Morlet and Db2 have principal role in opposite direction. In PC(5) Haar has central role opposite to Db2. Figure 12f advocates that 95% variance of the downhole data are explained by first two PCs. The PCA-based convincing role among Haar, Gaus 1,

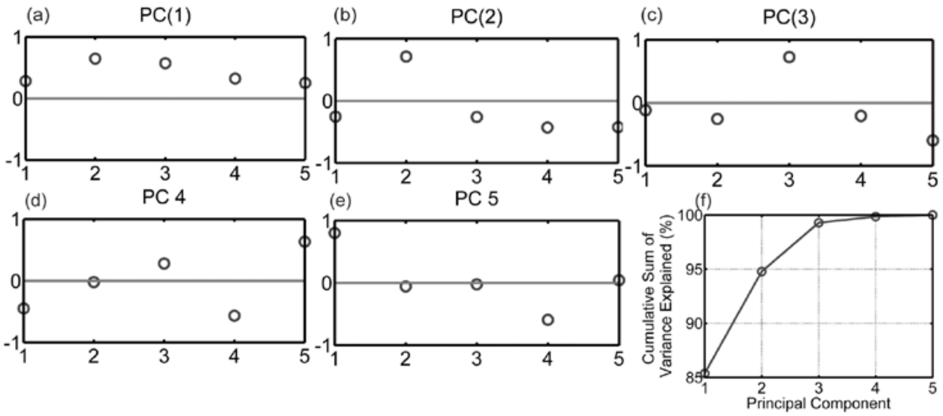

Figure 12. (a-e) PCA plot demonstrates the impact of each variable (CWT coefficient series at scale 4 of various mother wavelets of density log of main hole) for modelling of well log signal. In the x-axis, position of Haar, Gaus 1, Gaus 3, Db2 and Morlet wavelet are represented by 1, 2, 3, 4, and 5 respectively. Y-axis denotes the impact of each wavelet and the value is normalized between -1 and +1. (f) The PCA analysis of well log data from cumulative sum of variance is explained by the different PCs.

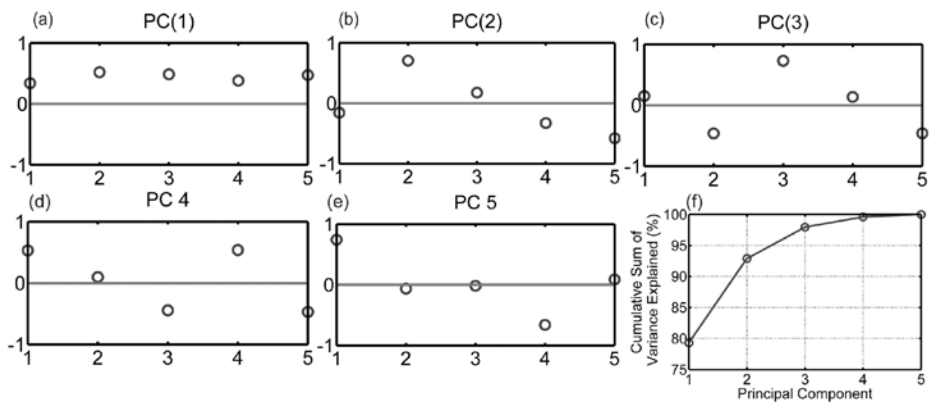

Figure 13: (a-e) PCA plot demonstrates the impact of each variable (CWT coefficient series at scale 8 of various mother wavelets of density log of main hole) for modelling of well log signal. In the x-axis, position of Haar, Gaus 1, Gaus 3, Db2 and Morlet wavelet are represented by 1, 2, 3, 4, and 5 respectively. Y-axis denotes the impact of each wavelet and the value is normalized between -1 and +1. (f) The PCA analysis of well log data from cumulative sum of variance is explained by the different PCs.

Gaus 3, Db 2 and Morlet at scale 4 for the depth 3000-7000 m interval of density log is demonstrated in figures 12a-e.

Figures 13(a-e) exhibit the role of each PC corresponding to each mother wavelet for modeling well log at scale 8. Figures 13a-e suggest that the Gaus 1 shares slightly convincing role in modeling density in panel PC(1), although, mother wavelets have significant positive involvement in PC(1). In PC(2), Gaus 1 and Morlet have strong role in opposite direction. In PC (3), Gaus 1 and Gaus 3 have strong role in opposite direction. In PC (4), Gaus 3 and Db 2 have strong role in opposite direction. In PC(5), Haar and Db2 have strong role in opposite direction. Figure 13f submits that 92% variance of the downhole data are explained by first two PCs. The PCA based strong role among Haar, Gaus1, Gaus3, Db2 and Morlet at scale 8 for the depth 3000-7000 m interval of gamma ray log is demonstrated in figures 13a-e.

Figures 14(a-e) divulge the role of each PC corresponding to each mother wavelet for modeling well log at scale 16. Figures 14a-e suggest that the Gaus 1 shares slightly strong role in modeling density in panel PC(1), although, mother wavelets have significant positive involvement in PC(1). As seen in PC(2) panel, Gaus 1 and Morlet play major role to characterize the signal but their influence is found in opposite direction. PC(3) demonstrates dominance of Gaussian wavelets although they are acting in opposite direction, to match with the signal. It is evident from panel PC(4) that Db2 dominates over Morlet wavelet but the role of action is in opposite direction. PC(5) guides that Haar and Db2 can be more influential than the rest of the wavelets used.

Figure 14f advocates that 90% variance of the downhole data are explained by first two PCs. The PCA-based dominant role among Haar, Gaus 1, Gaus 3, Db2

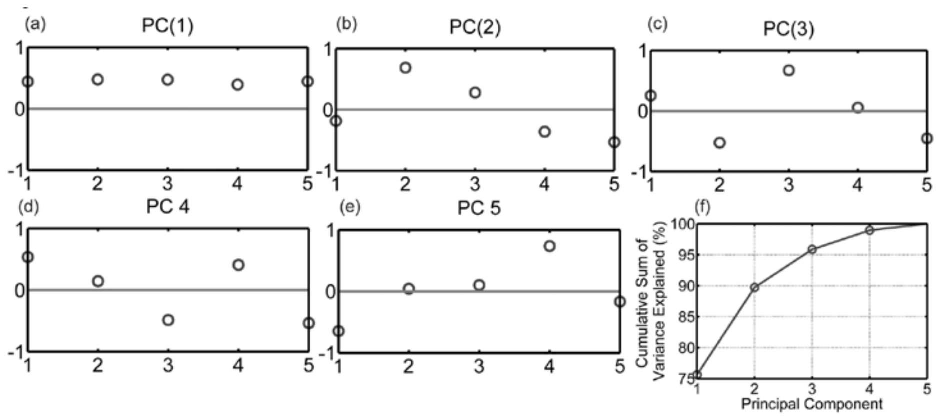

Figure 14: (a-e) PCA plot demonstrates the impact of each variable (CWT coefficient series at scale 16 of various mother wavelets of density log of main hole) for modelling of well log signal. In the x-axis, position of Haar, Gaus 1, Gaus 3, Db2 and Morlet wavelet are represented by 1, 2, 3, 4, and 5 respectively. Y-axis denotes the impact of each wavelet and the value is normalized between -1 and +1. (f) The PCA analysis of well log data from cumulative sum of variance is explained by the different PCs.

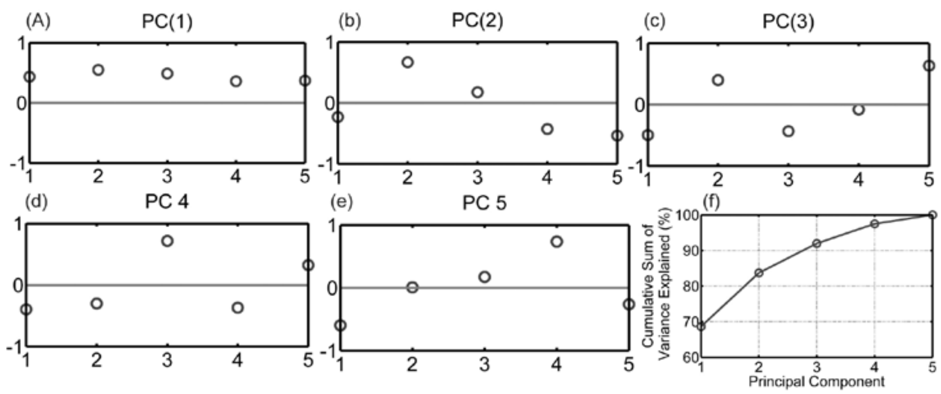

Figure 15. (a-e) PCA plot demonstrates the impact of each variable (CWT coefficient series at scale 32 of various mother wavelets of density log of main hole) for modelling of well log signal. In the x-axis, position of Haar, Gaus 1, Gaus 3, Db2 and Morlet wavelet are represented by 1, 2, 3, 4, and 5 respectively. Y-axis denotes the impact of each wavelet and the value is normalized between -1 and +1. (f) The PCA analysis of well log data from cumulative sum of variance is explained by the different PCs.

and Morlet at scale 16 for the depth 3000-7000 m interval of density log is demonstrated in figures 14a-e.

Figures 15(a-e) suggest the role of each PC corresponding to each mother wavelet for modeling well log at scale 32. Figures 15a-e imply that the Gaus1 shares slightly forceful role in modeling gamma ray in panel PC(1), although, mother wavelets have significant positive contribution in PC(1). In PC(2), Gaus1 and Morlet have powerful role in opposite direction. In PC(3), Morlet and Gaus 3 have clear role in opposite direction. In PC (4), Gaus 3 and Db2 have clear role in opposite direction. In PC (5) Haar and Morlet have key role in opposite direction. Figure 15f proposes that 82% variance of the downhole data are explained by first two PCs. Thus the multivariate data set can be described using only two coordinate axes. The PCA based central role among Haar, Gaus 1, Gaus 3, Db2 and Morlet at scale 32 for the depth 3000-7000 m interval of density log is demonstrated in figures 15a-e.

Figures 16a-e demonstrate the role of each PC corresponding to each mother wavelet for modeling well log at scale 64. Figures 16a-e suggest that the Gaus 1 shares slightly central role in modeling gamma ray in panel PC(1), although, mother wavelets have significant positive involvement in PC(1). In PC(2), Gaus1 and Morlet have key role but in opposite direction. In PC(3), Gaus 3 and Morlet have key role in opposite direction. In PC (4), Gaus 3 and Db2 have key role in opposite direction. In PC (5) Haar and Morlet have key role in opposite direction. Figure 16f recommends that 74% variance of the downhole data are explained by first two PCs. The PCA-based key role among Haar, Gaus 1, Gaus 3, Db2 and Morlet at scale 64 for the depth 3000-7000 m interval of density log is demonstrated in figures 16a-e.

The scalogram plots corresponding to mother wavelet Haar, Gaus 1, Gaus 3, Db2 and Morlet of gamma ray log of KTB pilot hole shown in figure 3 demonstrate that

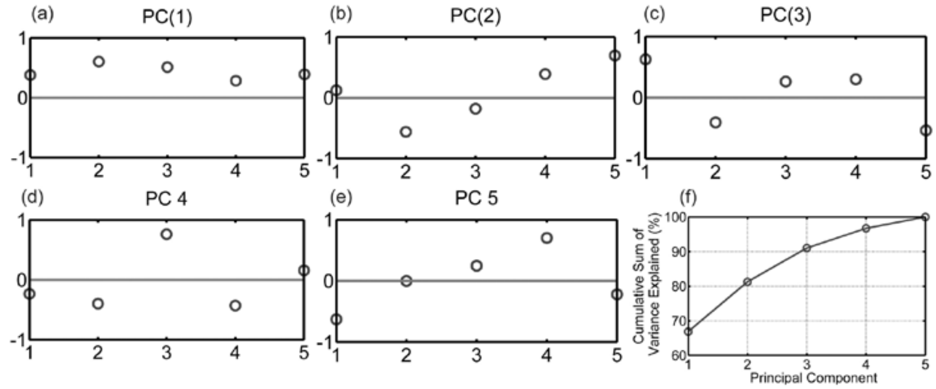

Figure 16. (a-e) PCA plot demonstrates the impact of each variable (CWT coefficient series at scale 64 of various mother wavelets of density log of main hole) for modelling of well log signal. In the x-axis, position of Haar, Gaus 1, Gaus 3, Db2 and Morlet wavelet are represented by 1, 2, 3, 4, and 5 respectively. Y-axis denotes the impact of each wavelet and the value is normalized between -1 and +1. (f) The PCA analysis of well log data from cumulative sum of variance is explained by the different PCs.

Table 2. Calculating depths of formation tops from the scalogram plots of the gamma ray intensity log in pilot hole data by using Haar, Gaus1, Gaus3, Morlet and Db2 wavelets.

Actual depths of the formation top obtained from log data (m)	Depths to the formation top by using different wavelets from scalogram plots (m)				
	Haar	Gaus1	Gaus3	Db2	Morlet
60.04	60.04	59.74	59.89	59.89	58.82
112.77	112.31	112	110.49	111.55	Not clear
196.44	196.13	Not clear	Not clear	195.98	Not clear
303.58	303.58	302.51	302.97	303.12	Not clear
336.65	336.65	335.73	334.67	336.04	Not clear
511.45	511.45	510.84	Not clear	510.08	Not clear
1150.01	1150.01	1150.01	1149.85	1150.01	Not clear
1597	1597	1597	1596.84	1596.84	1596.69
2683.61	2683.30	2683.15	2683	2683.30	Not clear
2733.29	2733.14	2732.83	2732.53	2783.83	2732.68
3564.02	3564.02	3564.02	3563.72	3563.87	3563.56

the formation boundary are well resolved grossly against the log response changes. The detailed comparison of identified formation boundary for KTB pilot hole and main hole by using CWT-based scalogarms of various mother wavelets is presented in the tables 2 and 3 respectively. Overall, the boundary picked by the different scalograms of corresponding mother wavelet is found to be satisfactory and is well tuned with the boundary detected from the changes of the well log at the KTB site (Table 2 and 3). Looking at the scalogram figures, Gaus 1 gives better resolution (spectral bands are more distinct) in comparison to the rest of the mother wavelets used, however, it also provides thicker spectral distribution at the sharp boundary of the bed. In the case of sharp bed boundary picking, Haar-based scalogram gives spectral distribution, which is relatively sharp at the boundary (Figure 3 and 4). The blocky kernel functions of the Haar wavelet, which helps to find the depth of the boundary with less smearing of spectral bands, is appropriate to model blocky signal at the boundary.

Conversely, Gaus 1 provides attractive structures for the interpreter for the overall signal matching for pay zone/litho-facies zone because it captures over all changes of the spectral band and or/distribution of CWT coefficients at different scales. However, comparatively poor resolution of non-Gaussian wavelets is evident because there is more miss-match of shape between mother wavelet and well log gross signal. Moreover, ~~shifts~~ and ~~dilations~~ parameters and their averaging at the boundary could be the cause for poor resolution. Therefore, in many of the cases, there is no clarity of boundary detection (table 2 and 3). The distribution and changes from positive to negative and vice versa of CWT coefficients over the colour panel clearly demonstrates the lithology/litho-facies changes at the KTB

Table 3. Calculating depths of formation tops from the scalogram plots of the density log in main hole data by using Haar, Gaus1, Gaus3, Db2 and Morlet.

Actual depths of the formation top obtained from log data (m)	Depths to the formation top by using different wavelets from scalogram plots (m)				
	Haar	Gaus1	Gaus3	Db2	Morlet
3409.79	3409.79	3409.64	3409.49	3409.18	3410.10
3546.34	3546.34	3546.19	3545.89	3546.19	3545.12
4000.51	4007.81	4007.51	4007.05	4008.12	4008.12
5204.61	5204.61	5204.61	5204.91	5204.15	5204.15
5773.21	5773.21	5773.21	5773.52	5773.82	Not clear
6007.30	6007.30	6007.30	Not clear	6007.30	6006.69
6436.46	6436.46	6436.31	Not clear	6436.31	6435.85
6566.30	6566.45	6566.30	6566.76	6566.45	6566.00
6709.10	6709.10	6709.10	6708.95	6709.25	6708.80
6882.38	6882.38	6882.38	6882.23	6882.53	6882.07

site. The boundary detected by the scalogram analysis is closely matching with the boundary obtained by the KTB research team using multiple methods (Pechnig et al., 1997; Maiti and Tiwari, 2009, 2010a-b; Singh et al., 2016).

CONCLUSIONS

In this paper, CWT based wavelet analysis has been carried out and scalogram was prepared using various mother wavelets to identify the very complex formation interfaces using the KTB well log data. For this histogram analysis, statistical significance test and PCA-based analysis were performed to understand how each CWT coefficient plays role in overall signal modeling and characterizing the KTB well log data. These results will be useful to provide future guidelines for selecting appropriate wavelet functions for such complex well log signal modeling.

From the above study, we reached at the following conclusions.

Histogram analysis shows that the CWT coefficients of Gaus 1 occur maximum times in the entire well log signals of KTB pilot and main hole. Hence, Gaus 1 is found to be the relatively best mother wavelet for CWT- based scalogram analysis of well log signal. Results after significance test demonstrate that spatial series at even number scale are statistically significant among all mother wavelets. PCA- based analysis suggests that CWT coefficient of Gaus 1 plays a major role in most of the cases at PC (1) and PC (2) for both pilot and main hole well log data.

ACKNOWLEDGEMENTS

AS and SM are gratified to Director, IIT (ISM), Dhanbad for permitting to publish the work. AS is thankful to IIT(ISM) for SRF fellowship. Financial support from the Ministry of Earth Sciences, Govt. of India, New Delhi (Grant No: MoES/P.O. (Geosci)/44/2015) is acknowledged. RKT is grateful to DAE for award of RRR. We are thankful to Dr. Gautam Gupta, Indian Institute of Geomagnetism for meticulous review, which has greatly improved the paper. Authors are also thankful to Dr.M.R.K.Prabhakar Rao for constructive editing of the manuscript. We thank the Chief Editor for his support.

Compliance with Ethical Standards

The authors declare that they have no conflict of interest and adhere to copyright norms.

REFERENCES

Adamowski, J., and Chan, H.F., 2011. A wavelet neural network conjunction model for groundwater level forecasting, J. Hydrol., v.407, pp: 28-40.

Chandrashekhar, E., and Rao, V.E., 2012. Wavelet analysis of Geophysical Well- log Data of Bombay offshore Basin, India Math. Geosci., v.44, pp: 901-928.

Daubechies, I., 1992. Ten lectures on wavelets, Soc. for Ind. and Appl. Math. Philadelphia, Pa. pp: 357.

Doveton, J.H., 1986. Log Analysis of Subsurface Geology Concepts and Computer Methods Wiley, New York, NY., pp: 273.

Farge, M., 1992. Wavelet transforms and their applications to turbulence, Annu. Rev. Fluid Mech., v.24, pp: 395-457.

Goupillaud, R.A., Grossmann, A., and Morlet, J., 1985. Cycle-octave and related transform in seismic signal analysis, Geoex., v.23 pp: 85-102.

Javid, M., and Tokhmechi, B., 2012. Formation interface detection using Gamma Ray log: A novel approach, J. Mining & Env., v.3, no.1, pp: 41-50.

Jolliffe, I.T., 1972. Discarding variables in a principle components analysis 1: Artificial Data, Appl. Stat., v.21, pp: 160-173.

Kisi, O., 2009. Wavelet regression model as an alternative to neural networks for monthly streamflow forecasting, Hydrol. Process., v.23, no.25, pp: 3583-3597.

Kumar, P., and Foufoula-Georgiou, E., 1997. Wavelet analysis for geophysical applications Review. Geophys., v.35, no.4, pp: 385-412.

Labat, D., 2008. Wavelet analysis of the annual discharge records of the world's largest rivers, Adv. Water Resour., v.31, no.1, pp: 109–117.

Liu, Z., Zhou, P., Chen, G., and Guo, L., 2014. Evaluating a coupled discrete wavelet transform and support vector regression for daily and monthly stream flow forecasting, J. Hydrol., v.519, pp: 2822-2831.

Maheswaran, R., and Khosa, R., 2012. Comparative study of different wavelets for hydrologic forecasting, Comput. Geosci., v.46, pp: 284–295.

Maiti, S., and Tiwari, R. K., 2009. A hybrid Monte Carlo method based artificial neural networks approach for rock boundaries identification: A case study from the KTB bore hole, Pure and Appl. Geophys., v.166, pp: 2059-2090.

Maiti, S., and Tiwari, R. K., 2010a. Automatic discriminations among geophysical signals via the Bayesian neural networks approach, Geophys., v.75, no.1, pp: E67-E78.

Maiti, S., and Tiwari, R. K., 2010b. Neural network modeling and an uncertainty analysis in Bayesian framework: A case study from the KTB borehole site, J. Geophy. Res., B10208., v.115.

Maraun, D., Kurths, J., and Holschneider, M., 2007. Nonstationary Gaussian processes in wavelet domain: synthesis, estimation, and significance testing. Physical Rev., E, v.75, pp: 016707.

Morlet, J., Arens, G., Fourgeau, E., and Giard, D., 1982. Wave propagation and sampling theory-part I:Complex signal and scattering in multilayered media Geophysics., v.47, no.2, pp: 203-221.

Nourani, V., Baghanam, A.H., Adamowski, J., and Kisi, O., 2014. Applications of hybrid wavelet–artificial intelligence models in hydrology: A review J. Hydrol., v.514, pp: 358–377.

Nourani, V., Kisi, O., and Komasi, M., 2011. Two hybrid artificial intelligence approaches for modelling rainfall-runoff process, J. Hydrol., v.402, no.1–2, pp: 41–59.

Ojha, M., and Maiti, S., 2016. Sediment classification using neural networks: an example from the site-U1344A of IODP Expedition 323 in the Bering Sea Deep-Sea Research Part II: Topical Studies in Oceanography, v.125-126, pp: 202-213.

Pan, S., Hsieh, B., Lu, M., and Lin, Z., 2008. Identification of stratigraphic formation interfaces using Wavelet and Fourier transform Comput. Geosci., v.34, pp: 77-92.

Pechnig, P., Haverkamp, S., Wohlenberg, J., Zimmermann, G., and Burkhardt, H., 1997. Integrated interpretation in the German Continental Deep Drilling Program: Lithology, porosity, and fracture zones. J. Geophys. Res., v.102, pp: 18363-18390.

Percival, D., and Walden, A. T., 2000. Wavelet methods for time series analysis Cambridge University Press, Cambridge, U.K.

Perez-Munoz, T., Velasco-Hernandez, J., and Hernandez-Martinez, E., 2013. Wavelet transform analysis for lithological characteristics identification in siliciclastic oil fields, J. Appl. Geophys., v.98, pp: 298-308.

Prokoph, A., and Agterberg, F. P., 2000. Wavelet analysis of well-logging data from oil source rock, Egret Member offshore eastern Canada Am Assoc Pet. Geol. Bull., v.84, pp: 1617–1632.

Sang, Y.F., Singh, V.P., Sun, F., Chen, Y., Liu, Y., and Yang, M., 2016. Wavelet-based hydrological time series forecasting J. Hydrol. Eng., v.21, no.5, pp: 06016001.

Schaefli, B., Maraun, D., and Holschneider, M., 2007. What drives high flow events in the Swiss Alps? Recent developments in wavelet spectral analysis and their application to hydrology Adv. Water Resour., v.30, no.12, pp: 2511–2525.

Shoaib, M., Shamseldin, A.Y., and Melville, B.W., 2014. Comparative study of different wavelet based neural network models for rainfall runoff modelling, J. Hydrol., v.515, pp: 47–58.

Singh, A., Maiti, S., and Tiwari, R.K., 2016. Modelling discontinuous well log signal to identify lithological boundaries via wavelet analysis: An example from KTB borehole data, J. Earth Sys. Sci., v.125, no.4, pp: 761-776.

Singh, R.M., 2011. Wavelet-ANN model for flood events Adv. Intel. Software Comput., v.131, pp: 165–175.

Strang, G., and Nguyen, T., 1995. Wavelets and filter banks. Wellesley–Cambridge Press, Prentice Hall.

Torrence, C., and Compo, G.P., 1998. A practical guide to wavelet analysis B. Am. Meteorol. Soc., v.79, no.1, pp: 61–78.

Walker, J.S., 1999. A primer on wavelets and their scientific applications, Chapman and Hall, CRC, New York.

NEWS AT A GLANCE

Forthcoming Events:

*April 27-28, 2017
4^{th} International Conference on Geology and Geoscience
"Exploring the Recent trends and analytical techniques in the field of Geology and Geosciences".
DUBAI, UAE. For details Email-geology@conferenceseries.net

*RSCy2017 — Fifth International Conference on Remote Sensing and Geo-Information of the Environment
20 Mar 2017 - 23 Mar 2017; Paphos, Cyprus
"Remote Sensing Applications, Geo-information, Geophysics, Remote sensing & geo-information in education, Ecosystems, Environment and Sustainable Development"
website: http://www.cyprusremotesensing.com/rscy2017/

*Association of Petroleum Geologists Annual Convention and Exhibition 2017
02 Apr 2017 - 05 Apr 2017; Houston, United States
"Petrophyscis , Petrochemistry and Petrochemical Industry"
website: http://www.aapg.org/events/conferences/ace/announcement/articleid/5663/aapg-2017-annual-convention-exhibition

*Engineering Geophysics 2017 Conference and Exhibition
24 Apr 2017 - 28 Apr 2017; Kislovodsk, Russia
website: http://www.eage.org/event/index.php?eventid=1508&Opendivs=s3

*Vernacular, Life-Style, Architecture, Design, and Place-making — TRIKONA Conference: VERNACULAR
03 Mar 2017 - 05 Mar 2017; Cheyyur Taluk, Kancheepuram District, India
"Architecture, Disaster-Management, Resilience, Sustainability, Engineering (general), Civil Engineering".
website: http://www.midas.ac.in

Scientific and Technology related news

***Prime Minister Narendra Modi moots Scientific Social Responsibility**

While inaugurating the 104^{th} Indian Science Congress on 3^{rd} January, 2017 at Tirupati (A.P.) Narendra Modi said as in the case of Corporate Social Responsibility, the concept of Scientific Social Responsibility needs to be developed to connect leading institutions to all stakeholders, including schools and colleges. He re-iterated that National Laboratories should connect with schools and colleges to develop appropriate training programmes. He is of the opinion that we have to develop innovative ideas focusing on societal needs. While appreciating India has become 6^{th} in the world as far as scientific publications as per the SCOPUS data base of peer-reviewed literature from science, he wanted scientists to focus on scientific studies of societal importance at par with basic and application oriented basic sciences. (**Source**: 4^{th} January issue of Deccan Chronicle).

I have mentioned in number of editorials the need to spare some of the valuable time to address various types of problems faced by the common man, due to non implementation of scientific procedures.

***CSIR-NGRI to identify underground sewer leakages in the twin-cities**

The Metro Water and Sewerage Board is working with CSIR-NGRI to identify underground sewer leakages by using Ground Penetrating Radar Technology. This has become essential as roads have caved in forming large craters (sink holes) at three different places in Hyderabad due to collapse of sewerage and water supply pipes. NGRI has requisite technical knowhow and experience, which would help to detect land subsidence zones/areas. NGRI will deploy technically qualified team of experts to study vulnerable pipe lines. (**Source:** 3^{rd} January issue of Deccan Chronicle)

NGRI earlier extended its help in lessening pollution in number of lakes present within GHMC limits.

Science News

***Groundwater Contamination in Karst Regions Affects Human Health**

Some characteristics of limestone aquifers, in contrast to porous media, make them particularly susceptible to contamination. Sinking streams and sinkholes provide a rapid route for unfiltered contaminants from the land surface to the underlying aquifer. This characteristic, along with swift groundwater flow in conduits that have been widened by mineral dissolution (karst aquifers) and difficulty characterizing and monitoring the highly heterogeneous karst subsurface, contributes to an elevated risk for degradation of water quality. The reliance on groundwater for drinking supplies in karst regions creates the potential for public health effects. The non profit Karst Waters Institute of Virginia State, USA held an interdisciplinary conference (http://bit.ly/ Karst-Conf) to explore knowledge gaps between the science of contaminant transport in karst aquifers and our understanding of exposure pathways and health outcomes. Seventy experts from seven countries attended. They specialized in karst hydrogeology, contaminant geochemistry, microbiology, public health sciences, and environmental law and regulation. Attendees grappled with identifying conceptual and practical obstacles while they learned of new tools, findings, and promising perspectives for protecting human health. Sessions highlighted emerging tools for investigating contaminant transport, for quantifying exposure concentrations, and for demonstrating linkages to human health outcomes. Numerous presenters demonstrated that karst is particularly prone to groundwater contamination that may undermine human health, with several studies documenting higher concentrations of bacteria and protozoa in karst than in porous media aquifers. In addition, molecular tools for tracing and identifying potential pathogens in groundwater revealed large numbers of viruses derived from humans as well as from wildlife and livestock. Most conclusions about human health outcomes are based on interpretation of public health data that are collected independent of information on the factors that exacerbate groundwater contamination. One of the studies presented at the meeting had sufficient data to link the timing of disease outbreak to the occurrence of storm flow that mobilized contaminant migration into groundwater supplies used for drinking. Participants discussed ways that general regulations for water quality protection may not be appropriate in karst regions, where contaminants are transmitted rapidly from the land surface to the water table, and they debated creative non-regulatory approaches to managing land use as another means of protecting water supplies. The significant time lag between the occurrence of water supply contamination, particularly by chemical agents, and the subsequent health outcomes in the population represents a fundamental misalignment of environmental and human data. An edited volume of research papers from the meeting is under contract for publication by Janet S. Herman, Department of Environmental Sciences, University of Virginia, Charlottesville; email: jherman@virginia.edu (**Weblink**: https://eos.org/wp-content/uploads/2016/08/01-Sept_magazine.pdf).

This study is of significant importance to Indian Karst regions as considerable amount of groundwater usage has become a necessity in these regions. It is time for our hydrogeologists and groundwater geophysicists to collect as much data as possible from Kurnool and Kadapa districts of A. P. and interact with the University of Virginia to help the large number of people residing in drought prone Karst locales of Rayalaseema.

*Bacteria Preserve Record of Earth's Magnetic Fields

In the waters of a prehistoric ocean, a minuscule bacterium swims back and forth, seeking food. As it does so, it leaves tiny metallic particles swirling in its wake—some already present in the water column, some excreted as the bacteria's by-products. As the water churns from the motion of other bacteria, some of these particles (magnetic ones) attract each another, coalescing into larger, but still tiny, magnetized crystals of magnetite, goethite, hematite, and other minerals. These iron-rich crystals drift slowly downward to land on the ancient seabed, aligning with the Earth's magnetic field as they're buried by other sediment and eventually locked into place. A scene much like this has unfolded again recently in a glass experimental vessel holding bacteria-filled water in a Russian laboratory. A team of scientists was curious to see how large the crystals could grow and whether they could become substantial enough to maintain a stable magnetic orientation over millions, or even billions, of years. Their findings, published recently in Geophysical Journal International (see http://bit.ly/ FeBacteria), shed light on how sediments gain and retain magnetism. Answers in sludge for their study, the team used "bacteria that are taken from nature, normal groundwater bacteria," said Alexandra Abrajevitch, a paleomagnetist at the Institute of Tectonics and Geophysics of the Russian Academy of Sciences in Khabarovsk, Russia, and lead author on the study. The scientists seeded the vessel of water with iron, food, and sand. Then they waited. Two years later, when the team looked at the reddish sludge that had formed at the bottom of their experiment, they found that the sample contained large crystals of magnetite and goethite. These are stable minerals, capable of carrying a magnetic signature over long periods of time. The team also found lepidocrocite, a magnetically unstable mineral that can transform into more stable forms over time. According to the paper, tests of the sludge's magnetism revealed that it contained a broad range of particle sizes. Some were tiny and unstable like those found in previous experiments, but many were more than 30 nanometers long, large enough to hold a magnetic direction for as long as billions of years. These particles confirmed for the researchers that given enough time, bacteria could prompt larger and larger magnetic crystals to grow in their environment, just by moving and stirring up the water and excreting iron-rich waste. In ancient waters, large particles recorded the direction of the Earth's magnetic field when they settled on the seabed. Most of the stable particles aligned with the Earth's magnetic field. Sediment settled on top of them, holding them in place. The different layers in sedimentary rock provide a continuous timeline of the shifting strength and direction of the magnetic field over time—"almost like a bar code," according to David Heslop, a geophysicist at the Australian National University in Canberra, Australia. If the common bacteria in the experiment could generate stable magnetic particles, he said, a similar process could have been happening throughout Earth's oceans, rivers, and lakes farther back in time than scientists have even looked, back when microbes first became abundant. However, Bacteria Preserve Record of Earth's Magnetic Fields Magnetic minerals, such as the dark stripes of magnetite seen in beach sand in India, can form layers in sediments. Researchers had no proof that bacteria could produce them. Because there was no proof that they could be stable, the particles were dismissed as a potential data source. But the authors of the new study say that prior researchers didn't wait long enough for the particles to mature and grow to their full size. Heslop expects that with this new knowledge in hand, scientists will be able to scan more rocks with better accuracy to find the direction of Earth's ancient magnetic field and to determine the strength of that magnetic field as well. Magnetic minerals from different sources and of different sizes vary in how readily they will align with a field, Heslop said. When researchers are looking at a rock's magnetism, they have to know either the strength of the Earth's magnetic field when the rock was formed or how responsive the magnetic alignment of that type of iron- rich particle was to the field. Knowing one can allow researchers to figure out the other. Figuring out exactly what kinds of particles the majority of bacteria produce and how strongly they align with Earth's magnetic field could help scientists refine their estimates of the strength and orientation of Earth's magnetic field in the deep geologic past. This new experiment was small, Heslop said, but its results may encourage scientists to revisit archives of sedimentary rock samples with new, more reliable information on the origins of their magnetic properties. (Source: https://eos.org/wp-content/uploads/2016/09/15-Sept_magazine.pdf)

Outstanding Contribution

M.S. Swaminathan
- Architect of "Green Revolution"

Mankombu Sambasivan Swaminathan (born 7 August 1925) is an Indian geneticist and international administrator, renowned for his leading role in India's Green Revolution a program under which high-yield varieties of wheat and rice seedlings were planted in the fields of poor farmers. Swaminathan is known as "Indian Father of Green Revolution" for his leadership and success in introducing and further developing high-yielding varieties of wheat in India. He is the founder and chairman of the MS Swaminathan Research Foundation. His stated vision is to rid the world of hunger and poverty. Swaminathan is an advocate of moving India to sustainable development, especially using environmentally sustainable agriculture, sustainable food security and the preservation of biodiversity, which he calls an "evergreen revolution".

Early career

Swaminathan decided to pursue a career in agricultural sciences. He enrolled in Madras Agricultural College (now the Tamil Nadu Agricultural University) where he graduated as valedictorian with another Bachelor of Science degree, this time in Agricultural Science. He explained this career decision thus: "My personal motivation started with the great Bengal famine of 1943, when I was a student at the University of Kerala. There was an acute rice shortage, and in Bengal about 3 million people died from starvation. All of our young people, myself included, were involved in the freedom struggle, which Gandhi had intensified, and I decided I should take to agricultural research in order to help farmers produce more."

In 1947, the year of Indian independence he moved to the Indian Agricultural Research Institute (IARI) in New Delhi as a post-graduate student in genetics and plant breeding. He obtained a post-graduate degree with high distinction in Cytogenetics in 1949.

He chose to accept the UNESCO Fellowship to continue his IARI research on potato genetics at the Wageningen

Agricultural University, Institute of Genetics in the Netherlands. Here he succeeded in standardising procedures for transferring genes from a wide range of wild species of Solanum to the cultivated potato, Solanum tuberosum. In 1950, he moved to study at the Plant Breeding Institute of the University of Cambridge School of Agriculture. He earned a Doctor of Philosophy (PhD) degree in 1952. His work presented a new concept of the species relationships within the tuber-bearing Solanum. His Cambridge college, Fitzwilliam, made him an Honorary Fellow in 2014.

Swaminathan then accepted a post-doctoral research associateship at the University of Wisconsin, Department of Genetics to help set up a USDA potato research station. Despite his strong personal and professional satisfaction with the research work in Wisconsin, he declined the offer of a full-time faculty position, returning to India in early 1954.

Professional achievements

Swaminathan has worked worldwide in collaboration with colleagues and students on a wide range of problems in basic and applied plant breeding, agricultural research and development and the conservation of natural resources. His professional career began in 1949:

Some of the important professional career particulars(out of many) are listed below

- 1972–79 – Director-General, Indian Council of Agricultural Research (ICAR), established the National Bureau of Plant, Animal, and Fish Genetic Resources of India. Established the International Plant Genetic Resources Institute (changed in 2006 to Bioversity International).
- 1979–80 – Principal Secretary in the Ministry of Agriculture, Government of India. Transformed the Pre-investment Forest Survey Programme into the Forest Survey of India.
- 1981–85 – Independent chairman, Food and Agriculture Organization (FAO) Council, Rome.Played a significant role in establishing the Commission on Plant Genetic Resources.
- 1982–88 – Director General, International Rice Research Institute (IRRI).
- 1984–90 – President of the International Union for Conservation of Nature and Natural Resources IUCN, develop the Convention on Biological Diversity CBD.
- 1986–99 – Chairman of the editorial advisory board, World Resources Institute, Washington, D. C., conceived and produced the first "World Resources Report."
- 1988–91 – Chairman of the International Steering Committee of the Keystone International Dialogue on Plant Genetic Resources, regarding the availability, use, exchange and protection of plant germplasm.
- 1988–99 – Chairman/Trustee, Commonwealth Secretariat Expert Group, organised the Iwokrama International Centre for Rainforest Conservation and Development, for the sustainable and equitable management of tropical rainforests in Guyana.
- 1990–93 – Founder/President, International Society for Mangrove Ecosystems (ISME)
- 1995–1999 chairman, Auroville Foundation
- 2001 – Chairman of the Regional Steering Committee for the India – Bangladesh joint Project on Biodiversity Management in the Sundarbans World Heritage Site, funded by the UN Foundation and UNDP.
- 2002 – President of the Nobel Peace Prize-winning Pugwash Conferences on Science and World Affairs .
- 2004 – 2014 – Chairman, National Commission on Farmers.
- Over 68 students have done their PhD thesis work under his guidance.

Publications

Dr. Swaminathan is a prolific scientific researcher and writer. In addition he has written a few books on the general theme of his life's work, biodiversity and sustainable agriculture for alleviation of hunger.

Honours, awards and international recognition

Swaminathan has received several outstanding awards and prizes.

- H.K. Firodia award for excellence in Science & Technology
- Four Freedoms Award, 2000
- Planet and Humanity Medal of the International Geographical Union, 2000
- UNEP Sasakawa Environment Prize
- The Tyler Prize for Environmental Achievement, 1991
- Honda Prize, for achieving outstanding results in the field of ecotechnology, 1991
- Padma Vibhushan 1989
- World Food Prize for advancing human development through increased quantity, quality or accessibility of food, 1987
- Golden Heart Presidential Award of the Philippines,1987
- Albert Einstein World Award of Science as a recognition for his contributions to plant genetics and his influence on international agricultural development. 1986
- Borlaug Award, given by Coromandel Fertilizers, 1979

- Padma Bhushan 1972
- Ramon Magsaysay Award for Community Leadership 1971
- Padma Shri 1967

He holds more than 50 honorary Doctorate degrees from universities around the world.

National Awards

He has been honoured with several awards in India for his work to benefit the country.

- Karmaveer Puraskaar Noble Laureates, March, 2007 by iCONGO- Confederation of NGOs.
- Dupont-Solae Award for his contribution to the field of food and nutrition security 2004
- Life Time Achievement Award from BioSpectrum 2003
- Indira Gandhi Gold Plaque by the Asiatic Society for his significant contribution towards human progress. 2002
- Lokmanya Tilak Award by the Tilak Smarak Trust, 2001
- Indira Gandhi Prize for Peace, Disarmament and Development, 2000
- Millennium Alumnus Award by the Tamil Nadu Agricultural University 2000
- Prof P N Mehra Memorial Award 1999
- Legend in his Lifetime Award by the World Wilderness Trust- India 1999
- Dr. B.P. Pal Medal, 1997
- V. Gangadharan Award,1997
- Lal Bahadur Shastri Deshgaurav Samman 1992
- Dr. J.C. Bose Medal, Bose Institute 1989
- Krishi Ratna Award, 1986
- Rabindranath Tagore Prize of Visva Bharati University 1981
- R.D. Misra Medal of the Indian Environmental Society 1981
- Barclay Medal of the Asiatic Society, 1978
- Moudgil Prize of the Bureau of Indian Standards, 1978
- Birbal Sahni Medal, 1965.
- Shanti Swarup Bhatnagar Award, 1961
- Indira Gandhi Award for National Integration of the Indian National Congress

International Awards

He has been honoured with recognition from several international organisations for spreading the benefits of his work to other countries.

Fellowships

- Indian Academy of Sciences – Elected Fellow (1957)
- Indian National Science Academy – Elected Fellow (1962)
- National Academy of Sciences, India – Elected Fellow (1976)
- Royal Society of London – Elected Fellow (1973)
- National Academy of Sciences, USA – Elected Fellow (1977)
- Russian Academy of Agricultural Sciences – Elected Fellow (1978)
- Royal Swedish Academy of Agriculture and Forestry – Elected Fellow (1983)
- National Academy of Arts and Sciences, USA – Elected Fellow (1984)
- Accad. Naz. Delle Sciencz detta del XL, Italy – Elected Fellow (1985)
- European Academy of Arts, Science and Humanities – Elected Fellow (1988)
- Am. Assn. For the Advancement of Science – Elected Fellow
- The World Academy of Sciences (TWAS) – Founder Fellow (1983)
- National Academy of Agricultural Sciences – Elected Fellow (1990)
- Swaminathan is a Fellow of the Royal Society of London, the U.S. National Academy of Sciences, the Russian Academy of Sciences, the Chinese Academy of Sciences, and the Italian Academy of Sciences.

Current work

He currently holds the UNESCO -Cousteau Chair in Ecotechnology at the M. S. Swaminathan Research Foundation in Chennai, India.

- He is the chairman of the National Commission on Agriculture, Food and Nutrition Security of India (National Commission on Farmers).

- He is currently spearheading a movement to bridge the Digital divide called, "Mission 2007: Every Village a Knowledge Centre".

- M. S. Swaminathan is also a member of the Leadership Council of Compact 2025, a partnership that develops and disseminates evidence-based advice to politicians and other decision-makers aimed at ending hunger and undernutrition in the coming 10 years.

P.R.Reddy

Carbon cycle and climate interactions—Recent study

Below are some of the most critical questions about carbon cycle and climate interactions that are driving current research. Answers to those questions are relevant not only for predicting future atmospheric carbon dioxide concentration and its impact on climate and ecosystems but also for understanding historical changes over past decades and millennia.

Permafrost

How much carbon will be released from permafrost? How quickly will the carbon –rich soil release its contents and in what form-carbon dioxide or methane?

Current estimates indicate that thawing permafrost might release upwards of 150 Pg of carbon, equivalent to roughly 15 years of current carbon dioxide emissions from fossil fuel combustion. Furthermore, depending on how much microbial respiration occurs underwater in lakes and ponds, a significant fraction of permafrost carbon could be released as methane, a stronger greenhouse gas than carbon dioxide.

Ocean circulation

How will be ocean circulation be altered by climate change, and what are the implications for ocean ecosystems and ocean carbon dioxide absorption?

Whereas most of the ocean has been warming, the northwest Atlantic has been cooling.The cooling there could reflect a weakening in the northward transport of heat, possibly related to Arctic warming, loss of sea ice, and melting of the Greenland ice sheet. Over the Southern Ocean, winds have been strengthening because of climate change and because of the ozone hole in the stratosphere.

Nutrient cycling

How will nutrient demand and availability affect ecosystem function and carbon dioxide uptake?

Photosynthesis by plants on land and by phytoplankton in the ocean is often limited by nutrient availability. Ocean-circulation changes associated with climate change are expected to reduce nutrient supply to low and mid-latitude surface waters, with potential impacts on ecosystems and fisheries.

(**Source:** Physics Today, Nov2016, vol 69, no 11, pp-52).

OBITUARY

Prof. David M Boyd
(26-6-1926 - 2-11-2016)

Professor David M Boyd, an internationally renowned Geophysicist passed away at Adelaide, South Australia on November 2, 2016,at the age of 90 years succumbing to the head injury he sustained when he fell while walking. He leaves behind his wife Jenny Boyd, two sons James and Hugh and a daughter Sarah, besides scores of his students and admirers the world over.

David was born in Scotland on June 26, 1926. He entered Glasgow University (UK) in 1943, after a mildly disrupted secondary education during World War II, and obtained double Honours in Natural Philosophy (Physics) and Geology – a first for Glasgow University. After graduation in 1947, he served as a Lecturer in the new science of Geophysics and spent 9 years teaching and conducting exploration field work in the UK, Iceland, and the Rift Valley in Uganda. After spending 2 years with John Taylor and Sons working on many mines in the UK and also in Cyprus he secured a position of a Chief Geophysicist at Hunting Geology and Geophysics (London) in 1956 and thus began 12 very busy, productive and happy years working predominantly on large airborne magnetic projects worldwide, including Ghana and Uganda. During this period, working directly with the field geologists, he developed the methodology, which may be classed as a pioneering work, for integrating aeromagnetics with geology, that culminated in his classic paper *"The contribution of airborne magnetic surveys to geological mapping"* presented at the Canadian Centennial Mineral and Ground Water Conference in Niagara, 1967, and has helped in training and creating generations of competent interpreters of Aeromagnetic data.

Passion for teaching, imbibed during his Glasgow university years, prompted David Boyd to return to academic life joining as inaugural Chairman of Geophysics in the Department of Economic Geology at the University of Adelaide, South Australia in 1969. He retired in 1992. His main focus was nurturing honours graduates who would be sought after by the mining industry. This has resulted in a very competent 'breed' of geophysicists who have become leaders and achievers in the exploration industry in Australia. While best known for his passion for aeromagnetics and the accompanying emphasis on 'hard-rock' geology, many of his graduates have made their mark in the Oil & Gas industry, in seismic research, well logging and as founders and operators of successful exploration companies.

Besides being a Professor of Geophysics, he held positions of Dean of the Faculty of Science; Chairman of the University's Education Committee and further served as Acting Vice-Chancellor in 1982-83. Outside of geosciences, David was Chairman of the Animal Ethics Committee of the Waite Institute (1983-92) and Chairman of the organising committees for ANZAAS congress in 1991 and 1997. His zealous campaign for the Government airborne survey programmes, contributed to the innovations by the South Australian government in launching the 'South Australian Exploration Initiative (SAEI)' and airborne survey funding during 1992-1996 thereby raising exploration profile of South Australia within Australia as well as internationally and becoming a model for other countries to follow. He nurtured relationships with the airborne geophysics industries in Finland, India, China and Africa and was a frequent visitor to these countries, as guest lecturer and counsel. He was key person in initiating courses on 'Geophysics for Geologists' at the Australian Mineral Foundation (AMF) and presented them with zest and zeal, until 1994. From 1997 until his recent passing, he was the key geophysics advisor to 'Archimedes Consulting' and actively working on projects on every inhabited continent of the Earth.

His earliest connection with the Aeromagnetic Survey projects in India goes back to the mid sixties. Interestingly his first contact with Indian programs, as I far as I know, was with the NGRI when, Dr. P.V.Sanker Narayan met him in 1966 at the Hunting Geophysics office in London in connection with the acquiring of a Proton Precision Magnetometer for NGRI's Aeromagnetic Survey Facility project just being started. In 1968 he was associated with the airborne survey in Tamil Nadu by M/s Hunting's (UNDP project) and later in

1972 -73, in his association with the Mineral Development Teams in Australia and the government geologists from India visiting under a Colombo Plan programme. He was instrumental in setting up the 'India-Australia scientific and technology co-operation program (1975)', which helped finance Indian scientists to come to Australia and vice-versa.

Interactions further strengthened and continued with my going to University of Adelaide on a Colombo Plan Fellowship spending the years from 1974 to 1976 and conducting Post-Doctoral Research on the Broken Hill, the Middleback and Hamersley Aeromagnetic data interpretation projects in Australia. The Broken Hill Aeromagnetic data interpretation project was a project close to his heart, in which besides me (Indian), David Isles (Australian), Koya Suto (Japanese) and D.M.Khan (Pakistani), really an international team, participated and successfully completed under his able and inspiring guidance. Later Shanti Rajagopalan, a brilliant student from Osmania University, who did her Ph.D under Prof Boyd's guidance, settled in Australia and played a significant role in the field of Airborne Geophysics and made invaluable contributions in the development of new interpretation techniques. Even after her premature demise, the Australian geophysical community gratefully remembers her and acknowledges her contributions.

Prof Boyd's keen interest in espousing the need for development of skilled manpower in the effective interpretation of Aeromagnetic data in the developing countries took him on several visits to India, particularly to the government institutions like NGRI, Geological Survey of India centers in Calcutta, Hyderabad and Bangalore, Atomic Minerals Division and, NRSA in Hyderabad, and Universities like the Osmania University, Hyderabad and Andhra University, Visakhapatnam. His lectures and practical demonstrations especially using the Indian data were of particular value and inspiration to the geologists and geophysicists at these institutions. This has encouraged the authorities of some of these institutions to depute their officers for further intensive training to the University of Adelaide! Armed with the command over the subject and with humane approach and personal rapport, he won the hearts of every one whom he met in India and they all look at him with admiration and reverence.

He is a Foreign Fellow of the Indian Geophysical Union, Fellow of the Geological Society of India and Association of Exploration Geophysicists (India). He was the President of the Geological Society of Australia (1986-87). He was awarded Honorary Membership of the ASEG in 1997. For his achievements in developing a special breed of geophysics graduates and for his successes in promoting the effective integration of aeromagnetics in geological mapping and exploration, the ASEG, at its 25th Conference, honored him with the presentation of the Society's Gold Medal on August 21, 2016, coinciding with his 90th birth day celebrations.

This was the auspicious occasion when nearly 60 of his students, including me, from world over, gathered in Adelaide in the celebration and paid respects and conveyed gratitude to their teacher. Prof. Boyd was full of energy, enthusiasm and was extremely happy to be with his students who made him proud, but at the same time he was an embodiment of humility and grace when he said *"Learning is a two way business. Learning goes through both for the student and from the student. I am indebted to all of you, although I cannot be specific on what I learnt from you, but I know each one of you have taught me something all the time I have been teaching you. I am greatly honoured. Thank you very much."*

After the celebrations every one left with joy, hope and wish that we all would be meeting again on his 100th birth day. But, alas, fate had a different plan and we had to bear the shocking news of his passing away so soon. He lived a full life, inspiring one and all who came in contact with him, a life to be cherished, emulated and celebrated. We are all very sure, wherever he is; he'll be smiling and will make others smile!

Dr.Dasu Atchuta Rao.
Scientist (Retired), CSIR-NGRI
F 201, Sri Sairam Aditya Residency
Engineers Colony, Yellareddyguda
Hyderabad 500073
Email: araodasu@gmail.com
Ph: 9490023947

OBITUARY

Prof. Y.J. Rao
(1929-2016)

Professor Yerramilli Janardan Rao; a doyen amongst university teachers is popularly known as Prof. Y.J.Rao. He is a pioneer teacher and a well known academician who taught Igneous Petrology and Structural Geology in Osmania University for over three and half decades.

Born on 16th September 1929 at Tanuku, Andhra Pradesh, Prof. Rao had his school education at Tanuku, Intermediate at Presidency college, in erstwhile Madras. He After completing graduation and post graduation from Banaras Hindu University, joined Osmania University as part time lecturer in the year 1954. He was awarded Ph.D. degree in Geology in the year 1960. He served Geology department as lecturer (1955-1963), Reader (1963-1966) and Professor (1966-1989). He served as Principal, University college of Science, Osmania University during 1981-1983 and Dean, faculty of Science during 1988-1989.

Prof. Rao was a Post-Doctoral Research associate at University of Chicago (1960), visiting Asst. Professor at Rutgers, University of New Jersey (1961). He was a visiting Professor at Sulaimania University and Salahddin University, Iraq (1977-1982), Brooklyn and Hunter colleges of the City University, New York (1985 & 1987) and Sultan Qaboos University, Muscat (1988).

An active researcher in Earth Science, Prof. Y.J. Rao has several scientific publications in national and international journals. He supervised about 2 dozen doctoral works. He was a member of the governing body of Institute of Himalayan Geology, Member of Indian scientific Committee that visited USSR (1968), Honorary Director of Indian Institute of Peninsular Geology (1974-1977), Member, Advisory panel for Bhatnagar Award in Earth Sciences (1973-1976).

Apart from his outstanding contribution as an academician and administrator, Prof. Y.J. Rao, is remembered by his students and admirers as one of the finest orators and a graceful human being with noble personality.

Dr.V.V.Sesha Sai,
G.S.I, Southern Region,
Bandlaguda, Hyd-500068

ANNOUNCEMENT

54th Annual Convention of
Indian Geophysical Union (IGU)

will be held at CSIR-NGRI, Hyderabad

During December 4-7, 2017

on

"RECENT ADVANCES IN GEOPHYSICS: SPECIAL REFERENCE TO EARTHQUAKES"

Hon. Secretary
Indian Geophysical Union
CSIR-NGRI Campus, Uppal Road
Hyderabad- 500 007, India
Email: igu123@gmail.com

GUIDE LINES TO AUTHORS

The Journal of Indian Geophysical Union (J-IGU), published quarterly by the Indian Geophysical Union (IGU), is an interdisciplinary journal from India that publishes high-quality research in earth sciences with special emphasis on the topics pertaining to the Indian subcontinent and the surrounding Indian Ocean region. The journal covers several disciplines of earth sciences such as the Geosphere, its watery and gaseous envelopes (the Hydrosphere, the Cryosphere and the Atmosphere), and life (the Biosphere). It also publishes articles on Space and Planetary sciences. J-IGU welcomes contributions under the following categories:

- Research papers reporting new findings, results, etc.
- Review articles providing comprehensive overview of a significant research field related to earth sciences

In addition, J-IGU also welcomes short communications on opinion and report on scientific activity, personal information, book reviews, news and views, etc.

The manuscript should be submitted electronically as a single pdf file including the main text, figures, tables, and any other supplementary information along with the signed "Declaration Letter". The manuscript should be submitted by email ((jigu1963@gmail.com) to the Editor.

After acceptance of the manuscript the corresponding author would be required to submit all source files (text and Tables in word format) and figures in high resolution standard (*.jpg, *.tiff, *.bmp) format. These files may be submitted to the Editor as a single *.zip file along with the "Copyright Transfer Statement".

IMPORTANT INFORMATION

Ethics in publishing

J-IGU is committed to ensuring ethics in publication and takes a serious view of plagiarism including self-plagiarism in manuscripts submitted to the journal. Authors are advised to ensure ethical values by submitting only their original work and due acknowledgement to the work of others in case used the manuscript. Authors must also refrain from submitting the same manuscript to more than one journal concurrently or publish the same piece of research work in more than one journal which is unethical and unacceptable. Editor of J-IGU is committed to make every reasonable effort to investigate any allegations of plagiarism brought to his attention, as well as instances that come up during the peer review process and has full authority to retract any plagiarized publication from the journal and take appropriate action against such authors if it is proven that such a misconduct was intentional.

Similarly, Editor and Reviewers are also expected to follow ethical norms of publishing by ensuring that they don't use any unpublished information, communicated to them for editorial or review purpose, in their own research without the explicit written consent of the author. They are also expected to keep manuscript/ data/ observations/ any other information related to the peer review confidential to protect the interest of the authors. Reviewers should refrain from reviewing the manuscripts in which they have conflicts of interest resulting from competitive, collaborative, or other relationships or connections with any of the authors, companies, or institutions connected to the manuscript.

Conflict of interest

All authors are requested to disclose any actual or potential conflict of interest including any financial, personal or other relationships with other people or organizations within three years of beginning the submitted work that could inappropriately influence, or be perceived to influence, their work.

Submission declaration

Submission of a manuscript implies that the work has not been published previously and it is not under consideration for publication elsewhere, and that if accepted it will not be published elsewhere in the same or any other form, in English or in any other language, without the written consent of the publisher. It also implies that the authors have taken necessary approval from the competent authority of the institute/organization where the work was carried out.

Copyright

After acceptance of the manuscript the corresponding author would be required to sign and submit the "Copyright Transfer Statement".

MANUSCRIPT PREPARATION

The corresponding author should be identified (include E-mail address, Phone/Mobile number). Full affiliation and postal address must be given for all co-authors.

Abstract:

An abstract of not more than 300 words must be included.

Text:

The manuscript should be structured to include a front page containing the title, Author(s) name, affiliation and address of the institute where the work was carried out, a short title, and 5-to-6 index terms/Key words. Author(s) present address, if different from the above mentioned address, may be given in the footnote. The corresponding author should be identified with an asterisk and his/her email ID should be provided. This page should be followed by the main text consisting of Abstract, Introduction, Methods/ Techniques/ Area description, Results, Discussion, Conclusions, Acknowledgements, and References. Tables and Figures with captions should be inserted in the main text of the manuscript at appropriate places.

Figures/ Illustrations:

All figures should be provided in camera-ready form, suitable for reproduction (which may include reduction) without retouching. Figures in high-resolution (at least 300 dpi) standard formats (*.jpg, *.tiff, *.bmp) are acceptable. Figures should be numbered according to their sequence in the text. References should be made in the text to each figure. Each figure should have a suitable caption.

Tables:

Authors should take note of the limitations set by the size and layout of the journal. Table should not exceed the printed area of the page. They should be typed on separate sheets and details about the tables should be given in the text. Heading should be brief. Large tables should be avoided and may be provided as supplementary information, if required.

Equations:

Equations should be numbered sequentially with Arabic numerals and cited in the text. Subscripts and Superscripts should be set off clearly. Equation writing software that presents each equation as an object in MS Word will be accepted. Style and convention adopted for the equations should be uniform throughout the paper.

References:

All references to publications cited in the main text should be presented as a list of references following the text and all references in the list must be cited in the text. References should be arranged chronologically, in the text. The list of references should be arranged alphabetically at the end of the paper.

References should be given in the following form:

Kaila, K.L., Reddy P.R., Mall D.M., Venkateswarlu, N., Krishna V.G. and Prasad, A.S.S.S.R.S., 1992. Crustal structure of the west Bengal Basin from deep seismic sounding investigations, Geophys. J. Int., v.111,no., pp:45-66.

REVIEW PROCESS:

All manuscripts submitted to the journal are peer-reviewed. It is advisable to send the contact details of **4 potential reviewers** along with the manuscript to expedite the review process. Editor has the option to select reviewers from the list or choose different reviewers. The review process usually takes about 3 months. All enquiries regarding the manuscript may be addressed to the Editor.

GALLEY PROOF:

Technical editing of manuscripts is performed by the editorial board. The author is asked to check the galley proof for typographical errors and to answer queries from the editor. Authors are requested to return the corrected proof **within two days** of its receipt to ensure uninterrupted processing. The editor will not accept new material in proof unless permission from the editorial board has been obtained for the addition of a "note added in proof". Authors are liable for the cost of excessive alterations to galley proof.

PUBLICATION CHARGES:

There are no page charges for publication and printing charges for b/w figures. However, in view of substantial cost involved in printing of color figures, author will be charged for printing of pages containing color figures @ Rs. 2,500/- per page. The charges may be revised at any time based on cost of printing and production. Author will receive an estimate/ invoice of the color figures reproduction cost along with the galley proof. It is the responsibility of the author to remit the color figures reproduction cost **within one month** of the receipt of the estimate/invoice.

The corresponding author will receive a soft copy (pdf format) of his/her published article. Should the author desire to purchase reprints of his/her publication, he/she must send the duly signed Reprint Order Form (accompanies the galley proof and contains price details) along with the corrected galley proof to the Editor. The reprint charges must be paid **within one month** of sending the Reprint Order Form.

Any payment related to printing of color figures and/or purchase of reprints should be made in the form of a Demand Draft in the name of **Treasurer, Indian Geophysical Union**, payable at **Hyderabad**.

You may download the pdf file here: Guide for Authors